Dissertation

submitted to the
Combined Faculty of Natural Sciences and Mathematics
of the Ruperto Carola University Heidelberg, Germany
for the degree of

Doctor of Natural Sciences

Presented by
M.Sc. Ahmed Eltokhi
born in: Kalyobia, Egypt
Oral-examination:

Dissecting hormonal and transient effects in Shankopathies associated with autism spectrum disorder

Referees: Prof. Dr. Gudrun A. Rappold

Dr. Rolf Sprengel

SWORN AFFIDAVIT ACCORDING TO §8 OF THE DOCTORAL DEGREE REGULATIONS OF THE COMBINED FACULTY OF NATURAL SCIENCES AND MATHEMATICS

I herewith declare that:

1. The thesis I have submitted entitled "Dissecting hormonal and transient effects in Shankopathies associated with autism spectrum disorder" is my own work. I have only used the sources indicated and have not made unauthorized use of services of a third party. Where the work of others has been quoted or reproduced, the source is always given.

2. I have not yet presented this thesis or parts thereof to a university as part of an examination or degree.

3. I am aware of the importance of a sworn affidavit and the criminal prosecution in case of a false or incomplete affidavit.

4. I affirm that the above is the absolute truth to the best of my knowledge and that I have not concealed anything.

Place and date: Signature:

Heidelberg,

Ahmed Eltokhi

PRESENTATIONS

Some data of this thesis were presented at the following conferences:

- The 28th Annual Meeting of the German Society of Human Genetics
  March 29-31, 2017 – Bochum, Germany

- Winter School: Sex Hormones and the Brain
  January 31- February 2, 2018 – Tübingen, Germany

- The annual meeting of the American Society of Human Genetics
  October 16-20, 2018 – San Diego, USA

- The annual meeting of the Society for Neuroscience
  November 3-7, 2018 – San Diego, USA

- The annual meeting of the Society for Neuroscience
  October 19-23, 2019 – Chicago, USA

PUBLICATIONS

The following publications were prepared in the context of this thesis:

- Sprengel R, Eltokhi A, and Single FN (2017). Gene Targeted Mice with Conditional Knock-In (-Out) of NMDAR Mutations. In NMDA Receptors Methods in Molecular Biology, Burnashev N., and S P., eds., pp 201-230. doi: 10.1007/978-1-4939-7321-7_11.

- Eltokhi, A., Rappold, G., and Sprengel, R. (2018). Distinct Phenotypes of Shank2 Mouse Models reflect Neuropsychiatric Spectrum Disorders of Human Patients with SHANK2 Variants. Frontiers in Molecular Neuroscience 11, 240-240. doi: 10.3389/fnmol.2018.00240.

- Berkel, S.*, Eltokhi, A.*, Fröhlich, H., Porras-Gonzalez, D., Rafiullah, R., Sprengel, R., Rappold, G. (2018). Sex Hormones Regulate SHANK Expression. Frontiers in Molecular Neuroscience 11(337). doi: 10.3389/fnmol.2018.00337.

- Eltokhi, A., Hüser, M., Bus, T., Rozov, A., Harten, A., Rappold, G.*, and Sprengel, R.* "Dissecting developmental and transient effects in Shankopathies associated with Autism spectrum disorder" (in preparation).

ACKNOWLEDGMENTS

This section is dedicated to thank many people who supported me over the last five years.

Prof. Dr. Gudrun Rappold: Thanks a lot for giving me the opportunity to work as a PhD student in your lab. I learned a lot from you, science-, career- and life-wise. Thank you for putting tremendous efforts in paving the way to find collaborators and for advancing this amazing project. Because of you, I know now how to work on myself to be a better person. This is a huge impact of you on my life, which I really don't know how to thank you for. I would like also to thank you for having enough patience to deal with me, and I 'm really fascinated by the way you dealt with my hot temper.

Dr. Rolf Sprengel: It all started on the 16th of September, 2015 with a simple email to introduce myself to you. I did not know back then that this would be a turning point in my life. I can spend much time trying to explain how you were supportive, kind and patient with me. However, I'm sure that I won't be able to describe you in simple words. Therefore, I will be straightforward and just say that I wouldn't be the person I 'm today without you and your help. Everything I have achieved or will achieve is based on your support. I will never forget what you have done for me. You will be definitely a big part of my acceptance speech in case I get the Nobel prize one day ☺.

Many thanks go to Prof. Dr. Ulrike Müller for being my TAC member and contributing with suggestions to the development of my PhD project through the years. I would like to thank Dr. Claudio Acuna for the long conversations and for the support. He changed my way of thinking and gave me the motivation to be a better scientist and to advance my scientific career.

HBGIS was such an amazing graduate school. Thanks to it, I was supported financially with a fellowship for 3 years, had several great scientific and career trainings. I also had the chance to meet nice people through it.

I would like to thank all the current and former members of AG Rappold. Special thanks go to Simone Berkel for working together in close proximity and helping me to get my first research article. Thanks for the other people from the lab, Dr. Beate Niesler, Dr. Stefanie Schmitteckert, Dr. Sandra Hoffmann, Dr. Anna-Eliane Müller, Tanja Mederer, Birgit White, Diana Gonzalez, Dr. Antonino Montalbano, Dr. Henning Fröhlich and Ralph Roeth. Without you all, my life would never be the same ☺. Each time I talk to someone of you, I get to know something new.

This part of the acknowledgment is dedicated to Simon Sumer and Flavia-Bianca Cristian. Complaining to you when things didn't go as planned was my way to tell you that you are very close to my heart. Yes, I know it was/is annoying. But I kept doing it because it is my untraditional way to express feelings ☺. I hope that I 'm close to your heart too. All the best with your PhD. You are great scientists. Academia needs people like you. I believe in you.

For the people from AG Sprengel, Thorsten Bus, Hannah Sonntag and Annette Herold, you can't imagine how grateful I 'm for the fruitful time I spent with you. I would like to express my deepest gratitude and thankfulness to you for the wonderful working atmosphere and for helping me every time when I needed. Every one of you has a special place in my heart. I hope that I had an impact on you similar to your big impact on me.

I would like to thank Dr. Claudia Pitzer and Barbara Kurpiers from the INBC, Heidelberg. I spent most of my PhD in your lab doing the behavior analysis on mice. Thanks a lot for your high tolerance and huge support. Without you, I wouldn't be able to get the marvelous opportunities I have right now.

For all the people who shared my joy and sadness. Thank you. Thanks a lot, Shehab Elzoheiry for all the support, negotiations and fun. I wish you will achieve your dream and become an astronaut. Don't forget to analyze the neuronal ensembles in aliens' brains. A message to the Egyptian/Syrian community in Heidelberg, Doaa Ali, Fadwa El Tahry, Hala Ghiias and Mohamed Belal, I survived my PhD because of your help. For the people who supported me from the motherland, Egypt, Yumna/Youmna Ibrahim ☺ and Esraa Samy. Yumna, I hope you already got the life you dreamt of. Esraa, I hope someday you will get the life you are dreaming of.

This part is dedicated to my family. Seven years ago, I decided to leave Egypt and take the risk. Although you didn't think it was a good idea, you still supported me financially and emotionally. I think now we can agree that it was the best decision ever. My father, mother, brother and sisters, I couldn't manage anything without your prayers. Although some people don't believe in that, your prayers have an amazing role in my life. I did many experiments on them, ran different statistical tests and even corrected for multiple tests, and I can say now that they significantly affected my life in a better way. I won't be able to thank you enough. In addition, special thanks go to Dr. Osman Fekry for his constant support. He is a brother to me ☺.

In the acknowledgment section of my master thesis, I wrote this about you "I would like to thank my special one who believes in me more than I believe in myself". Here I'm, five years later, and still, this is the first thing that pops in my head when I talk about you. The only difference is that you are now my wife. We had to go together through very difficult times. However, we managed to destroy all the obstacles. I can't imagine achieving what I have achieved without you. You gave me the strength and support. I hope I succeeded to describe what I feel about you. Thanks a lot, Shaimaa Madbouly "My sweetheart".

SUMMARY

Postsynaptic scaffolding proteins like SHANK1-3 stabilize the formation, organization and signal transmission at the glutamatergic synapses through numerous protein interactions. All three *SHANK* genes are expressed in multiple isoforms that cooperate to form a complex and a developmental-dependent scaffold organization at glutamatergic synapses. Those modulatory proteins are involved in the spatial organization of postsynaptic receptors, the efficiency of synaptic transmission and the plasticity of synapses. As a consequence, the synaptic transmission is responsive to structural changes within the SHANK scaffold, as evidenced by (I) the high number of ASD patients with mutations and copy number variations in the *SHANK* genes, (II) the diverse clinical phenotypes ranging from ASD to mania-like phenotypes in numerous *Shank* knock-out mouse models and (III) the 4-fold higher prevalence of ASD in males, which might be explained in some cases by the sex dimorphic expression of *SHANK*. Indeed, the here presented investigation of *Shank* expression in mice revealed significantly higher SHANK levels both in late stage male embryos and early-postnatal male pups during their peak of testosterone level. Moreover, the treatment of human neuroblastoma cells with dihydrotestosterone and 17β-estradiol increased the expression of all three *SHANK* genes, demonstrating a direct sensitivity of *SHANK* genes to the sex hormones.

For the functional analysis of specific SHANK isoforms in mice, the endogenous regulation of the Shank scaffold was blunted in favor of a strong constitutive, doxycycline-regulated overexpression of transgenic SHANKs. The spatiotemporal-controlled overexpression of either SHANK2A or the truncated SHANK2A(R462X) in the mouse glutamatergic forebrain neurons was correlated with specific ASD-like phenotypes including hyperactivity, repetitive behavior and impairments in social and novelty behaviors. When the transgenes were switched off in adulthood, specifically the impaired sociability was unexpectedly rescued in mice of both mouse lines. The effect of SHANK2A but not SHANK2A(R462X) overexpression inhibited the developmental-dependent AMPAR subtype switch in the basal dendrites of the hippocampus. In addition, the synaptic protein components were altered differently in both mouse lines, indicating mainly presynaptic components in SHANK2A(R462X) and more postsynaptic components in SHANK2A overexpressing mice. These results identified the differential regulation of endogenous SHANK as critical modulators of neuronal networks that are critically involved in learning and social behaviors.

ZUSAMMENFASSUNG

Das postsynaptische Proteingerüst der SHANK1-3 Proteine stabilisiert die Bildung, Organisation und Signalübertragung glutamaterger Synapsen durch zahlreiche Proteininteraktionen. Dabei ermöglicht die Vielzahl von SHANK Isoformen eine entwicklungsabhängige Reifung des postsynaptischen Netzwerks und somit eine räumliche Umorganisation postsynaptischer Rezeptoren, die für die synaptische Übertragung wesentlich sind. Dies wurde zum einen durch die vergleichsweise hohe Zahl von ASD-Patienten mit Veränderungen in den drei SHANK Genen deutlich und durch die extrem hohe phänotypische Variabilität der Patienten und der zahlreichen Shank-Knock-out-Mausmodelle. Weiterhin ist eine 4-fach höhere Prävalenz von ASD bei Männern beschrieben, was in einigen Fällen durch die geschlechtsdimorphe Expression von SHANK erklärt werden könnte. Tatsächlich zeigten Mäuse signifikant höhere SHANK Expressionslevel bei männlichen Embryonen in späten Stadien und männlichen Jungtieren während früher postnataler Stadien, wenn der Testosteronspiegel besonders hoch ist. Darüber hinaus führte die Behandlung von menschlichen Neuroblastomzellen mit Dihydrotestosteron und 17β-Östradiol zu einer erhöhten Expression aller drei SHANK-Gene, was den direkten Einfluss der Sexualhormone auf die Regulation neuronaler SHANK-Gene zeigen konnte.

Zur Funktionsanalyse definierter SHANK-Isoformen in Mäusen wurde die endogene Regulation des SHANK-Gerüsts zugunsten einer konstitutiven, Doxycyclin-regulierten Überexpression transgener SHANKs in den Hintergrund gedrängt. Die räumlich und zeitlich kontrollierte Überexpression von SHANK2A, oder des verkürzten SHANK2A(R462X), in den glutamatergen Vorderhirnneuronen korrelierte dabei mit mauslinienspezifischem, ASD-ähnlichem Verhalten wie Hyperaktivität, repetitives Verhalten und Beeinträchtigungen des Sozial- und Neuheitsverhaltens. Wenn die Transgene im Erwachsenenalter ausgeschaltet wurden, konnte bei adulten Tieren beider Mauslinien erstaunlicherweise ein normales Sozialverhalten beobachtet werden. Im Gegensatz zu SHANK2A (R462X) hemmte die Wirkung der Überexpression von SHANK2A den entwicklungsabhängigen Austausch von AMPAR-Subtypen in Basaldendriten des Hippokampus. Auch die Proteinzusammensetzung der Synapsen in beiden Mauslinien war unterschiedlich verändert: bei SHANK2A (R462X) waren überwiegend präsynaptische Komponenten, bei SHANK2A-überexprimierenden Mäusen überwiegend postsynaptische Komponenten betroffen. Diese Ergebnisse belegen eine entscheidende Rolle der SHANK Proteine als kritische Modulatoren neuronaler Netzwerke, die Lernvorgänge und soziales Verhalten beeinflussen.

Table of Contents

ABBREVIATIONS

β-gal	Beta-galactosidase
5-HT_{2A}	Serotonin receptor 5-HT_{2A}
ACSF	Artificial cerebrospinal fluid
ADHD	Attention deficit hyperactivity disorder
AMPA	α-Amino-3-hydroxy-5-methyl-4-isoxazolepropionic acid
AMPAR	AMPA receptor
ANK	Ankyrin
AR/Ar	Androgen receptor
ASD	Autism spectrum disorder
BSA	Bovine serum albumin
CamKII	Ca^{2+}/calmodulin-dependent protein kinase II
CB	Cerebellum
cDNA	Complementary DNA
CNV	Copy-number variation
Cre	Cre recombinase
D2	Dopamine receptor 2
DAB	3,3'-Diaminobenzidine
dB	Decibel
ddH2O	Double distilled water
DG	Dentate gyrus
DHT	dihydrotestosterone
DLGAP1	Disks large-associated protein 1
DMEM	Dulbecco’s modified Eagle medium
DNA	Deoxyribonucleic acid
dNTP	Deoxynucleotide triphosphate
Dox	Doxycycline
EPSC	Excitatory postsynaptic current
ER/Er	Estrogen receptor
EtOH	Ethanol

FDR	False Discovery Rate
FERM	4.1, Ezrin, Radixin, Moesin
FRT	Flippase recognition target
GABA	Gamma-Aminobutyric acid
$GABA_AR$	$GABA_A$ receptor
GAPDH	Glyceraldehyde 3-phosphate dehydrogenase
GFP	Green fluorescent protein
GKAP	Guanylate kinase- associated protein
GluA1/ 2/ 3	Glutamate receptor 1/ 2/ 3
GluN1/ 2A/ 2B	NMDA receptor subunit GluN1, GluN2A, GluN2B
GPI1	Glucose phosphate isomerase 1
GRIP	Glutamate receptor-interacting protein
HCl	Hydrogen Chloride
HPC	Hippocampus
HPRT1	Hypoxanthine phosphoribosyltransferase 1
HSPD1	Heat shock protein family D member1
Hz	Hertz
IBF	Interfacultary Biomedical Facility, Heidelberg University
ID	Intellectual disability
INBC	Interdisciplinary Neurobehavioral Core, Heidelberg University
kDa	Kilo dalton
Kegg	Kyoto Encyclopedia of Genes and Genomes
LABORAS	Laboratory animal behavior observation registration and analysis system
LTP	Long term potentiation
MGI	Mouse genome informatics
mGluR1/ 5	Metabotropic glutamate receptor 1 / 5
mRNA	Messneger Ribonucleic acid
NaCl	Sodium chloride
NaOH	Sodium hydroxide
Naspm	1-Naphthyl acetyl spermine trihydrochloride
NCBI	National Center for Biotechnology Information

Neo	Neomycin
Nes	Nestin
NGS	Normal goat serum
NMDA	N-methyl-D-aspartate receptor
NMDAR	NMDA receptor
OB	Olfactory bulb
Oxtr	Oxytocin receptor
PBS	Phosphate-buffered saline
PC	Purkinje cells
PCR	Polymerase chain reaction
PDZ	PSD-95-Discs Large-zona occludens-1
PFA	Paraformaldehyde
PGK1	Phosphoglycerate kinase 1
Pr	Promoter
PRR	Proline-rich region
PSD	Postsynaptic density
PSD95	Postsynaptic density protein 95
Ptet-bi	Bidirectional tetracycline-responsive promoter element
PV	Parvalbumin
qPCR	Quantitative PCR
rAAV	Recombinant adeno-associated virus
RIPA	Radioimmunoprecipitation assay buffer
RNA	Ribonucleic acid
RORA	Retinoic acid-related orphan receptor alpha
RPM	Revolutions per minute
SAM	Sterile alpha motif
SC-CA1	Schaffer collateral-CA1
SCZ	Schizophrenia
SD	Standard deviation
SDHA	Succinate dehydrogenase complex subunit A
SEM	Standard error of the mean

SH3	Src homology 3
SHANK	SH3 and multiple ankyrin repeat domain
SHARPIN	SHANK-associated RH domain interactor
SHIRPA	SmithKline Beecham, Harwell, Imperial College School of Medicine, Royal London Hospital, Phenotype, Assessment
SSTR2	Somatostatin receptor type 2
SYNGAP1	Synaptic Ras GTPase-activating protein 1
TAE	Tris acetic acid EDTA
TBS	Tris-buffered saline
TBS-T	Tris-buffered saline with Tween 20 (1%)
Tris	Tris-(hydroxymethyl)-aminomethane
tTA	Tetracycline transactivator
Venus	Green fluorescent protein variant
vGlut1	Vesicular glutamate transporter 1
VVA	Vicia Villosa Agglutinin
WT	Wild-type

Chapter 1

Introduction

1.1 Autism spectrum disorder (ASD)

Autism spectrum disorder (ASD) is a heritable complex neurodevelopmental disorder [1]. It refers to a constellation of clinical conditions with two main phenotypic characteristics: impairment in social communication and patterns of repetitive restrictive behaviors [2,3] with a 40% prevalence of developmental delay and intellectual disability (ID) [4]. Along with the core symptoms of ASD, comorbidities including hyperactivity, anxiety, epilepsy, hypotonia, sleep disruption and gastrointestinal disorders usually occur in ASD patients [5-8]. Moreover, other genetic disorders such as fragile X syndrome, tuberous sclerosis and Rett syndrome often present autistic features [9-17]. ASD symptoms are usually noticed before the age of three and persist throughout life, suggesting that prenatal impairments in brain development can turn into postnatal manifestations [18]. It has been suggested that specific brain regions mediate the phenotype observed in ASD patients: the frontoparietal cortex, amygdala, hippocampus, basal ganglia and striatum [19].

In ASD, information processing in the brain is disrupted by the altered connectivity of nerve cells and their functional network organization. There is also an excess of neurons, causing local over-connectivity and an abnormal formation of synapses and dendritic spines [20]. In the last decade, mutations in several genes that encode proteins required in synapse formation, development, plasticity and pruning were linked to ASD. This supports the hypothesis that ASD is, to a large extent, the consequence of a developmental synaptopathy. These genes include *NLGN3* [21], *NLGN4* [21], *NRXN1* [22,23], *CNTNAP2* [24] and *SHANKs* [4,25,26]. In addition to the genetic risk factors, a combination of different environmental factors influencing early brain

development likely contributes to ASD. These environmental triggers include maternal physical and mental health [27] as well as exposure to medication during pregnancy and hypoxia during birth [27] (for reviews, see [28-30]).

1.1.1 Sex bias in ASD

ASD affects more males than females in a 4:1 ratio and with a worldwide prevalence of about 1% [31-34]. The mechanism behind this sex-differential risk is not well understood. In part, the risk difference can be explained by a diagnostic bias as ASD symptoms are more visible and easier diagnosed in males [35], whereas female ASD patients are better at masking social challenges in school [36-38]. Since genetics play a major role in ASD, an increasing number of studies have proposed hypotheses related to the level and pattern of gene expression as a reason for the ASD sex-differential risk [31,39-44]. One hypothesis suggests that ASD risk genes are sex-differentially expressed due to genes on the X or Y chromosomes, skewed X inactivation or sex-specific imprinting defects on autosomes. A growing number of studies support this hypothesis by revealing that sex chromosomes aneuploidies modulate ASD risk with an increased rate of ASD diagnosis in Turner syndrome (XO, 3% ASD) [45-47], Klinefelter syndrome (XXY, 10% ASD) [48,49], and 47,XYY syndrome (20% ASD), but no increased rate in X chromosome trisomy [50,51]. This may indicate that the Y chromosome is a risk factor for ASD, while a second X chromosome is protective, possibly *via* genes that escape X-inactivation [39]. Another hypothesis suggests that ASD risk genes are expressed at the same level in both males and females, but they interact with sexually dimorphic pathways [44,52]. Due to the fact that early (prenatal and neonatal) brain development is influenced by sex hormones, a central role of sex hormones in the ASD sex-differential risk has been proposed [31]. One example is estrogen, which is known to enhance synaptogenesis and to modulate synaptic plasticity [53,54]. This, in turn, may have a protective effect against ASD [55]. Fetal testosterone levels, in contrast, are correlated with autistic traits [56,57] (for a review, see [58]). In addition, a subset of adolescent and adult patients with ASD showed elevated androgen levels [59]. Therefore, high levels of testosterone during early and late development have been hypothesized as an ASD risk factor due to a hypermasculinization of the brain (also known as the androgen theory of ASD [52,60]). However, the precise cellular and molecular mechanisms by which sex hormones interact with ASD pathways are not well understood. One potential mechanism of sex hormones was observed in the cortices of adult ASD patients. Here, the expression of genes involved in the immune system and glia function

were upregulated [61] and modulated by estradiol levels [62,63]. Another potential mechanism involves the expression of Retinoic acid-related orphan receptor alpha (*RORA*), a gene known to be associated with ASD [64,65]. *RORA* expression has been shown to be activated by estradiol and inhibited by testosterone hormones [66] *via* the estrogen receptor (ER) and androgen receptor (AR) [67]. Moreover, the expression of *RORA* displayed a pattern of sex-bias in certain brain regions in humans and mice [68]. The expression of ASD risk genes that encode synaptic proteins might also be regulated by sex hormones during brain development [69]. However, the effect of sex hormones on the expression of these genes have not been thoroughly investigated so far.

1.2 The excitatory glutamatergic synapses

At the most fundamental level, brain function is based mainly on computations performed by neurons that receive input through their synapses. The synapses permit the flow of electrochemical signals from one neuron to another [70]. The glutamatergic synapses are the most abundant type of excitatory synapses. They are composed of pre- and postsynaptic sides, separated by a 15-25 nm synaptic cleft [71]. The presynaptic region contains vesicles filled with the neurotransmitter glutamate. Glutamate is released when the presynaptic membrane is depolarized by an action potential [72]. The released glutamate binds to the fast ionotropic glutamatergic receptors including N-methyl-d-aspartate (NMDA), α-amino-3-hydroxy-5-methylisoxazole-4-propionic acid (AMPA) and kainate as well as to metabotropic glutamatergic receptors (mGluRs) [73]. Binding of glutamate to the ionotropic glutamatergic receptors usually induces an influx of positively charged ions such as Na^+ and sometimes Ca^{2+}, which, in turn, triggers the depolarization of the postsynaptic membrane [74]. At a depolarized postsynaptic membrane, the glutamate activation of NMDA receptor (NMDAR) leads to a very selective Ca^{2+} influx, a subsequent activation of second messenger cascades and finally to a long lasting change of synaptic transmission at this synapse. This is a central mechanism for the plasticity of the neuronal system, which is underlying learning and memory [75].

Fine-tuning of synaptic transmission and synaptic plasticity requires a rigorous spatiotemporal organization of the proteins at the excitatory synapses. Also, the specific coupling of the postsynaptic receptors to their downstream signaling pathways has to be orchestrated. Therefore, it is not surprising that the analysis of the molecular organization of the excitatory glutamatergic postsynapse in humans *via* mass spectrometry revealed around 1500 proteins including

intercellular cell adhesion molecules (Neurologins, N-cadherin) and a variety of signaling proteins (kinases, phosphatases, etc.) [76,77]. In the excitatory postsynapse, intracellular scaffolding proteins regulate the organization and the dynamics of those multiple protein complexes that are usually composed of several subunits and associated proteins [78]. These scaffolding proteins feature multiple protein- and/or cytoskeleton-binding domains that enable the trafficking, anchoring and clustering of receptors and adhesion molecules in the postsynaptic density (PSD) [78]. They also support and mediate the cellular processes critical for synaptic transmission and plasticity [79]. The most important scaffolding proteins include the postsynaptic density molecule 95 (PSD95) and the members of the SH3 and multiple ankyrin repeat domains (SHANK) protein family, which are involved in multiple aspects of synaptic function [34,80-82].

1.3 The SHANK family as major scaffolding proteins

The human SHANK family embodies three known synaptic scaffolding proteins, SHANK1, SHANK2 and SHANK3, with ~2000 amino acid residues in length and >200 kDa in molecular mass [34]. SHANK proteins are localized at the interface between the membrane receptors and cytoskeleton (24-26 nm inside the membrane) [83]. They organize a cytoskeleton-associated signaling complex at the PSD of nearly all excitatory glutamatergic synapses in the mammalian brain [84-87]. Thus, the SHANK proteins play an important role in the formation, organization and signaling of the glutamatergic synapses. For instance, they connect NMDAR and AMPA receptors (AMPAR) to the actin cytoskeleton of the PSD [34]. Several studies identified more than 30 synaptic proteins interacting with SHANKs by binding to their domains [87], which accounts for the complexity of SHANK protein function. A full-length SHANK protein contains five protein-protein interaction sites: the N-terminal multiple ankyrin (ANK) repeats, the Src homology 3 (SH3) domain, the PSD-95/Discs large/zona occludens (PDZ) domain, the long (>1000 residue) proline-rich region (PRR) and the sterile alpha motif (SAM) in the C-terminal domain [34] **(Figure 1)**. The ANK repeat domain is a 33-residue sequence motif [88] and interacts with the cytoskeletal protein α-fodrin [89] and SHANK-associated RH domain interactor (SHARPIN) that plays a role in the dendritic spine development [90]. The SH3 domain binds to the glutamate receptor-interacting protein (GRIP) that is required for AMPAR trafficking [91]. It also binds to Densin-180 for dendritic spines remodeling [92] and to $Ca_v1.3a$ for the synaptic clustering of $Ca_v1.3$ L-type Ca^{2+} channels [93]. The PDZ site in SHANK proteins binds to the C-terminal of

the adaptor protein guanylate kinase-associated protein (GKAP) (Naisbitt et al., 1999). GKAP itself can bind to PSD95 [94] which, in turn, is in contact with NMDAR [95] and AMPAR [96,97] (for a review, see [98]). The combined interaction of the PDZ domain and GKAP allows SHANK protein recruitment to the postsynaptic sites. Moreover, the PDZ domain recognizes a consensus C-terminal sequence X-T/S-X-L that is prevalent in many membrane proteins such as the group I mGluRs and the somatostatin receptor type 2 (SSTR2) [99]. However, the binding of the PDZ domain to SSTR2 was confirmed neither *in vitro* nor *in vivo* [85,100]. Importantly, the SHANK proteins have been shown to interact with Homer via the PRR [86,101]. This interaction allows the coupling of mGluRs to Ca^{2+} release from the endoplasmic reticulum in the PSD, which helps the assembly of signaling complexes in excitation-Ca^{2+} coupling [102]. Cortactin, a molecule involved in the actin cytoskeleton organization and polymerization in the cell cortex and dendritic spine [86], has been shown to bind to the PRR as well [103]. The SAM domains of SHANK proteins can bind to each other in homomeric and heteromeric manners, enabling the SHANK proteins to multimerize tail-to-tail by a Zn^{2+}-dependent mechanism [104,105]. In addition, the SAM domain is also essential for the localization of SHANK2 and SHANK3 proteins to the PSD [106]. Thus, the oligomerization of SHANK protein permits the cross-linking of multiple sets of protein complexes at the postsynaptic sites. In summary, the full-length SHANK proteins exert their versatile functions by binding directly to multiple synaptic proteins *via* their protein-binding domains and interacting indirectly with three major classes of postsynaptic glutamate receptors: NMDAR by the GKAP complex, mGluRs by Homer and AMPAR by GRIP.

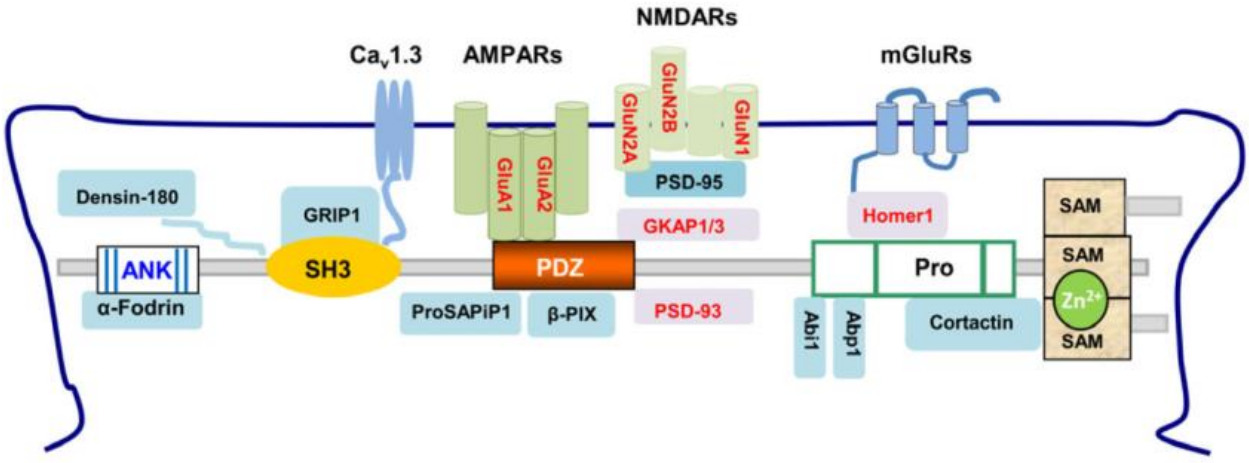

Figure 1: Simplified model of SHANK proteins in the PSD of the excitatory glutamatergic synapses

Schematic diagram of SHANK proteins, their protein-protein interaction sites (the N-terminal ANK repeats, the SH3, the PDZ, the PRR and the C-terminal SAM domain) and their direct partners. The figure and figure legend are adapted from [87].

Another layer of complexity in the SHANK protein function is added by a multitude of alternative splice variants as well as multiple internal promoters in their genes (*SHANK1*: 2; *SHANK2*: 3 and *SHANK3*: 6 internal promoters) [87], resulting in several isoforms [84,107]. The splicing appears to be regulated during brain development, albeit the functional significance of the alternative splicing of the *SHANK* genes is still unknown [87]. The differential spatiotemporal expression of the SHANK proteins adds another layer of complexity. Although SHANKs are predominantly expressed in the brain [108,109], *SHANK2* mRNA is also expressed in peripheral tissues like liver and kidney [84,110-112], and *SHANK3* mRNA is expressed in all tissues, predominantly in the heart and moderately in the brain and spleen [34,84] (see http://www.proteinatlas.org). In the brain, all three SHANK proteins are co-expressed in the cortex and hippocampus, whereas other brain regions showed differential expression [34]. The temporal expression of SHANK patterns identified by the *in situ* RNA hybridization studies in rats revealed the co-expression of SHANK1 and SHANK2 during the early days of development, whereas SHANK3 reaches its maximum expression at postnatal day (P) 16 [113].

Although all SHANK proteins can respond to synaptic events, there is still functional divergence between these three proteins. SHANK1 lacks the capability to localize to immature/inactive synapses, which seems to be SAM domain/Zn^{2+}-dependent. Therefore, it is recruited to the PSD to a pre-formed scaffold *via* its PDZ domain [104,105,114]. In contrast, SHANK2 and SHANK3 seem to be essential elements for the proper organization of the PSD by their localization *via* the SAM domain, which can be enhanced by the activity and synaptic release of Zn^{2+} [115]. Interestingly, on the electrophysiological level, the knockdown of SHANK1 and SHANK2, but not SHANK3, showed a decrease in the AMPAR responses at CA3-to-CA1 synapses in acute hippocampal slice cultures [116], which further supports their functional divergence.

1.4 *SHANK2* mutations and neuropsychiatric disorders

Mutations in the human *SHANK* genes are associated with a wide range of severe neuropsychiatric disorders including ASD, ID, schizophrenia (SCZ) and mania [117], likely reflecting the importance of a correctly organized PSD. These mutations include copy-number variations (CNVs), microduplications of nucleotides, as well as nonsense, missense and

frameshift mutations. Semi-identical *SHANK* mutations were found in patients with very distinct behavioral outcomes. First, the *SHANK* genes were associated with neurodevelopmental disorders by the studies of the Phelan-McDermid Syndrome which is characterized by autistic-like behaviors [118]. In nearly all reported Phelan-McDermid Syndrome cases, a deletion of *SHANK3* was identified [119,120]. Thereafter, *SHANK3* mutations have also been identified in genetic screenings of patients with ASD [121,122] and SCZ [123]. CNV deletions encompassing the *SHANK1* gene have been shown to segregate only in male carriers with high-functioning autism [26]. One explanation for this correlation between the mutation and the degree of cognitive impairment has to do with the expression pattern of this particular mutated *SHANK* gene [124].

The *SHANK2* gene, also known as ProSAP1, is the largest gene among the *SHANK* gene family (450 kb long, 25 exons). Its mRNA is enriched in the cortex, thalamus, hippocampus (CA1, CA3 and dentate gyrus (DG)) and Purkinje cells [125]. *SHANK2* loss-of-function mutations are assumed to result in synaptic dysfunction and were first identified in patients with ASD and ID [4]. Several other studies have described further variations in the *SHANK2* gene loci in patients with ASD and ID, which solidifies the causal link of *SHANK2* variants to neuropsychiatric disorders [110,124,126-132] (for a review, see [133]). Interestingly, an association between *SHANK2* gene mutations and SCZ was first described in 2015 [134]. By sequencing the *SHANK2* gene in 481 SCZ patients and 659 unaffected individuals, Peykov *et al.* identified several non-synonymous variants exclusively in SCZ patients [134]. This association was confirmed by a study reporting seven siblings in a family with SCZ spectrum disorders carrying a missense variant in *SHANK2* [135] (for a review, see [133]).

1.5 Possible explanations for the divergent phenotypes in patients with *SHANK2* variants

One explanation for the wide range of neuropsychiatric disorders caused by *SHANK2* mutations could be the unreliability of clinical data due to imprecise clinical diagnoses. Another explanation might be the nature of the *SHANK2* variants which might lead to an increase or decrease in the SHANK2 protein expression, altered SHANK2 protein domains or truncated SHANK2 protein products lacking one or more interaction domains. This, in turn, can alter the protein-protein interactions and the organization of the postsynaptic protein network. Therefore, different *SHANK2* mutations could potentially lead to different alterations in molecular and

cellular processes in neurons, resulting in a range of behavioral phenotypes [133]. This perspective finds support in the rescue experiment of SHANK2 knockdown by the overexpression of three different human SHANK2A variants (R462X, T1127M, L1008_P1009dup) in rat primary cultures [136]. These variants showed distinct localization patterns different to that of the SHANK2A-WT overexpression one [136], indicating that they can lead to a decrease in the total final amount of SHANK2 present at the synapse. They may also have other effects, e.g. in the soma and dendrites, which could be another important factor in the pathophysiology of neuropsychiatric disorders [133]. Moreover, the overexpression of SHANK2 variants revealed different degrees of rescue of the reduced spine volume caused by the SHANK2 knockdown [136], which indicates different influences of different SHANK variants on the regulation of spine size.

Other genetic, epigenetic and environmental factors have also a strong impact on the expression of *SHANK2* variant-mediated neuropsychiatric disorders. For example, the same *SHANK2* variants were found in patients with different clinical features **(Table 1)**. Additionally, synonymous variants were detected in patients with ASD, ID and SCZ, but not in healthy controls [4,134,137]. The effects of other genes on the phenotypic expression of *SHANK2* variants became most obvious in patients with an inherited *SHANK2* variant-associated ASD or SCZ, which have not been diagnosed in their parents. For example, the SHANK2A577V variant was found in 7 SCZ male brothers and inherited from a healthy mother [135]. This was also the case for other SHANK2 variants identified in SCZ [134] and ASD [133] patients, suggesting that sexually dimorphic pathways have an effect on the penetrance of *SHANK2* variants. Additionally, epigenetic factors are suggested to affect *SHANK2* expression [133,138], which, as well, may lead to different penetrances of similar *SHANK2* variants.

Table 1: Identical *SHANK2* variants causing different clinical features in patients

Point mutation	Amino acid residue exchange	Number of patients	Diagnosis	Trans-mission source	References
c.1604A>G	p.K535R	2	1 ASD 1 ID	n.a.	Berkel et al., 2010
c.1730C>T	p.A577V	7	5 SCZ 1 Schizotypal personality 1 Schizoaffective	Mother	Homann et al., 2016
c.1759C>T	p.P587S	2	1 Autism 1 ID	Mother n.a.	Berkel et al., 2010
c.1829C>A	p.S610Y	2	1 Catatonic SCZ 1 ID with Autistic features	n.a Father	Peykov et al., 2015 Berkel et al., 2010
c.5191G>T	p.A1731S	4	3 Paranoid SCZ 1 Disorganized SCZ	Mother	Peykov et al., 2015

Five different single point mutations in the coding region of the human *SHANK2* gene leading to five amino acid residue exchanges were associated with different neuropsychiatric disorders. n.a= not available. The table and table legend are adapted from [133].

To fully understand the function of SHANK2 and the effects of *SHANK2* mutations on synaptic function, mouse lines of *Shank2* were generated and characterized on electrophysiological, molecular and behavioral levels. Analyzing genetically comparable male and female inbred mice is suggested to minimize the environmental factors, especially when mice are raised and housed under similar conditions. This should help to reveal the influence of *SHANK2* mutations solely on the synaptic function and the behavioral outcomes. However, the analysis of *SHANK2* mutations in mice finds a challenge by the set of the available behavioral experiments. In particular, since the establishment of psychiatric diagnoses in physiological diseases in humans (*e.g.* hallucinations, delusions, sadness and guilt) cannot be convincingly ascertained in mice. On the other hand, mice are still considered a first entry point to study mutations found in human patients and thus are important to establish useful genotype-cellular phenotype correlations. They have the advantages of the multiple ways for genetic manipulation, a short reproduction cycle and a high breeding capability together with the possibility of molecular, cellular, physiological and behavioral analysis of the genetically modified mice. Most of our knowledge of the influence of *SHANK2* mutations on the anatomy and physiology of the mammalian CNS was derived from genetically-modified mice, as model organisms for Shankopathies.

1.6 *Shank2* knock-out mouse models

1.6.1 Generation of *Shank2* knock-out mouse models

The SHANK2 protein isoforms are suggested to have different functions during different developmental stages in different brain regions [87]. Therefore, the detailed knowledge of different SHANK2 isoforms and their expression patterns in the mouse brain was a prerequisite for the generation of *Shank2* gene-targeted mice. According to the NCBI database, 21 putative isoforms are predicted to be expressed by the *Shank2* gene locus on chromosome 7 in mice [133]. The expression of three SHANK2 isoforms was confirmed in the rat brain [108,109,139]. SHANK2E is the full-length SHANK2 isoform which is generated by a 5' located promoter and contains a 5'-untranslated exon, designated as exon 1 [133]. SHANK2E contains ANK, SH3, PDZ, PRR and SAM domains **(Figure 2)** [106]. It is expressed at different levels in different brain regions with the highest expression in the cerebellum [110]. The SHANK2A isoform is expressed by a promoter located in intron 10, and its transcript translation occurs by an intron-located translational start codon which opens the translational reading frame [133]. It seems to be underrepresented in peripheral tissues and primarily expressed in the brain [110,140]. It contains SH3, PDZ, PRR and SAM domains **(Figure 2)**. The SHANK2B isoform (named as SHANK2C in [125], **Figure 2**) is generated by a promoter located in intron 14, and its transcript translation occurs by an intron-located translational start codon. SHANK2B contains just PDZ, PRR and SAM domains **(Figure 2)**. It showed differential expression in all brain regions in rat [140] and human [110]. Another SHANK2 isoform was obtained by an alternative splicing event of exon 22 in humans. However, it could not be detected in the transcriptome of mice or rats [87,110].

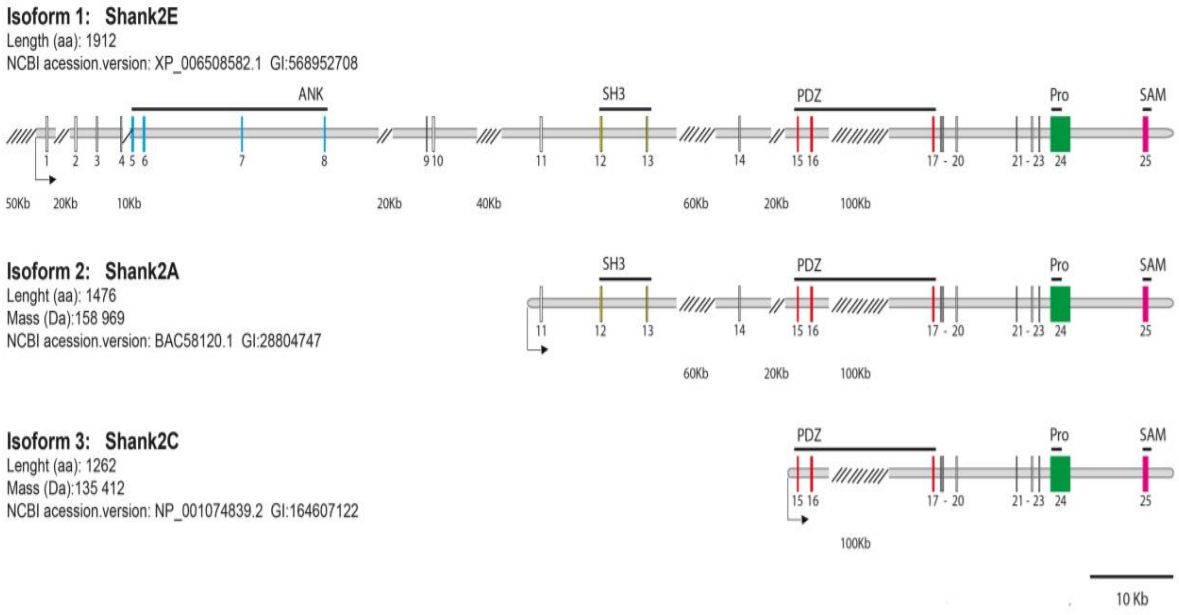

Figure 2: Schematic view of the full-length *Shank2* gene and the three transcripts produced by intragenic promoters
Shank2E is the full-length transcript and encodes for the SHANK2E isoform with 5 protein-protein interaction sites. The *Shank2A* transcript encodes for a brain-specific SHANK2A isoform which lacks the ANK domain. *Shank2C* encodes for a protein with 3 protein-protein interaction sites. Images are drawn to scale; each break symbol represents 10 Kb of intron sequence that has been deleted for simplification. The size of each total break deletion in Kb is indicated below each break. The image scale bar is 10 Kb. The figure and figure legend are adapted from [125].

Seven gene-targeted mouse lines of *Shank2* are listed in the mouse genome informatics (MGI) database **(Table 2)**. For most of these lines, the molecular, behavioral and physiological analyses have been published. The strategies for the published *Shank2* gene knock-out mouse models are schematically depicted (**Figure 3)**. Although these mouse lines were generated and characterized by the genetic deletion of *Shank2* exons encoding important protein domains, none of the gene-targeted events could confirm a complete knock-out of all putative SHANK2 isoforms [133].

Table 2: List of *Shank2* gene-targeted mouse lines in the MGI database

Shank2
Shank2$^{em1(IMPC)Rbrc}$
Shank2$^{em2(IMPC)Rbrc}$
Shank2$^{Gt(OST148685)Lex}$
Shank2$^{tm1.1Bcgen}$
Shank2^{tm1Tmb}
Shank2$^{tm1.1Tmb}$
Shank2^{tm1Mgle}

Seven genetically modified mouse lines encoding gene-targeted mutations of the endogenous *Shank2* were made public in the MGI database (http://www.informatics.jax.org). Mouse lines in blue are not published but commercially available. The table and the table legend are adapted from [133].

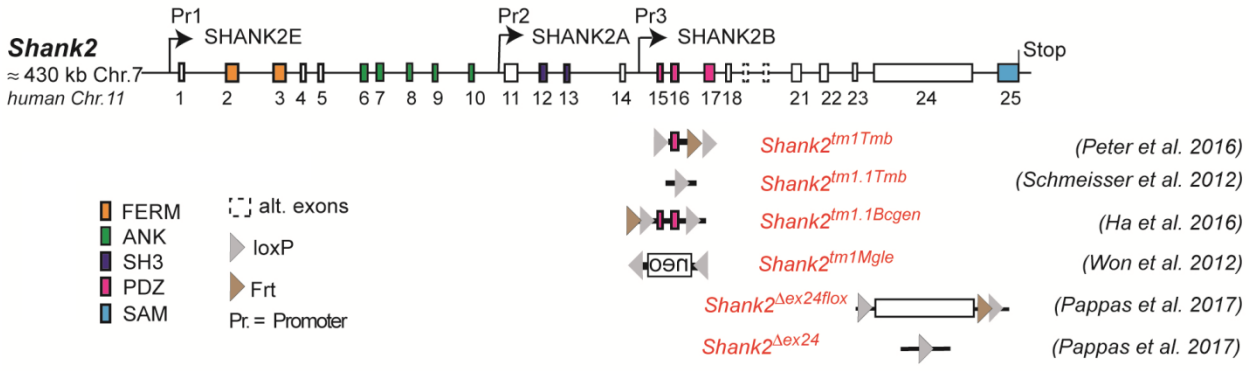

Figure 3: Gene structure and gene segment deletions in *Shank2* knock-out mouse models
The structure of the *Shank2* gene is depicted with exons given in rectangles and alternative spliced exons shown in dashed lines. The positions of promoters (Pr) for the expression of the different isoforms of the

Shank2 gene loci are indicated as well as those of the neomycin (neo) selection marker, loxP and Frt sites in the targeted alleles. Targeted gene segments flanked by two loxP elements can be removed or inverted by tissue-specific expression of Cre to generate conditional *Shank2* knock-out models. oen = neo selection marker, reverse orientation. References for the first publication of the mouse lines are given. The figure and figure legend are adapted from [133].

1.6.2 Characterization of *Shank2* knock-out mouse lines

As shown in **Figure 3**, the first two conventional *Shank2* knock-out mouse models (*Shank2*$^{-/-}$) were generated in 2012 and resembled two PDZ domain-encoding exons microdeletions found in two patients [4]. They were generated by replacing the exons 15-16-encoding gene segment by a loxP site flanked inverse-oriented neomycin resistance selection marker (*Shank2*$^{\Delta ex15\text{-}16}$) in one mouse model [141] and by deleting exon 16 (*Shank2*$^{\Delta ex16}$) in the other [142]. In 2017, a third conventional *Shank2* knock-out mouse model was generated by the out-of-frame deletion of *Shank2* exon 24 (*Shank2*$^{\Delta ex24}$) which removed the proline-rich region [143] **(Figure 3)**. Although both *Shank2*$^{\Delta ex15\text{-}16}$ and *Shank2*$^{\Delta ex16}$ mouse models displayed comparable ASD-like phenotypes with social impairment and repetitive behaviors **(Table 3)**, *Shank2*$^{\Delta ex24}$ mice exhibited bipolar-associated mania-like behaviors with hyperactivity and a decrease in the repetitive behavior, with no social preference in the social affiliation test as well as anhedonia-like behaviors and disturbed circadian rhythms **(Table 3)**. Moreover, the molecular, electrophysiological, synaptic composition and anatomical analyses revealed differences between the three *Shank2*$^{-/-}$ mouse lines despite their similar genetic background (C57Bl/6N and C57Bl/6J) **(Table 3).** By the direct comparison between *Shank2*$^{\Delta ex15\text{-}16}$ and *Shank2*$^{\Delta ex16}$ mouse models in a mixed C57Bl/6N x C57Bl/6J background, the differences in gene expression were correlated with the type of mutation as shown by the reduced expression of the GABA receptor gene, *Gabra2*, in *Shank2*$^{\Delta ex15\text{-}16}$, but not *Shank2*$^{\Delta ex16}$ mice [144]. Moreover, the inhibitory signaling, the AMPA/NMDA ratio and the long-term potentiation (LTP) analyses revealed significant differences between the two lines [144].

Table 3: Distinct endophenotypes in genetically very similar gene-manipulated, conventional *Shank2* knock-out mice (*Shank2*$^{-/-}$)

	Shank2$^{\Delta ex15\text{-}16}$	*Shank2*$^{\Delta ex16}$	*Shank2*$^{\Delta ex24}$
Body weight	Normal	Reduced	Normal
Spines morphology (hippocampus)	Spines density, number or length	Spines density and number	PSDs
Synaptic transmission	Basal synaptic transmission and mEPSC NMDA/AMPA ratio	Synaptic transmission, mEPSC amplitude and mEPSC frequency NMDA/AMPA ratio	n.a. NMDA/AMPA ratio
Synaptic plasticity (CA1)	LTP LTD	LTP LTD	n.a. n.a.
Hyperactivity	Yes	Yes	Yes
Anxiety	Yes	Yes	n.a.
Repetitive behavior	Jumping and upright scrabbling	Stereotypic behavior (self-grooming)	Self-grooming
Spatial learning	Spatial learning and memory in the Morris water maze	Spatial memory in the Morris water maze	Spatial learning in the Morris water maze
Social interact.	Social interaction	Social interaction	Social interaction
L838,417 treatment	Spatial memory deficit	Spatial memory deficit	n.a.
References	Won et al., 2012, Lim et al., 2017	Schmeisser et al., 2012, Lim et al., 2017	Pappas et al., 2017

The behavioral, electrophysiological, synaptic composition and anatomical analyses revealed differences between the three conventional *Shank2*$^{-/-}$ mouse lines despite their similar genetic background. n.a= not available, Green = no alteration; blue = decrease; red = increase. The table and table legend are adapted from [133].

Interestingly, a similar discrepancy between the phenotypic expression of *Shank2* ***Δex16***, ***Δex15-16*** gene and ***Δex24*** deletions was found when the three gene deletions were restricted to cerebellar Purkinje cells (PC) [143,145,146]. These mouse lines were generated by combining the floxed *Shank2* ***Δex16***, ***Δex15-16*** or ***Δex24*** gene segments, with transgenic Cre-expressing mouse lines that used the PC-specific Pcp2 promoter, also called L7 promoter, for PC-specific inactivation of the *Shank2* gene. *Shank2*$^{\Delta ex15\text{-}16\text{–}Pcp2\text{-}Cre}$ mice exhibited impaired motor

coordination and learning in the Erasmus ladder test, but normal motor performance in the rotarod test as well as normal social interaction without repetitive behavior and only mild anxiety. In contrast, *Shank2*$^{\Delta ex16–L7–Cre}$ mice exhibited normal motor performance in the Erasmus ladder with no anxiety, but deficits in social interaction. In contrast, *Shank2*$^{\Delta ex24\text{-}Pcp2\text{-}Cre}$ mice showed an impaired motor performance in the rotarod. Thus, similar inactivation of the *Shank2* gene in cerebellar Purkinje cells produced distinct phenotypes at the molecular and up to the behavioral levels. This finding in cell type-specific *Shank2* knock-out mice underlines the observation that very similar *SHANK2* mutations in human can lead to different phenotypes [133].

Similarly, in two recent mouse models restricting the ***Δex15-16*** deletion to two specific cell types: excitatory neurons (*Shank2*$^{\Delta ex15\text{-}16–CaMK2a\text{-}Cre}$) and GABAergic inhibitory neurons (*Shank2*$^{\Delta ex15\text{-}16–Viaat\text{-}Cre}$) [147], differences on the electrophysiological level were obvious as shown by the reduced mEPSC frequency in hippocampal CA1 neurons in *Shank2*$^{\Delta ex15\text{-}16–CaMK2a\text{-}Cre}$, but not in *Shank2*$^{\Delta ex15\text{-}16–Viaat\text{-}Cre}$ mice. On the behavioral level, *Shank2*$^{\Delta ex15\text{-}16–\ CaMK2a\text{-}Cre}$ mice exhibited increased anxiety but no repetitive behavior in contrast to *Shank2*$^{\Delta ex15\text{-}16–Viaat\text{-}Cre}$ mice that showed no anxiety but increased repetitive behavior.

The variability of the phenotype in the generated *Shank2* knock-out mouse models, despite similar genetic alterations, cannot be solely explained by the haploinsufficiency of SHANK2, but may rather indicate the presence of other protein isoforms or truncated versions that can manifest dominant-negative effects (**Figure 4**) [133]. This, in turn, might disrupt the structure and/or the flexibility of the SHANK and postsynaptic protein organization, leading to synaptic dysfunction. The impairment in synaptic function might vary in different neurons or even in different synapses of the same neuron, which may explain the divergent outcomes of the tested *Shank2* knock-out mice.

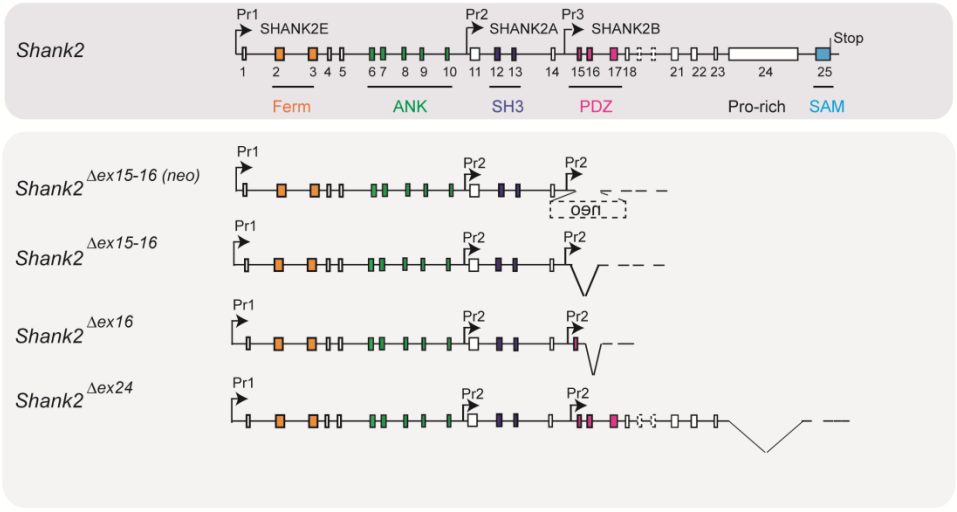

Figure 4: Putative pre-mRNA transcripts in homozygous *Shank2* knock-out mouse models
Schematic view of the *Shank2* gene and the putative pre-mRNA that can be expressed by the four different gene-targeted alleles of the *Shank2* mouse models with very distinct phenotypes. Symbols are the same as in **Figure 3**. The figure and figure legend are adapted from [133].

1.6.3 Limitations of the previous studies on *Shank2* knock-out mouse models

The gene-targeted conventional and conditional *Shank2* knock-out mouse models could not fully dissect the complex function of SHANK2. This complexity is also represented in the high similarity of SHANK2 to other SHANK proteins and by sharing evolutionarily conserved protein domains. Moreover, *SHANK2* generates several isoforms, some of which lack the conserved SHANK2 protein domains of the full-length isoform. Three of the SHANK2 isoforms were confirmed in mice; however, other putative isoforms may still be present and could play additional roles. The different isoforms of the SHANK2 protein are suggested to determine the different organization of the postsynaptic proteins at different developmental stages and/or in different brain regions [87]. The cellular and subcellular or activity-regulated expression of the SHANK2 isoforms in neurons have not been studied in detail yet.

The gene-targeted *Shank1*, *2* and *3* knock-out mouse models displayed recurrent features observed in animal models for ASD along with other neuropsychiatric-like phenotypes. However, whether these phenotypes are due to a complete loss of function of SHANKs or dominant negative effects by their truncated versions remains to be resolved. The different dominant negative effects exerted by the truncated SHANK versions may account for the distinct phenotype of genetically-similar mouse models. Until now, no mouse model with a compound loss of the three *Shank* members has been generated. Therefore, in the generated *Shank* knock-

out mouse models, other *Shank* members may compensate for the lack of some functions and might mask the functional analysis of the deleted *Shank2* gene or SHANK2 isoforms.

Although some behavioral phenotypes were rescued in adult *Shank2* knock-out mice using pharmacological approaches: *e.g.* social interaction using NMDAR agonist [141] and memory deficits using an allosteric modulator for the $GABA_A$ receptor ($GABA_AR$) [144], the reversibility of the phenotype *via* the genetic modification of *Shank2* and the rescue of the SHANK2 level was not analyzed. These mice could not provide any detailed insight into the dysfunction of the neuronal network communication nor the homeostasis impairments of the brain function. Also, the identities of the cell types contributing to the phenotypes in *Shank* knock-out mice and the exact molecular mechanisms have not been deciphered yet.

Another major issue with the previous *Shank2* knock-out mouse model studies was the comparison of the behavioral phenotypes determined in different laboratories [148]. Moreover, in most cases, the complete behavioral ethogram of *Shank2* knock-out mice was not performed: *e.g.* learning and memorizing fear in *Shank2* knock-out mice was not investigated. Multiple neuropsychiatric-like phenotypes can happen simultaneously and should only be addressed with a full behavioral ethogram.

Deletions or mutations in *Shank2* could affect the molecular structure and composition in various ways on different levels. Therefore, the generation of innovative animal models and an in-depth analysis of synaptic alterations are required to examine the multiple roles of *Shank2* mutations on multiple scales and to relate the synaptic defects to specific pathological behaviors. This goal can be achieved by combining proteomics to understand the synaptic protein composition, super-resolution imaging techniques to decipher the nanoscale organization of the synapse, as well as electrophysiology to link the synaptic structure and function.

1.7 Aim

Early brain development is strongly influenced by sex hormones which are suggested to play a role in the sex bias of ASD. However, the direct link between sex hormones and ASD remains unclear, and the effect of sex hormones on the expression of ASD risk genes has been poorly investigated. Therefore, the first aim of this thesis was to analyze whether the expression of *SHANK* genes is different in female and male embryos and pubs since it is known that sex hormone levels are very different between males and females during early development. The

analysis of *Shank* expression in mice lacking the androgen receptor in all neurons and the sensitivity of *SHANK* expression to sex hormone in a human cell line should clarify the direct effect of sex hormones on SHANK expression.

Due to the ethical limitations of studies with patients and the limitations of the previous *Shank2* knock-out mouse models, the second major aim of this thesis was to dissect the developmental and transient effects in Shankopathies associated with ASD in mice using another powerful technique. In a pilot study, rAAV-mediated overexpression of two isoforms, SHANK2A or SHANK2A(R462X) was performed in the forebrain of P0 mice. SHANK2(R462X) is a *de novo* nonsense mutation found in an ASD patient with a severe behavioral impairment and is suggested to lead to premature termination of *SHANK2* translation by producing a truncated protein [4]. Of note, the viral-mediated gene transfer led to a high variation and a strong mosaic expression of the transgene due to the variation in the virus injections. This made it hard to differentiate whether the number of neurons expressing the transgene or its expression level was crucial for the phenotype. Therefore, mouse models with well-defined SHANK2A and SHANK2A(R462X) were required to reveal whether the observed behavioral phenotypes in the viral-transduced mice could be recognized as a suitable experimental model for autistic disorder in humans. To this end, two transgenic mouse lines which allowed the spatiotemporal controlled overexpression of either SHANK2A or SHANK2A(R462X) in the glutamatergic neurons of the forebrain were generated in order to disturb the balanced and regulated expression of the endogenous SHANK2 protein. This can potentially disrupt the whole SHANK organization by shifting it into a scaffold structure which is mainly determined by the transgenically overexpressed SHANK2 isoform. By analyzing these mice on behavioral, electrophysiological and molecular levels, I aimed to identify signaling pathways affecting the SHANK-dependent organization of postsynaptic proteins. Moreover, I wanted to test whether the transient synaptic dysfunction of the glutamatergic system in the forebrain was sufficient for the behavioral impairment in ASD and reveal which behavioral phenotypes could be rescued in adulthood.

Chapter 2

Materials & Methods

2.1 Investigating the influence of sex hormones on *SHANK* expression

2.1.1 Animals

The mice used in this study were housed in the Interfacultary Biomedical Facility (IBF) at the Heidelberg University under a 12 hrs light-dark cycle and with *ad libitum* access to water and food. All procedures were conducted in strict compliance with the National Institutes of Health Guidelines for the Care and Use of Laboratory Animals and approved by the German Animal Welfare Act. Experiments on mice were performed according to the regulations of animal experimentation within Heidelberg University and the European Union (European Communities Council Directive 2010/63/EU (local license number: T-03/16, T-24/14)). CD1 (ICR) mice from Charles River were used for the sex-differential expression analyses in the cortex at two different developmental stages (E17.5 and P7.5) (n= 16 mice of each sex). The embryonic stage was calculated by vaginal plug check and by controlling the morphological parameters which accord to the respective Theiler stage. The day of birth was defined as postnatal day (P) 0.5. Neuron-specific androgen receptor knock-out mice (Ar^{NesCre}) were generated by crossing female homozygous floxed androgen receptor Ar^{flox} mice (*B6N.129-*$Ar^{tm1Verh}$*/Cnrm*) [149] with male Nestin-Cre deleter mice ($Tg^{(Nes\text{-}cre)1Kln}$; MGI:2176173) [150] hemizygous for the floxed *Ar* allele. Ar^{flox} mice were obtained from the European Mouse Mutant Archive (EMMA, #02579) and backcrossed into the C57Bl/6N background for over 12 generations prior to the arrival at the IBF as published previously [151].

2.1.2 Polymerase chain reaction (PCR) for genotyping

The genotyping of the mice was performed on tail biopsies and detected by PCR. Five mm of mouse tail were digested by adding 300 µl 10x PCR buffer (Qiagen, 203203) combined with proteinase K enzyme with a final concentration of 0.1 mg/ml. Samples were placed at 57°C shaking at 1000 rpm overnight. For tail PCR, 1 µl digested tail solution was amplified in a standard PCR reaction. For the sex genotyping of CD1 mice: Sry-F and Sry-R primers were used [cycling = 1 x 94°C 5 min, 35 x (94°C 50 sec, 65°C 45 sec, 72°C 30 sec), 1 x 72°C 5 min]. For the genotyping of Ar^{NesCre} mice for floxed androgen receptor: Flox-F and Flox-R primers were used [cycling = 1 x 95°C 5 min, 40 x (95°C 30 sec, 56°C 45 sec, 72°C 60 sec), 1 x 72°C 7 min]. For the genotyping of Ar^{NesCre} mice for Nestin-Cre: Cre-F and Cre-R primers were used [cycling = 1 x 95°C 5 min, 40 x (95°C 30 sec, 60°C 30 sec, 72°C 30 sec), 1 x 72°C 5 min].

The amplified gene fragments were separated and visualized *via* gel electrophoresis (2% agarose in 1x TAE buffer). The PCR primer sequences used for the genotyping of CD1 and Ar^{NesCre} mice are indicated in **Appendix 1**. For the TAE buffer recipe, refer to **Appendix 2**.

2.1.3 Cell culture

The human neuroblastoma cell line (SH-SY5Y) was obtained from the DSMZ (Leibniz Institute German collection of Microorganisms and Cell Cultures, no. ACC 209). Cells were seeded on 75 cm flasks in Dulbecco's modified Eagle medium (DMEM, Thermo Fisher Scientific), supplemented with 15% fetal calf serum, 1% non-essential amino acids and 1% Penicillin-streptomycin and incubated at 37°C in a humidified environment with 5% CO_2. Cells were split at 80-90% confluence and resuspended in phenol red-free DMEM (Thermo Fisher Scientific) containing 1% charcoal dextran-treated calf serum. 8 x 10^5 cells were plated per well on a 6 well cell culture plate and incubated at 37°C for 24 hrs. In each experiment, six replicates per condition were analyzed. Cells were treated either with 100 nM dihydrotestosterone (DHT) (dissolved in methanol) (Sigma-D-073-1ML), mock (100% methanol with the same dilution factor as DHT), 100 nM DHT combined with 1 µM flutamide (Sigma-F9397) or mock and flutamide together [152]. To investigate the effect of 17β-estradiol, cells were treated either with 100 nM 17β-estradiol dissolved in 100% ethanol (Sigma-E8875), mock (100% ethanol with the same dilution factor as 17β-estradiol), 100 nM 17β-estradiol combined with 100 nM MPP (1,3-*Bis(*4-hydroxyphenyl)-4-methyl-5-[4-(2-piperidinylethoxy)phenol]-1*H*-pyrazole

dihydrochloride) (Sigma-M7068), mock together with MPP, 100 nM 17β-estradiol plus 100 nM PHTPP (4-[2-Phenyl-5,7-*bis*(trifluoromethyl)pyrazolo[1,5-*a*]pyrimidin-3-yl]phenol) (Tocris-2662), mock plus PHTPP, 100 nM 17β-estradiol plus both MPP and PHTPP or mock plus both MPP and PHTPP [152]. Treatments of cells were followed by incubation at 37°C. Cells were harvested after 4 hrs of treatment for mRNA and 48 hrs for protein analyses.

2.1.4 Quantitative PCR (qPCR)

Total RNA from SH-SY5Y cells, CD1 and Ar^{NesCre} mouse cortices at E17.5 and P7.5 was extracted using TRIzol (Invitrogen) according to the manufacturer's instructions. Reverse transcription was performed using the SuperScript™ VILO™ cDNA Synthesis Kit (Invitrogen). qPCR was performed using the SensiFAST™ SYBR® Lo-ROX (Bioline) kit in the 7500 Fast Real-Time PCR System (Applied Biosystems). All samples from SH-SY5Y cells and CD1 mice were measured in technical triplicates, and their relative expression was assessed via the relative standard curve method by the normalization to the following reference: ribosomal *18S* RNA, glyceraldehyde 3-phosphate dehydrogenase (*GAPDH*) mRNA, heat shock protein family D (HSP60) member1 (*HSPD1*) mRNA, succinate dehydrogenase complex subunit A (*SDHA*) mRNA and hypoxanthine phosphoribosyltransferase 1 (*HPRT1*) mRNA. For the SH-SY5Y cell treatment with 17β-estradiol, only *18S*, *HSPD1* and *SDHA* were used as references, as *GAPDH* and *HPRT1* mRNA levels were reported to be influenced by estradiol [153]. The relative expression values for mock treatment and male CD1 mice were set to 1.

For Ar^{NesCre} mice and their littermate wild-type (WT) controls, Cre induced site-specific recombination was checked on the brain cortical cDNA at two developmental stages, E17.5 and P7.5, using a specific reverse primer residing in the floxed exon 2 of *Ar* gene in order to confirm the absence of *Ar* expression in Ar^{NesCre} mice due to exon 2 deletion. The relative expression was assessed via the relative standard curve method by normalization to ribosomal *18s* RNA, and the relative *Ar* expression values in WT mice were set to 1. The qPCR primer sequences for the oligonucleotides used are given in **Appendix 1**. The qPCR amplification protocol was [cycling = 1 x 94°C 2 min, 40 x (94°C 5 sec, 60°C 10 sec, 72°C 20 sec), 1 x 72°C 5 min].

2.1.5 Protein analysis

2.1.5.1 Immunofluorescent histology

SH-SY5Y cells were fixed using 4% paraformaldehyde (PFA) for 20 min at RT. Cells were then permeabilized with Day 1 buffer (1% BSA, 0.3% Triton X-100 in PBS), supplemented with 4% normal goat serum (NGS), for 1 hr. Immunofluorescence staining was carried out overnight using the primary antibodies, anti-androgen receptor (Abcam, ab74272, 1:100 dilution) and anti-estrogen receptor α (Abcam, ab661002, 1:100 dilution), in Day 1 buffer, supplemented with 1% NGS, at 4°C. In the next day, cells were washed three times with PBS in intervals of 10 min before applying the secondary antibodies, Alexa fluor 488 conjugated goat anti-rabbit or Alexa fluor 488 conjugated goat anti-mouse (Thermo Fisher Scientific, 1:1000 dilution), in Day 2 buffer (1:3 Day 1 buffer diluted with PBS). Cells were incubated with the secondary antibodies for 1 hr in the dark. Next, they were washed twice in PBS in intervals of 10 min followed by incubation with DAPI (1:5000 dilution) for 5 min. Cells were again washed twice with PBS in intervals of 10 min and covered by coverslips using Aqua Poly/Mount (Polysciences Cat. Nr. 18606) and allowed to dry overnight at 4°C in the dark. Images were taken using Leica DMI4000 B microscope and Leica application suite advanced fluorescence software.

2.1.5.2 Immunoblots

Protein extraction from SH-SY5Y cells and mouse cortices (using the Polytron PT1200E, Kinematica AG) was performed at 4°C using 1% RIPA buffer (diluted in PBS), supplemented with SIGMAFAST protease inhibitor (Sigma, S8820). The mixture was left for 20 min and then centrifuged at 13000 rpm at 4°C for another 20 min, and the supernatant was collected and measured for protein concentration with the BCA protein assay kit (Pierce). Western blot analysis was executed using the Odyssey Infrared Imaging System (LI-COR Biosciences). Around 20 μg of proteins were denatured in 5x SDS protein loading dye, boiled at 94°C for 3 min and separated on Novex WedgeWell 4-12% Tris-Glycine gels (Thermo Fisher Scientific) using a standard program at 130V and 35mA for 1.5 hr together with two size markers, the Page Ruler Prestained Protein ladder (10-180 kDa) and the Spectra Multicolor High Range Protein ladder (40-300 kDa) (Thermo Fisher Scientific). Wet transfer of proteins was performed for 2 hrs at 500V and 250mA onto PVDF membranes (Millipore). Blocking was performed in Odyssey® Blocking Buffer for 1 hr at room temperature. PVDF membranes were probed with mouse anti-pan-SHANK (1:500; Neuromab), mouse monoclonal β3-tubulin (1:20000; Promega-G7121),

anti-SHANK1 (Synaptic Systems, polyclonal rabbit purified antibody, 1:500 dilution), anti-SHANK2 (Synaptic Systems, polyclonal guinea pig antiserum, 1:500 dilution) and anti-SHANK3 (ab140030, Abcam, 1:1000 dilution) and incubated overnight at 4°C. IRDye 800CW donkey anti-mouse, IRDye 680LT donkey anti-guinea pig or IRDye 680RD donkey anti-rabbit (1:15000 dilution; LI-COR Biosciences) immuno-positive signals were quantified using the Image Studio Lite 3.1 software (LI-COR Biosciences). Shank protein expression was normalized to the amount of β3-tubulin and the values obtained for the male cortices were set to 1. Western blot solution recipes are listed in **Appendix 2**.

2.1.6 nCounter analysis

Total RNA from conditional Ar^{NesCre} mouse cortices was extracted with TRIzol (Invitrogen) according to the manufacturer's instructions. Gene expression profile was investigated at the nCounter Core Facility, Heidelberg University, using the nCounter Dx analysis system GEN1 (NanoString Technologies). A customized Elements codeset with 7 target genes (*Shank1*, *Shank2, Shank3, Mecp2, Psd95, Erα* and *Erβ*) as well as 4 reference genes (*Gapdh*, *Hspd1*, *Sdha* and *Hprt1*) was applied. The detailed workflow is described at https://www.nanostring.com/support/product-support/support-workflow. Background correction and normalization of data were performed using the nSolver Analysis Software 3.0 (NanoString Technologies). A positive control and reference gene normalization was performed according to the Gene expression analysis guideline from NanoString Technologies (https://www.nanostring.com/application/files/7715/1251/5220/Gene_Expression_Data_Analysis_Guidelines.pdf; accessed June 2018). All reference genes in the customized Elements codeset were found to be stable and were selected for normalization based on the geNorm method [154]. The unit of measurement is given in 'codeset counts', and the codeset counts of the WT mice were set to 100%. The designs of the probes are indicated in **Appendix 3**.

2.1.7 Statistical analysis

Data analysis was performed using IBM SPSS STATISTICS 21, Prism 6 software (GraphPad Software) and Microsoft Office Excel software. The two-way ANOVA statistical test was used for the comparison between hormone-treated and mock-treated SH-SY5Y cells, and the biological replicate was used as a covariate. To compare gene expression levels between male and female cortices, the two-way ANOVA statistical test was used assigning litters and sex as

influencing factors. According to Bonferroni correction for multiple testing, a *P*-value threshold of ≤ 0.01 was considered significant (n = 5 different tests). For the expression analysis of the conditional Ar^{NesCre} mouse model using nCounter and for the quantification of Shank proteins in male and female cortices of CD1 mice in the western blot experiments, unpaired two-tailed Student's t-test was used, with a *P*-value of ≤ 0.05 considered as nominal significant. All data are presented as mean values ± standard error of the mean (SEM).

2.2 Functional analysis of SHANK2A and SHANK2A(R462X) overexpression in the glutamatergic neurons in the mouse forebrain

2.2.1 Animals

The tTA responder transgenic mice were generated by the pronuclear injection of either SHANK2A or SHANK2A(R462X) constructs as described in the Master Thesis from Markus Hüser (2015, Hochschule Mannheim). The transgenic vectors contain a bidirectional tetracycline-responsive promoter element (Ptet-bi) which controls the expression of the lacZ gene on one side and a fusion transcript composed of green fluorescent protein variant (Venus), 2A self-cleaving peptide and either SHANK2A or SHANK2A(R462X) on the other side **(Figure 12)**. The responder transgenic mice were backcrossed with C57BL/6J mice for 5 generations, followed by mating with $Tg^{\alpha CaMKII\text{-}tTA}$ mice (activator mice) in a C57BL/6J background, which express the doxycycline-dependent transactivator (tTA) under the control of an 8.5 kb fragment of the αCaMKII promoter [155]. In turn, the $Tg^{SHANK2A/tTA}$ and $Tg^{SHANK2AR462X/tTA}$ double transgenic mice were generated **(Figure 12)**. The mouse lines expressing tTA in addition to either SHANK2A or SHANK2A(R462X), are referred throughout this thesis as either $Tg^{SHANK2A}$ or $Tg^{SHANK2AR462X}$, respectively. Littermate mice with a single transgene, either the activator or the responder transgene, were included in the control population along with the non-transgenic littermate controls to avoid any effect due to the insertion of the transgene. The mice were housed at the IBF of the Heidelberg University, under a 12-hrs light-dark cycle and given *ad libitum* access to water and food. The mice maintenance and procedures were performed according to the animal welfare guidelines of the Max Planck Society (Charles River). Transgenic animals were generated under the license number 35-9185.81/G-219/11 (Regierungspräsidium Karlsruhe). Killed mice were registered as (T28/1) at the IBF of the Heidelberg University. Behavioral analysis was performed at the INBC under the license number

35-9185.81/G-100/16. Within the last two years, a 50% death rate within the first month of life was noticed in $Tg^{SHANK2A}$ mice. This early postnatal lethality was facilitated either by the massive inbreeding of the line for five years or directly by the SHANK2A overexpression. The histological analysis of the 'survivors' showed no signs of cell loss or gliosis (data not shown), which is in favor of the inbreeding hypothesis.

To stop the transgene expression in $Tg^{SHANK2A}$ and $Tg^{SHANK2AR462X}$ adult mice, doxycycline hydrochloride (dox) (Sigma-Alderich, Deisenhofen, Germany) at a concentration of 2 g/l was dissolved in water, supplemented with 5% sucrose, and provided to adult mice in light-protected bottles. To switch on the transgene overexpression only after the prenatal and early postnatal stages, 50 mg/l dox were provided in water, supplemented with 5% sucrose, to pregnant mice until the day of delivery.

2.2.2 PCR for genotyping

The mice were genotyped by PCR of mouse tail genomic DNA with specific primers. Five mm of mouse tail was obtained and submerged in 300 µl of 50 mM NaOH. Samples were shaken at 850 rpm and 99°C for 2 hrs followed by a short session of mixing via vortex. Subsequently, 30 µl of 1 M Tris pH 8 were added to each tube, and the tubes were mixed again. Afterward, the samples were centrifuged for 10 min at 13000 rpm, and the supernatant containing the DNA was collected. Two PCR mixtures were prepared to identify the activator and the responder transgenes. The PCR amplification protocol was [cycling = 1 x 95°C 5 min, 40 x (94°C 20 sec, 55°C 30 sec, 72°C 50 sec), 1 x 72°C 5 min].

As the last step, the PCR samples were analyzed via gel electrophoresis (3% agarose in 1x E-buffer). The PCR primer sequences used for genotyping are indicated in **Appendix 1**, and the E-buffer recipe is listed in **Appendix 2**.

2.2.3 Behavioral assays

The behavioral analysis of adult mice (4-9 months) was performed under the license number 35-9185.81/G-100/16 at the Interdisciplinary Neurobehavioral Core (INBC) of the Heidelberg University. One week prior to the start of the behavioral experiments, the mice were single-housed in the animal room with a constant temperature (22°C) and free access to food and water. They were handled extensively (10 min per mouse per day) to get acquainted with the testing environment [156]. Behavioral studies were performed during the light phase between 9 a.m. and 6

p.m. except for the nesting and burrowing tests. All behavioral tasks were performed in a blind manner to the mice genotype. The behavioral studies were performed in the following order: SHIRPA, LABORAS, activity in the home cage, as well as the following tests: open field, dark-light box, burrowing, nesting, three-chamber social, novel object recognition, cliff avoidance reaction, puzzle box, neophobia, direct social interaction and fear conditioning. Before experiments and between different trials, all equipment was cleaned and wiped with 70% ethanol and allowed to evaporate completely. The automatic tracking of the mouse behavior was analyzed using the SYGNIS tracking software.

2.2.3.1 SHIRPA

SHIRPA (SmithKline Beecham, Harwell, Imperial College School of Medicine, Royal London Hospital, Phenotype Assessment) provided a behavioral and functional profile by observational assessment of mice [157]. First, the body weight of the mouse was measured. Then, the mouse was placed in a new transparent arena for 30 sec. Body position, spontaneous activity, tremor, twitches, defecation and urination were observed and scored. Next, the mouse was suspended via its tail and transferred from the arena to a horizontal wire-grid. While descending toward the grid, the mouse was evaluated and scored for visual placement. Once the mouse was on all four limbs on the grid, it was evaluated for body tone, pinna reflex, corneal reflex, withdrawal reflex after toe pinch and crossed extensor reflex of the hindlimbs. Subsequently, from a standing position, the mouse was held by tail suspension for 15 sec. While in mid-air, it was assessed for hindlimbs splay, trunk-curl and limb-grasp. After being suspended, the mouse was lowered again via its tail towards the horizontal wire-grid. Once the mouse had grasped the wire with only its forelimbs, it was rotated horizontally by the tail. The ability of the mouse to maneuver and to negotiate its position in the horizontal wire platform was scored, based on the hindlimbs response. Afterward, the mouse was placed on a vertical wire-grid with its head upward, then downward, and evaluated and scored for catalepsy and negative geotaxis, respectively.

2.2.3.2 LABORAS

LABORAS (Laboratory animal behavior observation registration and analysis system) is an advanced and non-invasive system that automatically recognizes several different behaviors of mice by analysis of the forces that are induced by their movement [158]. Each tested mouse was

caged individually on the system for 24 hrs to detect the duration and the frequency of locomotion, immobility, climbing, rearing, self-grooming, drinking and eating.

2.2.3.3 Activity in the home cage

Repetitive behaviors of mice in their home cage with fresh bedding were assessed during 6 min. These repetitive behaviors include jumping, defined as the behavior of a mouse when it rears on its hind legs in the corner of the cage and jumps, so that one or both hind legs come off the ground; self-grooming, defined as stroking or scratching of the face, head, body or tail with the both forelimbs, or licking of their body parts, whereas digging behavior is defined as the behavior of a mouse, who is coordinately using two forelegs or hindlegs to dig out or displace bedding materials.

2.2.3.4 Open field test

The mouse was placed in a corner of a white acryl open-field box (40×40×40 cm) and allowed to explore the arena freely for 10 min, while its path was monitored and tracked using a video camera placed 1 m above the center of the arena. Automatic detection of the mouse's traveled distance and the time spent in the central zone (15 cm apart from the walls) was recorded.

2.2.3.5 Dark-light box test

The dark-light box is an open white rectangle (30 x 20 x 20 cm), attached to a 3 x 3 cm opening to a dark chamber (with a lid and painted black) (15 x 20 x 20 cm). The light chamber was illuminated at 600 lux. Each mouse was put in the dark chamber, and the latency as well as the number of visits to the light chamber within 10 min were measured. Only when all four limbs of the subject crossed the entrance, it was considered as an entry to the light chamber.

2.2.3.6 Burrowing test

The burrowing test is based on the mouse's behavior regarding the displacement of items from the tube within their home cage [159,160]. The tube was filled with 200 g of food pellets covered with 60 g of bedding. The test was performed at 5 p.m. and the pellets remaining in the tube was weighted after 2 hrs, then put back again on the tube. After 12 hrs, the weight of the remaining pellets in the tube was assessed again.

2.2.3.7 Nesting test

The mouse was placed in a new home cage with a cotton nesting material at 5 p.m. The nest that was then built was checked the next day at 7 a.m., and its quality was assessed with a complexity score from 1 (no nest) to 5 (complex nest with a wall surrounding the mouse) [160,161].

2.2.3.8 Three-chamber social test

The test was performed as described previously [162-165], only with modifications. A social interaction box (Harvard Apparatus) divided into 3 compartments was used. The social arena was made of a transparent box (42 x 60 cm) with two transparent sliding doors that divided the left, right and center chambers (42 x 20 cm). In the first 5 min session, the tested mouse was placed in the central chamber with the sliding doors open to offer access to the two chambers for habituation. In the second session, an empty cylindrical cage and another cylindrical cage housing an unfamiliar C57BL/6J mouse of the same sex and age as the tested mouse were located in the corners of the left and right chambers. The tested mouse was placed in the central chamber and allowed to explore the arena for 5 min. Once this session was completed, another unfamiliar C57BL/6J mouse (novel mouse) with the same sex and age as the tested mouse was put in the empty cylindrical cage. The tested mouse was then allowed to explore the arena for 5 min. In the fourth session, the mouse in the cylindrical cage from session two was replaced by unfamiliar C57BL/6J mouse of the opposite sex, and the tested mouse was then allowed to explore the arena for 5 min. The location of the cages was alternated between tests. The number of observed contacts of the tested mice with the cages was manually counted.

2.2.3.9 Novel object recognition test

Each mouse was placed in the corner of a new arena measuring (40 x 40 x 40 cm) and allowed to run around freely for 5 min. Afterward, the mouse was returned to its home cage for 1 min and introduced again to the arena with an object (cube) fixed in the center for another 5 min. The number of observed contacts with the object was counted manually.

2.2.3.10 Balance test

The apparatus was composed of 7 rods with diameters of 6, 8, 12, 15, 20, 25 and 32 mm, a length of 50 cm and a height of 20 cm. The tested mouse was put on each rod for 10 sec starting from the widest to the narrowest. The score was calculated by the number of rods from which the tested mouse did not fall. The test was performed twice for each mouse with a 1 hr interval.

2.2.3.11 Cliff avoidance reaction test

The cliff avoidance reaction was assessed using a round wooden platform (diameter 20 cm; thickness 2 cm), supported by an iron rod (height 50 cm) [166]. The floor below the platform was carpeted to prevent injuries of fallen mice. The test was initiated by gently placing a mouse on a platform such that the forelimbs would approach the edge. The latency from the initial placement on the platform until the fall was recorded. The test was performed for 1 hr.

2.2.3.12 Puzzle box test

The test was slightly modified from the one described in Berkel et. al., 2012 [136]. The puzzle box consisted of two compartments (a brightly-lit start zone and a smaller covered goal zone) separated by a barrier which had a narrow underpass (about 4 cm wide). Each mouse was introduced into the start zone, and the task was to enter the goal zone with bedding from its home cage. The mice underwent a total of 11 trials over 4 consecutive days, with three trials per day on the first three days, and two trials on the last day. On the first day, during trial 1, the underpass was left open, and the barrier had an open door above the underpass. During trials 2 and 3, the barrier had no doorway and the mice were supposed to enter the goal zone via the small underpass. On the second day, trial 4 was identical to trials 2 and 3. During trials 5 and 6, however, the underpass was filled with sawdust and they had to dig through the sawdust. On the third day, trial 7 was identical to trials 5 and 6. During trials 8 and 9, the mice were presented with the underpass which was blocked by a cardboard plug that mice had to pull with teeth and paws to enter the goal zone. Trial 10 on the fourth day was again carried out to repeat trial 9. At the end of the test, during trial 11, the task was to repeat trial 1 on the first day. After each trial, the mice were left for 1 min inside the goal zone.

2.2.3.13 Neophobia test

Each subject was placed in an arena with an unfamiliar drink (100 μl sweetened condensed milk) in the center. The mouse was allowed to explore the arena freely for 10 min, and the latency as well as the number of contacts with the drink were manually assessed.

2.2.2.14 Direct social interaction

Each mouse was placed in a white acrylic open-field box (40×40×40 cm) for 1 min before a same-sex, similar-age, unfamiliar C57BL/6J mouse was added to the arena. The number of

contacts made by the tested mouse with the unfamiliar mouse was counted manually within 5 min.

2.2.3.15 Fear conditioning test

On the first day, the acquisition session started by putting each mouse in an arena and spending 180 sec as a habituation phase. Then, an auditory tone was presented for 30 sec at a level of 90 dB and frequency of 5000 Hz with a rise time of 50 msec. A mild foot shock (0.5 mA) was administered during the last 2 sec of the tone presentation and co-terminated with the tone. After the shock presentation, an intertrial interval of 90 sec preceded the second and third identical trials. Following the third shock presentation, the mouse was kept in the arena for an additional 90 sec. On the second day, the contextual testing was conducted, similarly to the training session including lighting and odor, but without the tone and the foot shock. The experiments lasted for 300 sec. On the third day, the cued memory was tested by placing the mouse in a new chamber with a different odor and lighting condition and allowing it to habituate for 180 sec. The same intensity tone cue used in the acquisition session was then activated for the next 30 sec. Then, an intertrial interval of 90 sec preceded the second and third trials. The third tone was activated for 300 sec until the end of the experiment. The video freeze software was used to record and measure the freezing percentage and frequency.

2.2.4 Protein analysis

2.2.4.1 Staining methods

2.2.4.1.1 Mouse brain dissection and slicing

The mouse was first anesthetized with Isofluran (CP-Pharma). The abdominal wall and the thorax of the mouse were cut carefully not to injure the liver. Once the still beating heart was exposed, a hollow needle connected to two syringes, one with PBS solution and the other with 4% PFA, was pierced in the left ventricle. First, the blood was washed out with PBS until the liver completely lost its red color. Then, PFA was channeled through the mouse as described for PBS. To access the brain, the mouse head was detached from the body, the skin and skull were cut open in a sagittal section, and the olfactory bulbs were removed from the bone structures. The brain was then detached from the skull and further preserved in 4% PFA for 2 hrs as a post-fixation process. The brain was then embedded in 2% agarose in PBS and sliced into 100 µm-thick coronal or sagittal slices using the microtome VT 1000 S by Leica Microsystems (serial

number 0804/12.2006). Once the hippocampus was showing, the slices were collected separately, one in each well of 24-well plates filled with cold PBS.

2.2.4.1.2 Eosin/X-gal staining

The enzymatic activity of β-galactosidase was assessed by Eosin/X-gal staining following a standard protocol of Aguzzi and Theuring [167], with modifications. First, the brain slices were washed in PBS for 20 min and incubated in LacZ solution (0.5 M $K_4Fe(CN)_6$, 0.5 M $K_3Fe(CN)_6$, 0.2 M $MgCl_2$, X-gal 20 mg/ml in PBS) for 2 hrs at 37°C. The slices were then washed three times with 1x PBS with intervals of 10 min and shortly in 10 mM TRIS (pH 7.6) before being mounted onto glass slides. After an overnight dry session at RT, 0.5% Eosin solution was used as a counterstain, and the slides were shortly washed in demineralized water, 70% EtOH, 80% EtOH and 100% EtOH, respectively. After drying, the slides were washed in Xylol, and one drop of Eukitt was put onto each slice. As the last step, the coverslip was placed onto the slide and allowed to air dry at RT overnight for polymerization.

2.2.4.1.3 Immunohistochemical analysis

2.2.4.1.3.1 Immunofluorescence staining

The brain slices were permeabilized for 1 hr using 2% NGS in Day1 buffer (1% BSA and 0.3% Triton X-100 in PBS). Then, they were stained overnight with primary antibodies (anti-rabbit GFP, Abcam, 1:1000 dilution) or anti-parvalbumin (mouse, Sigma-Aldrich, 035M4879V, 1:1000). On the following day, the brain slices were washed three times in Day 2 buffer (1:3 Day 1 buffer diluted with PBS) with intervals of 10 min and incubated with secondary antibodies (Cy™3-conjugated AffiniPure Goat Anti-Mouse IgG, 115-165-003, 1:300 in Day 2 Buffer), anti-rabbit (Cy™3-conjugated AffiniPure Goat Anti-Rabbit IgG, 111-165-144, 1:300 in Day 2 buffer) and anti-rabbit (FITC (Abcam) 1:200 in Day 2 buffer) for 2 hrs in the dark while shaking. The slices were again washed three times with intervals of 10 min in Day 2 buffer and mounted onto glass slides using Aqua Poly/Mount (Polysciences Cat. Nr. 18606).

2.2.4.1.3.2 DAB staining

The immunostaining of the brain slices was performed following the peroxidase immunolabeling standard protocol. Endogenous peroxidase activity was blocked with 0.5% H_2O_2 in PBS for 10 min at RT. The slices were then washed twice in PBS with intervals of 10 min, and the

unspecific protein binding was blocked using 2% NGS in Day 1 buffer (1% BSA and 0.3% TritonX-100 in PBS) for 1 hr. Afterward, the slices were incubated overnight with the primary antibody (anti-mouse β-galactosidase (1:10000, Promega Z3783)) diluted in Day 1 buffer. On the following day, the slices were washed with Day 2 buffer (1:3 Day 1 buffer diluted with PBS) twice with intervals of 10 min and then incubated with a peroxidase-labeled secondary antibody (anti-mouse HRP, Vector Laboratories, 1:600) diluted in Day 2 buffer for 1 hr. Afterward, the brain slices were washed twice with PBS for 10 min and incubated with freshly prepared and filtered Diaminobenzidine solution (DAB: 20 mg/50 ml 20 mM Tris pH 7.6 and 12.5 µl 30% H_2O_2). DAB staining was stopped by washing slices with PBS three times and once in Tris pH 7.6 for 10 min and mounted onto the glass slides. Dry slides were then shortly dunked in Xylol for 2 min. Lastly, Eukitt was put onto each slice and the coverslips were placed.

2.2.4.1.4 Imaging

Slices from Eosin/X-gal, DAB and immunofluorescence staining were imaged with Zeiss Axioimager M1 epi-fluorescence and bright-field microscope with the software AxioVision version 4.6. Image quantification and editing were done with ImageJ and Adobe Photoshop CC.

2.2.4.2 Immunoblots

All steps for total protein lysate preparation from different brain tissues were performed at 4°C. Cortex, hippocampus, olfactory bulb and cerebellum of the mouse brain were collected and homogenized in ice-cold buffer (25 mM HEPES, pH 7.4) containing a protease inhibitor cocktail (Complete, Roche, Pharma AG). After 5 min of centrifugation at 2000 rpm, the supernatant containing the total amount of proteins was collected. Fractions were aliquoted, frozen in liquid N_2 and stored at -80°C for further analysis. Protein concentration was determined with the BCA protein assay kit (Pierce). Then, 5 mg of protein were separated by SDS–PAGE (8-12% separating and 4% stacking gels) and transferred to nitrocellulose membranes (Amersham™, Sigma). Membranes were probed with monoclonal anti-GFP (1:10000, Abcam), monoclonal anti-Shank2 (1:1000, Neuromab, 75-088), monoclonal mouse anti-β-galactosidase (1:20000, Promega Z3783) monoclonal anti-β3-tubulin (1:20000, Promega-G7121), anti-5-HT2A (1:500, Abcam, ab66049), anti-$GABA_AR$ (1:10000, Abcam, ab33299), anti-mGluR1 (1:200, Thermofischer, PA1-4516), anti-mGluR5 (1:1000, Millipore „Merck“, MABN540), anti-OXTR (1:1000, Abcam, ab181077), anti-GluN2A (1:1000, Millopore „Merck“, 07-632), anti-GluN2B

(1:1000, Novus Biological, NB300-106), anti-GluA1 (1:1000, Chemicon international, LV1368418), anti-GluA2 (1:1000, Chemicon international, LV1350412), anti-GluA3 (1:1000, Abcam, ab40845), anti-GluN1 (1:1000, Millipore „Merck“, AB9864R), anti-Psd95 (1:1000, Millipore „Merck“, LV1824016), anti-Homer1 (1:1000, Synaptic Systems, 160011), anti-VGlut1 (1:1000, Neuromab, 75-066) and anti-D2 (1:1000, Abcam, ab130295). The secondary antibodies (anti-rabbit IgG (1:10000)) and (anti-mouse IgG (1:10000)), conjugated with horseradish peroxidase, were used. Chemiluminescence was developed using a detection reagent (GE Healthcare, Amersham^{TM}, ECLTM Prime Western Blotting Detection Regent, RPN2232) and scanned with the Fujifilm LAS-3000 Luminescent Image Analyzer (Object No.: B00000623). The Image Reader LAS-3000 software was used and the protein bands were quantified using ImageJ software. Western blot solution recipes are indicated in **Appendix 2**.

2.2.5 nCounter analysis

Total RNA from mice hippocampi was extracted with TRIzol (Invitrogen) according to the manufacturer's instructions. Gene expression profile was investigated at the nCounter Core Facility Heidelberg using the nCounter Dx analysis system GEN1 (NanoString Technologies). A customized elements codeset with 21 target and 6 reference genes was applied. The detailed workflow is described at https://www.nanostring.com/support/product-support/supportworkflow. Background correction and normalization of data were performed using the nSolver Analysis Software 3.0 (NanoString Technologies). A positive control and reference gene normalization was performed according to the Gene expression analysis guideline from NanoString Technologies (https://www.nanostring.com/application/files/7715/1251/5220/Gene_Expression_Data_Analysis_Guidelines.pdf; accessed June 2018). The most stable expressed genes *Gapdh*, *Sdha*, *Hprt1*, Glucose phosphate isomerase 1 (*Gpi1*), *Hspd1* and phosphoglycerate kinase 1 (*Pgk1*) were selected for normalization based on the geNorm method [154]. The unit of measurement is ‘‘codeset counts’’, and the codeset counts of the control mice were set to 1. The designs of the used probes are indicated in **Appendix 3**.

2.2.6 Electrophysiological analysis

The electrophysiological analysis was performed in collaboration with Dr. Andrey Rozov from the Institute of physiology and pathophysiology at the Heidelberg University. Transverse

hippocampal 300 μm-slices were prepared from the brains of $Tg^{SHANK2A}$, $Tg^{SHANK2AR462X}$ and control mice at the age of 4-7 weeks, killed by cervical dislocation. The slicing chamber contained an oxygenated ice-cold solution (modified from [168] and composed of (in mM): K-Gluconate, 140; N-(2-hydroxyethyl) piperazine-*N*′-ethanesulfonic acid (HEPES), 10; Na-Gluconate, 15; ethylene glycol-bis (2-aminoethyl)-*N,N,N′,N*′-tetraacetic acid (EGTA), 0.2; and NaCl, 4 (pH 7.2). Slices were incubated for 30 min at 35°C before being stored at RT in artificial cerebrospinal fluid (ACSF) containing (in mM): NaCl, 125; $NaHCO_3$, 25; KCl, 2.5; NaH_2PO_4, 1.25; $MgCl_2$, 1; $CaCl_2$, 2; and D-glucose, 25; bubbled with 95% O_2 and 5% CO_2. During experiments, brain slices were continuously perfused with the same ACSF. Patch electrodes were pulled from hard borosilicate capillary glass (Sutter Instruments flaming/brown micropipette puller). Electrodes for the postsynaptic pyramidal cells were filled with a solution which consisted of (in mM): Cs-gluconate, 100; CsCl, 40; HEPES, 10; NaCl, 8; MgATP, 4; MgGTP, 0.3; phosphocreatine, 10 (pH 7.3 with CsOH). The solution for the presynaptic interneurons consisted of (in mM): K-gluconate, 100; KCl, 40; HEPES, 10; NaCl, 8; MgATP, 4; MgGTP, 0.3; phosphocreatine, 10 (pH 7.3 with KOH).

CA1 pyramidal cells were visually identified using IR-video microscopy. Whole-cell recordings from these neurons were taken at RT in voltage-clamp mode using a HEKA EPC-7 amplifier (List Elektronik) with a sampling rate of 100 μsec and filtered at 3 kHz. Excitatory postsynaptic currents (EPSCs) were evoked from two independent inputs, basal and apical dendrites, with two patch pipettes as stimulating electrodes located in stratum oriens and stratum radiatum, respectively. The two stimulus pipettes were > 200 μm apart, located below and above the soma of a CA1 pyramidal cell. All measurements were performed at -70mV membrane potential.

The AMPA/NMDA current ratios were measured in Mg^{2+}-free ACSF. AMPA and NMDA receptor-mediated EPSCs were pharmacologically isolated by sequential bath application of APV and NBQX (Sigma Alderich), respectively. First, the compound AMPAR and NMDAR-mediated current was recorded in Mg^{2+}-free ASCF. After collecting at least 100 sweeps, the AMPA-mediated component was blocked by the application of 10 μM NBQX. Then, additional 100 sweeps of the putative NMDA-mediated currents were collected and the NMDA nature was confirmed by a subsequent application of APV. The AMPA-mediated component was then obtained by subtracting the averaged NMDA-mediated currents from the averaged compound

responses. For subsequent analysis, the mean amplitude of the AMPA currents was normalized to the level of the amplitude of the NMDA EPSCs.

In the LTP experiments, the control pathway was measured by stimulating synapses of the basal dendrites when the apical dendrite input was potentiated and vice versa: the input in the stratum radiatum was used as a control pathway when the paired pathway was input to synapses of the basal dendrites. LTP was evoked and recorded according to Chen et. al., 1999 [169] by voltage clamping the membrane potential of the postsynaptic pyramidal cell to 0 mV for 3 min while stimulating the paired pathway every 1.5 sec. The measured amplitudes were normalized to the mean EPSCs before pairing. The NMDA dependence was tested in the presence of 100 µMD-AP5.

2.2.7 Proteomic analysis

Large-scale proteomic analysis of synaptosome was performed in collaboration with Prof. A.B. Smit in the Center for Neurogenomics and Cognitive Research at VU University Amsterdam. Synaptic plasma membrane preparations from the hippocampus of $Tg^{SHANK2A}$, $Tg^{SHANK2AR462X}$ and control mice were produced according to the protocol described in [170,171]. The crude synaptosomal fraction was analyzed using the SWATH technology as a data independent method of mass spectrometry for protein identification and quantification, which enabled the analysis of synaptic proteins with high sensitivity without the need of prior isotopic labeling. For the identification of affected pathways in $Tg^{SHANK2A}$ and $Tg^{SHANK2AR462X}$ mice, pathway and gene ontology analyses of the differentially abundant proteins in the synaptosomes were investigated using the online software ConsensusPathDB.

2.2.8 Statistical analysis

For the behavioral analysis, the two-way ANOVA test was used to compare the transgenic and control mice, assigning sex and genotype as influencing factors. For nCounter and protein quantification, the unpaired two-tailed student's t-test was used. Data were analyzed using Prism6 software (GraphPad Software). All data are shown as mean ± SEM. For the electrophysiological analysis, the paired two-tailed student's t-test was used to compare the responses from the paired *vs.* unpaired input. Data between genotypes were compared by unpaired two-tailed student's t-test and given as means ± SD. For the synaptosome analysis, the differential abundance analysis between genotypes was performed on log-transformed protein

abundances. Empirical Bayes moderated t-statistics with multiple testing corrections by False Discovery Rate (FDR) was used, as implemented by the eBayes and topTable functions from the limma R package.

Chapter 3

Results

3.1 Investigating the influence of sex hormones on *SHANK* expression

3.1.1 Effect of DHT and 17β-estradiol on *SHANK* expression

To test if sex hormones have an effect on *SHANK* gene expression, a human neuroblastoma cell model (SH-SY5Y) was employed. This cell model has the advantage of expressing all three SHANKs, as well as the androgen, estrogen α and β receptors (AR, ERα and ERβ) [66,172-175]. First, the expression of AR and ERα in SH-SY5Y cells was confirmed by immunofluorescence staining **(Figure 5)**. After stimulation with DHT for 2 hrs, the overall expression of AR increased in the cells. The stimulation of SH-SY5Y cells with 17β-estradiol for 2 hrs did not affect the expression level of ERα, but more protein was found to be localized in the nucleus **(Figure 5)** [152].

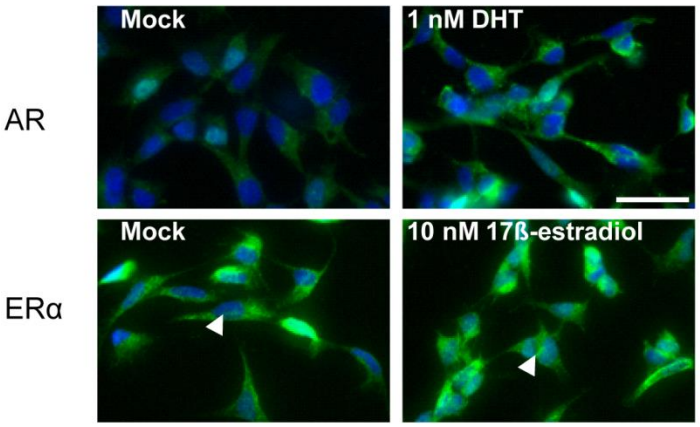

Figure 5: AR and ERα expression in SH-SY5Y cells
Immunofluorescence staining showing the expression of AR and ERα in SH-SY5Y cells after 1 nM DHT and 10 nM 17β-estradiol treatment, respectively. The expression of AR was increased after the DHT treatment. The expression of ERα was more localized in the nucleus after the 17β-estradiol treatment without an increase in the overall expression. DHT and 17β-estradiol treatments in SH-SY5Y cells were done for 2 hrs. Scale bar = 50 μm. The figure and figure legend were adapted from [152].

After the confirmation of AR and ER expression in SH-SY5Y cells and their response to DHT and 17β-estradiol, respectively, the regulatory influence of these sex hormones on *SHANK* gene expression was tested. Initially, SH-SY5Y cells were treated with two different concentrations of DHT, and the expression of *SHANK* was checked by qPCR and normalized against *18S*. For this analysis, *PSD95* was used as a positive control gene because its expression was found to be regulated by sex hormones [176-178]. As DHT concentrations between 1 and 100 nM are within the physiological range and have been used in similar studies [66,174], 1 nM and 10 nM DHT treatments of SH-SY5Y cells for 4 hrs was initially performed and revealed a trend of increased expression of all *SHANK* and *PSD95* genes without reaching statistical significance **(Figure 6)** [152].

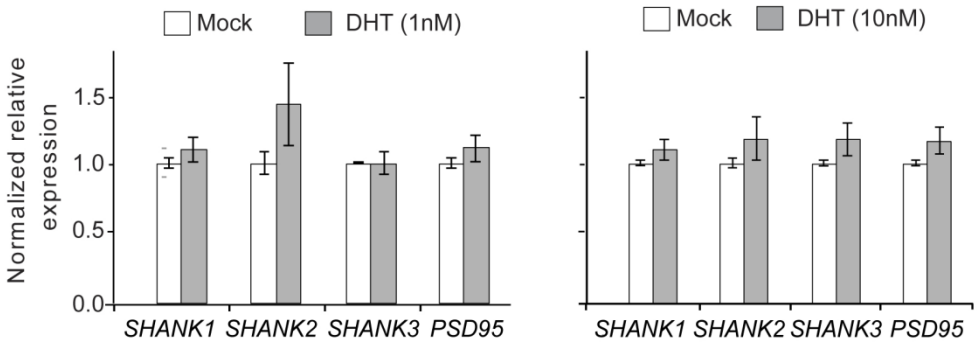

Figure 6: Effect of DHT treatment on *SHANK* expression in SH-SY5Y cells
Gene expression analysis of *SHANK1-3* after 4 hrs of treatment with 1 nM DHT (n = 3) and 10 nM DHT (n = 4) revealed a non-significant increase of their expression. *PSD95* was used as a positive control. Gene expression was normalized against *18S*. Error bars indicate standard error of the mean (SEM). The figure and figure legend were adapted from [152].

The effect of 100 nM DHT on *SHANK* gene expression in SH-SY5Y cells was then investigated and showed a strong increase of all three *SHANKs* and *PSD95* expression after 4 hrs of treatment (about 35% upregulation, *P*-values ≤ 0.001) **(Figure 7A)** [152]. *MECP2*, which shows a transient sex-specific expression difference in the developing rat brain [179], was included as an additional marker in the expression analysis, and its expression level was not influenced by the DHT treatment **(Figure 7A)**. Gene expression was normalized to five androgen independent reference

RNAs: the ribosomal *18S* RNA, the mRNAs for *GAPDH*, *HSPD1*, *SDHA* and *HPRT1*. The androgen independence of the reference genes was shown by their similar expression levels in DHT and mock-treated SH-SY5Y cells after normalization to *18S* **(Table 4)** [152].

The regulatory effect of DHT on *SHANK* gene expression on RNA level was confirmed by an increased SHANK immunosignal in western blots by 50%, using a pan anti-SHANK antibody after the treatment of SH-SY5Y cells with 100 nM DHT for 48 hrs **(Figure 7B)** [152]. To test whether the effect of DHT treatment on SHANK expression is mediated by the stimulation of the androgen receptor, SH-SY5Y cells were treated with 100 nM DHT for 4 hrs combined with 1 µM of the anti-androgen flutamide. The regulatory effect of DHT on *SHANK* and *PSD95* mRNA levels was completely abolished **(Figure 7A)**. Moreover, the regulatory effect of DHT on all SHANK proteins was absent in the presence of flutamide as shown with a pan-Shank antibody **(Figure 7B)**. These results demonstrate the role of AR modulation by DHT treatment on the increased *SHANK* and *PSD95* levels [152].

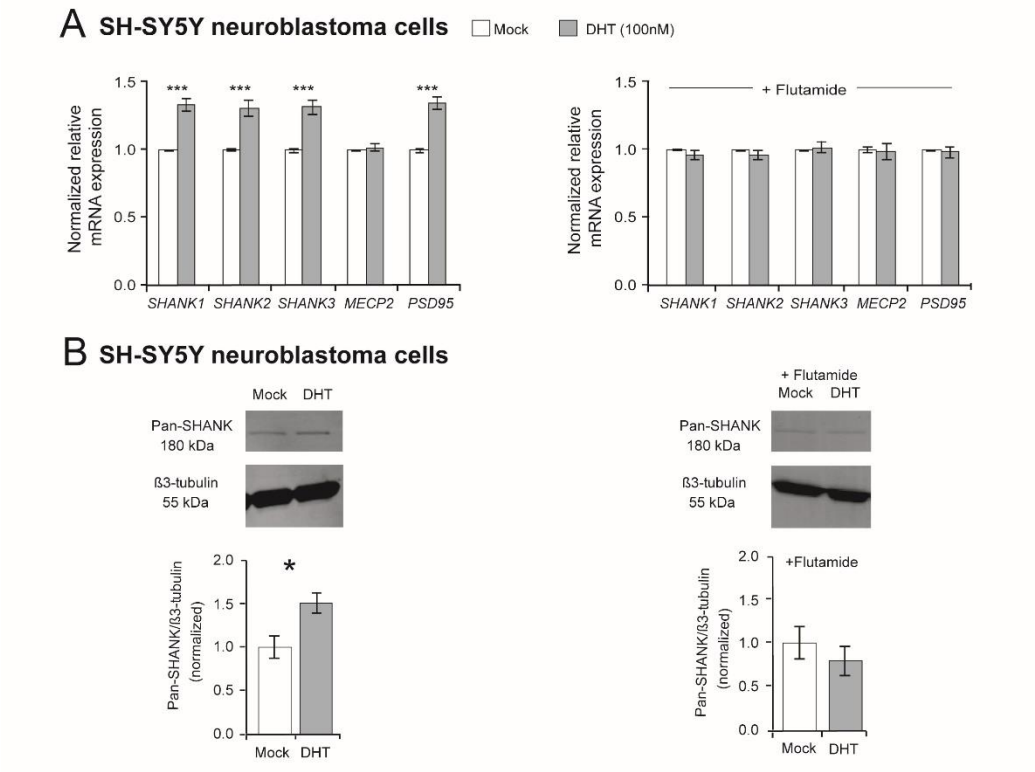

Figure 7: Effect of DHT on *SHANK* gene expression in SH-SY5Y cells
(A) Quantification of *SHANK*, *MECP2* and *PSD95* gene expression by qPCR after 4 hrs of treatment with either 100 nM DHT or a combination of 100 nM DHT and 1 µM flutamide (n = 5). Gene expression was normalized against 5 reference genes (*18S*, *GAPDH*, *HPRT1*, *HSPD1* and *SDHA*) (Two-way ANOVA, * $P \leq 0.05$, *** $P \leq 0.001$, versus mock; Bonferroni threshold: n = 5 tests, $P \leq 0.01$). **(B)** An increase of SHANK

protein levels by 50% was shown after 48 hrs of 100 nM DHT treatment (n = 5) by western blot analysis, whereas no difference was determined after 48 hrs of treatment with DHT combined with flutamide (n = 5). Error bars indicate SEM. The figure and figure legend were adapted from [152].

Table 4: Analysis of the influence of DHT treatment on reference gene expression

	GAPDH	*HPRT1*	*HSPD1*	*SDHA*
DHT versus Mock	0.202	0.335	0.316	0.194

Two-way ANOVA *P*-values are shown and showed no significant effect of 100 nM DHT treatment in SH-SY5Y cells for 4 hrs on the expression of reference genes *GAPDH*, *HPRT1*, *HSPD1* or *SDHA*. The analyzed reference genes were normalized against *18S*. The table and table legend were adapted from [152].

To elucidate if estrogens also regulate *SHANK* gene expression, SH-SY5Y cells were treated with 100 nM 17β-estradiol to stimulate the estrogen receptors. First, the expression of the reference genes was analyzed and revealed that *GAPDH* and *HPRT1* expression was affected by 17β-estradiol when normalized to *18S* **(Table 5)** [152]. Therefore, the gene expression analysis of *SHANK*, *MECP2* and *PSD95* genes in SH-SY5Y cells treated with 100 nM 17β-estradiol was normalized against *18S*, *HSPD1* and *SDHA*. A minor enhancement of *SHANK*, *MECP2* and *PSD95* expression could be observed on RNA level after 4 hrs of treatment (15% upregulation, *P*-value for *SHANK1*= 0.02; *P*-values for *SHANK2*, *SHANK3*, *MECP2* and *PSD95* ≤ 0.001) **(Figure 8A)** [152]. The minor regulatory effect of 17β-estradiol on *SHANK* gene expression on RNA level could not be confirmed on protein level in immunoblots after the treatment of SH-SY5Y cells with 10 and 100 nM 17β-estradiol for 48 hrs **(Figure 8B)** [152]. When blocking the ERα or ERβ receptor subtypes with the selective ERα antagonist MPP or ERβ antagonist PHTPP, the effect of 17β-estradiol on *SHANK* mRNA expression by MPP was gone, whereas the blocking of ERβ with the antagonist PHTPP abrogated the effect on *SHANK* and *PSD95* mRNA expression **(Figure 8A)** [152]. The combined blocking of both ERs antagonized the 17β-estradiol stimulated expression of *SHANK*, *PSD95* and *MECP2* **(Figure 8A)**. Thus, besides AR signaling, also ERα and ERβ signaling contribute to the expression of *SHANK* genes in the human SH-SY5Y cell line [152].

Table 5: Analysis of the influence of 17β-estradiol treatment on reference gene expression

	GAPDH	*HPRT1*	*HSPD1*	*SDHA*
17β-estradiol versus Mock	0.097	0.032	0.229	0.64

Two-way ANOVA *P*-values show no effect of 100 nM 17β-estradiol treatment of SH-SY5Y cells for 4 hrs on the expression of reference genes, *HSPD1* and *SDHA*. In contrast, there was a significant and borderline

significant effect on *HPRT1* and *GAPDH* expression, respectively. The analyzed reference genes were normalized against *18S*. As *HPRT1* and *GAPDH* expression was influenced by 17β-estradiol, both genes were excluded from the 17β-estradiol treatment analyses. The table and table legend were adapted from [152].

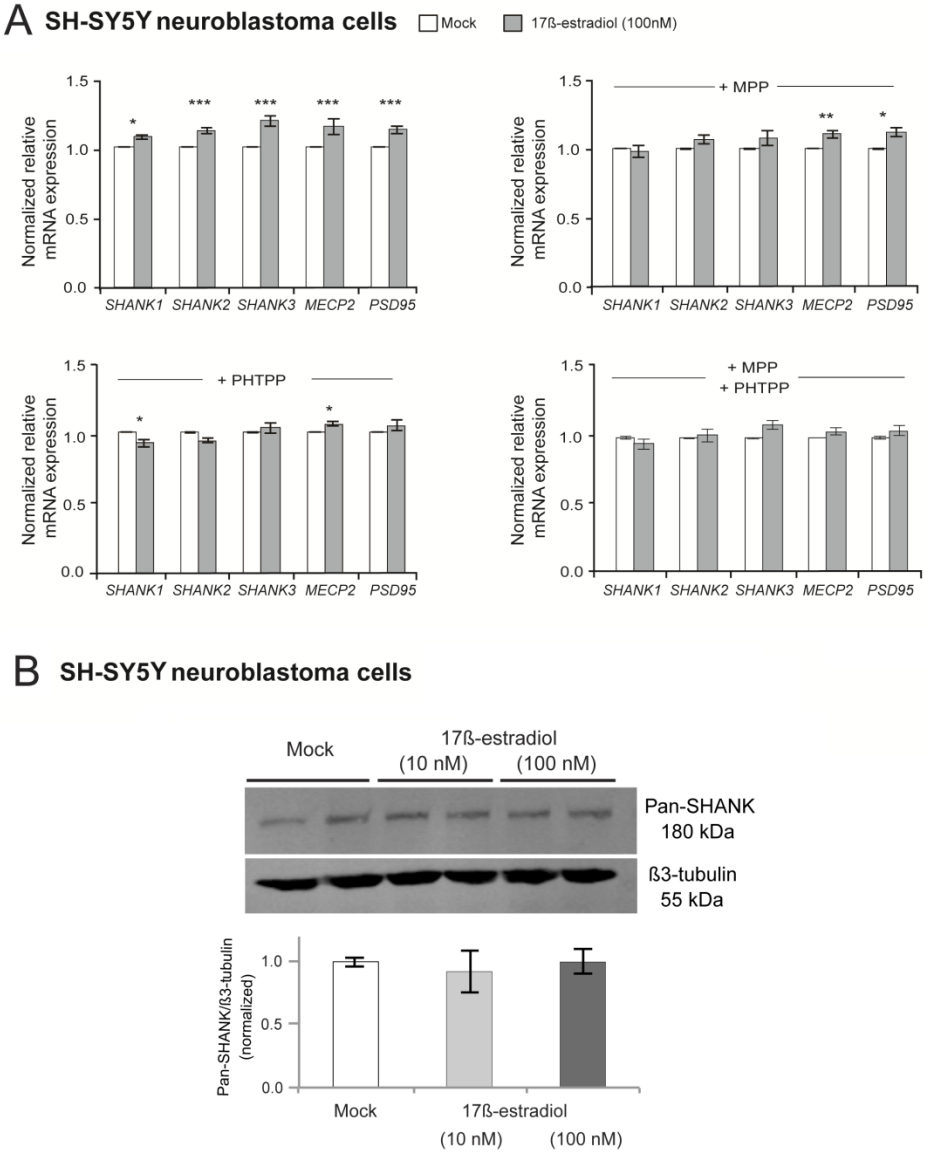

Figure 8: Effect of 17β-estradiol on *SHANK* gene expression in SH-SY5Y cells
(A) Gene expression analysis of *SHANK*, *MECP2* and *PSD95* after 4 hrs of treatment with 100 nM 17β-estradiol (n = 5). The expression was also analyzed after stimulation with 100 nM 17β-estradiol in combination with a selective blocking of ERα (100 nM MPP), ERβ (100 nM PHTPP) or a combination of both (n = 5 of each). Gene expression was normalized against three reference genes (*18S*, *HSPD1* and *SDHA*). Error bars indicate SEM (Two-way ANOVA, * $P \leq 0.05$, ** $P \leq 0.01$, *** $P \leq 0.001$, versus mock-treatment control; Bonferroni correction: n = 5 tests, $P \leq 0.01$). **(B)** Western blot analysis did not show any significant effect of 17β-estradiol treatment on SHANK protein expression in SH-SY5Y cells (10 nM, 100 nM 17β-estradiol, n = 3 per treatment group). Error bars indicate SEM. The figure and figure legend were adapted from [152].

3.1.2 Expression analysis of *Shank* genes in neuron-specific conditional androgen receptor knock-out mice (Ar^{NesCre})

To provide *in vivo* evidence for the Ar regulatory influence on *Shank* gene expression during neurodevelopment, a neuron-specific *Ar* knock-out mouse line (Ar^{NesCre}) [151] was analyzed. *Shank* mRNA expression in the cortex of Ar^{NesCre} mice was investigated by the nCounter analysis at two stages during brain development, E17.5 and P7.5. First, the loss of *Ar* expression in cortical neurons in Ar^{NesCre} mice was confirmed by qPCR at both E17.5 and P7.5 **(Figure 9)** [152]. Next, the effect of the absence of *Ar* expression was investigated in the cortex of Ar^{NesCre}, which revealed a nominal significant reduction of mRNA expression of all three *Shanks*, *Mecp2* and *Erα* at P7.5, but not E17.5, compared with WT mice **(Figure 9)** [152]. Gene expression analysis was normalized against 4 stable reference genes, *Gapdh*, *Hprt1*, *Hspd1* and *Sdha* based on the geNorm method [154]. These results support the contribution of androgen receptor signaling in the specific regulation of the *Shank* gene expression during development.

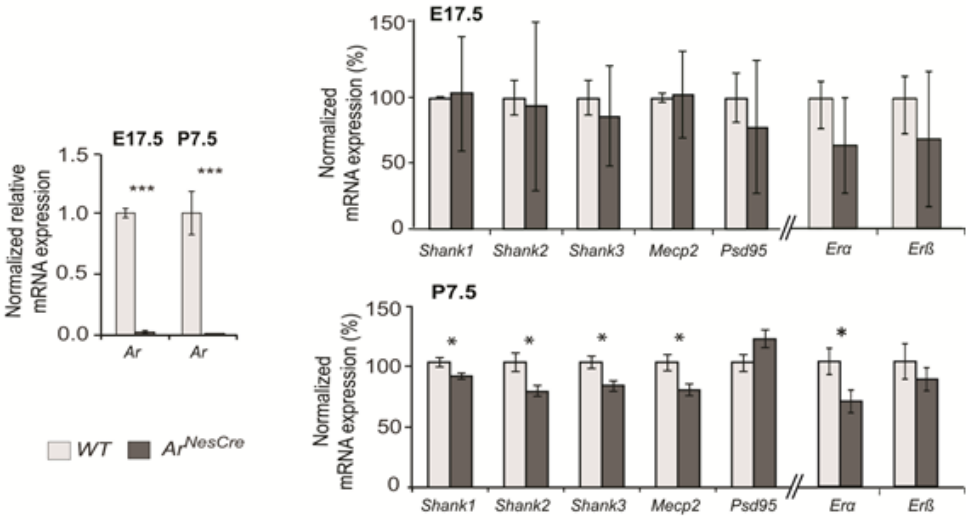

Figure 9: Comparative *Shank* gene expression by nCounter analysis in the cortex of wild-type and Ar^{NesCre} mice. (Left) Loss of *Ar* mRNA in the cortical neurons was confirmed by qPCR at E17.5 and P7.5. **(Right)** Gene expression analysis in the cortex of WT and Ar^{NesCre} mice at E17.5 **(top)** (n = 6 WT and 6 Ar^{NesCre} mice, 3 male and 3 female animals in each group) and P7.5 **(bottom)** (n = 7 WT and 7 Ar^{NesCre} mice, 2 male and 5 female animals in each group). The loss of *Ar* expression at E17.5 revealed no difference in the expression of the tested genes. In contrast, the loss of *Ar* expression at P7.5 resulted in a decreased expression of *Shank*, *Mecp2* and *Erα* genes. The analysis could not be stratified by sex due to the low number of mice. Gene expression was normalized against four reference genes (*Gapdh*, *Hprt1*, *Hspd1* and *Sdha*). Error bars indicate SEM (unpaired two-tailed Student's t-tests, * $P \leq 0.05$). The figure and figure legend were adapted from [152].

3.1.3 Expression of Shank1-3 in the male and female mouse cortex at E17.5 and P7.5

As sex hormone levels and the expression of *Ar*, *Erα* and *Erβ* differ between males and females during development [180,181], a sex-specific regulation of *Shank* expression was suggested. Therefore, the expression levels of *Shank* genes were investigated in the frontal cortices of male and female CD1 WT mice at two different developmental stages, E17.5 and P7.5. The sex-independent expression of the reference genes was confirmed by showing equal levels of *Gapdh*, *Sdha*, *Hprt1* and *Hspd1* expression, normalized to *18s*, in male and female mice cortices at the two investigated developmental stages **(Table 6)** [152]. In the comparative qPCR analysis, significantly elevated *Shank1*, *Shank3* and *Mecp2* expression levels could be detected in the cortices of female compared with male mice at E17.5 (about 20%, *Shank1* (*P*=0.001), *Shank3* (*P*= 0.007) and *Mecp2* (*P*=0.0005)) **(Figure 10)** [152]. At P7.5, the expression analysis revealed elevated *Shank1* mRNA expression in the cortices of female mice with nominal significance, as well as significantly elevated *Psd95* expression (about 20%, *Shank1* (*P*= 0.03) and *Psd95* (*P*= 0.001) **(Figure 10)** [152]. By comparing the expression of tested genes between E17.5 and P7.5, *Shank1*, *Shank2*, *Mecp2* and *Psd95* expression in both male and female mice increased in the cortex from E17.5 to P7.5 **(Figure 10)**. In contrast, the expression of *Shank3* decreased at P7.5 in both male and female mice **(Figure 10)**.

Table 6: Quantification of the relative reference gene expression in the cortex of male and female CD1 mice during different developmental stages

	Gapdh	*Hprt1*	*Hspd1*	*Sdha*
E17.5	0.2055	0.8219	0.2179	0.9228
P7.5	0.7953	0.1236	0.6343	0.9668

Two-way ANOVA *P*-values revealed no significant difference in the expression of reference genes, *Gapdh*, *Hprt1*, *Hspd1* and *Sdha*, between male and female CD1 mice cortices at E17.5 and P7.5. The analyzed reference genes were normalized against *18s*. The table and table legend were adapted from [152].

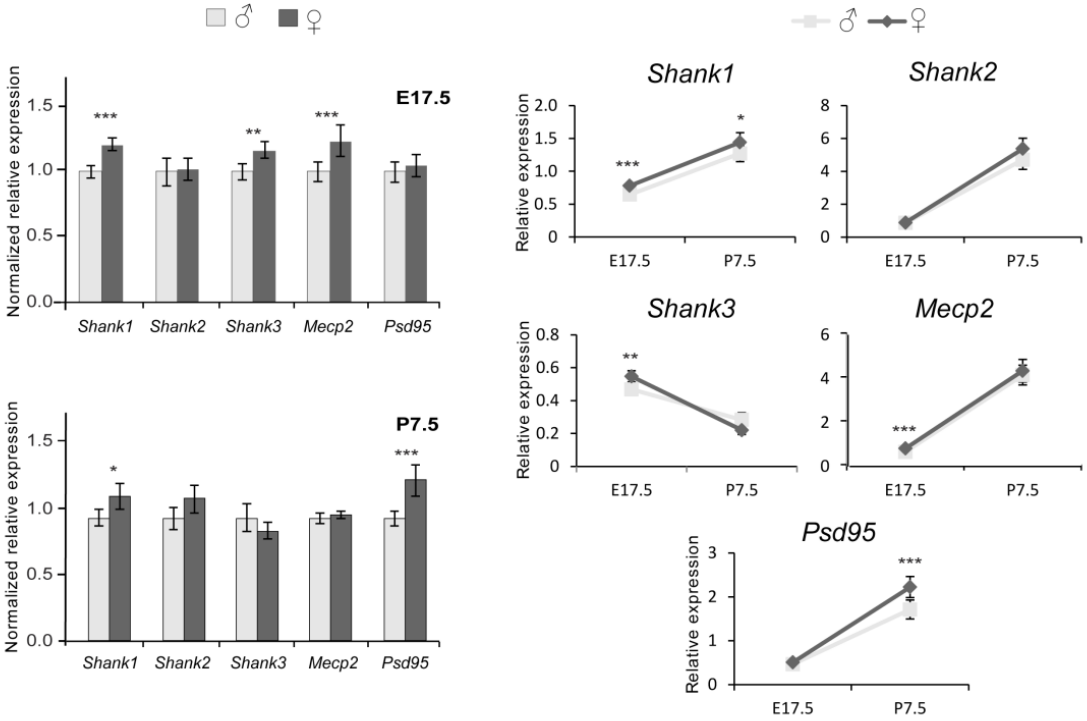

Figure 10: ***Shank*** **gene expression analysis in the male and female CD1 mouse cortex**
qPCR analysis revealed gene expression differences in the male and female mouse cortex at E17.5 for *Shank1* (*P*= 0.001), *Shank3 (P*= 0.007) and *Mecp2* (*P*= 0.0005) (n = 16 male, 16 female). At the developmental stage P7.5, a sex-differential expression was obtained for *Psd95* (*P*= 0.001) and *Shank1* (*P*= 0.03) with higher expression in female than male mice (n =18 male, 17 female). *Shank1*, *Shank2*, *Mecp2* and *Psd95* expression increased in the cortex from E17.5 to P7.5. For *Shank3*, the expression decreased at P7.5 in both male and female mice. The respective gene expression was normalized against five reference genes (*18s*, *Gapdh*, *Hprt1*, *Hspd1* and *Sdha*). Error bars indicate SEM (Two-way ANOVA, * $P \leq 0.05$, ** $P \leq 0.01$, *** $P \leq 0.001$; Bonferroni correction: n = 5 tests for each developmental stage, $P \leq 0.01$). The figure and figure legend were adapted from [152].

To confirm the sex-differential expression of *Shanks* in CD1 mice, the expression level of Shanks in total protein lysate from the frontal cortex of male and female mice at E17.5 and P7.5 was investigated by western blot analysis. In contrast to the *Shank* mRNA expression analysis, significantly higher expression levels for all three Shank proteins was found in the male compared with female cortices at both developmental stages **(Figure 11)** [152]. Shank expression was reduced in females by 50-77% at E17.5 and by 43-47% at P7.5 **(Figure 11)**, indicating that Shank expression differences were more pronounced at the earlier stages [152].

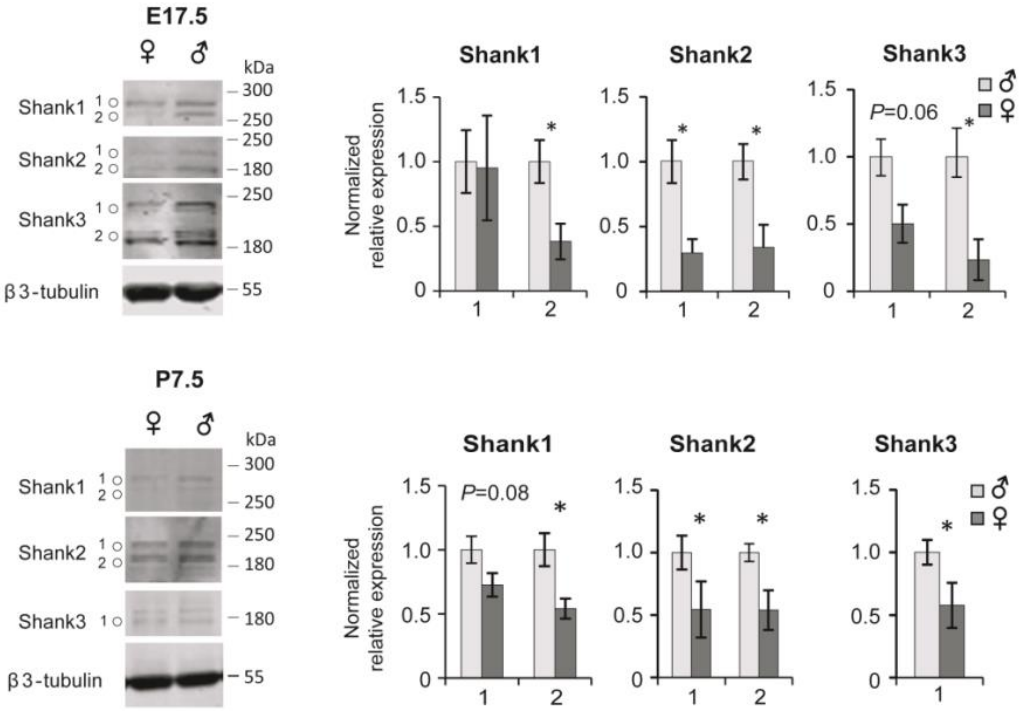

Figure 11: Shank protein analysis in the male and female CD1 mouse cortex
Levels of Shank1, 2 and 3 proteins in the cortex of male and female CD1 mice at E17.5 **(top)** and P7.5 **(bottom)** (n = 4 of each sex). Error bars indicate SEM (unpaired two-tailed Student's t-tests, *P < 0.05). Isoform expression differences were observed between the two developmental stages for Shank3. These data were provided by Dr. Simone Berkel from the Institute of Human Genetics, Heidelberg University. The figure and figure legend were adapted from [152].

3.2 Functional analysis of SHANK2A and SHANK2A(R462X) overexpression in the glutamatergic neurons in the mouse forebrain

3.2.1 Generation and characterization of $Tg^{SHANK2A}$ and $Tg^{SHANK2AR462X}$ mouse lines

To enable the study of the molecular, physiological and behavioral effects that originate from Shank dysfunctions in the glutamatergic neurons while maintaining the regular SHANK function in other cell types, two conditional transgenic *Shank2* mouse lines overexpressing human SHANK2A, the brain-specific isoform, or the truncated SHANK2A(R462X) isoform, were used. The overexpression of these isoforms is suggested to disturb the balanced SHANK-dependent organization of postsynaptic proteins. In the two mouse lines, the SHANK2A and SHANK2A(R462X) overexpression was achieved by combining two transgenes from $Tg^{\alpha CaMKII\text{-}tTA}$ mouse line with either the silent transgene that encodes SHANK2A or SHANK2A(R462X) together with reporter genes. $Tg^{\alpha CaMKII\text{-}tTA}$ mice express the synthetic doxycycline (dox)-dependent transcriptional activator (tTA) under the control of the forebrain-specific promoter for the alpha subunit of Ca^{2+}/calmodulin-dependent protein kinase II (αCaMKII) specifically in the excitatory neurons [155,182] **(Figure 12)**. The transgenes of $Tg^{SHANK2A}$ and $Tg^{SHANK2AR462X}$ mice encode a bidirectional expression module composed of the lacZ reporter gene and the SHANK2A variant fused by the 2A peptide bridge with Venus. Both lacZ and the Venus2A-SHANK2 genes were under the control of a bidirectional promoter (Ptet-bi) which can be activated by tTA in the absence of dox, and which can be silenced at any time by a dox diet. Thus for the activation of the SHANK2 encoding transgenes, the double transgenic lines $Tg^{\alpha CaMKII\text{-}tTA}/Tg^{SHANK2A}$ and $Tg^{\alpha CaMKII\text{-}tTA}/Tg^{SHANK2AR462X}$ have to be generated by breeding of both lines **(Figure 12)**. Double transgenic offspring have to be identified by PCR genotyping and are named $Tg^{SHANK2A}$ and $Tg^{SHANK2AR462X}$ for reasons of simplicity. Single transgenic littermates served in all experiments as controls.

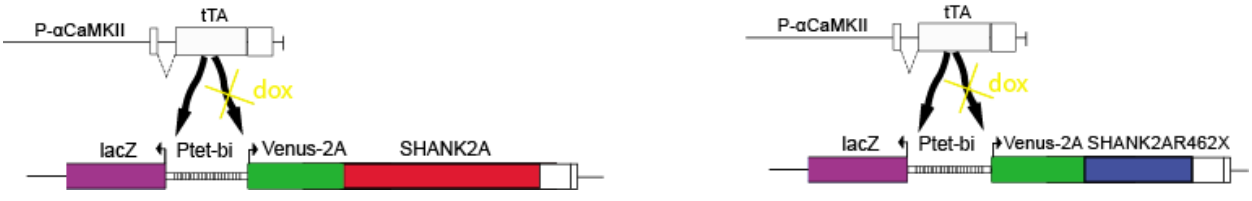

Figure 12: Schematic of the two transgenes used for the overexpression of SHANK2A and SHANK2A(R462X) in the glutamatergic forebrain neurons

Schematic drawing of the transgenes in $Tg^{\alpha CaMKII\text{-}tTA}/Tg^{SHANK2A}$ **(left)** and $Tg^{\alpha CaMKII\text{-}tTA}/Tg^{SHANK2AR462X}$ mice **(right)**. The transcription activator (tTA) is expressed under the control of αCamKII promoter in the glutamatergic neurons in the mouse forebrain. In the presence of the responder transgene, tTA binds to the Ptet-bi and activates the expression of the transgenes. These transgenes include the lacZ gene on one side of the Ptet-bi and a fusion transcript composed of green fluorescent protein variant (Venus), 2A self-cleaving peptide and either SHANK2A or SHANK2A(R462X) on the other side. The overexpression of SHANK2A and SHANK2A(R462X), along with reporter proteins, can be switched off when mice are provided with dox, dissolved in water. Dox binds to tTA and inhibits its binding to the Ptet-bi, leading to the inactivation of the transgene expression.

The expression of the reporter genes, Venus and lacZ, in $Tg^{SHANK2A}$ and $Tg^{SHANK2AR462X}$ mice was confirmed in histological and western blot analyses **(Figure 13)**. The Venus epifluorescence was restricted to the forebrain of both mouse lines with no detectable fluorescence in the cerebellum **(Figure 13A)**. The β-galactosidase expression of the lacZ gene was detected at the cellular level in the cortex and hippocampus in anti-β-galactosidase DAB-immunostains of coronal brain section **(Figure 13A).** The expression of β-galactosidase was also confirmed by the visualization of its enzymatic activity via Eosin/X-gal stainings **(Figure 13B)**. Immunoblots of protein lysates of different brain regions from $Tg^{SHANK2A}$ and $Tg^{SHANK2AR462X}$ mice revealed the expression of Venus, β-galactosidase and either SHANK2A or SHANK2A(R462X) in the olfactory bulb, forebrain and hippocampus, but not in the cerebellum **(Figure 13C)**. The highest expression was detected in the hippocampus. The levels of mRNA overexpression of both SHANK2A and SHANK2A(R462X) transgenes were measured, as represented by the Venus expression level, using the nCounter analysis. The expression of Venus mRNA in both $Tg^{SHANK2A}$ and $Tg^{SHANK2AR462X}$ mice revealed a ratio of 12 to the endogenous *Shank2* and 1.6 to the sum of all endogenous *Shanks* (*Shank1,2* and *3*) mRNA expression **(Figure 13D)**. Immunoblots of hippocampal total protein lysate from $Tg^{SHANK2A}$ and $Tg^{SHANK2AR462X}$ mice revealed no difference between SHANK2A and SHANK2A(R462X) expression **(Figure 13E)**, indicating their similar level of overexpression consistent with the mRNA results obtained from the nCounter analysis **(Figure 13D)**.

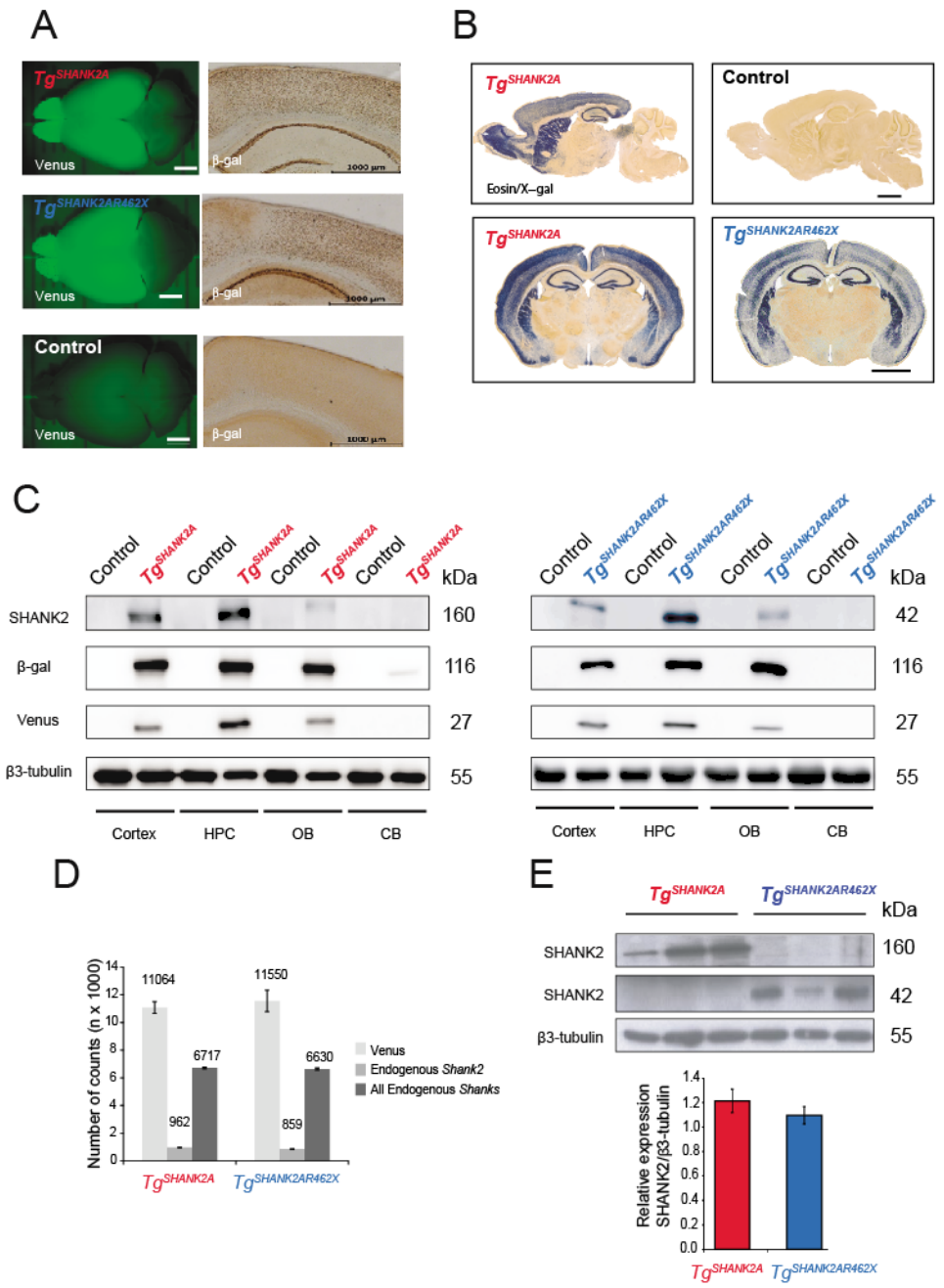

Figure 13: Forebrain-specific expression of the transgenic controlled β-galactosidase, Venus and SHANK2A or SHANK2A(R462X), as exemplified in some representative mice

(A) The overexpression of the polycistronic SHANK2 transgenes was visualized by the Venus epifluorescence in the forebrain of $Tg^{SHANK2A}$ mice **(upper row)** and of $Tg^{SHANK2AR462X}$ mice **(middle row)** (scale bar: 2 mm). β-galactosidase expression of the lacZ gene can be detected at the cellular level in anti-β-galactosidase DAB-immunostainings of coronal brain section (shown for the cortex and hippocampus; (scale bars: 1 mm). **(B, top row)** The β-galactosidase activity was visualized in sagittal brain section of $Tg^{SHANK2A}$ mice by Eosin/X-gal staining. X-gal of slices from control mice on the right shows no blue staining **(B, bottom row)**. Eosin/X-gal staining of coronal brain sections from $Tg^{SHANK2A}$ and $Tg^{SHANK2AR462X}$ mice (scale bars: 2 mm). **(C)** Protein lysates of different brain regions from $Tg^{SHANK2A}$ **(right)** and $Tg^{SHANK2AR462X}$ **(left)** mice (6 months) were analyzed by immunoblotting with the SHANK2, β-galactosidase and Venus antibodies. The hippocampus showed the highest expression of both transgenes. HPC: Hippocampus, OB: Olfactory bulb, CB: Cerebellum.

(D) The nCounter analysis revealed a ratio of Venus to endogenous *Shank2* mRNA expression of 12, and a ratio of Venus to all endogenous *Shank* mRNA expression of 1.6 (n = 8 $Tg^{SHANK2A}$ and 11 control mice; n = 7 $Tg^{SHANK2AR462X}$ and 7 control mice, 3 – 5 months). **(E)** Comparable quantification of SHANK2A and SHANK2A(R462X) transgene expression in the hippocampus by immunoblotting revealed no significant difference between $Tg^{SHANK2A}$ and $Tg^{SHANK2AR462X}$ mouse lines (3 mice per each mouse line, 3 – 5 months).

3.2.2 Behavioral analysis of $Tg^{SHANK2A}$ mice

The detailed behavior analysis including general, social and cognitive behavior analysis was performed in $Tg^{SHANK2A}$ mice (for a summary, see **Appendix 5**). $Tg^{SHANK2A}$ pups showed a 50% death rate in the first 4 weeks of life. First, the SHIRPA test, as a comprehensive screening method for qualitatively abnormal phenotypes in mice, was performed and revealed that the adult $Tg^{SHANK2A}$ mice suffered from muscle twitches and that their body weights were 30% less compared with their littermate controls **(Figure 14A)**. The general behavior of $Tg^{SHANK2A}$ mice was investigated using the LABORAS test, in which the movements of the mice were continuously monitored for 24 hrs. $Tg^{SHANK2A}$ mice displayed hyperactivity as shown by an increase in locomotion and a higher average speed compared with control mice **(Figure 14B)**. They also showed increased duration of eating periods **(Figure 14C)**. Moreover, an increase in the number of repetitive rearing was noted **(Figure 14D)**. The duration of drinking, self-grooming and climbing were not different between $Tg^{SHANK2A}$ and control mice **(Figure 14C, D)**. To manually examine the repetitive behavior, the time of jumping, self-grooming and digging in their home cages was measured within 6 min. $Tg^{SHANK2A}$ mice displayed an increase in the duration of self-grooming and a decrease in the duration of digging compared with control mice **(Figure 14E)**. Because building nests is considered a spontaneous home cage behavior of mice [160], the nesting behavior of $Tg^{SHANK2A}$ mice was assessed in their home cages during the evening. $Tg^{SHANK2A}$ mice were impaired in the nesting test as shown by building less complex nests compared to their littermate controls **(Figure 14F)**.

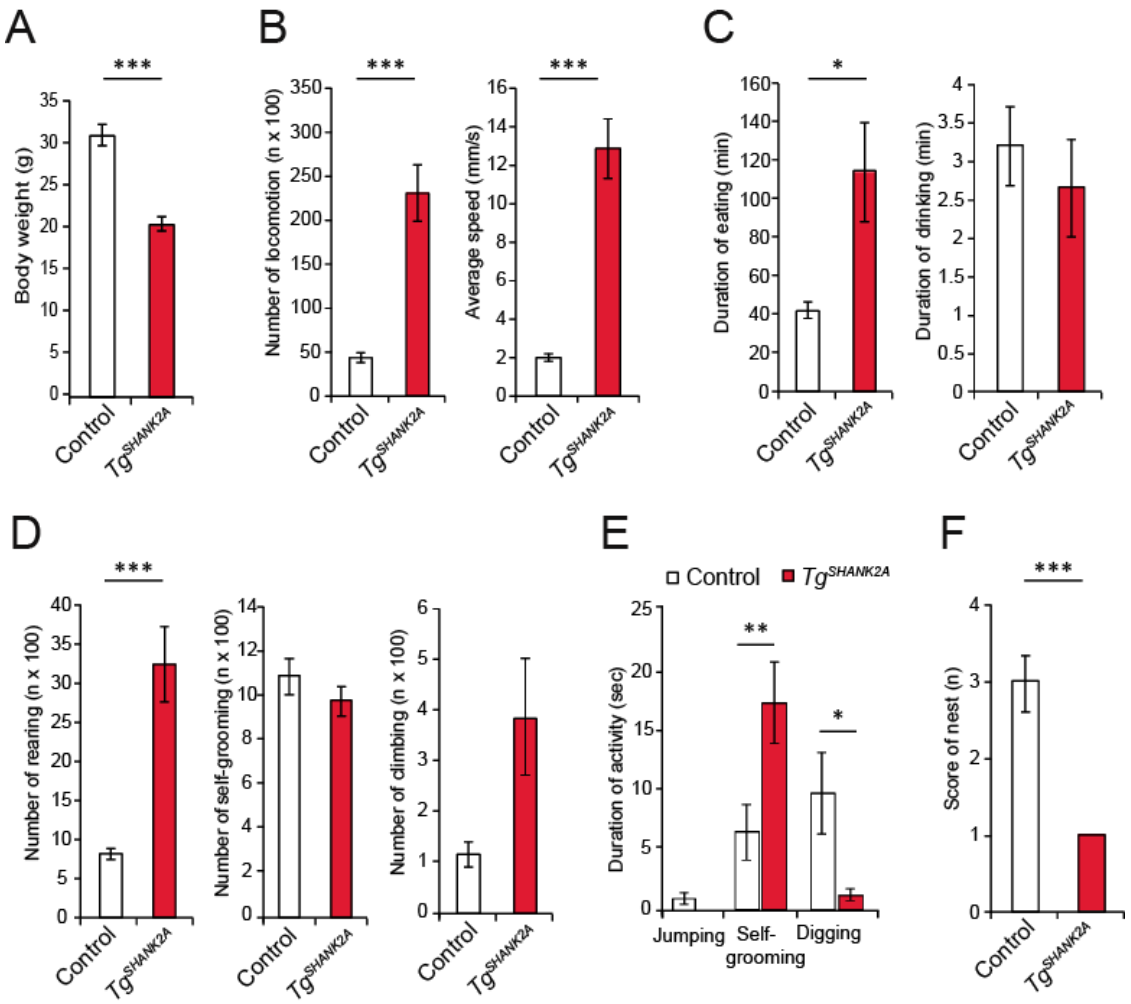

Figure 14: Analysis of general and repetitive behaviors in $Tg^{SHANK2A}$ mice
(A) Body weights of $Tg^{SHANK2A}$ mice were 30% less than that of control mice. **(B)** LABORAS test revealed that $Tg^{SHANK2A}$ mice were hyperactive as shown by the increased number of locomotion **(left)** and average speed **(right)**. **(C)** $Tg^{SHANK2A}$ mice displayed more time for eating **(left)**, but similar drinking time **(right)** compared with control mice in the LABORAS cages. **(D)** $Tg^{SHANK2A}$ mice showed increased rearing **(left)**, but normal self-grooming **(middle)** and climbing **(right)**. **(E)** Stereotypical behaviors in the home cage were investigated within 6 mins and revealed enhanced self-grooming and decreased digging durations in $Tg^{SHANK2A}$ mice compared with control mice. **(F)** The nests built by $Tg^{SHANK2A}$ mice were less complex as shown by the low score in the nesting test (n = 12 $Tg^{SHANK2A}$ and 15 control mice at 6 – 9 months of age). Error bars indicate SEM (Two-way ANOVA,*$p \leq 0.05$, **$p \leq 0.01$, ***$p \leq 0.001$).

In mice with an autistic-like phenotype, hyperactivity is often combined with anxiety. Therefore, three different experiments were performed to test anxiety in $Tg^{SHANK2A}$ mice and revealed clear signs of increased anxiety. In the dark-light box test, $Tg^{SHANK2A}$ mice showed a significant delay to the first entry to the light compartment with fewer total numbers of entries compared with control mice **(Figure 15A)**. In the open field test, $Tg^{SHANK2A}$ mice traveled less distance in the central zone of a new arena accompanied by fewer visits **(Figure 15B)**. In the neophobia test,

Tg^{SHANK2A} mice exhibited more fear of an unfamiliar drink as shown by the fewer contacts and the higher latency to the first contact to the unfamiliar drink compared with control mice **(Figure 15C)**.

To test the integrity of hippocampal function, the burrowing test, which measures the ability of mice to retrieve food pellets from a tube, was performed. *Tg*^{SHANK2A} mice retrieved fewer pellets from the tube after 2 and 12 hrs compared with control mice, indicating hippocampal dysfunction **(Figure 15D)**. *Tg*^{SHANK2A} mice showed impairment in maintaining their balance in two consecutive sessions in the balance test **(Figure 15E)**. Moreover, they showed a high impulsive or a lack of inhibition reaction in the cliff avoidance reaction test and fell faster and more often from the elevated platform than control mice **(Figure 15F)**.

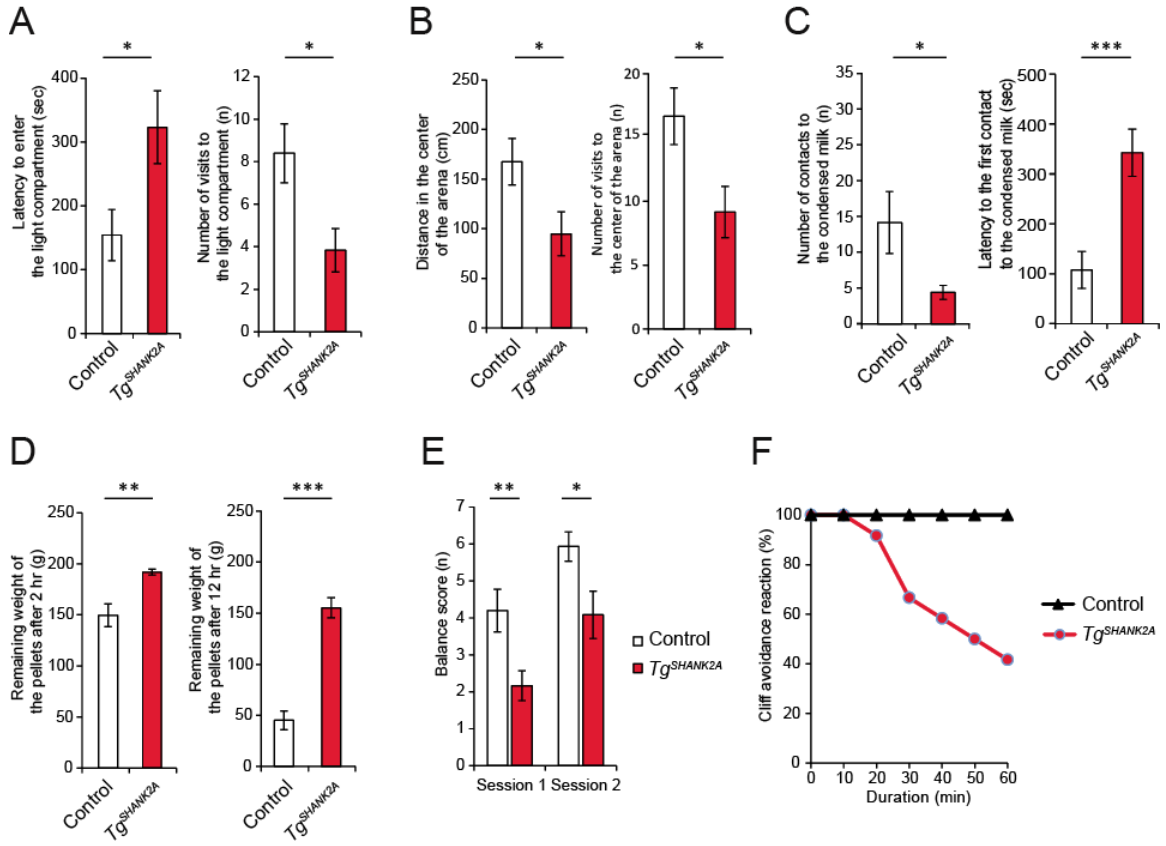

Figure 15: Characterization of anxiety and impulsivity in *Tg*^{SHANK2A} mice
(A) The dark-light box test revealed anxiety in *Tg*^{SHANK2A} mice as shown by the high latency **(left)** and reduced number of visits **(right)** to the light compartment compared with control mice. **(B)** *Tg*^{SHANK2A} mice exhibited anxiety in the open field test by showing less traveled distance **(left)** and fewer visits **(right)** to the center of a new arena than control mice. **(C)** *Tg*^{SHANK2A} mice displayed fear of an unfamiliar drink (condensed milk in the center of the arena) in the neophobia test as shown by fewer contacts **(left)** and higher latency **(right)** to the first contact to the unfamiliar drink than control mice. **(D)** In the burrowing test, *Tg*^{SHANK2A} mice retrieved fewer pellets from the tube after 2 hrs **(left)** and 12 hrs **(right)** than control mice. **(E)** *Tg*^{SHANK2A} had a

significant lower score in two successive sessions in the balance test compared with control mice. **(F)** $Tg^{SHANK2A}$ mice displayed a high impulsive reaction with less cliff avoidance reaction (n = 12 $Tg^{SHANK2A}$ and 15 control mice at 6 – 9 months of age). Error bars indicate SEM (Two-way ANOVA,*$p \leq 0.05$, **$p \leq 0.01$, ***$p \leq 0.001$).

As social impairment is a core phenotype in ASD, the sociability of $Tg^{SHANK2A}$ mice was investigated in three different tests. $Tg^{SHANK2A}$ mice showed social impairment in the three-chamber social test in all three sessions **(Figure 16A)**. They also made fewer contacts to same-sex unfamiliar mice in the direct social interaction test **(Figure 16B)**. In the novel object recognition test, $Tg^{SHANK2A}$ mice showed borderline significant fewer contacts to a novel object in the center of an arena than control mice **(Figure 16C)**. Together, these results indicate severe impairment of the social behavior of $Tg^{SHANK2A}$ mice. Because cognitive dysfunction is one of the comorbidities of ASD, cognitive and memory functions of $Tg^{SHANK2A}$ mice were assessed using the puzzle box test. $Tg^{SHANK2A}$ mice displayed a cognitive dysfunction and less ability to solve the puzzle in sessions 1, 8 and 10 compared with control mice **(Figure 16D)**. Lastly, the emotional learning of $Tg^{SHANK2A}$ mice was assessed by the fear conditioning test which revealed no impairment in the context or the cued memories in $Tg^{SHANK2A}$ mice **(Figure 16E)**.

In summary, the SHANK2A overexpression in the glutamatergic neurons in the mouse forebrain caused severe behavioral outcomes. The detailed behavioral analysis of $Tg^{SHANK2A}$ mice revealed ASD-like phenotypes including repetitive behavior and social impairment. Moreover, $Tg^{SHANK2A}$ mice exhibited three comorbidities of ASD, hyperactivity, anxiety and cognitive dysfunction. In addition, the integrity of the hippocampal function in $Tg^{SHANK2A}$ mice was affected, leading to a difficulty in managing daily activities such as nest building and burrowing.

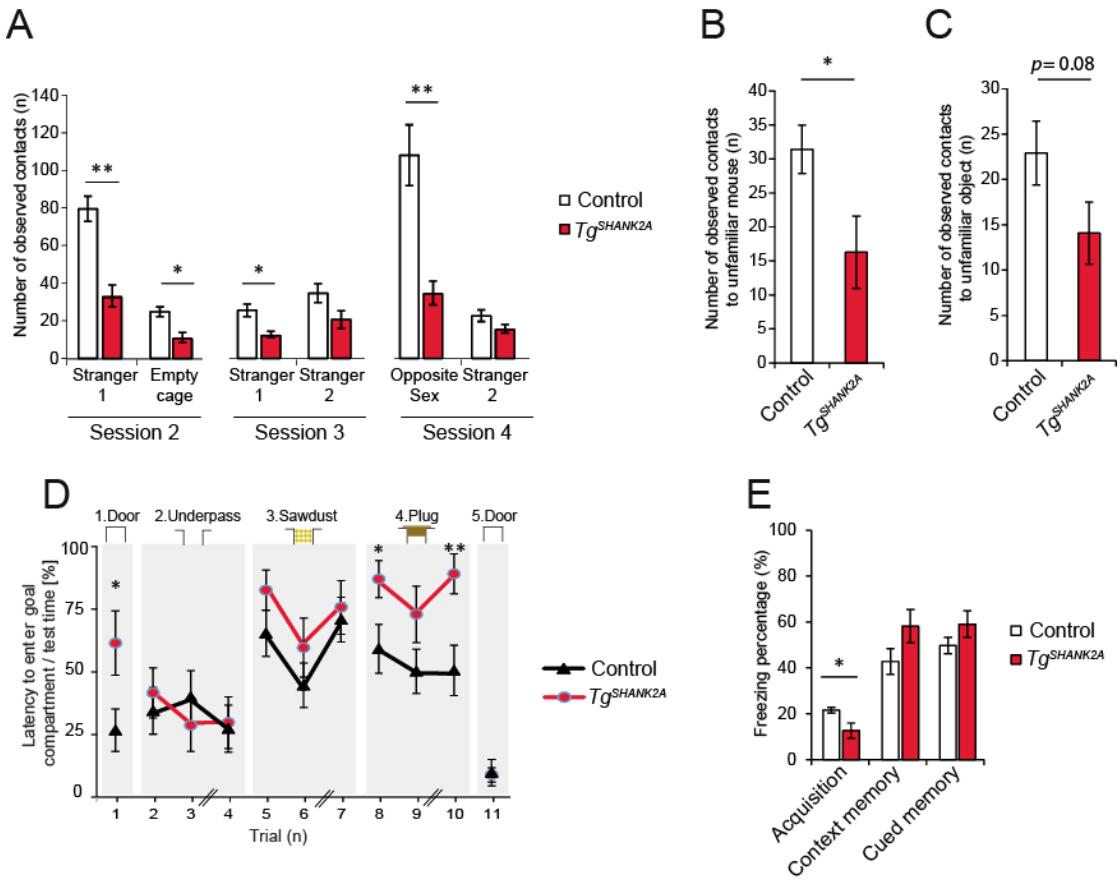

Figure 16: Characterization of the social behavior, cognitive function and emotional learning in *Tg*^{SHANK2A} mice

(A) Social interaction in the three-chamber social test. The graph shows the number of contacts to an empty cage and a caged stranger mouse in the first session, mouse and novel mouse in the second session, mouse and opposite-sex novel mouse in the third session. *Tg*^{SHANK2A} mice displayed fewer contacts to a stranger 1 in sessions one and two and fewer contacts to the opposite sex mouse in session three than control mice. **(B)** The direct social interaction test revealed fewer contacts of *Tg*^{SHANK2A} mice to unfamiliar same-sex mice than control mice. **(C)** The novel object recognition test showed a borderline significant reduction in the number of observed contacts to an unfamiliar object by *Tg*^{SHANK2A} mice. **(D)** In the puzzle box test, the door was open in trial 1, underpass in trials 2–4, underpass filled with sawdust in trials 5–7 and covered by a plug in trials 8–10, whereas trial 11 corresponded to trial 1. *Tg*^{SHANK2A} mice showed high latency to solve the puzzle in trials 1, 8 and 10. **(E)** The emotional learning ability was investigated using the fear conditioning test. The test was done over 3 days with the first day as an acquisition phase, the second day for testing the context memory and the third day for testing the cued memory. *Tg*^{SHANK2A} mice showed less freezing percentage in the acquisition phase compared with control mice but did not reveal any impairment in context or cued memory (n = 12 *Tg*^{SHANK2A} and 15 control mice at 6 – 9 months of age). Error bars indicate SEM (Two-way ANOVA,*$p \leq 0.05$, **$p \leq 0.01$).

3.2.3 Behavioral analysis of *Tg*^{SHANK2AR462X} mice

The detailed behavior of *Tg*^{SHANK2AR462X} mice was performed in analogy to the procedures used for *Tg*^{SHANK2A} mice. The SHIRPA test revealed around 10% reduced body weight compared to littermate controls **(Figure 17A)** (for a summary, see **Appendix 5**). The long term recording

LABORAS test revealed strong hyperactivity as shown by the increased numbers of locomotion and high average speed compared to controls **(Figure 17B).** *Tg*^{SHANK2AR462X} and control mice showed similar durations of eating and drinking periods **(Figure 17C)** and a similar number of rearing and climbing counts **(Figure 17D)**. In contrast, *Tg*^{SHANK2AR462X} mice revealed fewer self-grooming counts than control mice **(Figure 17D)**. By monitoring the activity in the home cage within 6 min, *Tg*^{SHANK2AR462X} mice showed an increase in the duration of jumping periods and a decrease in the duration of digging compared with control mice **(Figure 17E)**. In the nesting test, no significant difference in the nesting score was found between *Tg*^{SHANK2AR462X} and control mice, indicating normal nesting behavior **(Figure 17F)**.

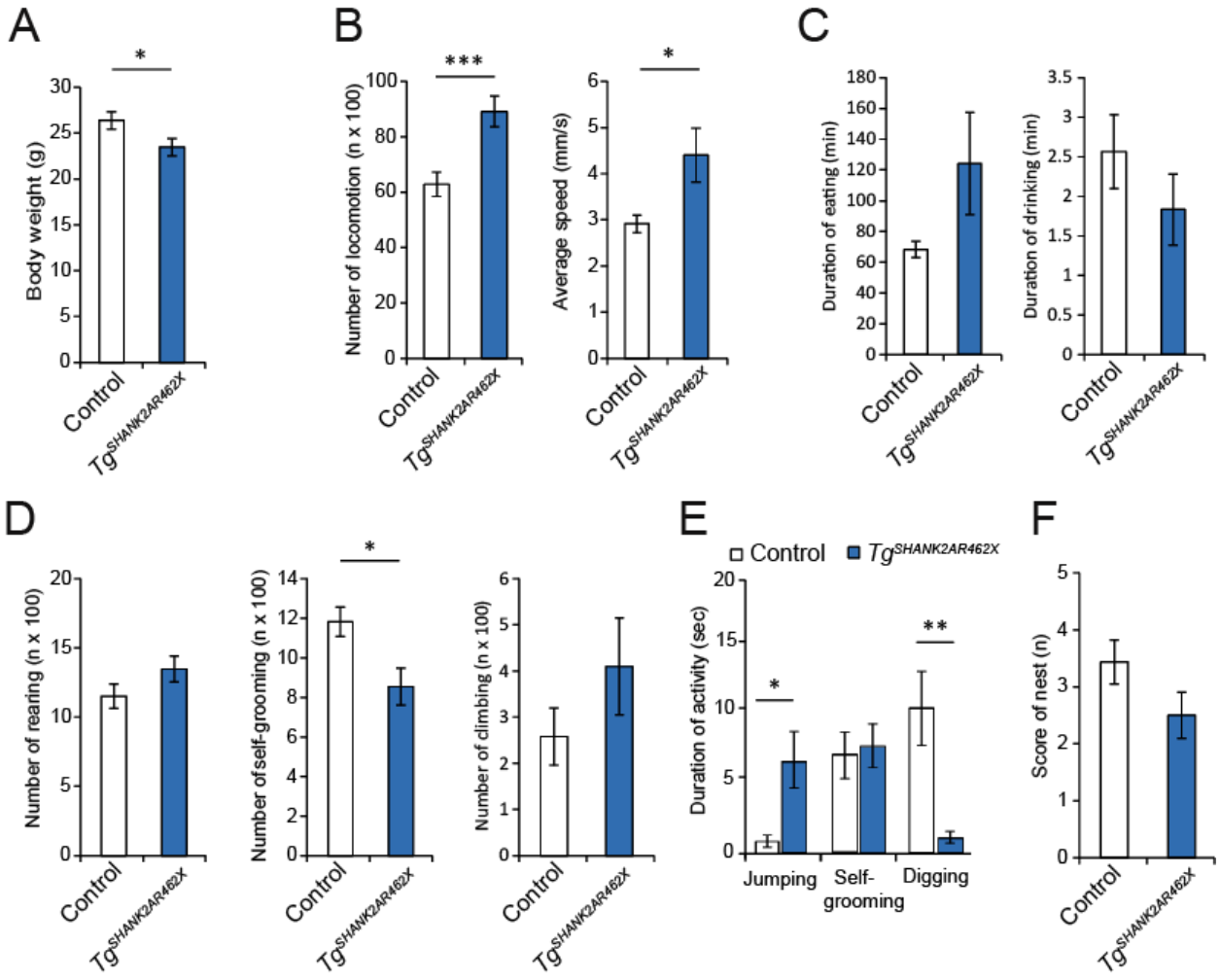

Figure 17: Analysis of general and repetitive behaviors in *Tg*^{SHANK2AR462X} mice
(A) Body weights of *Tg*^{SHANK2AR462X} mice were 10% reduced compared with control mice. **(B-D) The** LABORAS test of *Tg*^{SHANK2AR462X} mice revealed: **(B)** hyperactivity due to an increase in the number of locomotion events **(left)** and the average speed **(right)**, **(C)** no difference in the duration of eating **(left)** or drinking **(right)** periods, **(D)** similar rearing **(left)** and climbing **(right)** but less self-grooming **(middle)**. **(E)**

The stereotypical behaviors in the home cage were investigated within 6 min and revealed increased duration of jumping periods and decreased digging behavior in $Tg^{SHANK2AR462X}$ compared with control mice. **(F)** $Tg^{SHANK2AR462X}$ showed no impairment in the nesting behavior (n = 10 $Tg^{SHANK2AR462X}$ and 16 control mice at 6 – 9 months of age). Error bars indicate SEM (Two-way ANOVA,*$p \leq 0.05$, **$p \leq 0.01$, ***$p \leq 0.001$).

In the dark-light box test that measures anxiety level, $Tg^{SHANK2AR462X}$ mice showed a borderline significant delay and more visits to the light compartment compared with control mice **(Figure 18A)**. In the open field test, $Tg^{SHANK2AR462X}$ and control mice traveled a similar distance in the central zone of a new arena with similar numbers of visits, indicating no anxiety **(Figure 18B)**. In the neophobia test, $Tg^{SHANK2AR462X}$ mice showed a higher latency to the first contact to the unfamiliar drink than control mice but with a similar total number of contacts **(Figure 18C)**.

In the burrowing test, $Tg^{SHANK2AR462X}$ mice were unable to perform the test efficiently and they retrieved fewer pellets from the tube after 2 and 12 hrs **(Figure 18D)**. $Tg^{SHANK2AR462X}$ mice were able to balance normally in two consecutive sessions in the balance test **(Figure 18E)** but showed impairment in the cliff avoidance reaction test **(Figure 18F)**, which indicates impulsivity and/or a lack of behavioral inhibition.

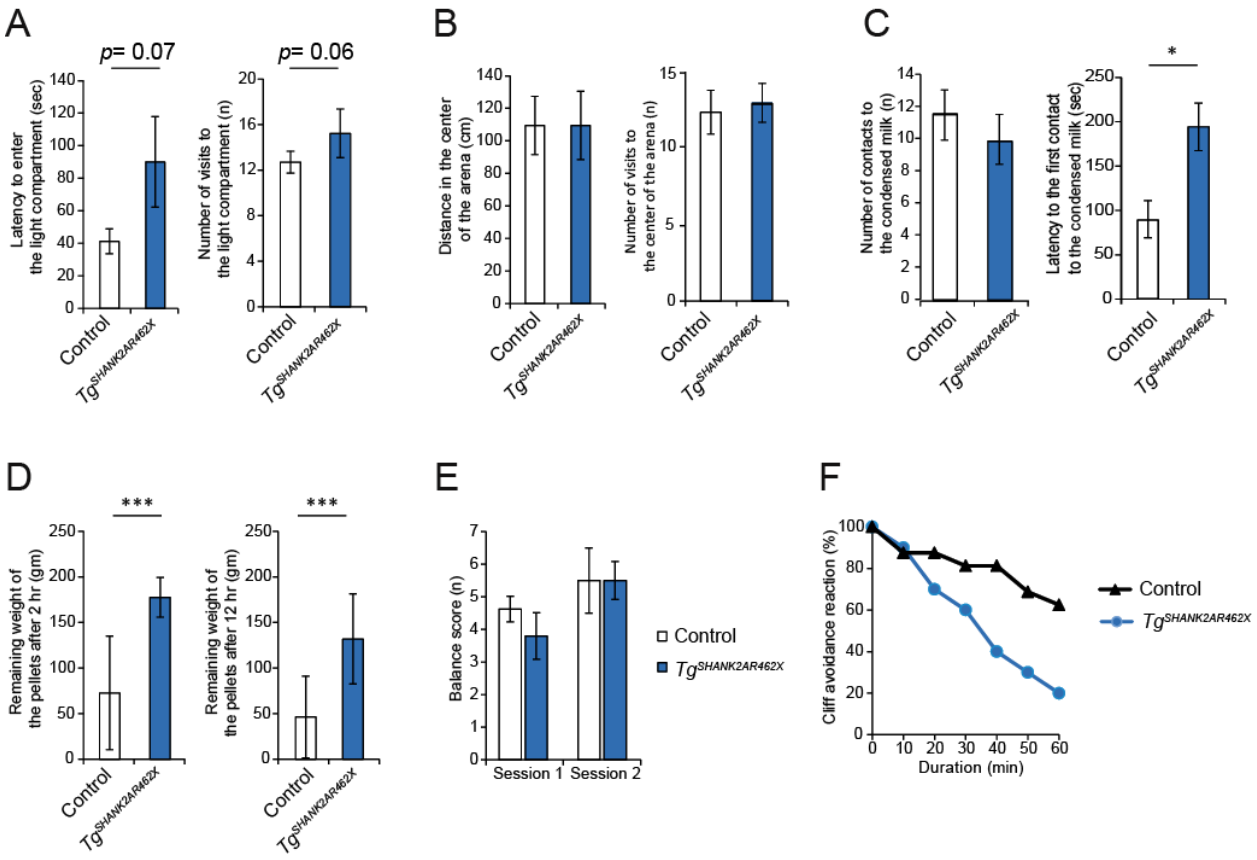

Figure 18: Characterization of anxiety and impulsive behaviors in $Tg^{SHANK2AR462X}$ mice
(A) The dark-light box test revealed borderline anxiety in $Tg^{SHANK2AR462X}$ mice with a tendency of increased latency **(left)** and visits **(right)** to the light compartment. **(B)** $Tg^{SHANK2AR462X}$ mice showed no anxiety in the open field test; they traveled a similar distance in the center of a new arena **(left)** and made a similar number of visits **(right)** as control mice. **(C)** $Tg^{SHANK2AR462X}$ and control mice made similar contacts to unfamiliar drink (condensed milk in the center of the arena) **(left)**, but $Tg^{SHANK2AR462X}$ mice had higher latency to the first contact **(right)**. **(D)** In the burrowing test, $Tg^{SHANK2AR462X}$ mice left more pellets in the tube after 2 hrs **(left)** and 12 hrs **(right)**. **(E)** $Tg^{SHANK2AR462X}$ had no impairment in two successive sessions in the balance test. **(F)** $Tg^{SHANK2AR462X}$ mice showed a high impulsive reaction and less cliff avoidance reaction percentage in the cliff avoidance reaction test (n = 10 $Tg^{SHANK2AR462X}$ and 16 control mice at 6 – 9 months of age). Error bars indicate SEM (Two-way ANOVA,*$p \leq 0.05$, ***$p \leq 0.001$).

In the three-chamber social test, $Tg^{SHANK2AR462X}$ and control mice made a similar number of contacts to stranger mice in all sessions **(Figure 19A)**. In contrast, $Tg^{SHANK2AR462X}$ mice made more social contacts to unfamiliar same-sex mice in the direct social interaction test **(Figure 19B)** and to a novel object in the center of an arena in the novel object recognition test **(Figure 19C)**. The cognitive dysfunction of $Tg^{SHANK2AR462X}$ mice became obvious in their higher latency to solve the puzzle box in trials 5–7 compared to control mice **(Figure 19D)**. In the fear conditioning test, $Tg^{SHANK2AR462X}$ mice were impaired in the contextual memory but showed no impairment in the cued memory **(Figure 19E)**.

In summary, $Tg^{SHANK2AR462X}$ mice exhibited some ASD/ADHD-like phenotypes including repetitive behaviors, hyperactivity and cognitive impairment with a tendency of increasing sociability. However, in general, they showed less severe phenotypes compared to $Tg^{SHANK2A}$ mice.

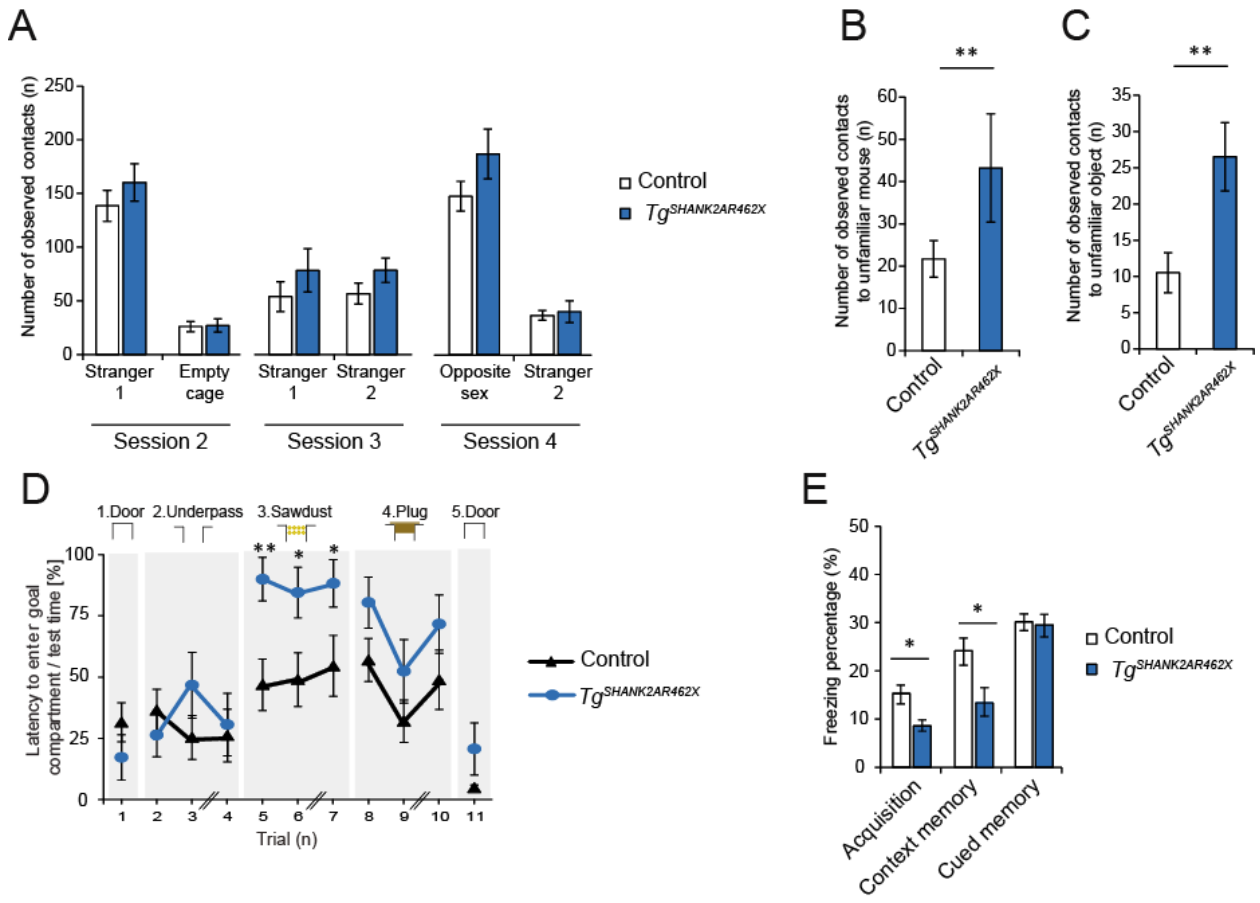

Figure 19: Characterization of the social behavior, cognitive function and emotional learning in *Tg*^{SHANK2AR462X} mice

(A) In the three-chamber social test, *Tg*^{SHANK2AR462X} and control mice made the same average number of contact to all stranger mice in all sessions. **(B)** The direct social interaction test revealed significant more contacts by *Tg*^{SHANK2AR462X} mice to unfamiliar same-sex mice than control mice. **(C)** The novel object recognition test revealed significant more observed contacts to an unfamiliar object by *Tg*^{SHANK2AR462X} mice than by control mice. **(D)** In the puzzle box test, *Tg*^{SHANK2AR462X} mice exhibited less ability and higher latency to solve the puzzle in trials 5, 6 and 7. **(E)** The emotional learning was investigated using the fear conditioning test and revealed less freezing percentages in the acquisition and context memory phases in *Tg*^{SHANK2AR462X} mice (n = 10 *Tg*^{SHANK2AR462X} and 16 control mice at 6 – 9 months of age). Error bars indicate SEM (Two-way ANOVA,*$p \leq 0.05$, **$p \leq 0.01$).

3.2.4 Electrophysiological analysis of *Tg*^{SHANK2A} and *Tg*^{SHANK2AR462X} mice

The results from the behavior analysis of *Tg*^{SHANK2A} and *Tg*^{SHANK2AR462X} mice implicated a possible disruption of synaptic function and transmission leading to the behavioral abnormalities. Therefore, the effects of SHANKA and SHANK2A(R462X) overexpression on the distribution of synaptic NMDARs and AMPARs in the hippocampus were evaluated. In collaboration with Dr. Andrey Rozov from the Institute of Physiology and Pathophysiology of the Heidelberg University, whole-cell voltage clamp recordings in CA1 pyramidal neurons from *Tg*^{SHANK2A}, *Tg*^{SHANK2AR462X} and control mice were performed. First, the contribution of AMPARs to the

synaptic response in $Tg^{SHANK2A}$, $Tg^{SHANK2AR462X}$ and control mice was found to be significantly higher at synapses located on the apical than on the basal dendrites, as indicated by larger AMPA/NMDA ratio values **(Figures 20)**. In $Tg^{SHANK2A}$ mice, a strong enhancement of AMPAR-mediated currents at the apical inputs was observed, and the ratio was significantly higher than in both $Tg^{SHANK2AR462X}$ and control mice. In contrast, the AMPA/NMDA ratios measured at basal dendrite synapses were similar in $Tg^{SHANK2A}$, $Tg^{SHANK2AR462X}$ and control mice **(Figures 20)**.

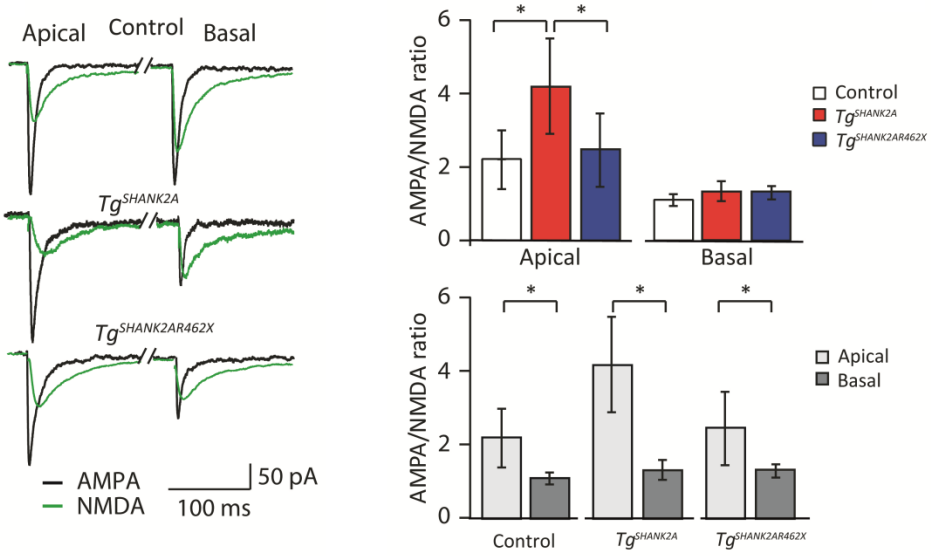

Figure 20: AMPA/NMDA ratio in the apical and basal dendrites in CA1 pyramidal neurons from $Tg^{SHANK2A}$ and $Tg^{SHANK2AR462X}$ mice
Averaged AMPAR (black) and NMDAR (green) mediated EPSCs evoked by stimulation of inputs to the apical and to the basal dendrites of CA1 pyramidal neurons. The AMPA/NMDA ratio measurements revealed a higher ratio in the apical dendrites in the CA1 hippocampal region from $Tg^{SHANK2A}$ but not $Tg^{SHANK2AR462X}$ mice, compared with control mice. No difference in the AMPA/NMDA ratio was found between $Tg^{SHANK2A}$, $Tg^{SHANK2AR462X}$ and control mice in the basal dendrites in CA1 hippocampal region (n = 10 neurons per each genotype of mice at 4 – 7 weeks of age). Error bars indicate standard deviation (SD) (unpaired two-tailed Student's t-test,*$p \leq 0.05$). Experimental data were provided by Dr. Andrey Rozov.

Selective enhancement of AMPAR-mediated EPSC at stratum radiatum synapses in $Tg^{SHANK2A}$ mice indicates either an increase of synaptic channel density or a change of AMPAR subunit composition from low conductance GluA2-containing to high conductance GluA2-lacking channels. To assess this, the sensitivity of these two inputs to the selective GluA2-lacking AMPAR channel blocker, 1-Naphthyl acetyl spermine (Naspm), was tested. After obtaining a stable baseline (more than 100 sweeps), Naspm was applied at a concentration of 100 µM. At the apical dendrite synapses of $Tg^{SHANK2AR462X}$ and control mice, the drug administration resulted in a small reduction of AMPAR-mediated EPSC **(Figure 21)**. However, in the basal dendrite

synapses, Naspm caused a robust reduction of EPSC amplitudes, suggesting a high expression of GluA2-lacking AMPARs in the basal dendrites. In contrast, AMPAR-mediating input to the apical dendrites in $Tg^{SHANK2A}$ gained a strong sensitivity to the blocker, while synapses in stratum oriens became totally resistant to the Naspm application **(Figure 21)**.

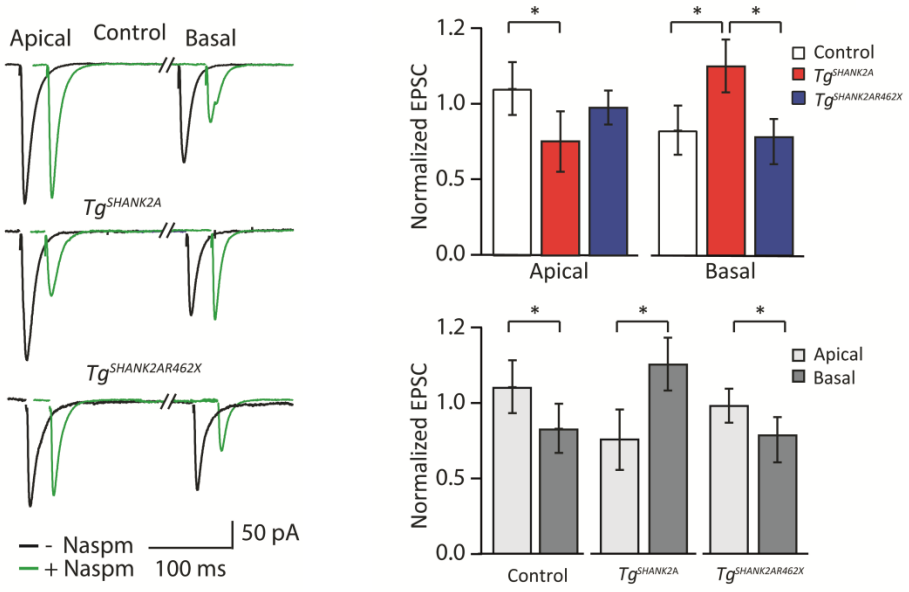

Figure 21: Analysis of AMPAR-mediated EPSC in the apical and basal dendrites in CA1 pyramidal neurons from $Tg^{SHANK2A}$ and $Tg^{SHANK2AR462X}$ mice with selective GluA2-lacking AMPAR channel blocker
Averaged AMPAR mediated EPSCs before (black) and after (green) Naspm application, a blocker of AMPARs lacking the GluA2 subunit, recorded upon stimulation of stratum oriens and stratum radiatum. Naspm treatment decreased the current in the apical dendrites of $Tg^{SHANK2A}$ mice, but not of $Tg^{SHANK2AR462X}$ or control mice. In the basal dendrites, Naspm treatment decreased the current of $Tg^{SHANK2AR462X}$ and control mice, but not $Tg^{SHANK2A}$ mice. This suggests a difference of AMPAR subunit composition in the apical and basal dendrites between $Tg^{SHANK2A}$ compared with $Tg^{SHANK2AR462X}$ and control mice (n = 5 neurons per each genotype of mice at 4 – 7 weeks of age). Error bars indicate SD (unpaired two-tailed Student's t-test,*$p \leq 0.05$). Experimental data were provided by Dr. Andrey Rozov.

The effect of sub-cellular redistribution of GluA2-lacking AMPAR on the long-term plasticity in CA1 pyramidal cells was tested by comparing the levels of LTP evoked at apical or basal dendrite synapses between $Tg^{SHANK2A}$, $Tg^{SHANK2AR462X}$ and control mice. At stratum radiatum, synapses pairing protocol induced similar LTP in the three genotypes **(Figure 22)**. At the basal dendrite synapses in $Tg^{SHANK2AR462X}$ and control mouse slices, pairing triggered small but stable potentiation **(Figure 22)**. In contrast, the same induction protocol in $Tg^{SHANK2A}$ mice did not result in LTP at stratum oriens synapses **(Figure 22)**.

In summary, $Tg^{SHANK2A}$ but not $Tg^{SHANK2AR462X}$ mice revealed impairment on the electrophysiological level due to the inhibition of the developmental dependent AMPAR subtype switch in the basal dendrites of the hippocampus.

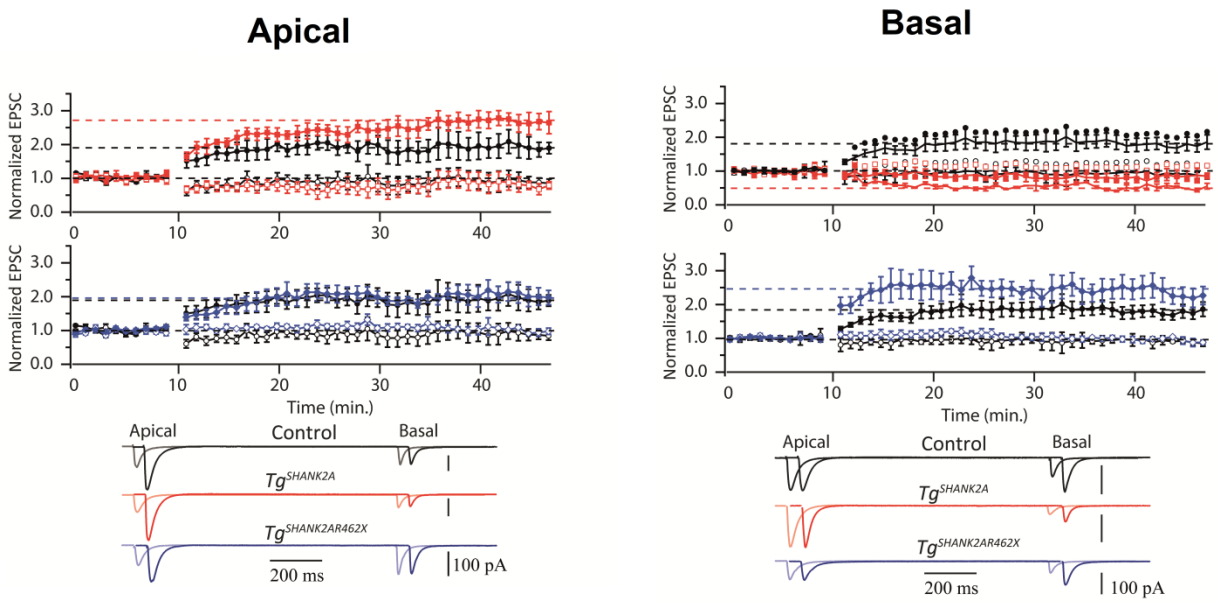

Figure 22: long-term potentiation measurement in CA1 pyramidal neurons from $Tg^{SHANK2A}$, $Tg^{SHANK2AR462X}$ and control mice

(Left) LTP evoked by pairing stimulation of synaptic inputs to the synapses located on CA1 pyramidal cell apical dendrites (filled symbols). Inputs to the basal dendrite were used as control pathway (open symbols). $Tg^{SHANK2A}$, $Tg^{SHANK2AR462X}$ and control mice had similar induced LTP in the apical dendrites using synapses pairing protocol. **(Right)** Results of pairing stimulation of synaptic inputs to the synapses located on CA1 pyramidal cell basal dendrites (filled symbols). Inputs to the apical dendrite were used as control pathway (open symbols). The same pairing protocol induced stable LTP in $Tg^{SHANK2AR462X}$ and control mice, but not in $Tg^{SHANK2A}$ mice (n = 10 neurons per each genotype of mice at 4 – 7 weeks of age). Experimental data were provided by Dr. Andrey Rozov.

3.2.5 Gene expression analysis in the hippocampus of $Tg^{SHANK2A}$ and $Tg^{SHANK2AR462X}$ mice

To identify disrupted neural signaling pathways in the hippocampus of $Tg^{SHANK2A}$ and $Tg^{SHANK2AR462X}$ mice, the expression levels of key signaling proteins in AMPA-, NMDA-, mGluR-, and GABA-pathways were studied on RNA level using the nCounter analysis. The comparative expression analysis of $Tg^{SHANK2A}$ and $Tg^{SHANK2AR462X}$ mice revealed a downregulation of AMPAR and mGluR genes in both transgenic mouse models **(Figure 23)**. Additionally, $Tg^{SHANK2A}$ mice showed a downregulation in the expression of two NMDAR genes *Grin2a* and *Grin2b*, while $Tg^{SHANK2AR462X}$ mice showed a downregulation of Oxytocin and Serotonin 2A receptor gene expression. Both $Tg^{SHANK2A}$ and $Tg^{SHANK2AR462X}$ mice did not show any difference in

the expression of endogenous *Shank* genes or the gene for $GABA_A$ receptor subunit alpha 1 gene (*Gabra1*) **(Figure 23)**.

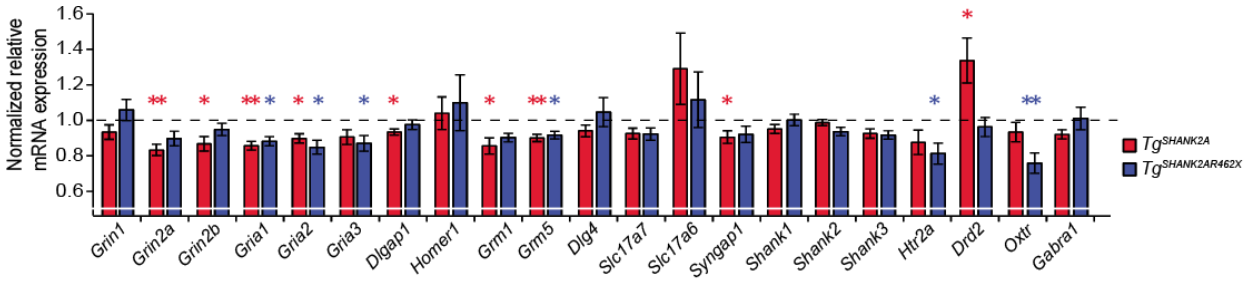

Figure 23: Comparative expression analysis of genes in the hippocampus of $Tg^{SHANK2A}$ and $Tg^{SHANK2AR462X}$ mice

Normalized RNA expression analysis of $Tg^{SHANK2A}$ mice using the nCounter analysis revealed a nominal significant upregulation of *Drd2* and a downregulation of the NMDAR genes (*Grin2a* and *Grin2b*), AMPAR genes (*Gria1* and *Gria2*), mGluR genes (*Grm1* and *Grm5*), in addition to *Dlgap1*, and *Syngap1* (n= 8 $Tg^{SHANK2A}$ and 11 control mice, 3 – 5 months). The expression analysis of $Tg^{SHANK2AR462X}$ mice revealed a nominal significant downregulation of the AMPAR genes (*Gria1*, *Gria2* and *Gria3*), *Grm5*, Serotonin 2A receptor (*Htr2a*) and Oxytocin receptor (*Oxtr*) genes (n= 7 $Tg^{SHANK2AR462X}$ and 7 control mice, 3 – 5 months). Error bars indicate SEM (Unpaired two-tailed Student's t-test, $*p \leq 0.05$, $**p \leq 0.01$).

The expression level of various proteins in the total protein lysate from the hippocampus of $Tg^{SHANK2A}$ and $Tg^{SHANK2AR462X}$ mice was investigated by western blot analysis in order to confirm the results obtained on RNA level. In $Tg^{SHANK2A}$ mice, the protein levels of NMDAR subunit (GluN2A) and Homer 1 were significantly increased **(Figure 24)**, whereas the levels of the AMPAR subunits (GluA1 and GluA2) and mGluR1 were decreased **(Figure 24)**. In $Tg^{SHANK2AR462X}$ mice, immunoblots confirmed the downregulation of the AMPAR subunits (GluA1 and GluA2) and Serotonin 2A receptor (5-HT2A), which was obtained from the nCounter analysis **(Figure 24)**.

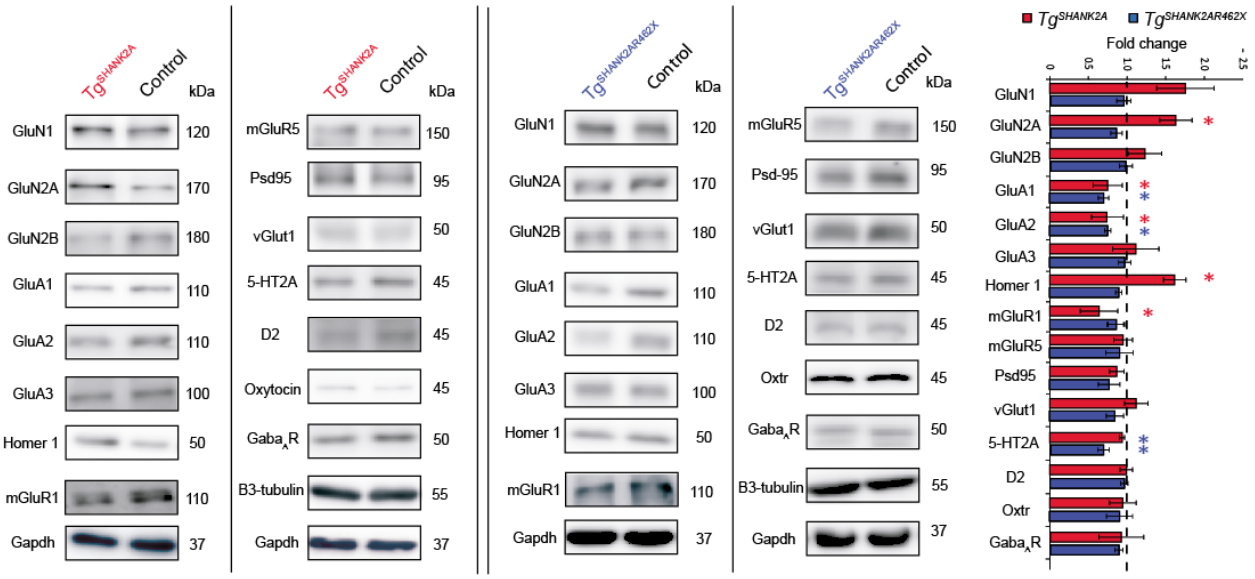

Figure 24: Protein analysis in the hippocampus of *Tg*^{SHANK2A} and *Tg*^{SHANK2AR462X} mice
Total protein lysate analysis in the hippocampus of *Tg*^{SHANK2A} revealed increased levels of GluN2A and Homer1, and a decreased amounts of GluA1, GluA2 and mGluR1 (n = 5 mice for each genotype, 3 – 5 months old). For *Tg*^{SHANK2AR462X}, total protein lysate analysis of the hippocampus revealed lower GluA, GluA2 and 5-HT2A levels (n = 6 mice for each genotype, 3 – 5 months). Error bars indicate SEM (Unpaired two-tailed Student's t-test, *$p \leq 0.05$, **$p \leq 0.01$).

The Excitatory/ inhibitory imbalance has been shown to play a role in the pathophysiology of ASD [183-188]. Therefore, the expression of the interneuronal marker, parvalbumin (PV), was investigated in the hippocampus of *Tg*^{SHANK2A}, *Tg*^{SHANK2AR462X} and control mice and revealed fewer PV-positive cells in the DG and CA1 regions of the hippocampus of *Tg*^{SHANK2A} mice compared with *Tg*^{SHANK2AR462X} and control mice **(Figure 25)**.

In summary, *Tg*^{SHANK2A} mice showed more severe dysregulation of gene expression in the hippocampus compared to *Tg*^{SHANK2AR462X} mice, which is consistent with the more severe behavioral phenotypes observed in *Tg*^{SHANK2A} mice.

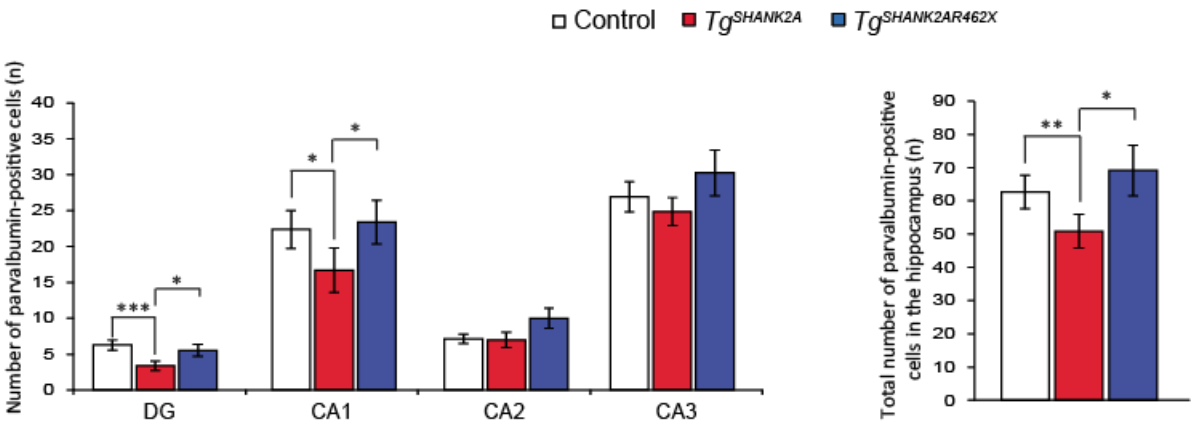

Figure 25: Quantitative expression analysis of parvalbumin in the hippocampus of $Tg^{SHANK2A}$ and $Tg^{SHANK2AR462X}$ mice
(Left) The numbers of PV-positive cells in the DG, CA1, CA2 and CA3 regions are shown. **(Right)** The total number of PV-positive cells in the whole hippocampus of $Tg^{SHANK2A}$ mice was reduced compared with $Tg^{SHANK2AR462X}$ and control mice. The displayed values show the mean values of 3 mice per each group (6 slices/mouse). Error bars indicate SEM (Unpaired two-tailed Student's t-test, *$p \leq 0.05$, **$p \leq 0.01$).

3.2.6 Synaptosome and gene ontology analysis in the hippocampus of $Tg^{SHANK2A}$ and $Tg^{SHANK2AR462X}$ mice

Large-scale proteomic analysis of synaptosome was performed in order to check the localization of proteins in the synapse using the mass spectrometry. In total, 2466 proteins were identified in the synaptosomal fractions from the hippocampus. For the $Tg^{SHANK2A}$ mice, 107 proteins were differentially expressed in synaptosomes compared with control mice ($p \leq 0.05$) (25 more and 82 less abundant) **(Appendix 4) (**data provided by Prof. A.B. Smit). For the $Tg^{SHANK2AR462X}$ mice, 55 proteins were differentially expressed in synaptosomes compared with control mice ($p \leq 0.05$) (19 more and 36 less abundant) **(Appendix 4) (**data provided by Prof. A.B. Smit). Next, the gene ontology analysis using the free online database ConsensusPathDB was performed. The Kegg pathway analysis of the differentially abundant proteins in the synaptosomes of $Tg^{SHANK2A}$ mouse hippocampus suggested that the glutamatergic synapses were affected **(Figure 26)**. For $Tg^{SHANK2AR462X}$, the Kegg pathway analysis revealed that the axon guidance pathway was mainly disrupted **(Figure 26)**.

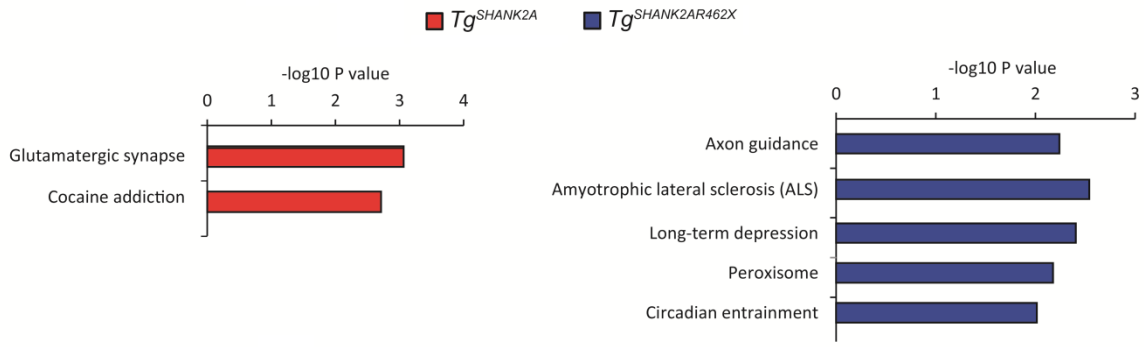

Figure 26: Synaptosome and pathway analysis in the hippocampus of $Tg^{SHANK2A}$ and $Tg^{SHANK2AR462X}$ mice The online database ConsensusPathDB predicted the affected pathways in $Tg^{SHANK2A}$ and $Tg^{SHANK2AR462X}$ mice by the analysis of differentially abundant proteins in the synaptosome of the hippocampus.

With regard to the biological processes, social, vocalization, learning and memory behaviors were predicted to be affected in $Tg^{SHANK2A}$ mice, in addition to an effect on neurogenesis, long term synaptic potentiation and regulation of AMPAR activity **(Figure 27)**. In $Tg^{SHANK2AR462X}$

mice, the behavioral functions and the regulation of the molecular functions were predicted to be disturbed **(Figure 27)**.

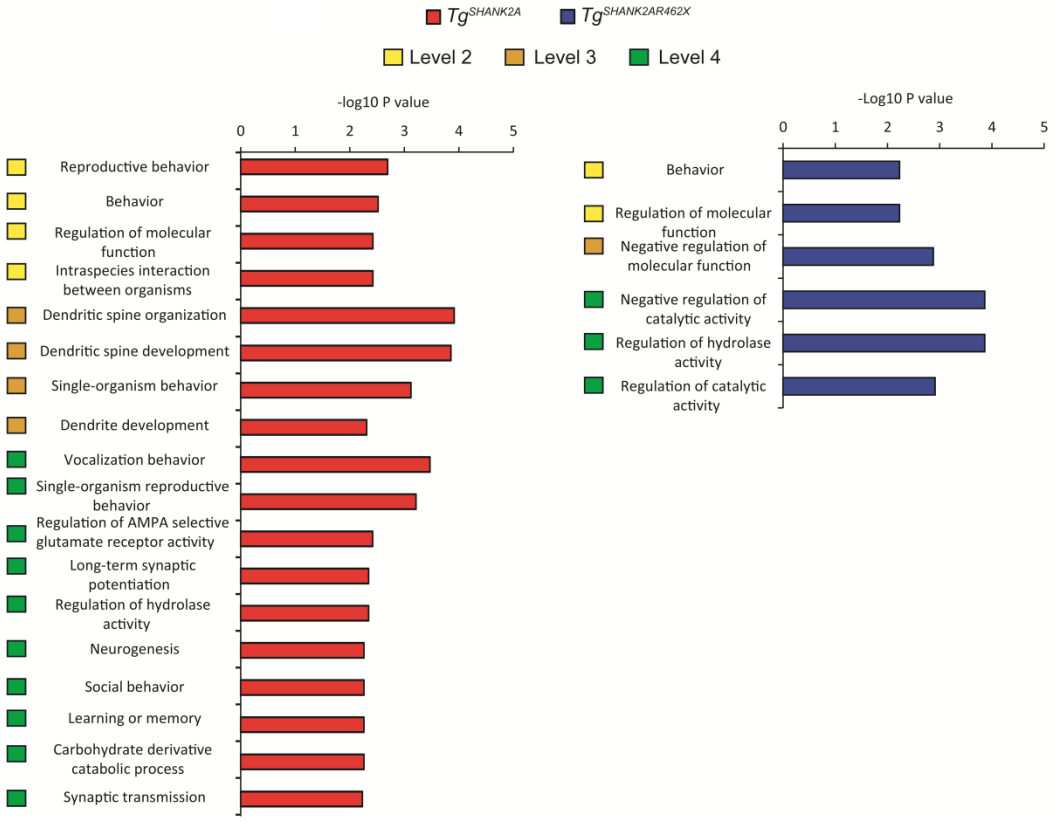

Figure 27: Biological process analysis in the hippocampus of $Tg^{SHANK2A}$ and $Tg^{SHANK2AR462X}$ mice
The figure shows a list of the affected biological processes in $Tg^{SHANK2A}$ and $Tg^{SHANK2AR462X}$ mice predicted by the online database ConsensusPathDB by the analysis of differentially abundant proteins in the synaptosome of the hippocampus. The terms used in the biological process analysis appear at different levels (level 2, 3 and 4). The higher the level, the more specific is the respective term.

With respect to the molecular function, the protein complex scaffold and binding, especially for the glutamatergic receptors were predicted to be affected in $Tg^{SHANK2A}$ mice **(Figure 28)**. In $Tg^{SHANK2AR462X}$, the semaphorin receptor activity was likely affected **(Figure 28)**.

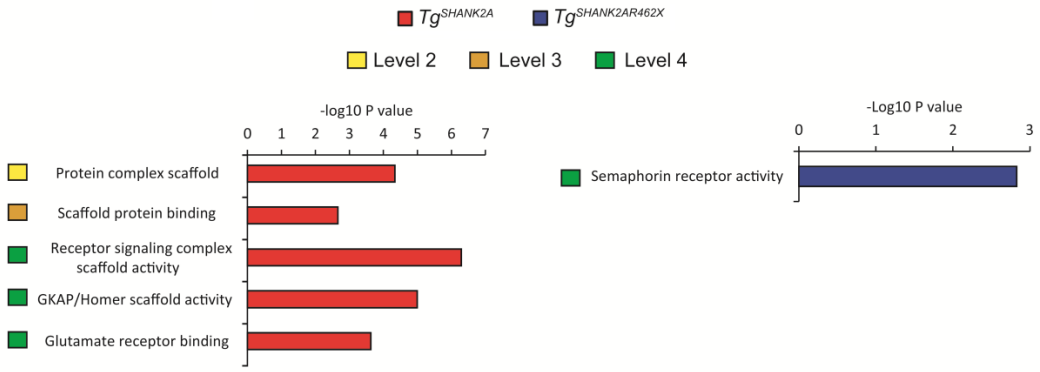

Figure 28: Molecular function analysis in the hippocampus of *Tg*^{SHANK2A} and *Tg*^{SHANK2AR462X} mice
The molecular function analysis of differentially abundant proteins in the synaptosome of the hippocampus, which was done by the online database ConsensusPathDB, predicted affected synaptic protein complex in *Tg*^{SHANK2A} mice and affected semaphorin receptor activity in *Tg*^{SHANK2AR462X} mice. The terms used in the molecular function analysis appear at different levels (level 2, 3 and 4). The higher the level, the more specific is the respective term.

Regarding the cellular components, the synaptic membranes, neuronal parts, postsynaptic density and cell projection parts were suggested to be affected in both *Tg*^{SHANK2A} and *Tg*^{SHANK2AR462X} mice **(Figure 29)**.

In summary, the synaptic protein composition was altered differently in both mouse lines, indicating mainly presynaptic components in SHANK2A(R462X) and more postsynaptic components in SHANK2A overexpressing mice. The function of the glutamatergic synapse in *Tg*^{SHANK2A} mice was mainly disturbed, leading to more severe behavioral and electrophysiological dysfunction. In contrast, the axon and dendrites branching in *Tg*^{SHANK2AR462X} mice were suggested to be dysregulated, which can account for some of the behavioral abnormalities of *Tg*^{SHANK2AR462X} mice.

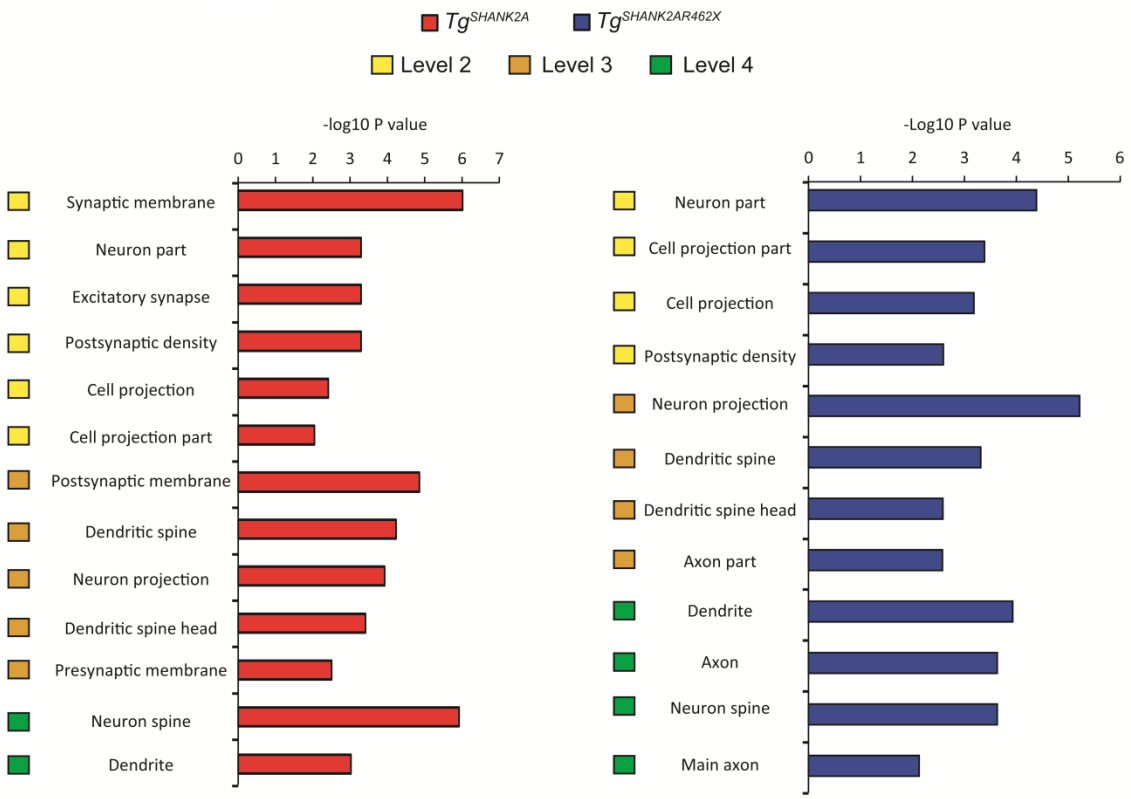

Figure 29: Cellular component analysis in the hippocampus of *Tg*^{SHANK2A} and *Tg*^{SHANK2AR462X} mice
The cellular component, synaptic membrane, neuron part, postsynaptic density and cell projection part were likely affected in both *Tg*^{SHANK2A} and *Tg*^{SHANK2AR462X} mice. The terms used in the cellular component analysis appear at different levels (level 2, 3 and 4). The higher the level, the more specific is the respective term.

3.2.7 Switching off the SHANK2A overexpression in adult *Tg*^{SHANK2A} mice

To analyze which phenotype described in chapter **3.2.2** can be rescued by the stop of SHANK2A overexpression in adulthood, adult *Tg*^{SHANK2A} mice (5 – 8 months) were received drinking water, supplemented with 2 g/l dox and 5% sucrose **(Figure 30A)**. The duration of dox intake was 1 month to assure the total elimination of the transgene expression and to enable the affected synapses to recover. Using immunofluorescence staining, the total absence of Venus expression after 1 month of dox intake was confirmed in dox-treated *Tg*^{SHANK2A} mice **(Figure 30B)**. In contrast, Eosin/X-gal staining revealed a low enzymatic activity of β-galactosidase at the cellular level in the hippocampus **(Figure 30B)**. The complete absence of SHANK2A and Venus overexpression and the low expression of β-galactosidase were confirmed in dox-treated *Tg*^{SHANK2A} mice by immunoblotting of proteins from the cortex, hippocampus and olfactory bulb **(Figure 30C)**.

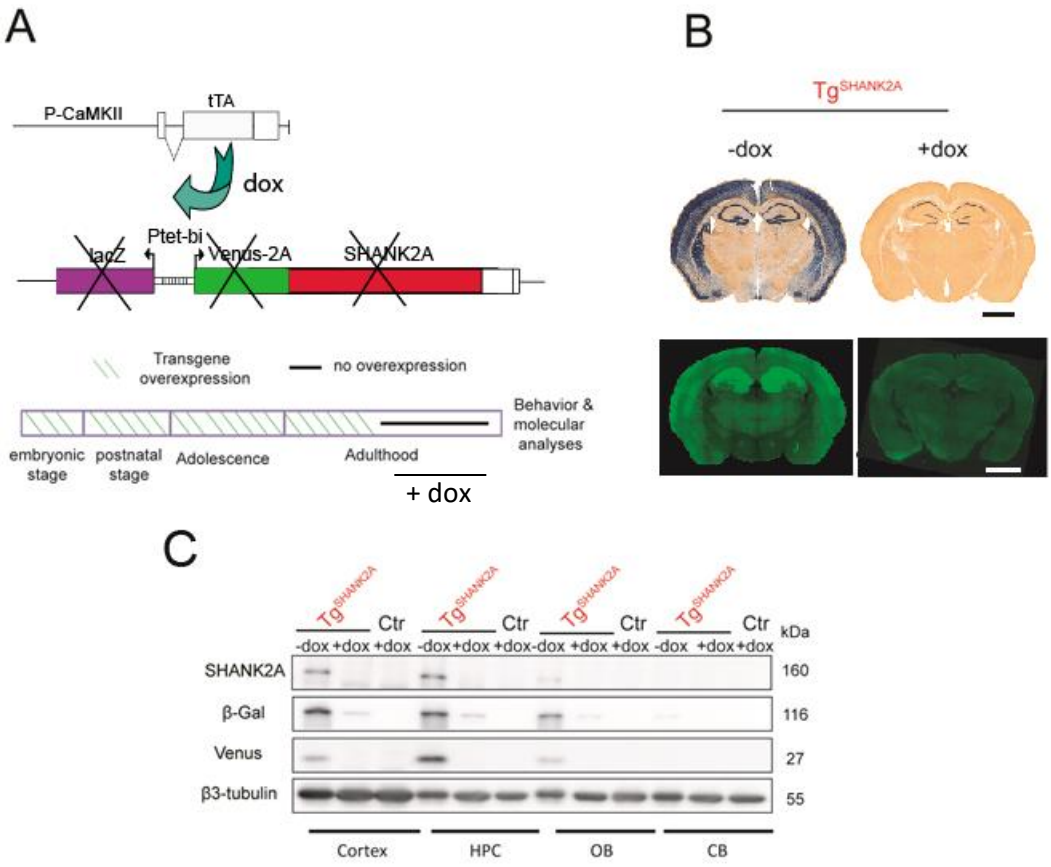

Figure 30: Characterization of *Tg*^{SHANK2A} mice after switching off the transgene overexpression in adulthood

(A) Schematic of the transgenes that were used for the overexpression of SHANK2A. The binding between the transcription activator (tTA) and the bidirectional Ptet-bi promoter of the SHANK2A responder transgene was inhibited by providing the adult mice with 2 g/l dox in water, supplemented with 5% sucrose, for 1 month which caused the inactivation of the transgene expression. **(B)** Eosin/X-gal staining detected some β-galactosidase expression of the lacZ gene at the cellular level in the hippocampus of *Tg*^{SHANK2A} mice after 1 month of dox intake **(upper row)** (scale bar: 2 mm). In contrast, the Venus expression in the forebrain of *Tg*^{SHANK2A} mice was completely absent **(lower row)** (scale bar: 2 mm). **(C)** Protein lysates of different brain tissues from adult *Tg*^{SHANK2A} (*Tg*^{SHANK2A}-dox), dox-treated *Tg*^{SHANK2A} (*Tg*^{SHANK2A}+dox) and dox-treated control mice (Ctr+dox) were analyzed by immunoblotting with SHANK2, β-galactosidase and Venus antibodies and revealed no expression of Venus or SHANK2A and a little expression of β-galactosidase in the cortex, hippocampus and olfactory bulb of dox-treated *Tg*^{SHANK2A} mice. (6 – 9 months), HPC: Hippocampus, OB: Olfactory bulb, CB: Cerebellum.

The detailed behavior analysis of dox-treated *Tg*^{SHANK2A} mice started by applying the SHIRPA test (for a summary, see **Appendix 5**). Dox-treated *Tg*^{SHANK2A} mice showed a reduced body weight compared to dox-treated control mice **(Figure 31A)**. The reduced body weight of dox-treated *Tg*^{SHANK2A} mice is similar to the reduced body weight of *Tg*^{SHANK2A} mice that continuously overexpress SHANK2A transgene in adulthood **(Figure 14A)**. Next, the general behavior of

dox-treated $Tg^{SHANK2A}$ mice was assessed in the LABORAS test. Dox-treated $Tg^{SHANK2A}$ mice were hyperactive **(Figure 31B)** and had longer eating duration **(Figure 31C)** and increased episodes of repetitive rearing **(Figure 31D)**, similar to the previously shown behavior of $Tg^{SHANK2A}$ mice **(Figure 14B-D)**. With regard to the number of self-grooming and climbing in the LABORAS cages, there was no difference between dox-treated $Tg^{SHANK2A}$ and dox-treated control mice. In the nesting test, the impaired nesting behavior of $Tg^{SHANK2A}$ mice **(Figure 14F)** was not rescued by switching off the SHANK2A overexpression in adulthood by dox intake **(Figure 31E)**.

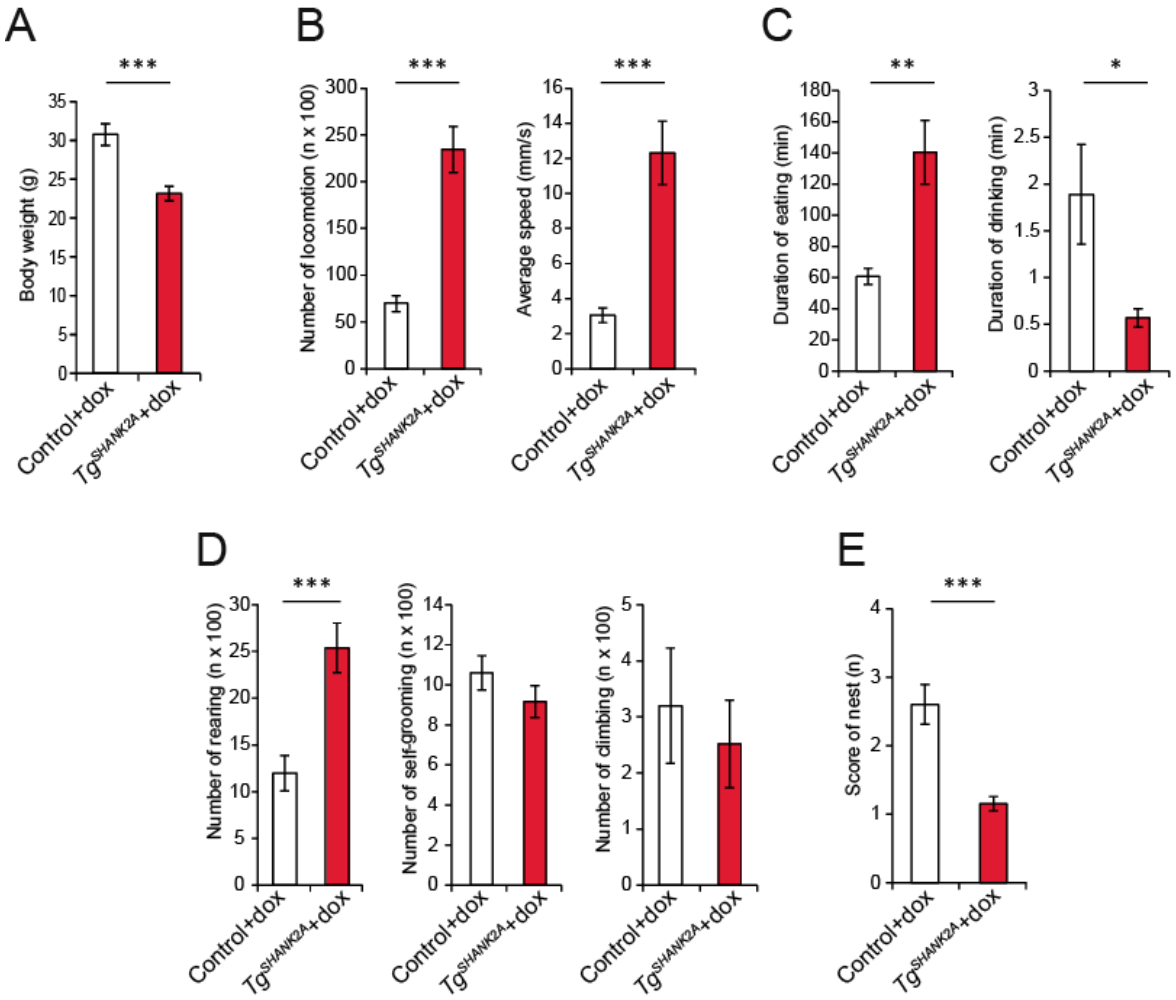

Figure 31: Analysis of general and repetitive behaviors in $Tg^{SHANK2A}$ mice after switching off the transgene overexpression in adulthood
(A) Body weight of dox-treated $Tg^{SHANK2A}$ mice was 30% less than of dox-treated control mice. **(B-D)** The LABORAS test of dox-treated $Tg^{SHANK2A}$ mice revealed hyperactivity behavior as shown by the increased number of locomotion **(B, left)** and the average speed **(B, right)**, increased eating **(C, left)** and decreased drinking durations **(C right)**, increased repetitive rearing **(D, left)** and normal self-grooming **(D, middle)** and climbing **(D, right)**. **(E)** The nesting behavior was impaired in dox-treated $Tg^{SHANK2A}$ (n = 12 dox-treated

$Tg^{SHANK2A}$ and 15 dox-treated control mice at 6 – 9 months of age). Error bars indicate SEM (Two-way ANOVA,*$p \leq 0.05$, **$p \leq 0.01$, ***$p \leq 0.001$).

In the dark-light box and neophobia tests for investigating anxiety, dox-treated $Tg^{SHANK2A}$ mice exhibited anxiety **(Figure 32A, C),** similar to $Tg^{SHANK2A}$ mice without dox treatment **(Figure 15A, C)**. On the other hand, the anxiety displayed by $Tg^{SHANK2A}$ mice in the open field test **(Figure 15B)** was rescued by switching off the transgene overexpression in adulthood **(Figure 32B)**.

In the burrowing test, the retrieval of pellets from the tube was impaired in dox-treated $Tg^{SHANK2A}$ mice after 2 and 12 hrs **(Figure 32D)** similar to $Tg^{SHANK2A}$ mice that continuously express SHANK2A **(Figure 15D)**. In the balance and cliff avoidance tests, the impaired balance ability of $Tg^{SHANK2A}$ mice, but not the impulsive behavior, was rescued in dox-treated $Tg^{SHANK2A}$ mice **(Figure 32E, F)**.

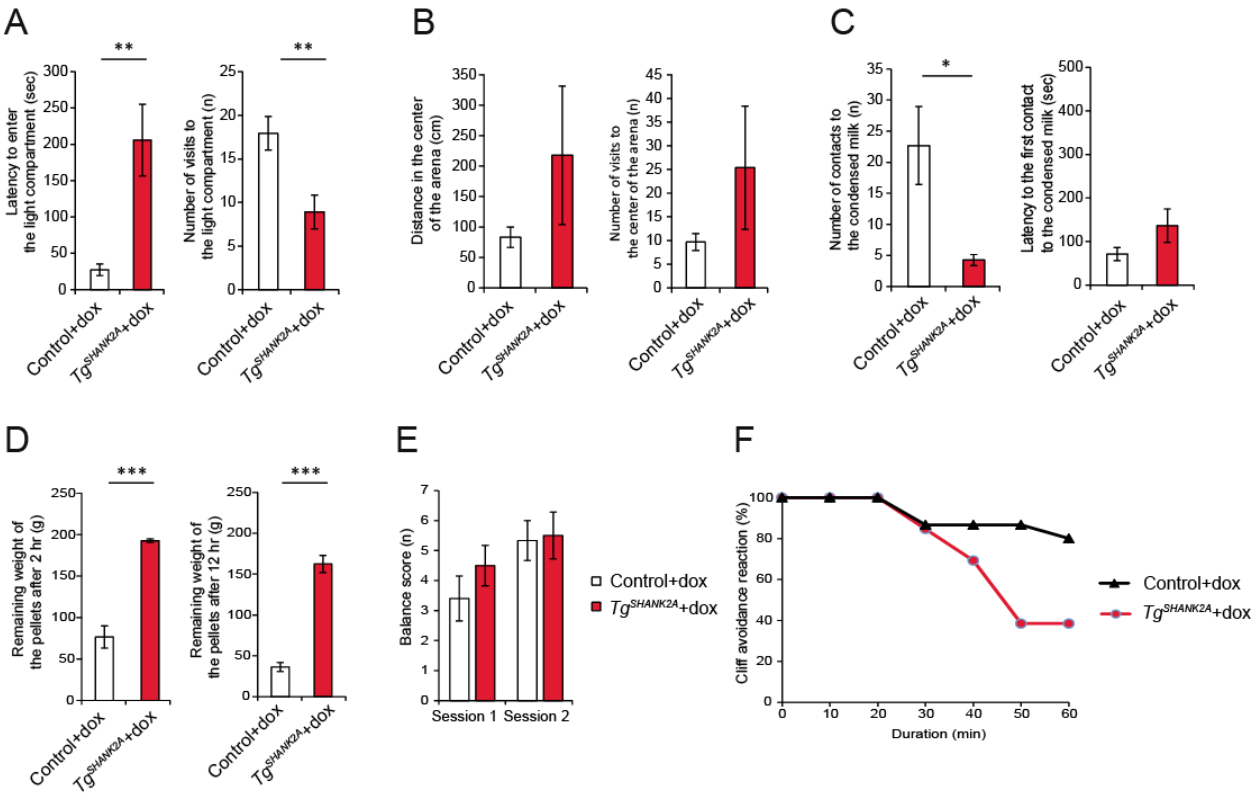

Figure 32: Characterization of anxiety and impulsive behaviors in $Tg^{SHANK2A}$ mice after switching off the transgene overexpression in adulthood

(A) The dark-light box test revealed anxiety in dox-treated $Tg^{SHANK2A}$ as shown by the high latency **(left)** and the decreased number of visits **(right)** to the light compartment compared with dox-treated control mice. **(B)** Dox-treated $Tg^{SHANK2A}$ and control mice traveled a similar distance **(left)** and made a similar number of visits **(right)** to the center of a new arena in the open field test. **(C)** Dox-treated $Tg^{SHANK2A}$ mice exhibited fear of the unfamiliar drink (condensed milk in the center of the arena) in the neophobia test by making few contacts. **(D)**

In the burrowing test, dox-treated $Tg^{SHANK2A}$ mice left more pellets in the tube after 2 hrs **(left)** and 12 hrs **(right)** compared with control mice. **(E)** Dox-treated $Tg^{SHANK2A}$ had no balance impairment in two successive sessions in the balance test. **(F)** Dox-treated $Tg^{SHANK2A}$ mice had a high impulsive reaction in the cliff avoidance test (n = 12 dox-treated $Tg^{SHANK2A}$ and 15 dox-treated control mice at 6 – 9 months of age). Error bars indicate SEM (Two-way ANOVA,*$p \leq 0.05$, **$p \leq 0.01$, ***$p \leq 0.001$).

In the social interaction tests, dox-treated $Tg^{SHANK2A}$ mice exhibited normal social behavior in the three-chamber social test **(Figure 33A)** and the direct social interaction test **(Figure 33B)**. In the novel object recognition test, dox-treated $Tg^{SHANK2A}$ and control mice likewise contacted a novel object in the center of an arena **(Figure 33C)**. This demonstrated that the restoration of balanced, endogenous Shank expression rescued the social impairment of $Tg^{SHANK2A}$ mice in three different social tests. Cognitive and memory functions of dox-treated $Tg^{SHANK2A}$ mice were assessed using the puzzle box and revealed the inability of dox-treated $Tg^{SHANK2A}$ to perform the test efficiently in all trials **(Figure 33D)**. In the fear conditioning test, dox-treated $Tg^{SHANK2A}$ showed increased freezing behavior during the cued memory phase compared with dox-treated control mice, indicating improved memory retrieval **(Figure 33E)**.

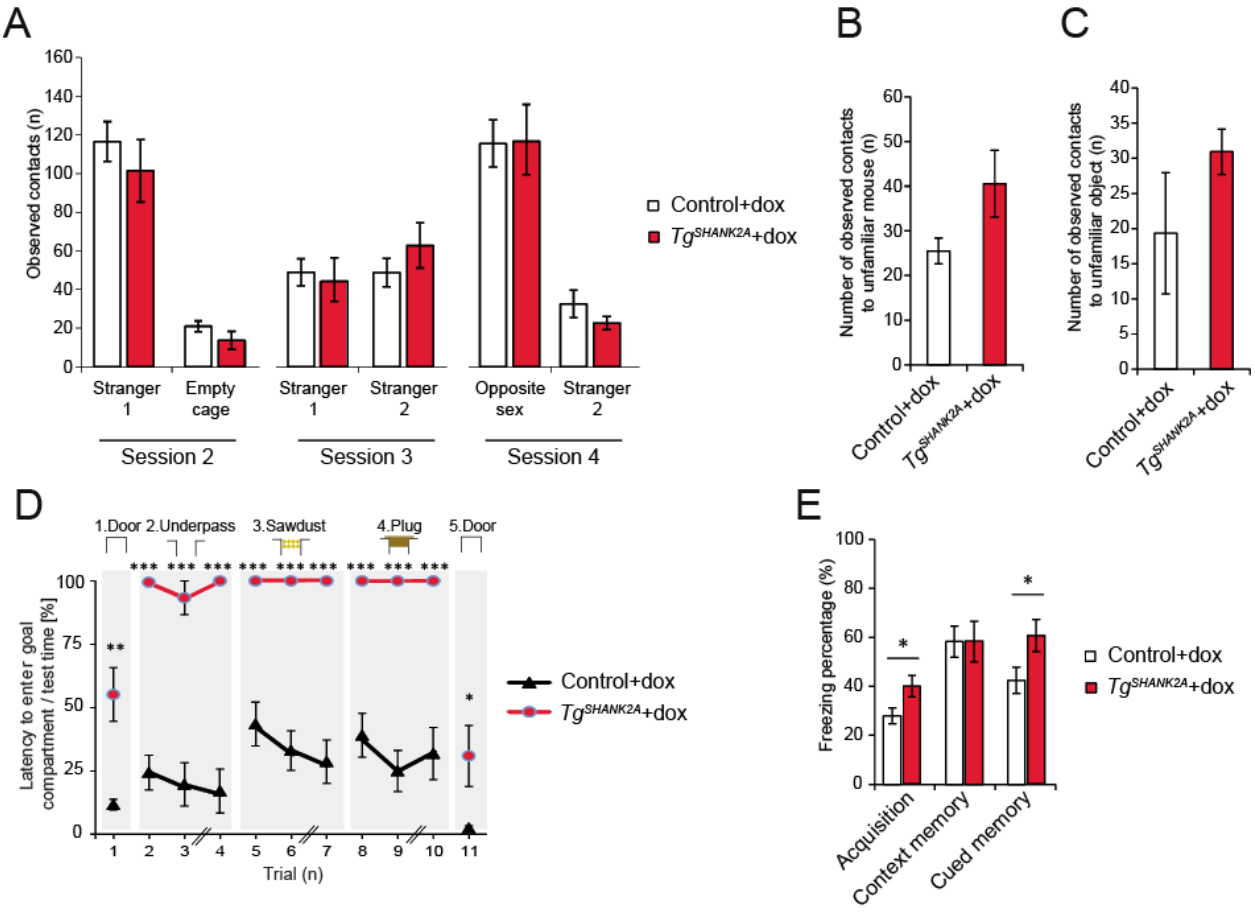

Figure 33: Characterization of the social behavior, cognitive function and emotional learning in $Tg^{SHANK2A}$ mice after switching off the transgene overexpression in adulthood
(A) In the three-chamber social test, dox-treated $Tg^{SHANK2A}$ and control mice displayed similar numbers of contacts to strangers in all sessions. **(B)** In the direct social interaction test, dox-treated $Tg^{SHANK2A}$ and control mice revealed similar numbers of contacts to unfamiliar same-sex mice. **(C)** In the novel object recognition test, dox-treated $Tg^{SHANK2A}$ and control mice made similar numbers of contacts to an unfamiliar object in the center of an arena. **(D)** In the puzzle box test, dox-treated $Tg^{SHANK2A}$ mice showed less ability and higher latency to solve the puzzle in all trials of the test. **(E)** In the fear conditioning test, dox-treated $Tg^{SHANK2A}$ mice showed more freezing percentages in the acquisition and cued memory phases than dox-treated control mice (n = 12 dox-treated $Tg^{SHANK2A}$ and 15 dox-treated control mice at 6 – 9 months of age). Error bars indicate SEM (Two-way ANOVA,*$p \leq 0.05$, **$p \leq 0.01$, ***$p \leq 0.001$).

The comparative nCounter expression analysis in dox-treated $Tg^{SHANK2A}$ mice revealed a downregulation of the AMPAR genes (*Gria1-3*), *Grm1* and *Grm5* **(Figure 34)**. Different from $Tg^{SHANK2A}$ mice that express SHANK2A in adulthood **(Figure 23)**, the expression of the Serotonin 2A receptor (*Htr2a*) and Oxytocin receptor (*Oxtr*) genes in dox-treated $Tg^{SHANK2A}$ mice were downregulated, and the expression of *Grin2a* and *Grin2b* was normal **(Figure 34)**.

In summary, stopping SHANK2A overexpression in adulthood revealed a rescue of the social impairment that was shown before in $Tg^{SHANK2A}$ mice, but not other ASD-like behaviors. The normal social behavior was accompanied by a normal expression of NMDAR genes in the hippocampus.

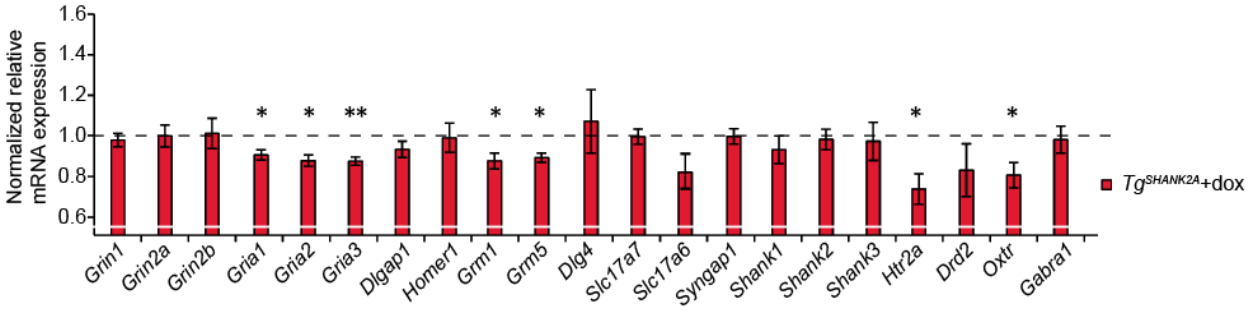

Figure 34: Comparative expression analysis of genes in the hippocampus of $Tg^{SHANK2A}$ mice after switching off the transgene overexpression in adulthood
Normalized RNA expression analysis of dox-treated $Tg^{SHANK2A}$ mice using nCounter analysis revealed a nominal significant downregulation of the AMPAR (*Gria1*, *Gria2* and *Gria3*) and mGluR genes (*Grm1* and *Grm5*), in addition to *Htr2a* and *Oxtr* (n= 7 dox-treated $Tg^{SHANK2A}$ and 8 dox-treated control mice, 3 – 5 months). Error bars indicate SEM (Unpaired two-tailed Student's t-test, *$p \leq 0.05$, **$p \leq 0.01$).

3.2.8 Switching off the SHANK2A(R462X) overexpression in adult $Tg^{SHANK2AR462X}$ mice

The SHANK2A(R462X) overexpression was switched off in adult mice as described above for SHANK2A overexpressing mice. Using immunofluorescence staining, the absence of Venus expression in the sagittal sections of dox-treated $Tg^{SHANK2AR462X}$ mouse brains was confirmed **(Figure 35B)**. Moreover, Eosin/X-gal staining revealed no β-galactosidase expression of the

lacZ gene **(Figure 35B)**. The complete absence of SHANK2A(R462X), Venus and β-galactosidase expression was confirmed using immunoblots of total protein lysates from the cortex, hippocampus and olfactory bulb **(Figure 35C)**.

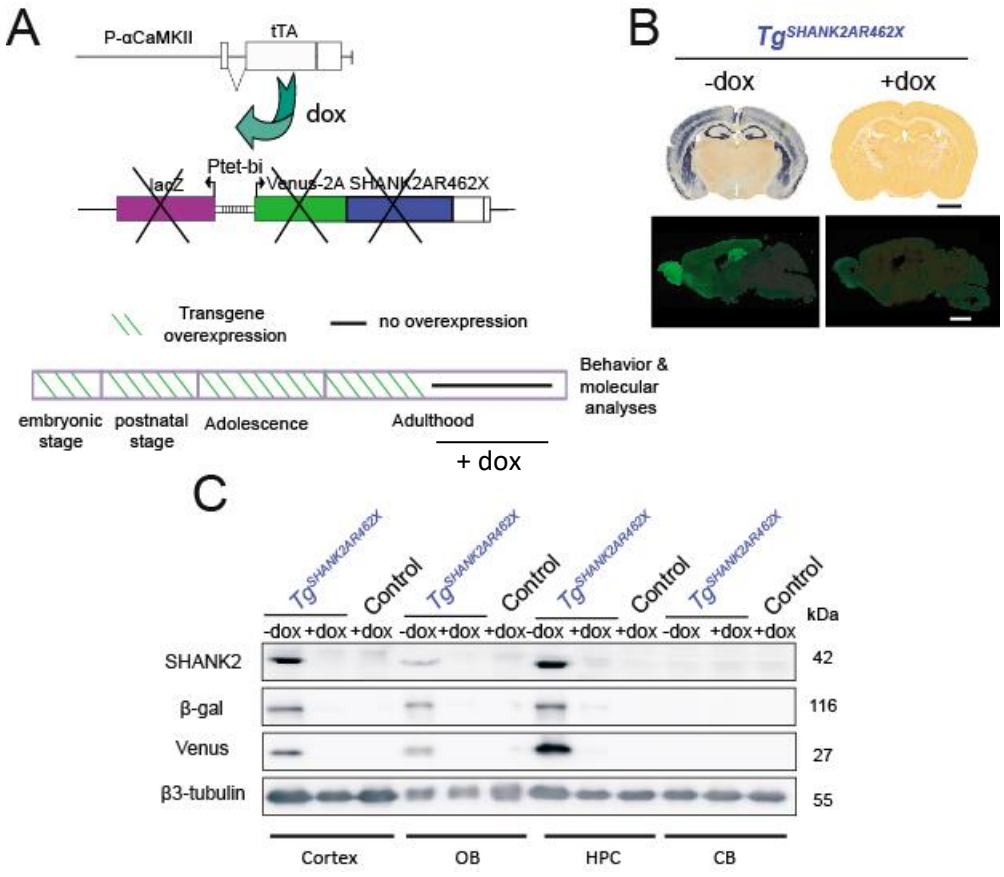

Figure 35: Characterization of *Tg*^{SHANK2AR462X} mice after stopping the transgene overexpression in adulthood

(A) Schematic of the transgenes that were used for the overexpression of SHANK2A(R462X). The binding between tTA and the bidirectional Ptet-bi promoter of the SHANK2A(R462X) transgene was inhibited by providing adult mice with dox in the water for 1 month which inactivated the transgene overexpression. **(B)** Eosin/X-gal staining revealed no β-galactosidase expression of the lacZ gene at the cellular level of *Tg*^{SHANK2AR462X} mice after 1 month of dox intake **(upper row)** (scale bar: 2 mm). Immunofluorescence of the sagittal sections of *Tg*^{SHANK2AR462X} mouse brains revealed no Venus expression in the forebrain of dox-treated *Tg*^{SHANK2AR462X} mice **(lower row)** (scale bar: 2 mm). **(C)** Protein lysates of different brain tissues from adult *Tg*^{SHANK2AR462X} without dox treatment (-dox), dox-treated *Tg*^{SHANK2AR462X} (*Tg*^{SHANK2AR462X}+dox) and dox-treated control mice (Ctr+dox) were analyzed by immunoblotting with SHANK2, β-galactosidase and Venus antibodies and revealed the absence of the transgene expression in dox-treated *Tg*^{SHANK2AR462X} (6 – 9 months), HPC: Hippocampus, OB: Olfactory bulb, CB: Cerebellum.

Dox-treated *Tg*^{SHANK2AR462X} mice showed no abnormal behavior in the SHIRPA test as noticed before for *Tg*^{SHANK2AR462X} mice (for a summary, see **Appendix 5**). Only the 10% body weight reduction of *Tg*^{SHANK2AR462X} was blunted, most likely due to the sucrose supplement in the

drinking water **(Figure 36A)**. Similarly, in the LABORAS test, dox-treated *Tg*^{SHANK2AR462X} mice showed similar phenotype as SHANK2A(R462X) overexpressing adult mice **(Figure 17B-D)** including hyperactivity **(Figure 36B)**, decreased self-grooming **(Figure 36D)**, normal drinking duration **(Figure 36C)** and a normal number of rearing and climbing **(Figure 36D)**. Moreover, dox-treated *Tg*^{SHANK2AR462X} mice had no impairment in the nesting test **(Figure 36E)** similar to *Tg*^{SHANK2AR462X} mice **(Figure 17F)**.

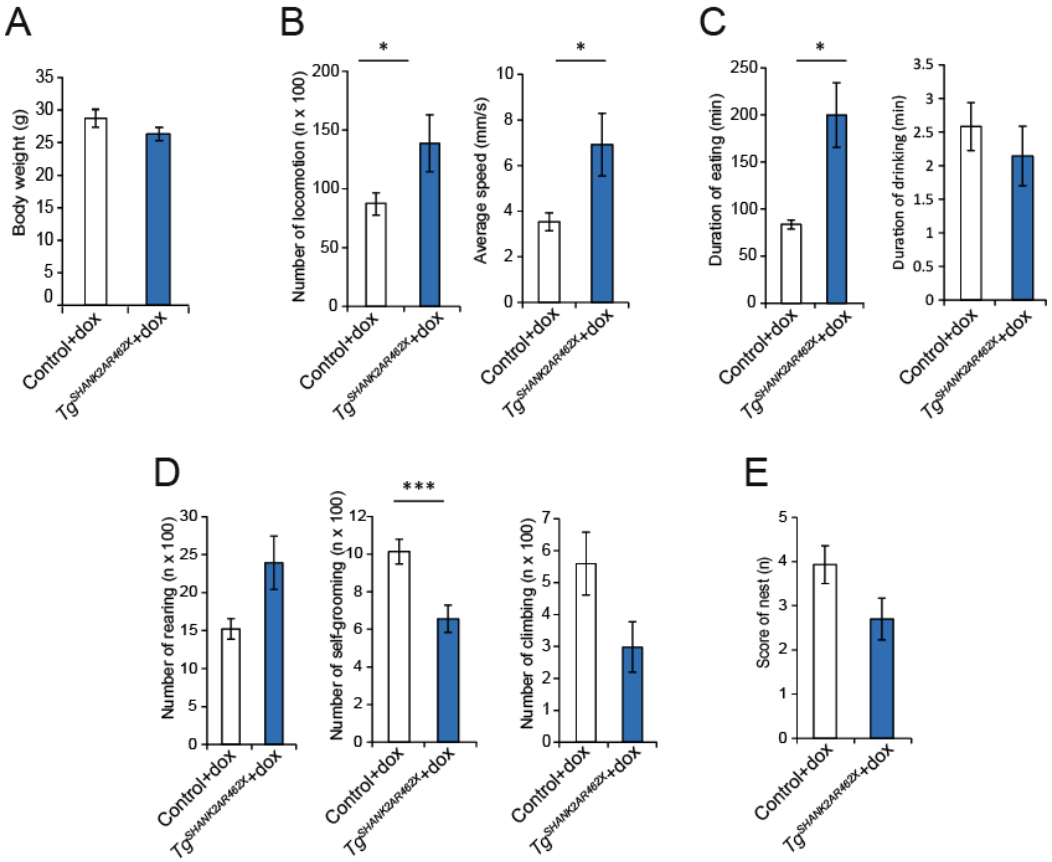

Figure 36: Analysis of general and repetitive behaviors in *Tg*^{SHANK2AR462X} mice after switching off the transgene overexpression in adulthood
(A) Body weights of dox-treated *Tg*^{SHANK2AR462X} mice were similar to dox-treated control mice. **(B-D)** LABORAS test of dox-treated *Tg*^{SHANK2AR462X} mice revealed hyperactivity as shown increased number of locomotion **(B, left)** and average speed **(B, right)**, increased eating **(C, left)** but normal drinking **(C, right)** durations, and normal number of rearing **(D, left)** and climbing **(D, right)** but less self-grooming **(D, middle)**. **(E)** Dox-treated *Tg*^{SHANK2AR462X} had no impairment in the nesting test (n = 10 dox-treated *Tg*^{SHANK2AR462X} and 14 dox-treated control mice at 6–9 months of age). Error bars indicate SEM (Two-way ANOVA,*$p \leq 0.05$, ***$p \leq 0.001$).

In contrast to *Tg*^{SHANK2AR462X} mice **(Figure 18A-C)**, the dox-treated *Tg*^{SHANK2AR462X} mice showed high anxiety levels in the dark-light box, open field and neophobia tests **(Figure 37A-C)**.

However, they had similar impairment in the burrowing and cliff avoidance tests, and no impairment in the balance test **(Figure 37D-F)**

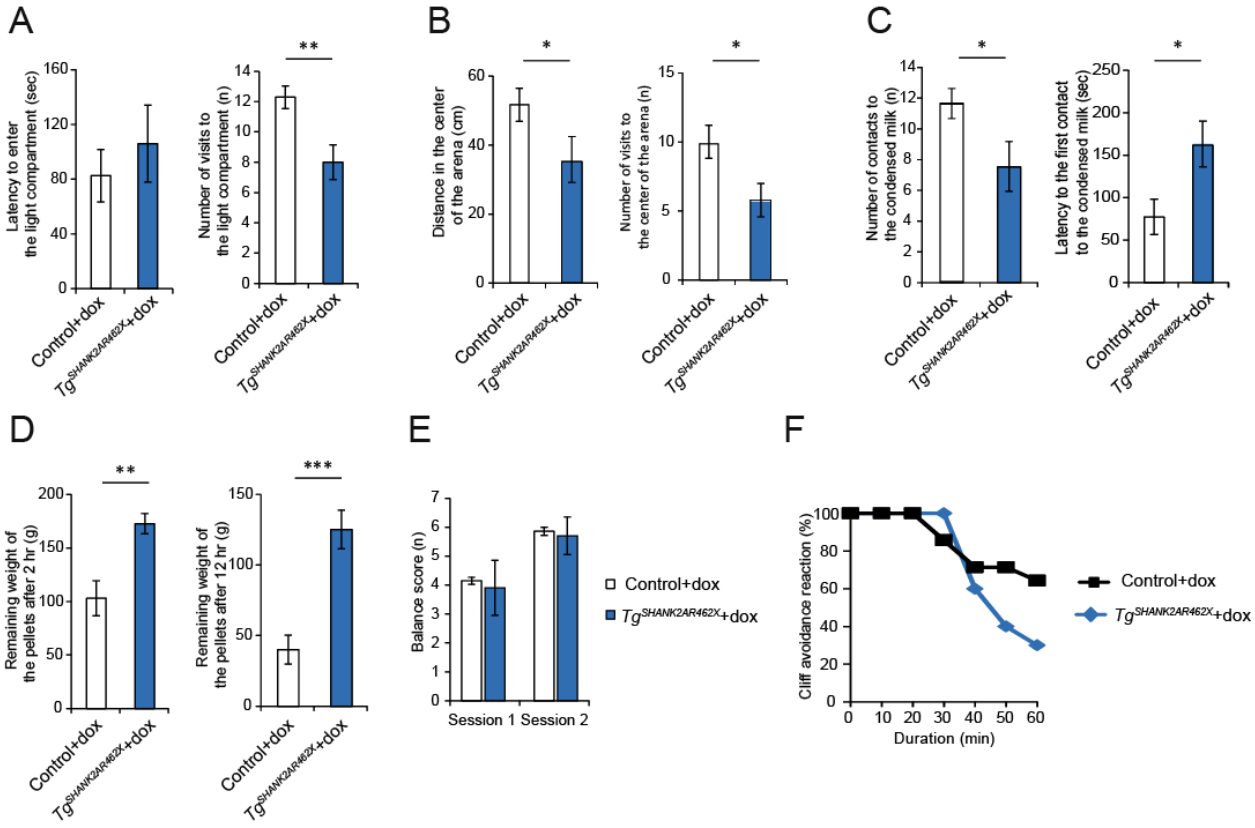

Figure 37: Characterization of anxiety and impulsive behaviors in *Tg*^{SHANK2AR462X} mice after stopping the transgene overexpression in adulthood
(A) The dark-light box test revealed that dox-treated *Tg*^{SHANK2AR462X} made fewer visits to the light compartment **(right)** but had similar latency of the first visit **(left)** compared with dox-treated control mice. **(B)** Dox-treated *Tg*^{SHANK2AR462X} mice were anxious in the open field test by displaying reduced distance **(left)** and numbers of visits **(right)** to the center of a new arena compared with dox-treated control mice. **(C)** Dox-treated *Tg*^{SHANK2AR462X} mice had fear of unfamiliar drink (condensed milk in the center of the arena) in the neophobia test by showing high latency to the first contact **(right)** and reduced numbers of contacts **(left)** to the unfamiliar drink. **(D)** In the burrowing test, dox-treated *Tg*^{SHANK2AR462X} mice left more pellets in the tube after 2 hrs **(left)** and 12 hrs **(right)**. **(E)** Dox-treated *Tg*^{SHANK2AR462X} mice were not impaired in two successive sessions in the balance test. **(F)** Dox-treated *Tg*^{SHANK2AR462X} mice showed high impulsive behavior and less cliff avoidance reaction percentage in the cliff avoidance test (n = 10 dox-treated *Tg*^{SHANK2AR462} and 14 dox-treated control mice at 6 – 9 months of age). Error bars indicate SEM (Two-way ANOVA,*$p \leq 0.05$, **$p \leq 0.01$, ***$p \leq 0.001$).

Similarly to *Tg*^{SHANK2AR462X} mice **(Figure 19A)**, dox-treated *Tg*^{SHANK2AR462X} mice made a normal number of contacts to the same/opposite-sex strangers in all sessions in the three-chamber social test **(Figure 38A)**. However, the increase in the number of contacts to same-sex mice in the direct social interaction test and to the novel object in the novel object recognition test, shown

previously by $Tg^{SHANK2AR462X}$ mice **(Figure 19B, C),** was rescued after the stop of SHANK2A(R462X) overexpression in adulthood **(Figure 38B, C)**.

The puzzle box test revealed that dox-treated $Tg^{SHANK2AR462X}$ mice were unable to solve the puzzle task in trials 5, 6 and 10, where executive performance was tested **(Figure 38D)**. In the fear conditioning test, dox-treated $Tg^{SHANK2AR462X}$ and control mice showed a similar freezing percentage during acquisition and context memory recall **(Figure 38E)**. This demonstrates that the reduced freezing percentage, shown previously in $Tg^{SHANK2AR462X}$ mice **(Figure 19E**), was rescued after turning down the SHANK2A(R462X) overexpression in adults. Additionally, dox-treated $Tg^{SHANK2AR462X}$ mice showed more freezing percentage during the cued memory phase than dox-treated controls, which might indicate a better memory retrieval **(Figure 38E)**.

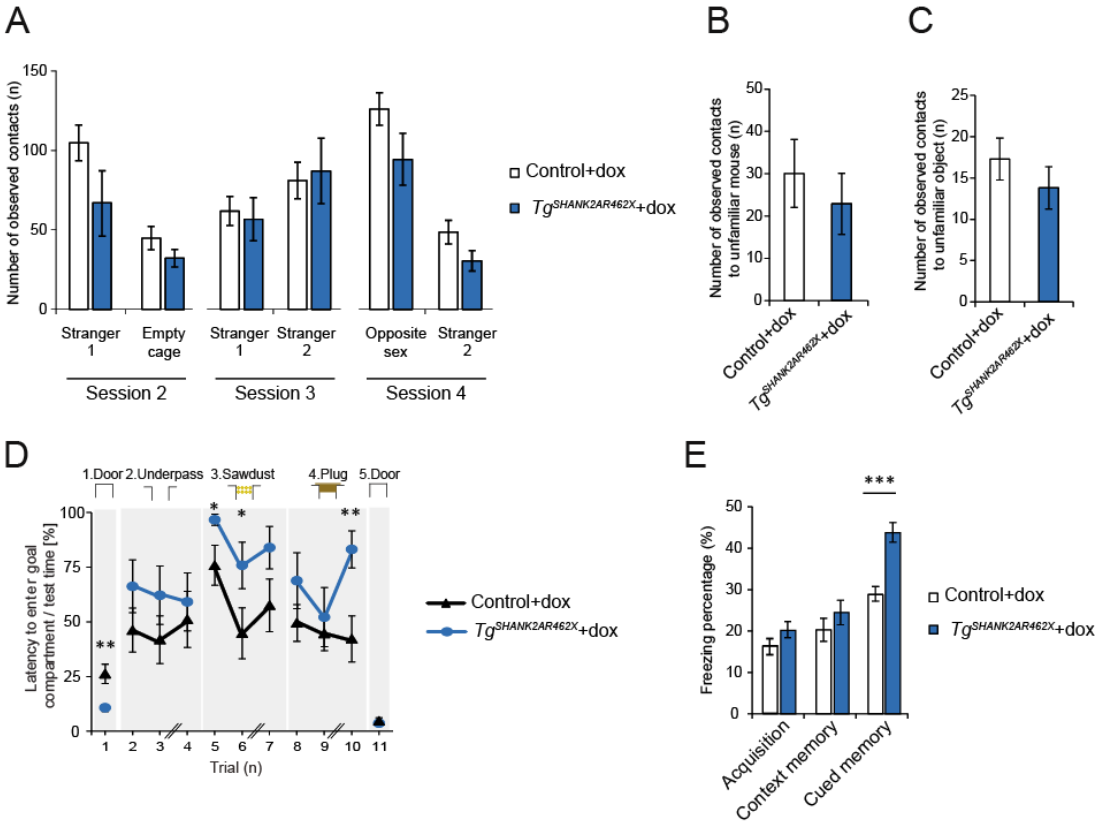

Figure 38: Characterization of the social behavior, cognitive function and emotional learning in $Tg^{SHANK2AR462X}$ mice after switching off the transgene overexpression in adulthood

(A) Dox-treated $Tg^{SHANK2AR462X}$ and control mice displayed similar numbers of contacts to stranger mice in all sessions in the three-chamber social test. **(B)** Dox-treated $Tg^{SHANK2AR462X}$ and control mice made similar numbers of contacts to unfamiliar same-sex mice in the direct social interaction test. **(C)** Dox-treated $Tg^{SHANK2AR462X}$ and control mice made similar numbers of contacts to an unfamiliar object in the novel object recognition test. **(D)** In the puzzle box test, dox-treated $Tg^{SHANK2AR462X}$ mice showed high latency to solve the puzzle in trials 5, 6 and 10. On the other hand, they had lower latency to solve the puzzle in the first trial compared with dox-treated control mice. **(E)** Dox-treated $Tg^{SHANK2AR462X}$ mice showed more freezing

percentage in the cued memory phase in the fear conditioning test (n = 10 dox-treated $Tg^{SHANK2AR462X}$ and 14 dox-treated control mice at 6 – 9 months of age). Error bars indicate SEM (Two-way ANOVA,*$p \leq 0.05$, **$p \leq 0.01$, ***$p \leq 0.001$).

The nCounter expression analysis of genes in the hippocampus of dox-treated $Tg^{SHANK2AR462X}$ mice revealed that the downregulation of AMPAR, mGluR, Serotonin 2A receptor or Oxytocin receptor genes, shown previously in $Tg^{SHANK2AR462X}$ mice **(Figure 23),** cannot be rescued by switching off the SHANK2A(R462X) overexpression in adult $Tg^{SHANK2AR462X}$ mice **(Figure 39)**.

In summary, stopping SHANK2A(R462X) overexpression in adulthood was able to rescue the unusual social behavior of $Tg^{SHANK2AR462X}$ mice but resulted in higher anxiety levels. However, the expression pattern of genes that encode synaptic proteins in the hippocampus was not different between dox-treated and dox-naive $Tg^{SHANK2AR462X}$ mice.

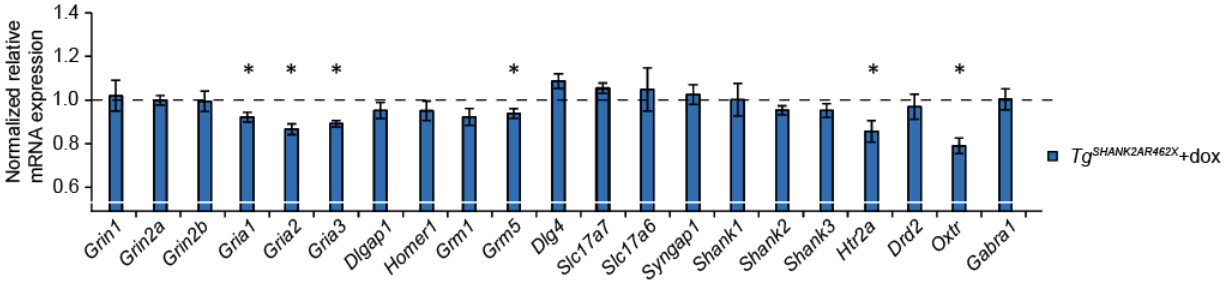

Figure 39: Comparative expression analysis of genes in the hippocampus of $Tg^{SHANK2AR462X}$ mice after stopping the transgene overexpression in adulthood
Normalized RNA expression analysis in dox-treated $Tg^{SHANK2AR462X}$ mice using nCounter analysis revealed a nominal significant downregulation of the AMPAR (*Gria1*, *Gria2* and *Gria3*) and the mGluR5 gene (*Grm5*), in addition to *Htr2a* and *Oxtr* (n= 8 dox-treated $Tg^{SHANK2AR462X}$ and 8 dox-treated control mice, 3 – 5 months). Error bars indicate SEM (Unpaired two-tailed Student's t-test, *$p \leq 0.05$).

3.2.9 SHANK2A overexpression after the critical developmental stage

ASD is known to be a neurodevelopmental disorder which is noticed in the first 3 years of life [189]. However, whether some autistic-like behaviors can still be developed after the critical developmental stage is still unknown. As shown above, the behavioral symptoms of $Tg^{SHANK2A}$ mice include the typical ASD-like phenotypes, including social impairment and repetitive behavior, along with anxiety, hyperactivity and cognitive dysfunction. To analyze which of those ASD-like phenotypes are developmentally mediated, the SHANK2A overexpression was induced in juvenile mice after the critical developmental stage which starts at the beginning of embryonic stage until P21 (for a detailed explanation of the developmental stage, see https://embryology.med.unsw.edu.au/embryology/index.php/Mouse_Timeline_Detailed).

Pregnant female mice received the described dox diet (50 mg/l) to inactivate tTA in embryos. Immunoblots of total protein lysates from the forebrains of P0 dox-treated $Tg^{SHANK2A}$ mice detected β-galactosidase first at P20, while Venus became immuno-visible 10 days later **(Figure 40A)**. After all, the hippocampal Venus, β-galactosidase and transgenic SHANK2A protein levels were comparable between $Tg^{SHANK2A}$ and P0 dox-treated $Tg^{SHANK2A}$ mice **(Figure 40B)**. However, immunofluorescence and Eosin/X-gal stainings revealed that the patterns of Venus and β-galactosidase overexpression in the hippocampus of P0 dox-treated $Tg^{SHANK2A}$ mice was different from the positive control, showing more localized signals in the hippocampal CA1 and CA2 regions, but not in the DG **(Figure 40C)**.

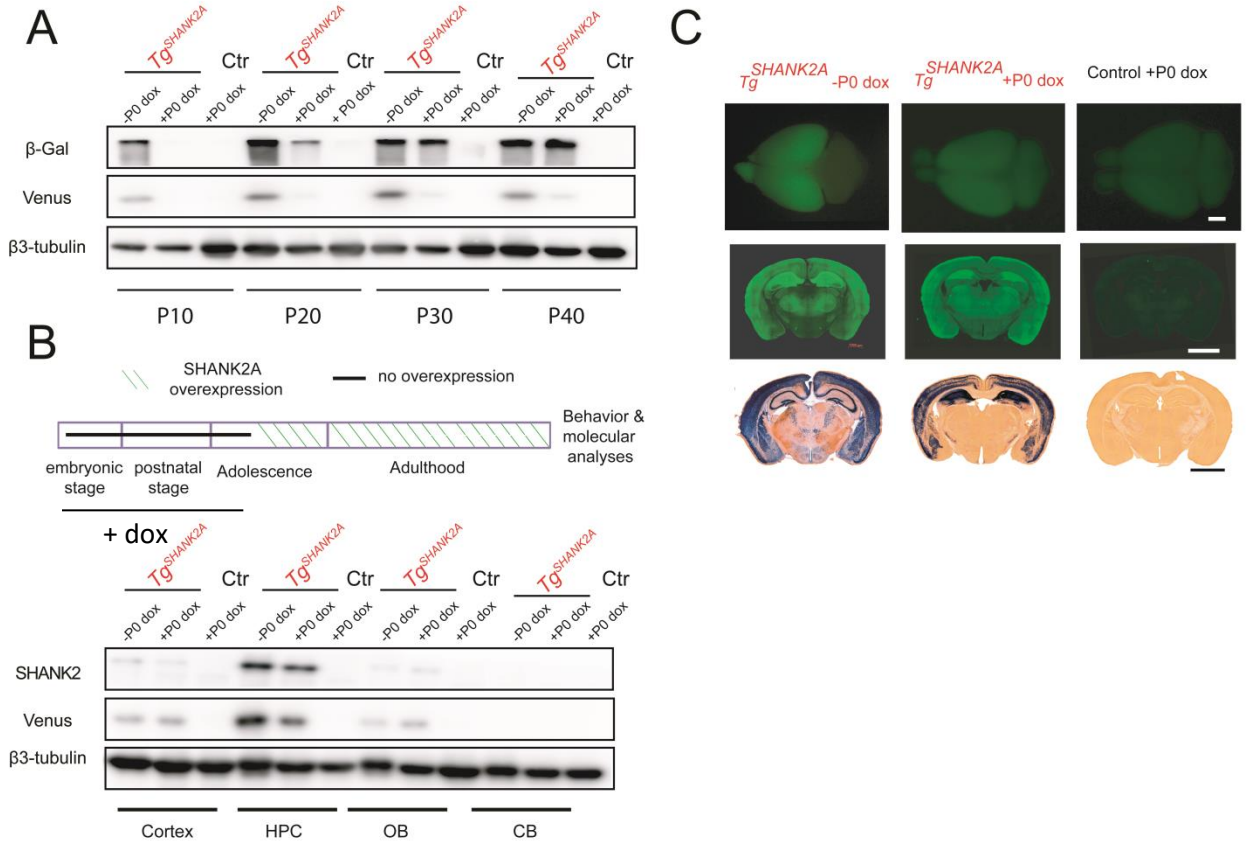

Figure 40: Characterization of $Tg^{SHANK2A}$ mice that overexpress SHANK2A after development
(A) Total protein lysates from forebrains of pups at different developmental stages, when their dams were treated with dox until labor, were analyzed by immunoblotting with β-galactosidase and Venus antibodies. The expression of the Venus transgene started at P30. **(B)** Total protein lysates of different brain tissues from adult $Tg^{SHANK2A}$, P0 dox-treated $Tg^{SHANK2A}$ and control mice were analyzed by immunoblotting with SHANK2, β-galactosidase and Venus antibodies. (5 months) HPC: Hippocampus, OB: Olfactory bulb, CB: Cerebellum. **(C)** Expression of SHANK2A transgene was visualized by the Venus epifluorescence in the forebrain of $Tg^{SHANK2A}$-doxP0 mice **(upper row)** (scale bar: 2 mm). Immunofluorescence staining revealed Venus

expression at the cellular level in coronal brain sections of P0 dox-treated $Tg^{SHANK2A}$ mice **(middle row)** (scale bar: 2 mm). The β-galactosidase expression could be detected at the cellular level of P0 dox-treated $Tg^{SHANK2A}$ mice by Eosin/X-gal staining **(lower row)** (scale bar: 2 mm). The patterns of Venus and β-galactosidase overexpression in the hippocampus of P0 dox-treated $Tg^{SHANK2A}$ mice were different from the positive control, and the signals were more localized in the CA1 and CA2 regions, but not in DG.

Despite the prenatal exposure to the dox/sucrose by the dox diet of the dams, the body weights of P0 dox-treated $Tg^{SHANK2A}$ mice was still 10% lower than P0 dox-treated control mice **(Figure 41A)**. In the LABORAS test, adult P0 dox-treated $Tg^{SHANK2A}$ mice were hyperactive **(Figure 41B)** and showed increased repetitive rearing **(Figure 41D)** similar to $Tg^{SHANK2A}$ animals **(Figure 14 B, D)**. In contrast to $Tg^{SHANK2A}$ mice, the duration of eating and the nesting behaviors were not affected when SHANK2A overexpression was induced in adolescence **(Figure 41C, E)** (for a summary, see **Appendix 5**).

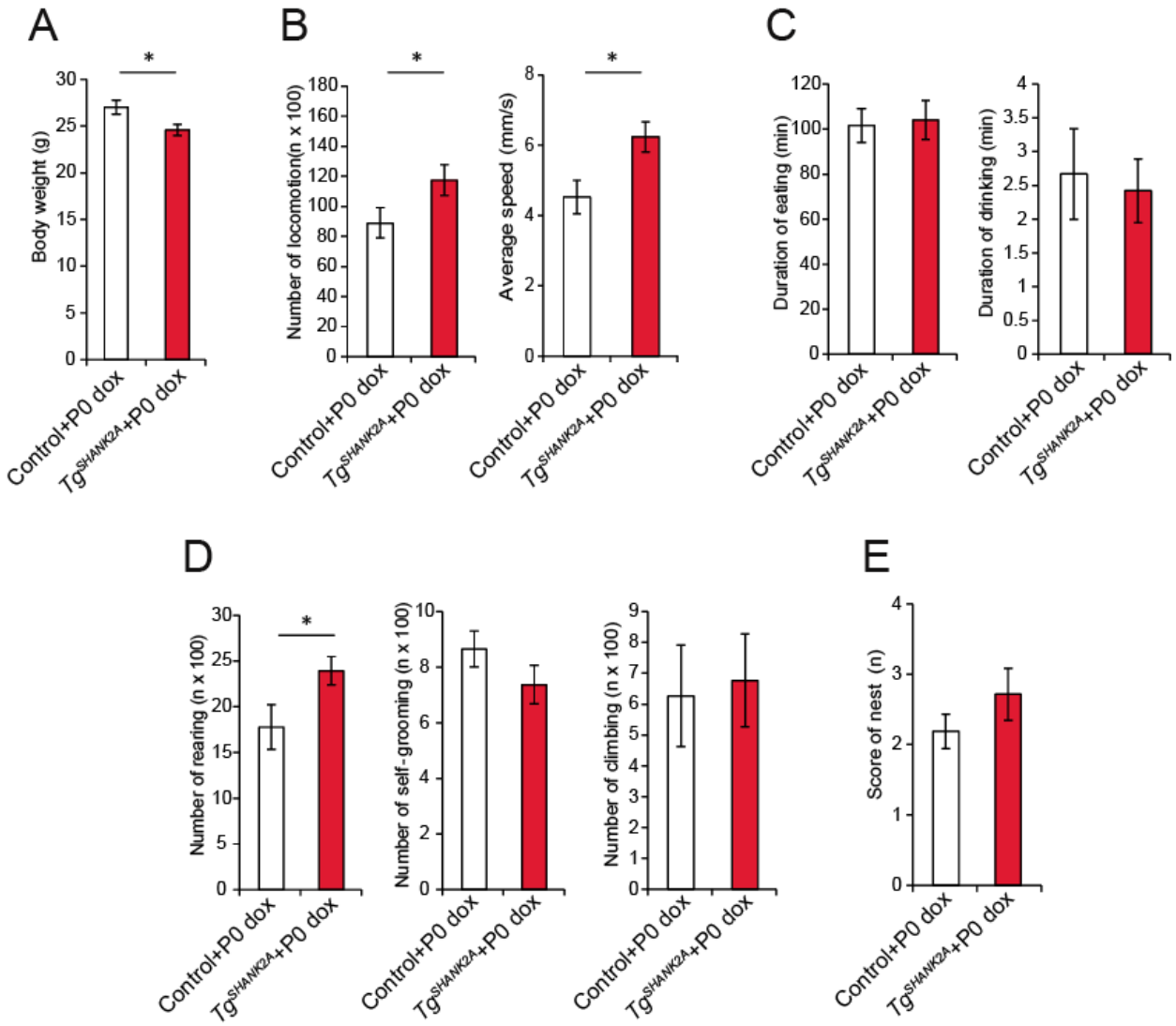

Figure 41: General and repetitive behaviors in $Tg^{SHANK2A}$ mice that overexpress SHANK2A after developmental

(A) The body weight of P0 dox-treated $Tg^{SHANK2A}$, when their dams were treated with dox until labor, was 10% less than of control mice. **(B-D)** The LABORAS test of P0 dox-treated $Tg^{SHANK2A}$ mice showed an increased number of locomotion events **(B, left)** and a high average speed **(B, right)**. P0 dox-treated $Tg^{SHANK2A}$ mice showed no difference in the duration of eating **(C, left)** or drinking **(C, right)**. P0 dox-treated $Tg^{SHANK2A}$ mice exhibited repetitive rearing **(D, left)**, but no difference in the number of self-grooming **(D, middle)** or climbing **(D, right)** compared with P0 dox-treated control mice. **(E)** P0 dox-treated $Tg^{SHANK2A}$ mice showed no impairment in the nesting test. (n = 14 P0 dox-treated $Tg^{SHANK2A}$ and 16 P0 dox-treated control mice at 6 – 9 months of age). Error bars indicate SEM (Two-way ANOVA,*$p \leq 0.05$).

To test anxiety in P0 dox-treated $Tg^{SHANK2A}$ mice, three different experiments were performed. P0 dox-treated $Tg^{SHANK2A}$ mice exhibited high anxiety level in the dark-light box **(Figure 42A)**, open field **(Figure 42B)** and neophobia **(Figure 42C)** tests similar to $Tg^{SHANK2A}$ mice **(Figure 15 A-C)**.

To test the integrity of hippocampal function, the burrowing test was performed and revealed the inability of P0 dox-treated $Tg^{SHANK2A}$ mice to perform the test efficiently with more remaining pellets in the tube after 2 hr, but not after 12 hrs **(Figure 42D)**. P0 dox-treated $Tg^{SHANK2A}$ mice were able to maintain their balance in two consecutive sessions in the balance test **(Figure 42E)** in contrast to $Tg^{SHANK2A}$ mice **(Figure 15E)**. The induction of SHANK2A overexpression after the developmental stage in P0 dox-treated $Tg^{SHANK2A}$ mice was still correlated with high impulsivity in the cliff avoidance reaction test **(Figure 42F)**.

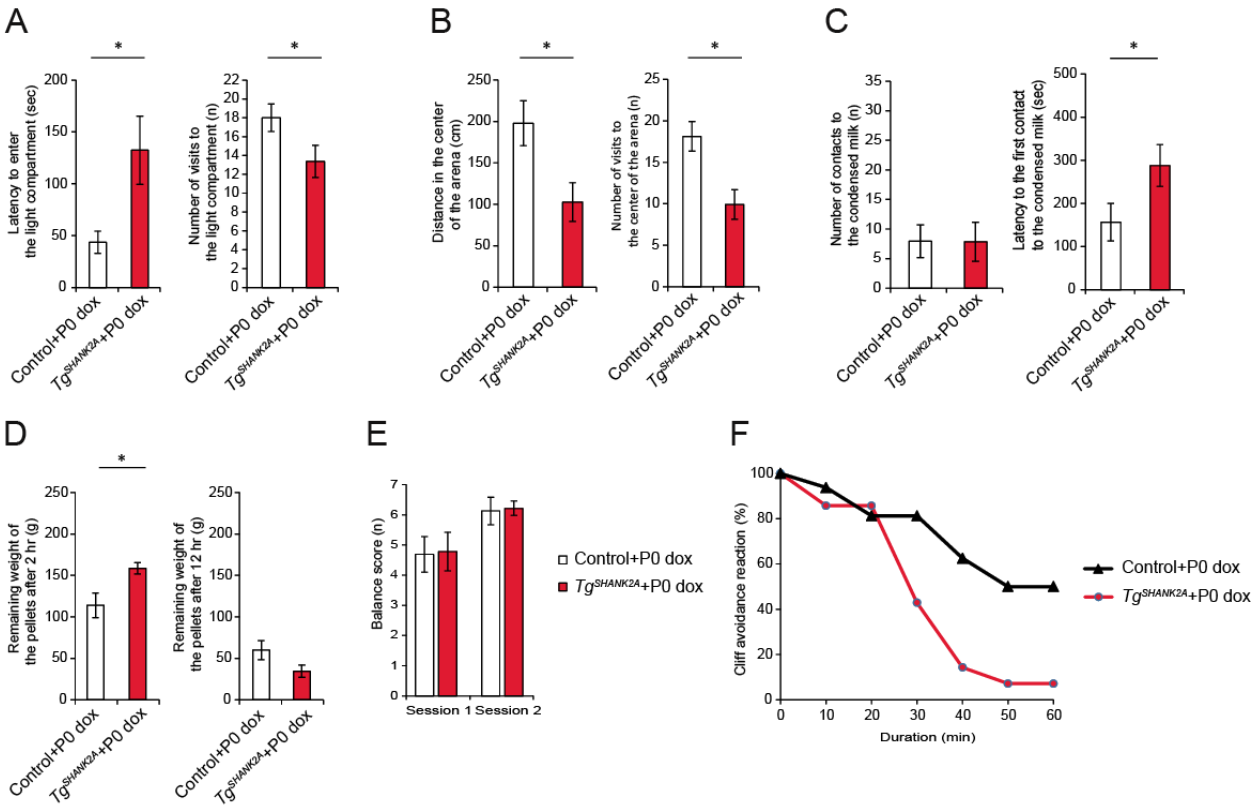

Figure 42: Characterization of anxiety and impulsive behaviors in *Tg*^{SHANK2A} mice that express SHANK2A after development

(A) The dark-light box test revealed anxiety in P0 dox-treated *Tg*^{SHANK2A} as shown by increased latency **(left)** and reduced numbers of visits **(right)** to the light compartment compared with P0 dox-treated control mice. **(B)** P0 dox-treated *Tg*^{SHANK2A} mice displayed anxiety in the open field test and showed less traveled distance **(left)** and fewer numbers of visits **(right)** to the center of a new arena than P0 dox-treated control mice. **(C)** P0 dox-treated *Tg*^{SHANK2A} mice exhibited fear of unfamiliar drink (condensed milk in the center of the arena) in the neophobia test by showing higher latency to the first contact **(right)**, but a similar number of contacts **(left)** to the unfamiliar drink. **(D)** In the burrowing test, P0 dox-treated *Tg*^{SHANK2A} mice showed more remaining pellets in the tube after 2 hrs **(left)**, but not after 12 hrs **(right)** than controls exposed to dox till P0. **(E)** P0 dox-treated *Tg*^{SHANK2A} mice showed no balance impairment in two successive sessions in the balance test. **(F)** P0 dox-treated *Tg*^{SHANK2A} mice showed impulsive behavior with less cliff avoidance reaction percentage in the cliff avoidance reaction test than P0 dox-treated control mice. (n = 14 P0 dox-treated *Tg*^{SHANK2A} mice and 16 P0 dox-treated control mice at 6 – 9 months of age). Error bars indicate SEM (Two-way ANOVA,*$p \leq 0.05$).

The social behavior of P0 dox-treated *Tg*^{SHANK2A} mice was assessed by performing the three-chamber social test, the direct social interaction and the novel object recognition tests. In contrast to *Tg*^{SHANK2A} mice with SHANK2A overexpression during the developmental stage **(Figure 16A-C)**, P0 dox-treated *Tg*^{SHANK2A} mice were not impaired in these three tests **(Figure 43A-C)**. In the puzzle box, P0 dox-treated *Tg*^{SHANK2A} mice showed a cognitive impairment and high latency to solve the puzzle in trials 1, 8, 9 and 10 **(Figure 43D)**. The emotional learning revealed no

impairment in the context or the cued fear memory in P0 dox-treated *Tg*^{SHANK2A} mice **(Figure 43E)** similarly to *Tg*^{SHANK2A} mice **(Figure 16E)**.

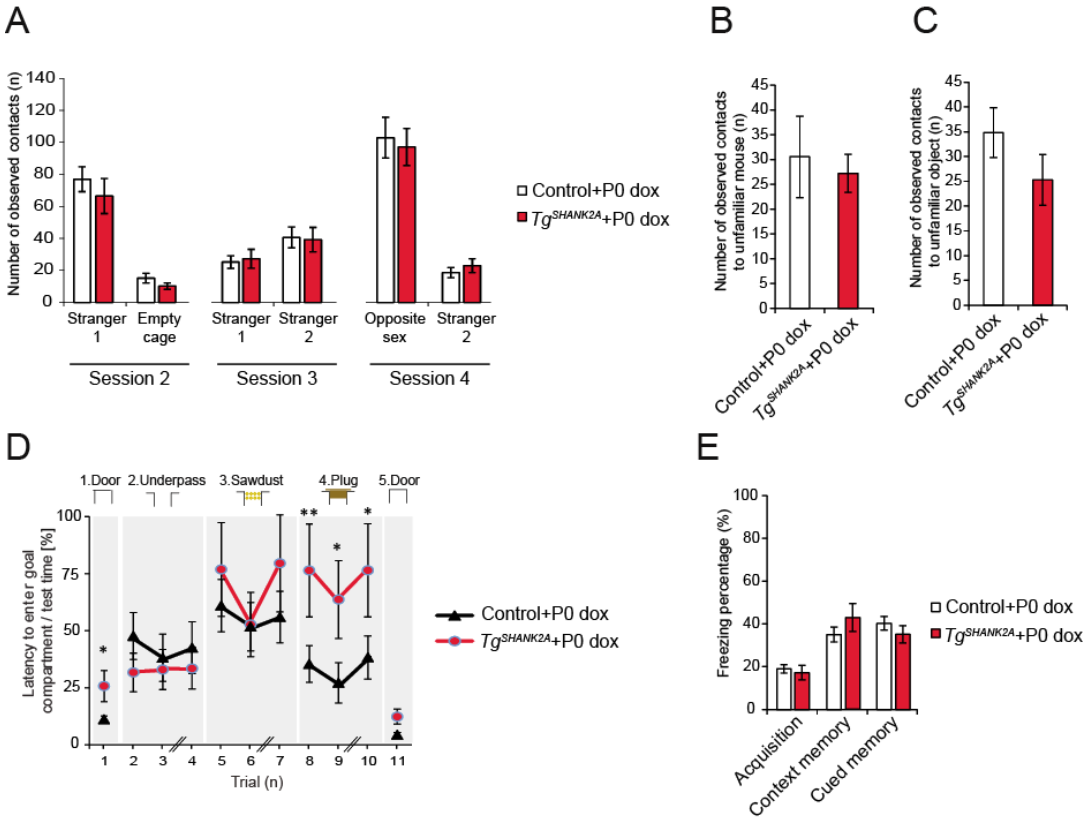

Figure 43: Characterization of the social behavior, the cognitive function and the emotional learning in *Tg*^{SHANK2A} mice that overexpress SHANK2A after development

(A) In the three-chamber social test, P0 dox-treated *Tg*^{SHANK2A} and control mice displayed similar numbers of contacts to strangers in all sessions. **(B)** In the direct social interaction, P0 dox-treated *Tg*^{SHANK2A} and control mice revealed similar numbers of contacts to unfamiliar same-sex mice. **(C)** In the novel object recognition test, P0 dox-treated *Tg*^{SHANK2A} and control mice showed similar numbers of observed contacts to an unfamiliar object. **(D)** In the puzzle box test, P0 dox-treated *Tg*^{SHANK2A} mice showed higher latency to solve the puzzle in trials 1, 8, 9 and 10 than P0 dox-treated control mice. **(E)** In the fear conditioning test, P0 dox-treated *Tg*^{SHANK2A} and control mice showed similar freezing percentages in the acquisition, context and cued memory phases. (n = 14 P0 dox-treated *Tg*^{SHANK2A} mice and 16 P0 dox-treated control mice at 6 – 9 months of age). Error bars indicate SEM (Two-way ANOVA,*$p \leq 0.05$, **$p \leq 0.01$).

The expression analysis of genes in the hippocampus of P0 dox-treated *Tg*^{SHANK2A} mice was investigated on RNA level using nCounter analysis. The comparative expression analysis revealed a downregulation of the AMPAR genes (*Gria2* and *Gria3*), *Grm1* and *Dlg4* **(Figure**

44). However, the activation of SHANK2A overexpression after development did not reveal the reduced expression of NMDAR genes, previously found in *Tg*^{SHANK2A} mice **(Figure 23)**.

In summary, P0 dox-treated *Tg*^{SHANK2A} mice displayed specific ASD-like features including hyperactivity, anxiety, repetitive behavior and cognitive dysfunction similar, but with less severity, to *Tg*^{SHANK2A} mice that overexpress SHANK2A during development. However, they did not show any social impairment in contrast to *Tg*^{SHANK2A} mice. The normal social interaction in P0 dox-treated *Tg*^{SHANK2A} mice was accompanied by a normal expression of NMDAR genes in the hippocampus.

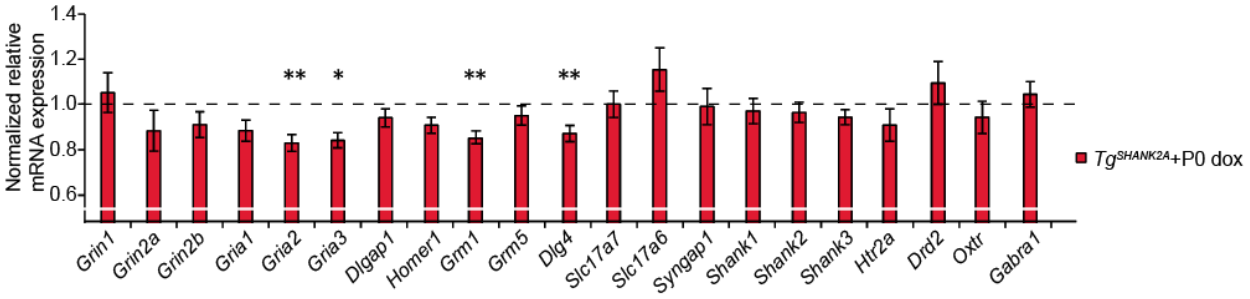

Figure 44: Comparative expression analysis of genes in the hippocampus of *Tg*^{SHANK2A} mice that overexpress SHANK2A after development

Normalized RNA expression analysis of P0 dox-treated *Tg*^{SHANK2A} mice using the nCounter analysis revealed a nominal significant downregulation of the AMPAR (*Gria2* and *Gria3*) and mGluR1 (*Grm1*), in addition to *Dlg4* genes. (n= 7 P0 dox-treated *Tg*^{SHANK2A} mice and 8 P0 dox-treated controls, 3 – 5 months). Error bars indicate SEM (Unpaired two-tailed Student's t-test, *$p \leq 0.05$, **$p \leq 0.01$).

Chapter 4

Discussion

4.1 The influence of sex hormones on *SHANK* expression

A clear link between testosterone and ASD has emerged from studying synaptic dysfunction [56]. As SHANKs are postsynaptic scaffolding proteins and known to be linked to ASD pathology [124], an influence of testosterone on their expression was suggested. Testosterone is metabolized in the brain into DHT or converted into 17β-estradiol by the enzyme aromatase (CYP19A1). Therefore, the effect of testosterone's metabolites on *SHANK* gene expression was investigated in a SH-SY5Y cell model, a widely used neuronal cell model to investigate hormonal influences of androgens and estrogens on the expression of genes [66,174,190,191]. Treating SH-SY5Y cells with DHT and 17β-estradiol, AR and ERα, respectively, revealed different expression levels and patterns, confirming their different signaling cascades in SH-SY5Y cells, as shown previously in humans [192]. Both DHT and 17β-estradiol increased *SHANK* mRNA expression, with a more pronounced effect of DHT (35%), compared to the effect of 17β-estradiol (15%). Moreover, the effect of DHT but not 17β-estradiol on *SHANK* expression was present on the protein level with a 50% increase in the level of SHANK protein isoforms. The increase in SHANK expression on protein level more than on mRNA level in response to DHT treatment indicates either reduced mRNA stability or that the major effect of DHT is at the level of translation [152]. The general regulatory influence of DHT and 17β-estradiol was modest, indicating a role as transcriptional fine-tuners [152]. In previous studies, the postsynaptic scaffolding protein PSD95 was shown to be regulated as well by sex hormones [176-178]. Moreover, the AMPAR subunits, GluA1 and GluA2, were reported to be androgen-responsive [193]. These results underline the important role of sex

hormones in regulating the expression of multiple synaptic proteins. Despite the small effect of sex hormones on individual gene expression, synergistic effects on several genes could influence the synaptic composition substantially, leading to the notable differences observed between male and female phenotypes.

The effect of DHT and 17β-estradiol on *SHANK* expression was absent in the presence of AR and ER antagonists. This suggests that the modulation of sex hormones on *SHANK* expression is mainly direct *via* androgen and estrogen receptor signaling, although other indirect effects of sex hormones on the regulation of *SHANK* expression can still be present. The direct contribution of AR signaling on the regulation of *SHANK* gene expression was confirmed by the reduced expression of *Shank* genes in the cortex of Ar^{NesCre} mice at P7.5, supporting the role of Ar activity in the regulation of *Shank* expression during mouse brain development. Surprisingly, Ar^{NesCre} and littermate control mice revealed similar expression levels of *Shank* genes at E17.5, which can be explained by the low level of *Ar* expression in the cortex of control mice at E17.5. Moreover, deletion of *Ar* by Nestin-Cre might need a longer duration before modulating the *Shank* gene expression. The period between E17.5 and P7.5 is considered a critical period for brain development [152]. In a previous study, sex differences in the spatiotemporal expression of *Ar*, *Erα* and *Erβ* in the mouse brain as well as differences in testosterone levels were reported, suggesting their interrelated roles in shaping the brain structure and synaptic function [181]. Therefore, it is not surprising that the human cortex differs in size between males and females, which can be correlated with sex hormone levels [194,195]. Moreover, the genetic involvement of androgen dysregulation in ASD has been previously reported [196]. A polymorphism in the androgen receptor gene (*SRD5A2*), which catalyzes the conversion of testosterone into DHT, was found in a Slovak cohort of ASD children, suggesting a direct role of AR impairment in ASD pathology [196].

Previous data has shown that *Ar* and *Shank* genes have overlapping expression patterns. This comprises of the cortex along with other brain regions including the striatum and hippocampus, suggesting a correlation between their functions [125,151,197]. Moreover, genes encoding for other proteins, that are known to be involved in the function of the glutamatergic synapses, were found to be regulated by androgens and estrogens in other brain regions such as the medial preoptic area and the ventromedial hypothalamus [198]. The effect of anti-androgenic treatment, estrogenic treatment and a combination of both treatments on the *Shank* gene expression was investigated in

male and female rats and revealed an alteration in *Shank1* and *Shank2* expression levels in males at P6. In females, the expression of *Shank2* and *Shank3* was modulated in response to anti-androgenic and estrogenic treatments [198]. In a previous study, *SHANK* promoters and enhancers were found to contain palindromic and dihexameric motifs of androgen responsive elements [199], and an AR-binding site was also identified in an intron and in the distant promoter region of *SHANK2* by ChIP-Seq [200]. Given these aforementioned studies, there is growing evidence that the effect of sex hormones on *SHANK* expression is direct *via* androgen and estrogen receptors.

In humans, the male cerebral cortex has more neurons than the female one. Those neurons are densely packed in the cerebral cortex of males but not in other brain regions [201]. The dense packing of neurons in the male brain is associated with more intrahemispheric white matter, suggesting a pattern of increased local connectivity and decreased interhemispheric connectivity in the male brain [202,203]. Furthermore, it is known that the size of the human cortex and its sex hormone levels differ between males and females [204,205], which may suggest a sex-differential expression of genes that encode for important neuronal and synaptic proteins. Therefore, the expression of *Shank* genes and proteins was investigated in the cortex of male and female wild-type CD1 mice. qPCR analysis showed a significant reduction of *Shank1* mRNA expression in the cortex of male compared to female mice at P7.5. In contrast, immunoblots revealed higher levels of all SHANKs in the cortex of male mice. This discrepancy between RNA and protein results suggests that they do not always correlate with each other, especially in proteins with a long half-life. Also, a negative feedback mechanism can sometimes occur when the increase in protein level decreases the expression of mRNA. Furthermore, a previous genome-wide study reported that the cellular abundance of a protein is predominantly controlled at the level of translation [206].

The sex-differential Shank expression can be explained by a different *Ar* expression and testosterone level between male and female brains during the critical developmental stage [181]. Male mouse embryos have about three times higher blood testosterone levels than female embryos at E17 [180] and show significantly higher testosterone levels in the brain of CD1 mice at E19 [181]. The finding that male mice brains with high testosterone levels have elevated Shank protein expression is consistent with the finding that DHT increases *SHANK* mRNA and protein expression in SH-SY5Y cells. However, caution is advised when comparing an *in vitro* to an *in vivo* model. Moreover, SH-SY5Y cells may not entirely reflect the regulatory potential regarding

testosterone signaling in cortical neurons, which are a heterogeneous population of cells that may respond differently to DHT [152].

In humans, the prenatal stage and the first few years in life are the most vulnerable times for ASD [207]. Showing that *Shank* expression in the cortex is different between male and female mice at two developmental stages indicates that the sex differences in the cortex intersect with ASD etiological pathways. The sex-differential expression of *Shanks* acts either as a male-risk factor or as a female-protective factor. Many studies support the female-protective factors hypothesis as female ASD patients usually carry a greater etiological load than affected males [208-214], indicating that females are able to withstand higher genetic liability than males without being affected [39]. The complementary model of the high male-specific risk for ASD was supported by many studies, suggesting a link between prenatal exposure to high fetal testosterone and ASD [58,60]. Therefore, male and female sex hormones may play a role in female protection or male susceptibility to ASD [215]. Males show higher prenatal and postnatal testosterone levels than females [31,60], which is suggested to increase the "masculinization" of the brain [215]. In one study, girls with congenital adrenal hyperplasia, a congenital condition associated with abnormally high levels of testosterone, showed autistic behavioral manifestations [216]. Moreover, it has been demonstrated that children with ASD have significantly elevated androgen levels [56,217-219]. In addition, a high testosterone level in children was found to be associated with moodiness, low attachment, and low sociability in prepubertal ages [220], which are common observations in children with ASD. Physiologically higher SHANK protein expression levels in males compared to females implicate that genetic variants can have a higher penetrance in males, resulting in a larger proportion of males diagnosed with ASD [152]. Although *SHANK2* and *SHANK3* variants are randomly distributed across male and female subjects, CNV deletions encompassing *SHANK1* segregated only in male carriers with high-functioning autism [26]. Most ASD individuals that have been identified with *SHANK* deletions and various point mutations are very likely to have reduced levels of SHANK. However, it cannot be excluded that a general dysregulation of *SHANK* expression contributes to ASD pathology, as *SHANK3* gene duplications have also been identified in individuals with Asperger syndrome [25].

Gene expression in the neocortex of human postmortem tissues was previously compared between males and females [44,193]. No evidence was obtained for sex-differential expression of *SHANKs* or other ASD-associated genes like *RORA* and *FOXP1* in the prenatal (16-22 weeks) or

the adult stages. However, these two stages do not match the investigated developmental windows in the presented study. This suggests that the regulation of *SHANK* expression is very sensitive to sex hormones in the days shortly before or after birth. In a very recent study, the DNA methylation patterns of ASD risk genes, including *NRXN1-3, FDE4A* and *SHANK2*, and ASD-related pathways were found to be sex-biased in human postmortem prefrontal cortical tissues in the adult stage [221]. This suggests that sex hormones may have an effect on DNA methylation, which impacts sexually different characteristics of the human brain. In a previous study, a DNA hypermethylation value of 5 CpG positions within the *SHANK2* gene was found in a male patient with ID and developmental delay [138]. In addition, SHANK3 CpG islands were highly methylated in tissues where protein expression is low and vice versa [222]. By performing an in-depth investigation of the *SHANK3* locus in human and mouse, it has been shown that DNA methylation patterns in *SHANK3* regulate intragenic promoter activity, leading to a tissue-specific differential expression [223]. These results indicate that the expression of *SHANK* genes is sensitive to the DNA methylation pattern. As DNA methylation is the upstream regulator of the gene expression, comprehensive analyses that combine methylation and gene expression are crucial to reach a better understanding of the sex bias in ASD [221].

Taken together, the data presented here revealed an effect of sex hormones on *SHANK* gene expression in addition to a sex-differential Shank expression in mice cortices. This can provide a novel insight into the understanding of the sex bias in the pathophysiology of ASD.

4.2 SHANK2A and SHANK2A(R462X) overexpression in the glutamatergic neurons in the mouse forebrain

Mutations in *SHANK* genes are associated with different severities of ASD, with *SHANK1* mutations displaying a mild phenotype, while *SHANK2* and *SHANK3* exhibit profound and severe phenotypes [124,224]. This suggests that SHANK proteins have different but complementary interrelated functions at the excitatory glutamatergic synapses during the course of mammals' development. By the overexpression of SHANK2A isoform or the truncated SHANK2A(R462X) in transgenic mice $Tg^{SHANK2A}$ and $Tg^{SHANK2AR462X}$, respectively, the developmental and physiological regulation of endogenous SHANK expression was bypassed. Thus, in contrast to the traditional *Shank* knock-out mouse models, compensatory mechanisms of the remaining endogenous *Shank* genes had a very minor impact on the phenotype of $Tg^{SHANK2A}$ and

Tg^{SHANK2AR462X} mice. Moreover, the expression of endogenous *Shank* genes in the hippocampus of *Tg*^{SHANK2A} and *Tg*^{SHANK2AR462X} mice was not altered, as shown by the nCounter analysis. Thus, the phenotypes of both transgenic mice were directly mediated by the transgenic SHANK2A variants. As indicated by the 12-fold overexpression of the transgenic SHANK2A variants (when compared to the endogenous SHANK2), the structure and organization of the SHANK scaffold was dominated by the transgenic, SHANK2A or SHANK2A(R462X). Nevertheless, the total hippocampal transgenic SHANK2A and SHANK2A(R462X) overexpression was only 1.6 fold relative to the total hippocampal SHANK1-3 expression, suggesting that the protein overload was still in a physiological and not in a toxic range. The transgenic overexpression of SHANK2A proteins might critically disrupt the postsynaptic organization in the brain regions that are known to be implicated in ASD - such as cortex, hippocampus and striatum [225-232]. This enabled the direct study of molecular, physiological and behavioral effects that originated from the transgenic SHANK2A-mediated dysfunctions in the glutamatergic neurons in mice. Due to the high complexity of the SHANK scaffold, cell-type specific *Shank* knock-out models could not solve the crucial function of the different *Shank2* genes and their isoforms. This is best exemplified by the mild ASD-like behavior of two mouse lines with a specific SHANK2 depletion in excitatory αCaMKII expressing neurons [143,147]. *Shank2*$^{\Delta ex15\text{-}16\text{–}CaMK2a\text{-}Cre}$ mice showed mild hyperactivity, and *Shank2*$^{\Delta ex24\text{–}CaMK2a\text{-}Cre}$ did not reveal any hyperactivity. Compared to *Tg*^{SHANK2A} and *Tg*^{SHANK2AR462X} mice, *Shank2*$^{\Delta ex15\text{-}16\text{–}CaMK2a\text{-}Cre}$ mice revealed normal body weight and no repetitive behaviors [147]. In contrast, the overexpression of SHANK variants in the same αCaMKII expressing neuronal population of *Tg*^{SHANK2A} and *Tg*^{SHANK2AR462X} mice showed a severe ASD-like phenotypes, demonstrating a more severe disruption of the SHANK organization compared to the loss of only Shank2 in *Shank2*$^{\Delta ex15\text{-}16\text{–}CaMK2a\text{-}Cre}$ and *Shank2*$^{\Delta ex24\text{–}CaMK2a\text{-}Cre}$ mice, which justifies the overexpression approach for the analysis of gene function in a complex protein networks.

4.2.1 Autistic-like behavior and dysregulated gene expression in *Tg*^{SHANK2A} and *Tg*^{SHANK2AR462X} mice

The analysis of locomotor activity, stereotypic, anxiety, social and cognitive behavior of *Tg*^{SHANK2A} and *Tg*^{SHANK2AR462X} mice revealed that both lines expressed a behavioral phenotype described for most of the published *Shank2* knock-out mice lines. Mice from both *Tg*^{SHANK2A} and *Tg*^{SHANK2AR462X} lines exhibited line-specific impairments in the balancing performance and

stereotypic self-grooming and jumping behavior. A similar line-specific difference in the repetitive behavior has been shown before in the two related *Shank2* knock-out mouse models, *Shank2*$^{\Delta ex15\text{-}16}$ and *Shank2*$^{\Delta ex16}$, which were actually expected to reveal very similar phenotype as both express a truncated version of SHANK2 due to a frameshift in the PDZ domain (**Figure 3)** [133]. *Shank2*$^{\Delta ex15\text{-}16}$ mice exhibited increased jumping and upright scrabbling in the home cage and increased self-grooming in the novel object recognition arena [141,145]. In contrast, *Shank2*$^{\Delta ex16}$ mice showed increased self-grooming in the home cage [146]. Self-grooming and jumping are associated with several brain regions including cortex, hypothalamus, striatum, cerebellum and amygdala [233,234]. This discrepancy suggests already the role of a small genetic variation of the SHANK2 gene mutation on the expression of ASD-like symptoms in mice by potentially affecting different signaling pathways in different brain regions.

In both *Tg*^{SHANK2A} and *Tg*^{SHANK2AR462X} mice, the SHANK2A variant overexpression was associated with different levels of increased locomotor activity. The locomotion speed in the 24 hrs LABORAS recording was found to be increased in both lines. The hyperactivity might also explain the reduced cliff avoidance reaction in *Tg*^{SHANK2A} and *Tg*^{SHANK2AR462X} mice. However, in the context of other behavioral impairments, the decreased cliff avoidance reaction was more likely due to a lack of behavioral inhibition that is closely linked to the attention and sociability deficits seen in animal models for ADHD [235-237] and ASD [238-241].

In the tests for the 'activities of daily living', the burrowing and nesting tests, *Tg*^{SHANK2A} mice performed very poorly. For *Tg*^{SHANK2AR462X} mice, the score for the nesting behavior was only slightly reduced. Since poor nest building is also recognized as a proxy for sociability [242], this result might already indicate a minor impairment in the sociability of *Tg*^{SHANK2AR462X} mice.

In the context of cognitive dysfunction, as a comorbidity of ASD, *Tg*^{SHANK2A} and *Tg*^{SHANK2AR462X} mice showed impairment in executive tasks in the puzzle box. The high latency to solve the puzzle by *Tg*^{SHANK2AR462X} mice is in line with a previous pilot study that showed cognitive dysfunction in mice with rAAV-mediated SHANK2A(R462X) overexpression [136]. This suggests a dominant negative effect exerted by the SHANK2A(R462X) truncated isoform on intra-hippocampal pathways that play a role in the formation and storage of memory [243]. Unfortunately, the cognitive behavior was analyzed for the *Shank2* knock-out mice just in the Morris water maze and for the transgenic animals just in the Puzzle box and therefore, the

detailed comparison of the cognitive impairment still needs to be analyzed. The cognitive dysfunction in both transgenic mouse lines was accompanied by a downregulation of AMPAR subunit expression in the hippocampus. Reduced function of AMPAR has been shown to induce cognitive impairments associated with ASD and SCZ symptoms [244,245]. Moreover, the loss of GluA1 subunit in GluA1 knock-out mice significantly impaired the problem-solving ability in the puzzle box [246]. Similar downregulation of AMPAR subunit expression was found in the hippocampus of *Shank2* knock-out mice: GluA1 subunit in *Shank2*$^{\Delta ex15\text{-}16}$ and *Shank2*$^{\Delta ex16}$ mice [146,247] and both GluA1 and GluA2 subunit in *Shank2*$^{\Delta ex24}$ mice [143].

In the memory of fear, the SHANK2A and SHANK2A(R462X) overexpression provided inconsistent results. *Tg*^{SHANK2A} mice associated the tone and the context with the painful electric shock, while *Tg*^{SHANK2AR462X} mice responded just in the context with reduced freezing. The impaired contextual fear memory in *Tg*^{SHANK2AR462X} but not *Tg*^{SHANK2A} mice may be a result of the downregulation of Serotonin receptor 2A subunit or Oxytocin receptor expression in the hippocampus of *Tg*^{SHANK2AR462X} mice. Serotonin and oxytocin are known to modulate contextual fear memory in mice [248-252], which is suggested to be a function of hippocampus activation, especially in DG and CA3 regions [253]. DG is suggested to impose a distinct firing pattern on the CA3 region which forms an auto-associative network through the extensive collaterals present in that region [254,255]. On the other hand, the role of the CA1 region is not completely understood, but it is thought to host a variety of both essential and modulatory functions including memory consolidation [256], generalization [257] and encoding of specific items and their inter-relation within the context [258-260]. Therefore, the DG and CA3 regions form the initial memory framework that supports rapid conditioning [261,262], and all other hippocampal regions subsequently expand upon this framework to create a more comprehensive representation as the session continues [253]. For the cued fear memory which is known to require amygdala function, *Tg*^{SHANK2A} and *Tg*^{SHANK2AR462X} mice did not reveal any impairment. This suggests that the amygdala is not affected in both mouse lines [263]. *Tg*^{SHANK2A} and *Tg*^{SHANK2AR462X} mice showed a decrease in the freezing percentage in the acquisition phase, which can be explained by the hyperactivity of both mouse lines in the new arena.

In summary, the line-specific alterations in the profiles of stereotypic behavior, hyperactivity, anxiety, life performance, fear conditioning and poor cognition of *Tg*^{SHANK2A} and *Tg*^{SHANK2AR462X}

mice are reminiscent to the heterogeneous ASD-like phenotypes in the three *Shank2* knock-out mouse models *Shank2*$^{\Delta ex15\text{-}16}$, *Shank2*$^{\Delta ex16}$ and *Shank2*$^{\Delta ex24}$ (for a review, see [133]).

The most radical behavioral difference between the two transgenic lines was found in their response to novel objects and unfamiliar mice. *Tg*^{SHANK2A} mice showed the typical ASD-like ignorance to novelty and were not interested in social contacts in the three-chamber and the direct social interaction test. *Tg*^{SHANK2AR462X} exhibited exactly the opposite activity pattern with increased contacts to novel objects and interactions to unfamiliar mice. Social novelty recognition of an old vs. new social stranger in the three-chamber social test could be observed neither in *Tg*^{SHANK2A}, *Tg*^{SHANK2AR462X} nor control mice, which was also observed in the PV-neuron cell type-specific knock-out of *Shank2* [264]. Thus, the overexpression of two related SHANK2A variants was associated with very selective and different phenotypic behaviors, similarly to the diverse *SHANK2* patients, who were diagnosed with different neuropsychiatric disorders as SCZ-like or ASD-like phenotypes. The dramatic opposite social behavior of *Tg*^{SHANK2A} and *Tg*^{SHANK2AR462X} mice is novel in *Shank* mutant mice. According to this parameter, *Tg*^{SHANK2A} mice showed a pure ASD-like phenotype, while the phenotype of *Tg*^{SHANK2AR462X} mice might belong to ADHD [235-237] since both ASD and ADHD mouse models share the lack of behavioral inhibition "ADHD [235-237] and ASD [238-241]". The discrepancy in the social behavior between *Tg*^{SHANK2A} and *Tg*^{SHANK2AR462X} mice suggests opposite effects of the two isoforms on the social circuits in the forebrain, *e.g.* the prefrontal-hippocampal-amygdala pathway. Moreover, the social impairment in *Tg*^{SHANK2A} but not *Tg*^{SHANK2AR462X} mice was accompanied by a downregulation of NMDAR 2A and 2B subunit expression in the hippocampus. As NMDAR-mediated neurotransmission is important in the regulation of normal sociability in mice [265-268], the dysregulation of NMDAR expression in the hippocampus may account for the severe social impairment in *Tg*^{SHANK2A} mice. In previous studies, *Shank2* knock-out mouse models showed a dysregulation in NMDAR subunit expression. GluN1 subunit expression was reduced in the hippocampus of *Shank2*$^{\Delta ex15\text{-}16}$ and *Shank2*$^{\Delta ex24}$ knock-out mice but increased in *Shank2*$^{\Delta e16}$ [141-143]. On the other hand, both GluN2A and GluN2B subunit expression was increased in the hippocampus of *Shank2*$^{\Delta e16}$ and *Shank2*$^{\Delta ex24}$ knock-out mice [141-143]. The reason for this discrepancy between these mice is still unknown, and the question is open as to whether the differential expression is a result of the loss of Shank2 or acts as a compensatory mechanism by other Shank members.

The imbalance of the excitatory and inhibitory signals and disturbance in network synchrony play a role in ASD manifestation [183-188,269,270]. Therefore, the interneuronal marker PV, known to be implicated in brain excitation and rhythms, as well as brain dysfunctions [271-276], was investigated in $Tg^{SHANK2A}$ and $Tg^{SHANK2AR462X}$ mice. The PV immunosignal in the hippocampus of $Tg^{SHANK2A}$ mice was reduced compared to $Tg^{SHANK2AR462X}$ and control mice. The observed reduction in the PV immunosignal can be either a result of a decrease in gene expression levels and/or a decrease in the numbers of PV-positive neurons due to perturbed developmental state or premature cell death [277]. If there is a decrease in the PV expression, it can result in enhanced inhibition [277]. In contrast, the loss of the PV-positive neurons can cause reduced inhibition [277]. One way to answer this question is to perform staining for *Vicia Villosa Agglutinin* (VVA) which recognizes the specific extracellular matrix enwrapping the PV-positive neurons [278]. The reduced expression of PV was previously shown in many mouse models of ASD including two *Shank1* and *Shank3* knock-out mouse lines [277,279,280]. However, the level of PV expression was not investigated before in conventional *Shank2* knock-out mouse models. Shank proteins were also found to be expressed in PV-positive neurons, and limiting the Shank2 deletion to these neurons has led to hyperactivity, enhanced self-grooming and suppressed brain excitation, indicating a direct link between Shank and PV and that Shank2 may regulate PV expression at the transcriptional level.

4.2.2 AMPAR conductance imbalance in the apical and basal dendrites in the CA1 hippocampal region of $Tg^{SHANK2A}$ mice

The electrophysiological studies in the hippocampal CA1 cells were used to identify the alternation in the fast glutamatergic neurotransmission at the synaptic level. The electrophysiological recordings of $Tg^{SHANK2A}$ mice revealed an impaired AMPA/NMDA ratio in the apical dendrites of the hippocampal CA1 region. AMPARs are composed of four types of subunits, designated as GluA1, GluA2, GluA3, and GluA4, which form tetramers [281,282]. Most AMPARs are heterotetrameric, consisting of symmetric 'dimer of dimers' of GluA2 and either GluA1, GluA3 or GluA4 [283,284]. The AMPAR impermeability to Ca^{2+} is mediated by the GluA2 subunit [285]. The increase in AMPA/NMDA ratio in the apical dendrites in $Tg^{SHANK2A}$ mice is due to either an increase in the number of AMPARs or switching the type of AMPARs into the GluA2-lacking Ca^{2+} permeable channels. The effect of the drug Naspm, which specifically blocks the Ca^{2+} permeable channels, revealed increased Ca^{2+} permeable channels in the apical

dendrites as EPSCs were reduced after the drug treatment. Moreover, the effect of Naspm on EPSCs in the basal dendrites was absent in $Tg^{SHANK2A}$ mice in contrast to control mice, suggesting an increase in the number of Ca^{2+} impermeable channels in the basal dendrites of $Tg^{SHANK2A}$ mice. The switch of AMPAR subunit between the apical and basal dendrites in $Tg^{SHANK2A}$ mice led to an absence of LTP in basal dendrites. However, the increase of GluA2-lacking channels in the apical dendrites and their decrease in the basal dendrites need to be confirmed by the immunostaining of GluA2 subunit. Recently, it has been shown that Shank proteins can mediate Zn^{2+}-dependent regulation of AMPAR function by allowing the AMPAR subunit switch in the developing neurons from GluA2-lacking to GluA2-containing AMPARs, which contributes to synaptic maturation and plasticity [286]. The SHANK protein family plays a major role in retaining and maintaining AMPAR at synapses by anchoring endocytic zones adjacent to the PSD [287,288]. Moreover, the SH3 protein domain of SHANKs has been shown to be important in AMPAR trafficking through interaction with GluA2 *via* GRIP or by direct modulation of GluA1 trafficking *via* the Rich2- or mGluR- dependent pathways [34,91,289-291]. Mutations in *GRIP1* have been found in ASD patients [292]. These mutations are suggested to have either a gain of function effect leading to accelerated GluA2 recycling [292] or a loss of function one resulting in delayed GluA2 recycling in primary neurons [293]. *Shank3* knockout mice revealed a reduction in GluA1 clusters and protein levels in the hippocampus, and an alteration in activity-dependent AMPAR synaptic plasticity [294,295]. In hippocampal neurons knocked down for Shank3, a reduction in cell surface expression of GluA1 without a reduction in its protein expression was noticed which was correlated with the reduced mEPSC frequency, reflecting impairment in activity-dependent synaptic recruitment of AMPARs at basal conditions [290]. Moreover, in the CA1 region of the hippocampus, $Shank2^{\Delta ex15\text{-}16}$ and $Shank2^{\Delta ex24}$ knockout mice showed increased AMPA/NMDA ratio [141,143]. In contrast, $Shank2^{\Delta ex16}$ mice showed a decreased AMPA/NMDA ratio which had subsequently an effect on the AMPAR function and synaptic development leading to ASD-like phenotypes in mice [142]. Therefore, SHANK2 is critical for AMPAR recruitment and functionality in multiple brain circuits and any change in this normal developmental process of AMPARs is likely to be particularly vulnerable to risk factors for ASD.

In contrast to $Tg^{SHANK2A}$ mice, $Tg^{SHANK2AR462X}$ mice had no impairment on the electrophysiological level. Previously, the rAAV-mediated SHANK2A(R462X) overexpression in the forebrain of P0 mice revealed an increase in the total number of AMPARs and AMPAR clusters in the stratum

radiatum of the hippocampus, which is thought to be mediated by alterations in the distribution of synaptic and extrasynaptic AMPAR [136]. Also, a reduced localization of AMPAR in spine heads was detected [136]. The effect of SHANK2A(R462X) overexpression demonstrated also a reduced average mEPSC amplitude, suggested to be caused by the postsynaptic reduction in the density of AMPARs [136]. In $Tg^{SHANK2AR462X}$ mice, however, no effect on EPSC amplitude or AMPA/NMDA ratio was detected. The discrepancy between these results can be explained by the overexpression of SHANK2A(R462X) only in the excitatory neurons in $Tg^{SHANK2AR462X}$ mice, while it was expressed in all neurons under the control of synapsin 1 promoter in rAAV-mediated SHANK2A(R462X).

4.2.3 Synaptosome proteomic analysis in $Tg^{SHANK2A}$ and $Tg^{SHANK2AR462X}$ mice

The effect of the SHANK2A and SHANK2A(R462X) overexpression on the expression of the synaptic proteins was investigated using mass spectrometry. The analysis of synaptosome proteomic can give insight into the synaptic dysfunction in $Tg^{SHANK2A}$ and $Tg^{SHANK2AR462X}$ mice. The overexpression of SHANK2A revealed a higher effect than SHANK2A(R462X) on the abundance of synaptic proteins, suggesting more synaptic dysfunction in $Tg^{SHANK2A}$ mice. In $Tg^{SHANK2A}$ mice, the total SHANK2 level at the synapse was 2.5 fold its level in control mice **(Figure 45)**. As suggested by the nCounter analysis measuring Venus expression on RNA level, SHANK2A expression is 12 times higher than that of the endogenous Shank2. This indicates that either not all the expressed SHANK2A transgene is localized in the PSD due to its size limitation or most of the overexpressed SHANK2A is degraded after translation. Due to the lack of an efficient Shank2 antibody that binds to both human and mouse Shank2 proteins with the same affinity, these hypotheses yet have to be confirmed. In $Tg^{SHANK2AR462X}$ mice, the abundance of SHANK2 protein in the synapses of the hippocampus was not different from the control mice **(Figure 45)**. This can be a result of the inefficiency of the mass spectrometry to identify the truncated form of SHANK2. Another explanation is that SHANK2A(R462X) does not localize in the spines but localizes mainly in the soma and dendrites where it exerts a dominant negative effect, as shown in the rAAV-mediated SHANK2A(R462X) overexpression [136]. The localization of SHANK2A(R462X) in the soma and not in spines where synapses are formed is consistent with the normal electrophysiological measurements in $Tg^{SHANK2AR462X}$ mice. To this end, another pathway of the effect of SHANK2A(R462X) overexpression leading to the behavioral abnormalities is considered. By taking a closer look at the proteins which were differentially

abundant, the organization of SHANK proteins in the PSD of $Tg^{SHANK2A}$ mice is clearly affected due to a 30% reduced localization of both Shank1 and Shank3 protein in response to the high abundance of SHANK2A (for a list of differentially expressed proteins, see **Appendix 4**). This suggests the close relationship between the three SHANK proteins and the compensation of their expression and function by each other. Previously, brain–region-specific biochemical analysis of synaptosomes in $Shank2^{\Delta e16}$ knockout mice revealed that the loss of Shank2 results in synaptic upregulation of Shank3. Most interestingly, this phenomenon also happens after the transient knock-down of Shank2 in rat primary hippocampal cultures and is only seen on the protein level implying a local regulatory mechanism, which may be a potential target for pharmacological intervention [142]. By comparing these results to the effect of SHANK2A overexpression on the expression of other SHANK members on RNA level, the endogenous *Shank1* and *Shank3* expression was not affected. Because mRNA was extracted from the whole hippocampus, the small difference in the expression level of *Shank1* and *Shank3* in specific cell types between $Tg^{SHANK2A}$ and control mice may be diluted. Moreover, the SHANK2A overexpression may have a specific effect only on the localization of other Shank members in the PSD but not on the expression level. In $Tg^{SHANK2AR462X}$ mice, no abundance difference of Shank1 or Shank3 was detected confirming the non-localization of SHANK2A(R462X) in the PSD **(Figure 45)**.

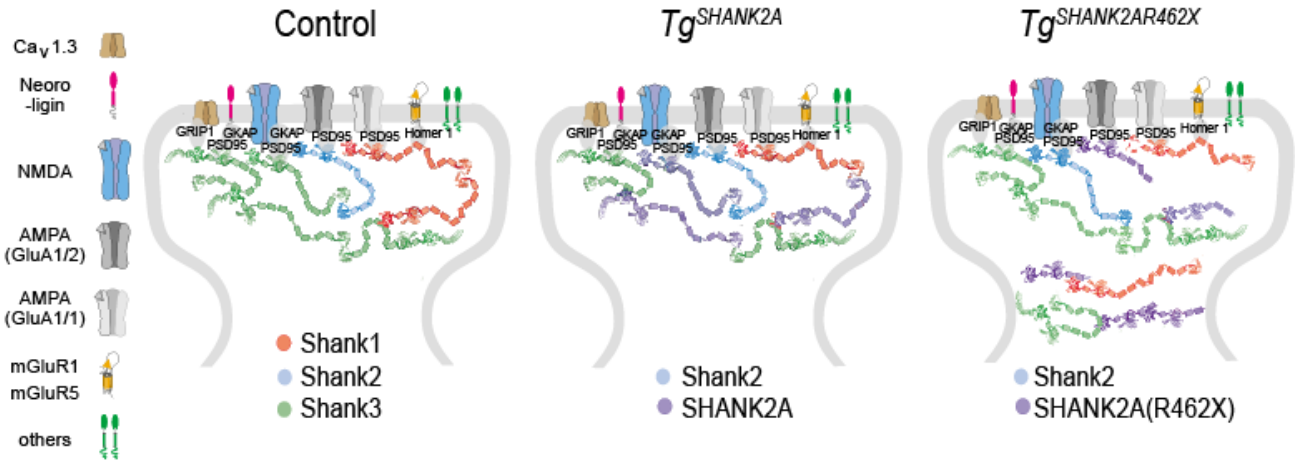

Figure 45: Putative Shank1-3 organization in the postsynaptic synaptosome compartment of the excitatory glutamatergic neurons in $Tg^{SHANK2A}$, $Tg^{SHANK2AR462X}$ and control mice
Schematic diagrams of the putative PSD in $Tg^{SHANK2A}$, $Tg^{SHANK2AR462X}$ and control mice. In control mice, the Shank3 expression is the highest compared to the expression of other Shank protein family members. In Tg^{SHANK2} mice, the organization of Shank proteins in the PSD is dominated by SHANK2A, and the expression of the endogenous Shank1 and Shank3 was 30% reduced compared to their expression control mice. In $Tg^{SHANK2AR462X}$ mice, the expression of SHANK2A(R462X) was not localized mainly in the synaptosome and

had no effect on the expression of the endogenous Shank1 or Shank3. However, other negative effects exerted by the SHANK2A(R462X) overexpression may dominate some functions of the Shank protein family.

The pathway analysis and molecular gene ontology of differentially abundant proteins in $Tg^{SHANK2A}$ and $Tg^{SHANK2AR462X}$ mice were performed using the online software ConsensusPathDB in order to study the most likely affected pathways. The analysis revealed a disruption of glutamatergic synapses and glutamate receptor binding affecting mainly the synaptic membrane in the spines of $Tg^{SHANK2A}$ mice. The dysfunction of glutamatergic synapses is well known to be associated with ASD phenotypes (for a review, see [296]). For the biological process analysis, mouse behaviors including social and learning and memory were predicted to be affected which is consistent with the behavioral analysis of $Tg^{SHANK2A}$ mice. Moreover, the regulation of AMPAR activity and LTP were suggested to be disturbed, consistent with the electrophysiological results of the AMPAR subunit switch in the apical and basal dendrites. The pathway and gene ontology analysis of differentially abundant proteins in the synaptosomes of $Tg^{SHANK2AR462X}$ mice revealed that axon and dendrites' branching due to the dysfunction of semaphorin receptor activity is most likely affected. Semaphorins are a class of secreted and membrane proteins that play an important role in neural system development by guiding axons to their target regions in the brain [297,298]. In a previous study, changes in the numbers and sizes of axons were found in the cortex of ASD patients [299]. Alterations of the morphology of dendrites were also found in human and mouse models of ASD (for a review, see [300]). Moreover, axon guidance pathways strongly influence human speech and language, and deficits in language and communication are hallmarks of ASD [301]. These findings stress the importance of normal axons and dendrites formation for proper brain development and provide a mechanism of the excessive connections between neighboring areas in the brain of ASD patients. These excessive connections may explain why individuals with ASD show the phenotypes of inability to shift attention, engaging in repetitive behavior and social impairment [299].

By performing biological process analysis of the differentially abundant proteins in the hippocampus of $Tg^{SHANK2A}$ and $Tg^{SHANK2AR462X}$ mice using the ConsensusPathDB software, both mouse lines are predicted to have abnormal behaviors. This indicates that ASD phenotypes are not exclusive to the synaptic dysfunction, and that the impairment in axon and dendrites' branching leading to excessive neurons that cause local over-connectivity could be a key feature

of ASD pathophysiology [302]. Therefore, the effect of the transgene overexpression on the structure of axons, dendrites and spines should be further investigated in detail by Golgi staining.

4.2.4 Rescue of some autistic phenotypes in *Tg*^{SHANK2A} and *Tg*^{SHANK2AR462X} mice after switching off the transgene overexpression in adulthood

It has been suggested that some symptoms of ASD are due to prenatal processes, like impaired neuronal migration during early gestation, for example, that cannot be reversed in adulthood. The temporal control of the transgene overexpression in *Tg*^{SHANK2A} and *Tg*^{SHANK2AR462X} mice allowed the investigation of the reversibility of autistic features in adulthood by recovering the SHANK organization and the normal level of the polycistronic SHANK2 expression. Here four weeks of dox diet in water was applied on adult mice (5 – 8 months), instead of one-week treatment [303], to switch off the tTA-dependent transgene expression.

In *Tg*^{SHANK2A} and *Tg*^{SHANK2AR462X} mice, the decrease and increase of the social interaction, respectively, were rescued after the stop of the transgene overexpression in adulthood. This indicates that certain circuits related to autistic features have a plasticity that can be rescued after the critical developmental stage. Thus, although SHANK2A overexpression inhibited the formation of networks involved in social learning during development, the action of the sociability network could be rebuilt when the genetic reason was eliminated. The rescue of the social impairment in dox-treated *Tg*^{SHANK2A} was accompanied by a rescue of the reduced expression of NMDAR subunits in the hippocampus. This is consistent with a previous study showing that the activation of NMDAR or enhancing its function using NMDAR agonists or *via* mGluR5 activation in adult mouse brains can rescue the social impairment but not other behavioral abnormalities in a *Shank* mouse model of ASD [141]. In that study, the treatment of *Shank2*$^{\Delta ex15\text{-}16}$ knock-out mice with D-cycloserine as a partial agonist at the glycine-binding site of NMDAR showed a rescue of the NMDA/AMPA ratio and social impairments [141]. Moreover, a positive allosteric modulator of mGluR5, (3-cyano-N-(1,3-diphenyl-1H-pyrazol-5-yl) benzamide) (CDPPB), which enhances the NMDAR function via mGluR5 activation, led to a normalization of NMDA/AMPA ratio and a restoration of the impaired LTP and LTD at Schaffer collateral-CA1 pyramidal (SC-CA1) synapses in the hippocampus of *Shank2*$^{\Delta ex15\text{-}16}$ mice [141]. Importantly, CDPPB did not rescue other autistic features like repeated jumping, anxiety-like behaviors or hyperactivity, which suggests that reduced NMDAR signaling in the hippocampus

leads to impaired social interaction but not other autistic-like behaviors. Another way to activate NMDAR in *Shank2*$^{\Delta ex15\text{-}16}$ knock-out mice was performed by the postsynaptic Zn^{2+} elevation induced by a Zn^{2+} chelator called clioquinol [304]. Zn^{2+} is mainly derived from presynaptic pools and activates NMDAR through postsynaptic activation of the tyrosine kinase Src [305]. Treating *Shank2* knock-out mice with clioquinol (2 hrs before the behavior experiment) has been shown to enhance social interaction [304]. On the other hand, the NMDA/AMPA ratio in the hippocampus of *Shank2*$^{\Delta e\text{-}16}$ knock-out mice was increased with enhancing LTP and upregulation of NMDAR subunits [142]. In this regard, it certainly has to be further clarified whether the loss of Shank2 leads to NMDAR hyper- or hypofunction and if the observed NMDAR upregulation can, therefore, be interpreted as causative or compensatory with respect to the corresponding physiological phenotype [133]. In general, it can be concluded that maintaining a normal range of NMDAR function in the brain is important, as both over- and under- regulation of NMDAR transmission may result in abnormal behavioral phenotypes [133].

The rescue of other SHANK2 overexpression-linked behaviors was not as clear-cut. The repetitive behavior patterns, hyperactivity, anxiety, impulsive behavior and cognitive dysfunction were not rescued in *Tg*^{SHANK2A} or *Tg*^{SHANK2AR462X} mice after the stop of the transgene overexpression in adulthood. Moreover, the non-rescue of cognitive dysfunction was accompanied by no rescue of the downregulation of AMPAR subunit expression in the hippocampus, confirming their role in the learning and memory [306,307]. In the fear conditioning test, both dox-treated *Tg*^{SHANK2} and *Tg*^{SHANK2AR462X} mice showed higher memory retrieval in the cued phase compared to their dox-treated littermates for unknown reasons.

In conclusion, continued neural plasticity is present in the adult mouse brain, especially regarding the social circuits. This can pave the way to rescue at least some ASD symptoms in adulthood. Moreover, the irreversible behavioral deficits may also be improved with early postnatal intervention, which should be further investigated.

4.2.5 Specific autistic-like behaviors in mice caused by SHANK2A overexpression after development

The SHANK2A overexpression in *Tg*^{SHANK2A} mice was temporally controlled after development to test whether some autistic-like behaviors can still be developed after the critical developmental stage. In a previous study, it has been shown that the expression of the GFP

transgene by tTA-dependent tetracycline promoter was already present at P0, which indicated that the functional activity of the αCaMKII-tTA transgene was already present in newborn mice [308]. Pregnant mice were given dox until labor to switch off the SHANK2A overexpression during the embryonic and early postnatal stages, confirming the absence of the transgene expression during most of the critical developmental period. Immunoblotting of protein lysates from different brain regions of adult P0 dox-treated $Tg^{SHANK2A}$ mice**,** when their mothers were given dox until birth, revealed high expression levels of SHANK2A and other reporter proteins, but lower than the transgenic SHANK2A expression in $Tg^{SHANK2A}$ mice that expressed SHANK2A during development. This indicates that the tTA-dependent tetracycline promoter did not return back to its complete efficiency due to its silencing during development in the absence of the active tTA, as shown previously [309]. According to that study, the tTA-dependent tetracycline promoter can be unsilenced only in cell types with very high tTA activity after the full washout of dox [309].

The behavioral analysis of adult P0 dox-treated $Tg^{SHANK2A}$ mice revealed hyperactivity, anxiety and repetitive rearing. Moreover, they displayed cognitive dysfunction accompanied by a downregulation of AMPAR subunits expression in the hippocampus. However, these mice exhibited no social impairment. This suggests that not all aspects of autistic disorders are mediated by early neurodevelopment, while social circuits may be formed mainly during the early developmental stage. This hypothesis is supported by studies showing that the preterm birth is associated with social difficulties in infants and increased risk of ASD [310-312] (for a review, see [313]).

The normal social interaction in these mice was accompanied by a normal NMDAR expression in the hippocampus. This confirms again that the social impairment in $Tg^{SHANK2A}$ mice is due to the NMDAR dysfunction, although NMDAR-independent mechanisms may also play a role.

In all performed behavioral tests, adult P0 dox-treated $Tg^{SHANK2A}$ mice did not show such a severe phenotype as $Tg^{SHANK2A}$ mice that express the transgene during development. This is in line with the study which revealed that autistic patients with late ASD manifestations were found to exhibit less severe and global developmental disruption [314]. This again highlights that ASD is mainly a neurodevelopmental disorder, however, some features with reduced severity can still be developed later in life.

4.2.6 Conclusion

The high prevalence of non-synonymous *SHANK* mutations in ASD and the variable phenotypes reported for different *Shank* mouse mutants suggest a broad repertoire of possible functional alterations in the SHANK-mediated organization that contribute to ASD. The approach used in this study provided a comprehensive model of synaptic alterations mediated by the disruption of SHANK proteins in the glutamatergic neurons. One conclusion from this study is that the disturbance in the expression of SHANKs has consequences on the function of the glutamatergic neurons and on the general, cognitive and social functions, ranging from ASD-like to ADHD-like phenotypes when SHANK2A variants are not localized in the PSD. SHANK proteins play an important role in AMPAR trafficking in specific tissues, which leads to balanced and organized AMPAR signaling, By the overexpression of SHANK2 variants, the AMPAR levels seem to be reduced, which is associated with the irreversible hyperactivity and cognitive dysfunction. Notably, not all affected neuronal circuits in *SHANK*-related ASD/ADHD are due to neurodevelopmental dysfunctions, hence, they can be reversed or treated in adulthood. The finding that a balanced NMDAR subunit expression in the hippocampus is necessary for a normal social behavior is of great interest and can pave the way for the development of novel molecular diagnoses and treatments for Shankopathies in ASD. In conclusion, a balanced expression and a proper dosage of SHANK2 along with other SHANK members throughout life are necessary for appropriate organization of synaptic proteins and receptors and for normal brain function.

4.2.7 Future perspective

This study has demonstrated that the truncated versions of SHANK2 can have dominant negative effects even when they are not localized at the PSD. Therefore, the expression of residual truncated Shank2 isoforms in the previously generated *Shank* knock-out mice should be further investigated, which can explain the distinct phenotype in these mice. Moreover, the full battery of behavioral analysis covering ASD, SCZ, mania and ADHD has to be applied to cover the wide range of expected phenotypes. In addition, male and female littermates need to be compared to unravel gender effects on the expression of the phenotypes.

Knock-in mice with genetic variants in *Shank* genes resembling the identical genetic defects of human ASD patients should contribute to explaining the distinct human phenotypes and help to

discover the affected crucial neuronal circuits and cell types underlying the abnormalities. An investigation as to whether there is a critical period of the affected circuits and underlying phenotypes should be carried out in these mice. The affected neuronal populations in these mice can then be targeted and analyzed in great detail during the behavioral analysis by novel physiological technologies, *e.g.* multicellular recordings and optogenetics. Once the impairments in these circuits are confirmed, strategies for effective treatment can be developed. However, the ultimate goal remains the translation of these new findings into treatment options for human.

Bibliography

1 Banerjee, S., Riordan, M. & Bhat, M. A. Genetic aspects of autism spectrum disorders: insights from animal models. *Frontiers in cellular neuroscience* **8**, 58-58, doi:10.3389/fncel.2014.00058 (2014).

2 *Diagnostic and statistical manual of mental disorders : DSM-5*. (American Psychiatric Association, 2013).

3 Yoo, H. J. Recent increase in autism and ADHD: true or inflated? *Journal of Korean medical science* **28**, 974-975, doi:10.3346/jkms.2013.28.7.974 (2013).

4 Berkel, S. *et al.* Mutations in the SHANK2 synaptic scaffolding gene in autism spectrum disorder and mental retardation. *Nature genetics* **42**, 489-491, doi:10.1038/ng.589 (2010).

5 Gillberg, C. & Billstedt, E. Autism and Asperger syndrome: coexistence with other clinical disorders. *Acta psychiatrica Scandinavica* **102**, 321-330 (2000).

6 Levy, S. E., Mandell, D. S. & Schultz, R. T. Autism. *Lancet (London, England)* **374**, 1627-1638, doi:10.1016/S0140-6736(09)61376-3 (2009).

7 Matson, J. L. & Cervantes, P. E. Assessing aggression in persons with autism spectrum disorders: an overview. *Research in developmental disabilities* **35**, 3269-3275, doi:10.1016/j.ridd.2014.08.004 (2014).

8 Hsiao, E. Y. Gastrointestinal issues in autism spectrum disorder. *Harvard review of psychiatry* **22**, 104-111, doi:10.1097/hrp.0000000000000029 (2014).

9 Abrahams, B. S. & Geschwind, D. H. Advances in autism genetics: on the threshold of a new neurobiology. *Nature reviews. Genetics* **9**, 341-355, doi:10.1038/nrg2346 (2008).

10 Geschwind, D. H. Advances in autism. *Annual review of medicine* **60**, 367-380, doi:10.1146/annurev.med.60.053107.121225 (2009).

11 Guo, X., Tu, W.-J. & Shi, X.-D. Tuberous sclerosis complex in autism. *Iranian journal of pediatrics* **22**, 408-411 (2012).

12 Vignoli, A. *et al.* Autism spectrum disorder in tuberous sclerosis complex: searching for risk markers. *Orphanet journal of rare diseases* **10**, 154-154, doi:10.1186/s13023-015-0371-1 (2015).

13 Percy, A. K. Rett syndrome: exploring the autism link. *Archives of neurology* **68**, 985-989, doi:10.1001/archneurol.2011.149 (2011).

14 Kaufmann, W. E. *et al.* Autism Spectrum Disorder in Fragile X Syndrome: Cooccurring Conditions and Current Treatment. *Pediatrics* **139**, S194, doi:10.1542/peds.2016-1159F (2017).

15 Chaste, P. *et al.* High-functioning autism spectrum disorder and fragile X syndrome: report of two affected sisters. *Molecular Autism* **3**, 5, doi:10.1186/2040-2392-3-5 (2012).

16 Abbeduto, L., McDuffie, A. & Thurman, A. J. The fragile X syndrome-autism comorbidity: what do we really know? *Frontiers in genetics* **5**, 355-355, doi:10.3389/fgene.2014.00355 (2014).

17 Hernandez, R. N. *et al.* Autism spectrum disorder in fragile X syndrome: a longitudinal evaluation. *American journal of medical genetics. Part A* **149A**, 1125-1137, doi:10.1002/ajmg.a.32848 (2009).

18 Rabaneda, Luis G., Robles-Lanuza, E., Nieto-González, José L. & Scholl, Francisco G. Neurexin Dysfunction in Adult Neurons Results in Autistic-like Behavior in Mice. *Cell Reports* **8**, 338-346, doi:10.1016/j.celrep.2014.06.022 (2014).

19 Amaral, D. G., Schumann, C. M. & Nordahl, C. W. Neuroanatomy of autism. *Trends in neurosciences* **31**, 137-145, doi:10.1016/j.tins.2007.12.005 (2008).

20 Belmonte, M. K. *et al.* Autism and Abnormal Development of Brain Connectivity. *The Journal of Neuroscience* **24**, 9228, doi:10.1523/JNEUROSCI.3340-04.2004 (2004).

21 Jamain, S. *et al.* Mutations of the X-linked genes encoding neuroligins NLGN3 and NLGN4 are associated with autism. *Nature genetics* **34**, 27-29, doi:10.1038/ng1136 (2003).

22 Ching, M. S. L. *et al.* Deletions of NRXN1 (neurexin-1) predispose to a wide spectrum of developmental disorders. *American journal of medical genetics. Part B, Neuropsychiatric genetics : the official publication of the International Society of Psychiatric Genetics* **153B**, 937-947, doi:10.1002/ajmg.b.31063 (2010).

23 Kim, H.-G. *et al.* Disruption of Neurexin 1 Associated with Autism Spectrum Disorder. *The American Journal of Human Genetics* **82**, 199-207, doi:10.1016/j.ajhg.2007.09.011 (2008).

24 Alarcon, M. *et al.* Linkage, association, and gene-expression analyses identify CNTNAP2 as an autism-susceptibility gene. *American journal of human genetics* **82**, 150-159, doi:10.1016/j.ajhg.2007.09.005 (2008).

25 Durand, C. M. *et al.* Mutations in the gene encoding the synaptic scaffolding protein SHANK3 are associated with autism spectrum disorders. *Nature genetics* **39**, 25-27, doi:10.1038/ng1933 (2007).

26 Sato, D. *et al.* SHANK1 Deletions in Males with Autism Spectrum Disorder. *American journal of human genetics* **90**, 879-887, doi:10.1016/j.ajhg.2012.03.017 (2012).

27 Chaste, P. & Leboyer, M. Autism risk factors: genes, environment, and gene-environment interactions. *Dialogues in clinical neuroscience* **14**, 281-292 (2012).

28 Karimi, P., Kamali, E., Mousavi, S. M. & Karahmadi, M. Environmental factors influencing the risk of autism. *Journal of research in medical sciences : the official journal of Isfahan University of Medical Sciences* **22**, 27-27, doi:10.4103/1735-1995.200272 (2017).

29 Dietert, R. R., Dietert, J. M. & Dewitt, J. C. Environmental risk factors for autism. *Emerging health threats journal* **4**, 7111-7111, doi:10.3402/ehtj.v4i0.7111 (2010).

30 Modabbernia, A., Velthorst, E. & Reichenberg, A. Environmental risk factors for autism: an evidence-based review of systematic reviews and meta-analyses. *Molecular Autism* **8**, 13, doi:10.1186/s13229-017-0121-4 (2017).

31 Werling, D. M. The role of sex-differential biology in risk for autism spectrum disorder. *Biology of sex differences* **7**, 58, doi:10.1186/s13293-016-0112-8 (2016).

32 Fombonne, E. Epidemiology of pervasive developmental disorders. *Pediatr Res* **65**, 591-598, doi:10.1203/PDR.0b013e31819e7203 (2009).

33 Gillberg, C., Cederlund, M., Lamberg, K. & Zeijlon, L. Brief report: "the autism epidemic". The registered prevalence of autism in a Swedish urban area. *J Autism Dev Disord* **36**, 429-435, doi:10.1007/s10803-006-0081-6 (2006).

34 Sheng, M. & Kim, E. The Shank family of scaffold proteins. *Journal of cell science* **113 (Pt 11)**, 1851-1856 (2000).

35 Bargiela, S., Steward, R. & Mandy, W. The Experiences of Late-diagnosed Women with Autism Spectrum Conditions: An Investigation of the Female Autism Phenotype. *J Autism Dev Disord* **46**, 3281-3294, doi:10.1007/s10803-016-2872-8 (2016).

36 Hiller, R. M., Young, R. L. & Weber, N. Sex differences in pre-diagnosis concerns for children later diagnosed with autism spectrum disorder. *Autism* **20**, 75-84, doi:10.1177/1362361314568899 (2015).

37 Hiller, R. M., Young, R. L. & Weber, N. Sex differences in autism spectrum disorder based on DSM-5 criteria: evidence from clinician and teacher reporting. *Journal of abnormal child psychology* **42**, 1381-1393, doi:10.1007/s10802-014-9881-x (2014).

38 Mandy, W. *et al.* Sex differences in autism spectrum disorder: evidence from a large sample of children and adolescents. *Journal of autism and developmental disorders* **42**, 1304-1313, doi:10.1007/s10803-011-1356-0 (2012).

39 Werling, D. M. & Geschwind, D. H. Sex differences in autism spectrum disorders. *Current opinion in neurology* **26**, 146-153, doi:10.1097/WCO.0b013e32835ee548 (2013).

40 Stone, J. L. *et al.* Evidence for sex-specific risk alleles in autism spectrum disorder. *American journal of human genetics* **75**, 1117-1123, doi:10.1086/426034 (2004).

41 Cantor, R. M. *et al.* Replication of autism linkage: fine-mapping peak at 17q21. *American journal of human genetics* **76**, 1050-1056, doi:10.1086/430278 (2005).

42 Szatmari, P. *et al.* Mapping autism risk loci using genetic linkage and chromosomal rearrangements. *Nature genetics* **39**, 319-328, doi:10.1038/ng1985 (2007).

43 Lamb, J. A. *et al.* Analysis of IMGSAC autism susceptibility loci: evidence for sex limited and parent of origin specific effects. *J Med Genet* **42**, 132-137, doi:10.1136/jmg.2004.025668 (2005).

44 Werling, D. M., Parikshak, N. N. & Geschwind, D. H. Gene expression in human brain implicates sexually dimorphic pathways in autism spectrum disorders. *Nature Communications* **7**, 10717, doi:10.1038/ncomms10717 (2016).

45 Donnelly, S. L. *et al.* Female with autistic disorder and monosomy X (Turner syndrome): parent-of-origin effect of the X chromosome. *American journal of medical genetics* **96**, 312-316 (2000).

46 Skuse, D. H. *et al.* Evidence from Turner's syndrome of an imprinted X-linked locus affecting cognitive function. *Nature* **387**, 705-708, doi:10.1038/42706 (1997).

47 Skuse, D. H. Autism in association with Turner syndrome: Genetic implications for male vulnerability to pervasive developmental disorders AU - Creswell, Catharine S. *Neurocase* **5**, 511-518, doi:10.1080/13554799908402746 (1999).

48 Jha, P., Sheth, D. & Ghaziuddin, M. Autism spectrum disorder and Klinefelter syndrome. *European child & adolescent psychiatry* **16**, 305-308, doi:10.1007/s00787-007-0601-8 (2007).

49 van Rijn, S., Bierman, M., Bruining, H. & Swaab, H. Vulnerability for autism traits in boys and men with an extra X chromosome (47,XXY): the mediating role of cognitive flexibility. *Journal of psychiatric research* **46**, 1300-1306, doi:10.1016/j.jpsychires.2012.06.004 (2012).

50 Ross, J. L. *et al.* Behavioral and social phenotypes in boys with 47,XYY syndrome or 47,XXY Klinefelter syndrome. *Pediatrics* **129**, 769-778, doi:10.1542/peds.2011-0719 (2012).

51 Bishop, D. V. *et al.* Autism, language and communication in children with sex chromosome trisomies. *Archives of disease in childhood* **96**, 954-959, doi:10.1136/adc.2009.179747 (2011).

52 Baron-Cohen, S. *et al.* Why are autism spectrum conditions more prevalent in males? *PLoS biology* **9**, e1001081, doi:10.1371/journal.pbio.1001081 (2011).

53 Babayan, A. H. & Kramár, E. A. Rapid effects of oestrogen on synaptic plasticity: interactions with actin and its signalling proteins. *Journal of neuroendocrinology* **25**, 1163-1172, doi:10.1111/jne.12108 (2013).

54 Jelks, K. B., Wylie, R., Floyd, C. L., McAllister, A. K. & Wise, P. Estradiol Targets Synaptic Proteins to Induce Glutamatergic Synapse Formation in Cultured Hippocampal Neurons: Critical Role of Estrogen Receptor-α. *The Journal of Neuroscience* **27**, 6903-6913, doi:10.1523/jneurosci.0909-07.2007 (2007).

55 Beyer, C. Estrogen and the developing mammalian brain. *Anatomy and embryology* **199**, 379-390 (1999).

56 Auyeung, B. *et al.* Fetal testosterone and autistic traits. *British journal of psychology (London, England : 1953)* **100**, 1-22, doi:10.1348/000712608x311731 (2009).

57 Auyeung, B., Taylor, K., Hackett, G. & Baron-Cohen, S. Foetal testosterone and autistic traits in 18 to 24-month-old children. *Molecular Autism* **1**, 11, doi:10.1186/2040-2392-1-11 (2010).

58 Geier, D. A., Kern, J. K., King, P. G., Sykes, L. K. & Geier, M. R. An evaluation of the role and treatment of elevated male hormones in autism spectrum disorders. *Acta neurobiologiae experimentalis* **72**, 1-17 (2012).

59 Tordjman, S., Ferrari, P., Sulmont, V., Duyme, M. & Roubertoux, P. Androgenic activity in autism. *The American journal of psychiatry* **154**, 1626-1627 (1997).

60 Baron-Cohen, S. The extreme male brain theory of autism. *Trends in cognitive sciences* **6**, 248-254 (2002).

61 Voineagu, I. *et al.* Transcriptomic analysis of autistic brain reveals convergent molecular pathology. *Nature* **474**, 380-384, doi:10.1038/nature10110 (2011).

62 Schwarz, J. M. & Bilbo, S. D. Sex, glia, and development: interactions in health and disease. *Hormones and behavior* **62**, 243-253, doi:10.1016/j.yhbeh.2012.02.018 (2012).

63 McCarthy, M. M., Todd, B. J. & Amateau, S. K. Estradiol modulation of astrocytes and the establishment of sex differences in the brain. *Annals of the New York Academy of Sciences* **1007**, 283-297 (2003).

64 Sayad, A., Noroozi, R., Omrani, M. D., Taheri, M. & Ghafouri-Fard, S. Retinoic acid-related orphan receptor alpha (RORA) variants are associated with autism spectrum disorder. *Metabolic brain disease* **32**, 1595-1601, doi:10.1007/s11011-017-0049-6 (2017).

65 Nguyen, A., Rauch, T. A., Pfeifer, G. P. & Hu, V. W. Global methylation profiling of lymphoblastoid cell lines reveals epigenetic contributions to autism spectrum disorders and a novel autism candidate gene, RORA, whose protein product is reduced in autistic brain. *FASEB journal : official publication of the Federation of American Societies for Experimental Biology* **24**, 3036-3051, doi:10.1096/fj.10-154484 (2010).

66 Sarachana, T., Xu, M., Wu, R. C. & Hu, V. W. Sex hormones in autism: androgens and estrogens differentially and reciprocally regulate RORA, a novel candidate gene for autism. *PloS one* **6**, e17116, doi:10.1371/journal.pone.0017116 (2011).

67 Sarachana, T. & Hu, V. W. Differential recruitment of coregulators to the RORA promoter adds another layer of complexity to gene (dys) regulation by sex hormones in autism. *Molecular Autism* **4**, 39, doi:10.1186/2040-2392-4-39 (2013).

68 Hu, V. W., Sarachana, T., Sherrard, R. M. & Kocher, K. M. Investigation of sex differences in the expression of RORA and its transcriptional targets in the brain as a potential contributor to the sex bias in autism. *Molecular Autism* **6**, 7, doi:10.1186/2040-2392-6-7 (2015).

69 McEwen, B. S. & Milner, T. A. Understanding the broad influence of sex hormones and sex differences in the brain. *Journal of neuroscience research* **95**, 24-39, doi:10.1002/jnr.23809 (2017).

70 Johns, P. in *Clinical Neuroscience* (ed Paul Johns) 81-89 (Churchill Livingstone, 2014).

71 Sheng, M. & Hoogenraad, C. C. The postsynaptic architecture of excitatory synapses: a more quantitative view. *Annu Rev Biochem* **76**, 823-847, doi:10.1146/annurev.biochem.76.060805.160029 (2007).

72 Südhof, T. C. The presynaptic active zone. *Neuron* **75**, 11-25, doi:10.1016/j.neuron.2012.06.012 (2012).

73 Glutamate (ionotropic). *British Journal of Pharmacology* **158**, S113-S116, doi:10.1111/j.1476-5381.2009.00502_5.x (2009).

74 Uzman, A. *Molecular Cell Biology (4th edition)*. Vol. 29 (2001).

75 Lüscher, C. & Malenka, R. C. NMDA receptor-dependent long-term potentiation and long-term depression (LTP/LTD). *Cold Spring Harbor perspectives in biology* **4**, a005710, doi:10.1101/cshperspect.a005710.

76 Bayés, A. *et al.* Characterization of the proteome, diseases and evolution of the human postsynaptic density. *Nature neuroscience* **14**, 19-21, doi:10.1038/nn.2719 (2011).

77 Okabe, S. Molecular anatomy of the postsynaptic density. *Molecular and cellular neurosciences* **34**, 503-518, doi:10.1016/j.mcn.2007.01.006 (2007).

78 Verpelli, C., Schmeisser, M. J., Sala, C. & Boeckers, T. M. Scaffold proteins at the postsynaptic density. *Advances in experimental medicine and biology* **970**, 29-61, doi:10.1007/978-3-7091-0932-8_2 (2012).

79 de Bartolomeis, A. & Fiore, G. Postsynaptic density scaffolding proteins at excitatory synapse and disorders of synaptic plasticity: implications for human behavior pathologies. *International review of neurobiology* **59**, 221-254, doi:10.1016/s0074-7742(04)59009-8 (2004).

80 Kreienkamp, H. J. Scaffolding proteins at the postsynaptic density: shank as the architectural framework. *Handbook of experimental pharmacology*, 365-380, doi:10.1007/978-3-540-72843-6_15 (2008).

81 Sala, C. *et al.* Regulation of dendritic spine morphology and synaptic function by Shank and Homer. *Neuron* **31**, 115-130 (2001).

82 Prybylowski, K. *et al.* The synaptic localization of NR2B-containing NMDA receptors is controlled by interactions with PDZ proteins and AP-2. *Neuron* **47**, 845-857, doi:10.1016/j.neuron.2005.08.016 (2005).

83 Valtschanoff, J. G. & Weinberg, R. J. Laminar organization of the NMDA receptor complex within the postsynaptic density. *J Neurosci* **21**, 1211-1217 (2001).

84 Lim, S. *et al.* Characterization of the Shank family of synaptic proteins. Multiple genes, alternative splicing, and differential expression in brain and development. *The Journal of biological chemistry* **274**, 29510-29518 (1999).

85 Zitzer, H., Honck, H. H., Bachner, D., Richter, D. & Kreienkamp, H. J. Somatostatin receptor interacting protein defines a novel family of multidomain proteins present in human and rodent brain. *The Journal of biological chemistry* **274**, 32997-33001 (1999).

86 Naisbitt, S. *et al.* Shank, a novel family of postsynaptic density proteins that binds to the NMDA receptor/PSD-95/GKAP complex and cortactin. *Neuron* **23**, 569-582 (1999).

87 Jiang, Y.-H. & Ehlers, M. D. Modeling autism by SHANK gene mutations in mice. *Neuron* **78**, 8-27, doi:10.1016/j.neuron.2013.03.016 (2013).

88 Mosavi, L. K., Cammett, T. J., Desrosiers, D. C. & Peng, Z.-Y. The ankyrin repeat as molecular architecture for protein recognition. *Protein science : a publication of the Protein Society* **13**, 1435-1448, doi:10.1110/ps.03554604 (2004).

89 Boeckers, T. M. *et al.* Synaptic scaffolding proteins in rat brain. Ankyrin repeats of the multidomain Shank protein family interact with the cytoskeletal protein alpha-fodrin. *J Biol Chem* **276**, 40104-40112, doi:10.1074/jbc.M102454200 (2001).

90 Lim, S. *et al.* Sharpin, a novel postsynaptic density protein that directly interacts with the shank family of proteins. *Molecular and cellular neurosciences* **17**, 385-397, doi:10.1006/mcne.2000.0940 (2001).

91 Lu, W. & Ziff, E. B. PICK1 interacts with ABP/GRIP to regulate AMPA receptor trafficking. *Neuron* **47**, 407-421, doi:10.1016/j.neuron.2005.07.006 (2005).

92 Quitsch, A., Berhorster, K., Liew, C. W., Richter, D. & Kreienkamp, H. J. Postsynaptic shank antagonizes dendrite branching induced by the leucine-rich repeat protein Densin-180. *J Neurosci* **25**, 479-487, doi:10.1523/jneurosci.2699-04.2005 (2005).

93 Zhang, H. *et al.* Association of CaV1.3 L-type calcium channels with Shank. *J Neurosci* **25**, 1037-1049, doi:10.1523/jneurosci.4554-04.2005 (2005).

94 Naisbitt, S. *et al.* Characterization of guanylate kinase-associated protein, a postsynaptic density protein at excitatory synapses that interacts directly with postsynaptic density-95/synapse-associated protein 90. *J Neurosci* **17**, 5687-5696 (1997).

95 Kornau, H. C., Schenker, L. T., Kennedy, M. B. & Seeburg, P. H. Domain interaction between NMDA receptor subunits and the postsynaptic density protein PSD-95. *Science* **269**, 1737-1740 (1995).

96 Kim, C. H., Chung, H. J., Lee, H. K. & Huganir, R. L. Interaction of the AMPA receptor subunit GluR2/3 with PDZ domains regulates hippocampal long-term depression. *Proc Natl Acad Sci U S A* **98**, 11725-11730, doi:10.1073/pnas.211132798 (2001).

97 Uemura, T., Mori, H. & Mishina, M. Direct interaction of GluRdelta2 with Shank scaffold proteins in cerebellar Purkinje cells. *Mol Cell Neurosci* **26**, 330-341, doi:10.1016/j.mcn.2004.02.007 (2004).

98 Boeckers, T. M., Bockmann, J., Kreutz, M. R. & Gundelfinger, E. D. ProSAP/Shank proteins - a family of higher order organizing molecules of the postsynaptic density with an emerging role in human neurological disease. *J Neurochem* **81**, 903-910 (2002).

99 Im, Y. J. *et al.* Crystal structure of the Shank PDZ-ligand complex reveals a class I PDZ interaction and a novel PDZ-PDZ dimerization. *The Journal of biological chemistry* **278**, 48099-48104, doi:10.1074/jbc.M306919200 (2003).

100 Zitzer, H., Richter, D. & Kreienkamp, H. J. Agonist-dependent interaction of the rat somatostatin receptor subtype 2 with cortactin-binding protein 1. *The Journal of biological chemistry* **274**, 18153-18156 (1999).

101 Tu, J. C. *et al.* Coupling of mGluR/Homer and PSD-95 complexes by the Shank family of postsynaptic density proteins. *Neuron* **23**, 583-592 (1999).

102 Cheng Tu, J. *et al. Coupling of mGluR/Homer and PSD-95 Complexes by the Shank Family of Postsynaptic Density Proteins*. Vol. 23 (1999).

103 Ammer, A. G. & Weed, S. A. Cortactin branches out: roles in regulating protrusive actin dynamics. *Cell Motil Cytoskeleton* **65**, 687-707, doi:10.1002/cm.20296 (2008).

104 Baron, M. K. *et al.* An architectural framework that may lie at the core of the postsynaptic density. *Science (New York, N.Y.)* **311**, 531-535, doi:10.1126/science.1118995 (2006).

105 Gundelfinger, E. D., Boeckers, T. M., Baron, M. K. & Bowie, J. U. A role for zinc in postsynaptic density asSAMbly and plasticity? *Trends in biochemical sciences* **31**, 366-373, doi:10.1016/j.tibs.2006.05.007 (2006).

106 Boeckers, T. M. *et al.* C-terminal synaptic targeting elements for postsynaptic density proteins ProSAP1/Shank2 and ProSAP2/Shank3. *Journal of neurochemistry* **92**, 519-524, doi:10.1111/j.1471-4159.2004.02910.x (2005).

107 Sala, C., Vicidomini, C., Bigi, I., Mossa, A. & Verpelli, C. Shank synaptic scaffold proteins: keys to understanding the pathogenesis of autism and other synaptic disorders. *Journal of neurochemistry* **135**, 849-858, doi:10.1111/jnc.13232 (2015).

108 Boeckers, T. M. *et al.* Proline-rich synapse-associated protein-1/cortactin binding protein 1 (ProSAP1/CortBP1) is a PDZ-domain protein highly enriched in the postsynaptic density. *J Neurosci* **19**, 6506-6518 (1999).

109 Boeckers, T. M. *et al.* Proline-rich synapse-associated proteins ProSAP1 and ProSAP2 interact with synaptic proteins of the SAPAP/GKAP family. *Biochemical and biophysical research communications* **264**, 247-252, doi:10.1006/bbrc.1999.1489 (1999).

110 Leblond, C. S. *et al.* Genetic and functional analyses of SHANK2 mutations suggest a multiple hit model of autism spectrum disorders. *PLoS genetics* **8**, e1002521, doi:10.1371/journal.pgen.1002521 (2012).

111 McWilliams, R. R. *et al.* Shank2E binds NaPi cotransporter at the apical membrane of proximal tubule cells. *American Journal of Physiology-Cell Physiology* **289**, C1042-C1051, doi:10.1152/ajpcell.00568.2004 (2005).

112 McWilliams, R. R., Gidey, E., Fouassier, L., Weed, S. A. & Doctor, R. B. Characterization of an ankyrin repeat-containing Shank2 isoform (Shank2E) in liver epithelial cells. *The Biochemical journal* **380**, 181-191, doi:10.1042/bj20031577 (2004).

113 Boeckers, T. M. *et al.* Differential expression and dendritic transcript localization of Shank family members: identification of a dendritic targeting element in the 3' untranslated region of Shank1 mRNA. *Mol Cell Neurosci* **26**, 182-190, doi:10.1016/j.mcn.2004.01.009 (2004).

114 Grabrucker, A. M. *et al.* Concerted action of zinc and ProSAP/Shank in synaptogenesis and synapse maturation. *The EMBO journal* **30**, 569-581, doi:10.1038/emboj.2010.336 (2011).

115 Grabrucker, A. M. A role for synaptic zinc in ProSAP/Shank PSD scaffold malformation in autism spectrum disorders. *Developmental neurobiology* **74**, 136-146, doi:10.1002/dneu.22089 (2014).

116 Shi, R. *et al.* Shank Proteins Differentially Regulate Synaptic Transmission. *eNeuro* **4**, doi:10.1523/eneuro.0163-15.2017 (2017).

117 Soler, J. *et al.* Genetic variability in scaffolding proteins and risk for schizophrenia and autism-spectrum disorders: a systematic review. *Journal of psychiatry & neuroscience : JPN* **43**, 170066, doi:10.1503/jpn.170066 (2018).

118 Phelan, K. & McDermid, H. E. The 22q13.3 Deletion Syndrome (Phelan-McDermid Syndrome). *Molecular syndromology* **2**, 186-201, doi:000334260 (2012).

119 Wilson, H. L. *et al.* Interstitial 22q13 deletions: genes other than SHANK3 have major effects on cognitive and language development. *European journal of human genetics : EJHG* **16**, 1301-1310, doi:10.1038/ejhg.2008.107 (2008).

120 Wilson, H. L. *et al.* Molecular characterisation of the 22q13 deletion syndrome supports the role of haploinsufficiency of SHANK3/PROSAP2 in the major neurological symptoms. *Journal of Medical Genetics* **40**, 575, doi:10.1136/jmg.40.8.575 (2003).

121 Gauthier, J. *et al.* Novel de novo SHANK3 mutation in autistic patients. *American journal of medical genetics. Part B, Neuropsychiatric genetics : the official publication of the International Society of Psychiatric Genetics* **150B**, 421-424, doi:10.1002/ajmg.b.30822 (2009).

122 Boccuto, L. *et al.* Prevalence of SHANK3 variants in patients with different subtypes of autism spectrum disorders. *European journal of human genetics : EJHG* **21**, 310-316, doi:10.1038/ejhg.2012.175 (2013).

123 de Sena Cortabitarte, A. *et al.* Investigation of SHANK3 in schizophrenia. *American journal of medical genetics. Part B, Neuropsychiatric genetics : the official publication of the International Society of Psychiatric Genetics* **174**, 390-398, doi:10.1002/ajmg.b.32528 (2017).

124 Leblond, C. S. *et al.* Meta-analysis of SHANK Mutations in Autism Spectrum Disorders: a gradient of severity in cognitive impairments. *PLoS genetics* **10**, e1004580, doi:10.1371/journal.pgen.1004580 (2014).

125 Monteiro, P. & Feng, G. SHANK proteins: roles at the synapse and in autism spectrum disorder. *Nature reviews. Neuroscience* **18**, 147-157, doi:10.1038/nrn.2016.183 (2017).

126 Pinto, D. *et al.* Functional impact of global rare copy number variation in autism spectrum disorders. *Nature* **466**, 368-372, doi:10.1038/nature09146 (2010).

127 Wischmeijer, A. *et al.* Olfactory Receptor-Related Duplicons Mediate a Microdeletion at 11q13.2q13.4 Associated with a Syndromic Phenotype. *Mol Syndromol* **1**, 176-184, doi:10.1159/000322054 (2011).

128 Schluth-Bolard, C. *et al.* Breakpoint mapping by next generation sequencing reveals causative gene disruption in patients carrying apparently balanced chromosome rearrangements with intellectual deficiency and/or congenital malformations. *J Med Genet* **50**, 144-150, doi:10.1136/jmedgenet-2012-101351 (2013).

129 Prasad, A. *et al.* A discovery resource of rare copy number variations in individuals with autism spectrum disorder. *G3 (Bethesda)* **2**, 1665-1685, doi:10.1534/g3.112.004689 (2012).

130 Chilian, B. *et al.* Dysfunction of SHANK2 and CHRNA7 in a patient with intellectual disability and language impairment supports genetic epistasis of the two loci. *Clin Genet* **84**, 560-565, doi:10.1111/cge.12105 (2013).

131 RK, C. Y. *et al.* Whole genome sequencing resource identifies 18 new candidate genes for autism spectrum disorder. *Nat Neurosci* **20**, 602-611, doi:10.1038/nn.4524 (2017).

132 Bowling, K. M. *et al.* Genomic diagnosis for children with intellectual disability and/or developmental delay. *Genome Med* **9**, 43, doi:10.1186/s13073-017-0433-1 (2017).

133 Eltokhi, A., Rappold, G. & Sprengel, R. Distinct Phenotypes of Shank2 Mouse Models Reflect Neuropsychiatric Spectrum Disorders of Human Patients With SHANK2 Variants. *Frontiers in molecular neuroscience* **11**, 240-240, doi:10.3389/fnmol.2018.00240 (2018).

134 Peykov, S. *et al.* Identification and functional characterization of rare SHANK2 variants in schizophrenia. *Mol Psychiatry* **20**, 1489-1498, doi:10.1038/mp.2014.172 (2015).

135 Homann, O. R. *et al.* Whole-genome sequencing in multiplex families with psychoses reveals mutations in the SHANK2 and SMARCA1 genes segregating with illness. *Mol Psychiatry* **21**, 1690-1695, doi:10.1038/mp.2016.24 (2016).

136 Berkel, S. *et al.* Inherited and de novo SHANK2 variants associated with autism spectrum disorder impair neuronal morphogenesis and physiology. *Human molecular genetics* **21**, 344-357, doi:10.1093/hmg/ddr470 (2012).

137 Rauch, A. *et al.* Range of genetic mutations associated with severe non-syndromic sporadic intellectual disability: an exome sequencing study. *Lancet* **380**, 1674-1682, doi:10.1016/S0140-6736(12)61480-9 (2012).

138 Kolarova, J. *et al.* Array-based DNA methylation analysis in individuals with developmental delay/intellectual disability and normal molecular karyotype. *European journal of medical genetics* **58**, 419-425, doi:10.1016/j.ejmg.2015.05.001 (2015).

139 Han, W. *et al.* Shank2 associates with and regulates Na+/H+ exchanger 3. *The Journal of biological chemistry* **281**, 1461-1469, doi:10.1074/jbc.M509786200 (2006).

140 Bockers, T. M. *et al.* Differential expression and dendritic transcript localization of Shank family members: identification of a dendritic targeting element in the 3' untranslated region of Shank1 mRNA. *Molecular and cellular neurosciences* **26**, 182-190, doi:10.1016/j.mcn.2004.01.009 (2004).

141 Won, H. *et al.* Autistic-like social behaviour in Shank2-mutant mice improved by restoring NMDA receptor function. *Nature* **486**, 261-265, doi:10.1038/nature11208 (2012).

142 Schmeisser, M. J. *et al.* Autistic-like behaviours and hyperactivity in mice lacking ProSAP1/Shank2. *Nature* **486**, 256-260, doi:10.1038/nature11015 (2012).

143 Pappas, A. L. *et al.* Deficiency of Shank2 causes mania-like behavior that responds to mood stabilizers. *JCI Insight* **2**, doi:10.1172/jci.insight.92052 (2017).

144 Lim, C. S. *et al.* Enhancing inhibitory synaptic function reverses spatial memory deficits in Shank2 mutant mice. *Neuropharmacology* **112**, 104-112, doi:10.1016/j.neuropharm.2016.08.016 (2017).

145 Ha, S. *et al.* Cerebellar Shank2 Regulates Excitatory Synapse Density, Motor Coordination, and Specific Repetitive and Anxiety-Like Behaviors. *J Neurosci* **36**, 12129-12143, doi:10.1523/jneurosci.1849-16.2016 (2016).

146 Peter, S. *et al.* Dysfunctional cerebellar Purkinje cells contribute to autism-like behaviour in Shank2-deficient mice. *Nature communications* **7**, 12627-12627, doi:10.1038/ncomms12627 (2016).

147 Kim, R. *et al.* Cell-Type-Specific Shank2 Deletion in Mice Leads to Differential Synaptic and Behavioral Phenotypes. *J Neurosci* **38**, 4076-4092, doi:10.1523/jneurosci.2684-17.2018 (2018).

148 Schellinck, H., P. Cyr, D. & Brown, R. *Chapter 7 - How Many Ways Can Mouse Behavioral Experiments Go Wrong? Confounding Variables in Mouse Models of Neurodegenerative Diseases and How to Control Them*. Vol. 41 (2010).

149 De Gendt, K. *et al.* A Sertoli cell-selective knockout of the androgen receptor causes spermatogenic arrest in meiosis. *Proc Natl Acad Sci U S A* **101**, 1327-1332, doi:10.1073/pnas.0308114100 (2004).

150 Tronche, F. *et al.* Disruption of the glucocorticoid receptor gene in the nervous system results in reduced anxiety. *Nature genetics* **23**, 99-103, doi:10.1038/12703 (1999).

151 Frohlich, H., Rafiullah, R., Schmitt, N., Abele, S. & Rappold, G. A. Foxp1 expression is essential for sex-specific murine neonatal ultrasonic vocalization. *Human molecular genetics* **26**, 1511-1521, doi:10.1093/hmg/ddx055 (2017).

152 Berkel, S. *et al.* Sex Hormones Regulate SHANK Expression. *Frontiers in Molecular Neuroscience* **11**, doi:10.3389/fnmol.2018.00337 (2018).

153 Schroder, A. L., Pelch, K. E. & Nagel, S. C. Estrogen modulates expression of putative housekeeping genes in the mouse uterus. *Endocrine* **35**, 211-219, doi:10.1007/s12020-009-9154-6 (2009).

154 Vandesompele, J. *et al.* Accurate normalization of real-time quantitative RT-PCR data by geometric averaging of multiple internal control genes. *Genome Biol* **3**, RESEARCH0034 (2002).

155 Mayford, M. *et al.* Control of memory formation through regulated expression of a CaMKII transgene. *Science (New York, N.Y.)* **274**, 1678-1683 (1996).

156 Deacon, R. M. & Rawlins, J. N. T-maze alternation in the rodent. *Nat Protoc* **1**, 7-12, doi:10.1038/nprot.2006.2 (2006).

157 Rogers, D. C. *et al.* Behavioral and functional analysis of mouse phenotype: SHIRPA, a proposed protocol for comprehensive phenotype assessment. *Mammalian genome : official journal of the International Mammalian Genome Society* **8**, 711-713 (1997).

158 Van de Weerd, H. A. *et al.* Validation of a new system for the automatic registration of behaviour in mice and rats. *Behavioural processes* **53**, 11-20 (2001).

159 Deacon, R. M. Burrowing in rodents: a sensitive method for detecting behavioral dysfunction. *Nat Protoc* **1**, 118-121, doi:10.1038/nprot.2006.19 (2006).

160 Jirkof, P. Burrowing and nest building behavior as indicators of well-being in mice. *Journal of neuroscience methods* **234**, 139-146, doi:10.1016/j.jneumeth.2014.02.001 (2014).

161 Deacon, R. M. Assessing nest building in mice. *Nature protocols* **1**, 1117-1119, doi:10.1038/nprot.2006.170 (2006).

162 Crawley, J. N. Mouse behavioral assays relevant to the symptoms of autism. *Brain Pathol* **17**, 448-459, doi:10.1111/j.1750-3639.2007.00096.x (2007).

163 Chadman, K. K. *et al.* Minimal aberrant behavioral phenotypes of neuroligin-3 R451C knockin mice. *Autism Res* **1**, 147-158, doi:10.1002/aur.22 (2008).

164 Yang, M., Clarke, A. M. & Crawley, J. N. Postnatal lesion evidence against a primary role for the corpus callosum in mouse sociability. *Eur J Neurosci* **29**, 1663-1677, doi:10.1111/j.1460-9568.2009.06714.x (2009).

165 Yang, M. *et al.* Social approach behaviors are similar on conventional versus reverse lighting cycles, and in replications across cohorts, in BTBR T+ tf/J, C57BL/6J, and vasopressin receptor 1B mutant mice. *Front Behav Neurosci* **1**, 1, doi:10.3389/neuro.08.001.2007 (2007).

166 Yamashita, M. *et al.* Impaired cliff avoidance reaction in dopamine transporter knockout mice. *Psychopharmacology (Berl)* **227**, 741-749, doi:10.1007/s00213-013-3009-9 (2013).

167 Aguzzi, A. & Theuring, F. Improved in situ beta-galactosidase staining for histological analysis of transgenic mice. *Histochemistry* **102**, 477-481 (1994).

168 Dugue, G. P., Dumoulin, A., Triller, A. & Dieudonne, S. Target-dependent use of co-released inhibitory transmitters at central synapses. *J Neurosci* **25**, 6490-6498, doi:10.1523/JNEUROSCI.1500-05.2005 (2005).

169 Chen, H. X., Otmakhov, N. & Lisman, J. Requirements for LTP induction by pairing in hippocampal CA1 pyramidal cells. *J Neurophysiol* **82**, 526-532, doi:10.1152/jn.1999.82.2.526 (1999).

170 Blackstone, C. D. *et al.* Biochemical characterization and localization of a non-N-methyl-D-aspartate glutamate receptor in rat brain. *Journal of neurochemistry* **58**, 1118-1126 (1992).

171 Lau, L. F. *et al.* Interaction of the N-methyl-D-aspartate receptor complex with a novel synapse-associated protein, SAP102. *The Journal of biological chemistry* **271**, 21622-21628 (1996).

172 Chamniansawat, S. & Chongthammakun, S. Estrogen stimulates activity-regulated cytoskeleton associated protein (Arc) expression via the MAPK- and PI-3K-dependent pathways in SH-SY5Y cells. *Neurosci Lett* **452**, 130-135, doi:10.1016/j.neulet.2009.01.010 (2009).

173 Chamniansawat, S. & Chongthammakun, S. Genomic and non-genomic actions of estrogen on synaptic plasticity in SH-SY5Y cells. *Neurosci Lett* **470**, 49-54, doi:10.1016/j.neulet.2009.12.053 (2010).

174 Grassi, D., Bellini, M. J., Acaz-Fonseca, E., Panzica, G. & Garcia-Segura, L. M. Estradiol and testosterone regulate arginine-vasopressin expression in SH-SY5Y human female neuroblastoma cells through estrogen receptors-alpha and -beta. *Endocrinology* **154**, 2092-2100, doi:10.1210/en.2012-2137 (2013).

175 Sarachana, T. & Hu, V. W. Differential recruitment of coregulators to the RORA promoter adds another layer of complexity to gene (dys) regulation by sex hormones in autism. *Mol Autism* **4**, 39, doi:10.1186/2040-2392-4-39 (2013).

176 Pan, W. *et al.* Effects of dihydrotestosterone on synaptic plasticity of the hippocampus in mild cognitive impairment male SAMP8 mice. *Experimental and therapeutic medicine* **12**, 1455-1463, doi:10.3892/etm.2016.3470 (2016).

177 Akama, K. T. & McEwen, B. S. Estrogen stimulates postsynaptic density-95 rapid protein synthesis via the Akt/protein kinase B pathway. *J Neurosci* **23**, 2333-2339 (2003).

178 Liu, F. *et al.* Activation of estrogen receptor-β regulates hippocampal synaptic plasticity and improves memory. *Nature Neuroscience* **11**, 334, doi:10.1038/nn2057 (2008).

179 Kurian, J. R., Forbes-Lorman, R. M. & Auger, A. P. Sex difference in mecp2 expression during a critical period of rat brain development. *Epigenetics* **2**, 173-178 (2007).

180 vom Saal, F. S., Grant, W. M., McMullen, C. W. & Laves, K. S. High fetal estrogen concentrations: correlation with increased adult sexual activity and decreased aggression in male mice. *Science (New York, N.Y.)* **220**, 1306-1309 (1983).

181 Mogi, K., Takanashi, H., Nagasawa, M. & Kikusui, T. Sex differences in spatiotemporal expression of AR, ERalpha, and ERbeta mRNA in the perinatal mouse brain. *Neuroscience letters* **584**, 88-92, doi:10.1016/j.neulet.2014.10.028 (2015).

182 Mack, V. *et al.* Conditional restoration of hippocampal synaptic potentiation in Glur-A-deficient mice. *Science (New York, N.Y.)* **292**, 2501-2504, doi:10.1126/science.1059365 (2001).

183 Ferguson, B. R. & Gao, W.-J. PV Interneurons: Critical Regulators of E/I Balance for Prefrontal Cortex-Dependent Behavior and Psychiatric Disorders. *Frontiers in neural circuits* **12**, 37-37, doi:10.3389/fncir.2018.00037 (2018).

184 Zikopoulos, B. & Barbas, H. Altered neural connectivity in excitatory and inhibitory cortical circuits in autism. *Frontiers in Human Neuroscience* **7**, doi:10.3389/fnhum.2013.00609 (2013).

185 Lee, E., Lee, J. & Kim, E. Excitation/Inhibition Imbalance in Animal Models of Autism Spectrum Disorders. *Biological Psychiatry* **81**, 838-847, doi:10.1016/j.biopsych.2016.05.011 (2017).

186 Selten, M., van Bokhoven, H. & Nadif Kasri, N. Inhibitory control of the excitatory/inhibitory balance in psychiatric disorders. *F1000Research* **7**, 23-23, doi:10.12688/f1000research.12155.1 (2018).

187 Nelson, Sacha B. & Valakh, V. Excitatory/Inhibitory Balance and Circuit Homeostasis in Autism Spectrum Disorders. *Neuron* **87**, 684-698, doi:10.1016/j.neuron.2015.07.033 (2015).

188 Gao, R. & Penzes, P. Common mechanisms of excitatory and inhibitory imbalance in schizophrenia and autism spectrum disorders. *Current molecular medicine* **15**, 146-167 (2015).

189 Park, H. R. *et al.* A Short Review on the Current Understanding of Autism Spectrum Disorders. *Experimental neurobiology* **25**, 1-13, doi:10.5607/en.2016.25.1.1 (2016).

190 Sun, J. *et al.* Androgen Receptor Regulates the Growth of Neuroblastoma Cells in vitro and in vivo. *Front Neurosci* **11**, 116, doi:10.3389/fnins.2017.00116 (2017).

191 Nakaso, K. *et al.* The estrogen receptor beta-PI3K/Akt pathway mediates the cytoprotective effects of tocotrienol in a cellular Parkinson's disease model. *Biochim Biophys Acta* **1842**, 1303-1312, doi:10.1016/j.bbadis.2014.04.008 (2014).

192 Mauvais-Jarvis, F. Estrogen and androgen receptors: regulators of fuel homeostasis and emerging targets for diabetes and obesity. *Trends in endocrinology and metabolism: TEM* **22**, 24-33, doi:10.1016/j.tem.2010.10.002 (2011).

193 Trabzuni, D. *et al.* Widespread sex differences in gene expression and splicing in the adult human brain. *Nature Communications* **4**, 2771, doi:10.1038/ncomms3771 (2013).

194 Lombardo, M. V. *et al.* Fetal testosterone influences sexually dimorphic gray matter in the human brain. *J Neurosci* **32**, 674-680, doi:10.1523/JNEUROSCI.4389-11.2012 (2012).

195 Lai, M. C. *et al.* Biological sex affects the neurobiology of autism. *Brain* **136**, 2799-2815, doi:10.1093/brain/awt216 (2013).

196 Schmidtova, E., Lakatosova, S., Celec, P., Ficek, A. & Ostatníková, D. *Polymorphisms in Genes Involved in Testosterone Metabolism in Slovak Autistic Boys*. Vol. 20 (2010).

197 Lein, E. S. *et al.* Genome-wide atlas of gene expression in the adult mouse brain. *Nature* **445**, 168-176, doi:10.1038/nature05453 (2007).

198 Lichtensteiger, W. *et al. Differential Gene Expression Patterns in Developing Sexually Dimorphic Rat Brain Regions Exposed to Antiandrogenic, Estrogenic, or Complex Endocrine Disruptor Mixtures: Glutamatergic Synapses as Target*. Vol. 156 (2015).

199 Wilson, S., Qi, J. & Filipp, F. V. Refinement of the androgen response element based on ChIP-Seq in androgen-insensitive and androgen-responsive prostate cancer cell lines. *Scientific reports* **6**, 32611, doi:10.1038/srep32611 (2016).

200 Quartier, A. *et al.* Genes and Pathways Regulated by Androgens in Human Neural Cells, Potential Candidates for the Male Excess in Autism Spectrum Disorder. *Biological Psychiatry* **84**, 239-252, doi:10.1016/j.biopsych.2018.01.002 (2018).

201 Pakkenberg, B. & Gundersen, H. J. Neocortical neuron number in humans: effect of sex and age. *The Journal of comparative neurology* **384**, 312-320 (1997).

202 Sheyn, D. *et al.* Structure of the Cerebral Cortex in Men and Women. *Journal of Neuropathology & Experimental Neurology* **61**, 46-57, doi:10.1093/jnen/61.1.46 (2002).

203 Witelson, S. F., Glezer, II & Kigar, D. L. Women have greater density of neurons in posterior temporal cortex. *J Neurosci* **15**, 3418-3428 (1995).

204 Lombardo, M. V. *et al.* Fetal Testosterone Influences Sexually Dimorphic Gray Matter in the Human Brain. *The Journal of Neuroscience* **32**, 674, doi:10.1523/JNEUROSCI.4389-11.2012 (2012).

205 Lai, M.-C. *et al.* Biological sex affects the neurobiology of autism. *Brain : a journal of neurology* **136**, 2799-2815, doi:10.1093/brain/awt216 (2013).

206 Schwanhausser, B. *et al.* Global quantification of mammalian gene expression control. *Nature* **473**, 337-342, doi:10.1038/nature10098 (2011).

207 Klin, A. [Autism and Asperger syndrome: an overview]. *Revista brasileira de psiquiatria (Sao Paulo, Brazil : 1999)* **28 Suppl 1**, S3-11, doi:/S1516-44462006000500002 (2006).

208 Sebat, J. *et al.* Strong association of de novo copy number mutations with autism. *Science (New York, N.Y.)* **316**, 445-449, doi:10.1126/science.1138659 (2007).

209 Iossifov, I. *et al.* De novo gene disruptions in children on the autistic spectrum. *Neuron* **74**, 285-299, doi:10.1016/j.neuron.2012.04.009 (2012).

210 Sanders, S. J. *et al.* Multiple recurrent de novo CNVs, including duplications of the 7q11.23 Williams syndrome region, are strongly associated with autism. *Neuron* **70**, 863-885, doi:10.1016/j.neuron.2011.05.002 (2011).

211 Levy, D. *et al.* Rare de novo and transmitted copy-number variation in autistic spectrum disorders. *Neuron* **70**, 886-897, doi:10.1016/j.neuron.2011.05.015 (2011).

212 Sanders, S. J. *et al.* De novo mutations revealed by whole-exome sequencing are strongly associated with autism. *Nature* **485**, 237-241, doi:10.1038/nature10945 (2012).

213 Neale, B. M. *et al.* Patterns and rates of exonic de novo mutations in autism spectrum disorders. *Nature* **485**, 242-245, doi:10.1038/nature11011 (2012).

214 O'Roak, B. J. *et al.* Sporadic autism exomes reveal a highly interconnected protein network of de novo mutations. *Nature* **485**, 246-250, doi:10.1038/nature10989 (2012).

215 Sato, T. *et al.* Brain masculinization requires androgen receptor function. *Proceedings of the National Academy of Sciences of the United States of America* **101**, 1673, doi:10.1073/pnas.0305303101 (2004).

216 Knickmeyer, R. *et al.* Androgens and autistic traits: A study of individuals with congenital adrenal hyperplasia. *Hormones and behavior* **50**, 148-153, doi:10.1016/j.yhbeh.2006.02.006 (2006).

217 Geier, D. A. & Geier, M. R. A prospective assessment of androgen levels in patients with autistic spectrum disorders: biochemical underpinnings and suggested therapies. *Neuro endocrinology letters* **28**, 565-573 (2007).

218 Al-Zaid, F. S., Alhader, A. A. & Al-Ayadhi, L. Y. Altered ghrelin levels in boys with autism: a novel finding associated with hormonal dysregulation. *Scientific reports* **4**, 6478, doi:10.1038/srep06478 (2014).

219 Auyeung, B. *et al.* Fetal testosterone predicts sexually differentiated childhood behavior in girls and in boys. *Psychological science* **20**, 144-148, doi:10.1111/j.1467-9280.2009.02279.x (2009).

220 Pennebaker, J. W., Groom, C. J., Loew, D. & Dabbs, J. M. Testosterone as a social inhibitor: two case studies of the effect of testosterone treatment on language. *Journal of abnormal psychology* **113**, 172-175, doi:10.1037/0021-843x.113.1.172 (2004).

221 Xia, Y. *et al.* Sex-differential DNA methylation and associated regulation networks in human brain implicated in the sex-biased risks of psychiatric disorders. *Molecular psychiatry*, doi:10.1038/s41380-019-0416-2 (2019).

222 Beri, S. *et al.* DNA methylation regulates tissue-specific expression of Shank3. *Journal of neurochemistry* **101**, 1380-1391, doi:10.1111/j.1471-4159.2007.04539.x (2007).

223 Maunakea, A. K. *et al.* Conserved role of intragenic DNA methylation in regulating alternative promoters. *Nature* **466**, 253, doi:10.1038/nature09165 (2010).

224 Schmeisser, M. & Verpelli, C. 151-160 (2016).

225 Parikshak, N. N. *et al.* Integrative functional genomic analyses implicate specific molecular pathways and circuits in autism. *Cell* **155**, 1008-1021, doi:10.1016/j.cell.2013.10.031 (2013).

226 Willsey, A. J. *et al.* Coexpression networks implicate human midfetal deep cortical projection neurons in the pathogenesis of autism. *Cell* **155**, 997-1007, doi:10.1016/j.cell.2013.10.020 (2013).

227 Shepherd, G. M. Corticostriatal connectivity and its role in disease. *Nat Rev Neurosci* **14**, 278-291, doi:10.1038/nrn3469 (2013).

228 Volk, D. W. & Lewis, D. A. Prefrontal cortical circuits in schizophrenia. *Curr Top Behav Neurosci* **4**, 485-508 (2010).

229 Lewis, D. A. Cortical circuit dysfunction and cognitive deficits in schizophrenia--implications for preemptive interventions. *Eur J Neurosci* **35**, 1871-1878, doi:10.1111/j.1460-9568.2012.08156.x (2012).

230 Brady, R. O., Jr. *et al.* State dependent cortico-amygdala circuit dysfunction in bipolar disorder. *J Affect Disord* **201**, 79-87, doi:10.1016/j.jad.2016.04.052 (2016).

231 Tang, S. *et al.* Altered Forebrain Functional Connectivity and Neurotransmission in a Kinase-Inactive Met Mouse Model of Autism. *Molecular Imaging* **18**, 1536012118821034, doi:10.1177/1536012118821034 (2019).

232 Smith, J., Xu, J. & Powell, E. *Age dependent forebrain structural changes in mice deficient in the autism associated gene MET tyrosine kinase*. Vol. 1 (2012).

233 Berridge, K. C. & Whishaw, I. Q. Cortex, striatum and cerebellum: control of serial order in a grooming sequence. *Experimental brain research* **90**, 275-290 (1992).

234 Kim, H., Lim, C.-S. & Kaang, B.-K. Neuronal mechanisms and circuits underlying repetitive behaviors in mouse models of autism spectrum disorder. *Behavioral and brain functions : BBF* **12**, 3-3, doi:10.1186/s12993-016-0087-y (2016).

235 Majdak, P. *et al.* A new mouse model of ADHD for medication development. *Sci Rep* **6**, 39472, doi:10.1038/srep39472 (2016).

236 Russell, V. A. Overview of animal models of attention deficit hyperactivity disorder (ADHD). *Curr Protoc Neurosci* **Chapter 9**, Unit9 35, doi:10.1002/0471142301.ns0935s54 (2011).

237 Sontag, T. A., Tucha, O., Walitza, S. & Lange, K. W. Animal models of attention deficit/hyperactivity disorder (ADHD): a critical review. *Atten Defic Hyperact Disord* **2**, 1-20, doi:10.1007/s12402-010-0019-x (2010).

238 Chadman, K. K. Animal models for autism in 2017 and the consequential implications to drug discovery. *Expert Opin Drug Discov* **12**, 1187-1194, doi:10.1080/17460441.2017.1383982 (2017).

239 Kazdoba, T. M. *et al.* Translational Mouse Models of Autism: Advancing Toward Pharmacological Therapeutics. *Curr Top Behav Neurosci* **28**, 1-52, doi:10.1007/7854_2015_5003 (2016).

240 Lazaro, M. T. & Golshani, P. The utility of rodent models of autism spectrum disorders. *Curr Opin Neurol* **28**, 103-109, doi:10.1097/WCO.0000000000000183 (2015).

241 Schroeder, J. C., Reim, D., Boeckers, T. M. & Schmeisser, M. J. Genetic Animal Models for Autism Spectrum Disorder. *Curr Top Behav Neurosci* **30**, 311-324, doi:10.1007/7854_2015_407 (2017).

242 Moy, S. S. *et al.* Sociability and preference for social novelty in five inbred strains: an approach to assess autistic-like behavior in mice. *Genes, brain, and behavior* **3**, 287-302, doi:10.1111/j.1601-1848.2004.00076.x (2004).

243 Gordon, R. *et al.* Intrahippocampal Pathways Involved in Learning/Memory Mechanisms are Affected by Intracerebral Infusions of Amyloid-beta25-35 Peptide and Hydrated Fullerene C60 in Rats. *Journal of Alzheimer's disease : JAD* **58**, 711-724, doi:10.3233/jad-161182 (2017).

244 Sanderson, D. J. *et al.* The role of the GluR-A (GluR1) AMPA receptor subunit in learning and memory. *Progress in brain research* **169**, 159-178, doi:10.1016/s0079-6123(07)00009-x (2008).

245 Wiedholz, L. M. *et al.* Mice lacking the AMPA GluR1 receptor exhibit striatal hyperdopaminergia and 'schizophrenia-related' behaviors. *Molecular psychiatry* **13**, 631-640, doi:10.1038/sj.mp.4002056 (2008).

246 Ben Abdallah, N. M. *et al.* The puzzle box as a simple and efficient behavioral test for exploring impairments of general cognition and executive functions in mouse models of schizophrenia. *Experimental neurology* **227**, 42-52, doi:10.1016/j.expneurol.2010.09.008 (2011).

247 Wegener, S. *et al.* Defective Synapse Maturation and Enhanced Synaptic Plasticity in Shank2 Δex7(-/-) Mice. *eNeuro* **5**, ENEURO.0398-0317.2018, doi:10.1523/ENEURO.0398-17.2018 (2018).

248 Dai, J. X. *et al.* Enhanced contextual fear memory in central serotonin-deficient mice. *Proc Natl Acad Sci U S A* **105**, 11981-11986, doi:10.1073/pnas.0801329105 (2008).

249 Pisansky, M. T., Hanson, L. R., Gottesman, I. I. & Gewirtz, J. C. Oxytocin enhances observational fear in mice. *Nature Communications* **8**, 2102, doi:10.1038/s41467-017-02279-5 (2017).

250 Guzmán, Y. F. *et al.* Role of oxytocin receptors in modulation of fear by social memory. *Psychopharmacology* **231**, 2097-2105, doi:10.1007/s00213-013-3356-6 (2014).

251 Homberg, J. R. Serotonergic modulation of conditioned fear. *Scientifica* **2012**, 821549-821549, doi:10.6064/2012/821549 (2012).

252 Uzefovsky, F. *et al.* The oxytocin receptor gene predicts brain activity during an emotion recognition task in autism. *Molecular Autism* **10**, 12, doi:10.1186/s13229-019-0258-4 (2019).

253 Leake, J., Zinn, R., Corbit, L. & Vissel, B. Dissociation between complete hippocampal context memory formation and context fear acquisition. *Learning & memory (Cold Spring Harbor, N.Y.)* **24**, 153-157, doi:10.1101/lm.044578.116 (2017).

254 O'Reilly, R. C. & Rudy, J. W. Conjunctive representations in learning and memory: principles of cortical and hippocampal function. *Psychological review* **108**, 311-345 (2001).

255 Krasne, F. B., Cushman, J. D. & Fanselow, M. S. A Bayesian context fear learning algorithm/automaton. *Frontiers in behavioral neuroscience* **9**, 112, doi:10.3389/fnbeh.2015.00112 (2015).

256 Remondes, M. & Schuman, E. M. Role for a cortical input to hippocampal area CA1 in the consolidation of a long-term memory. *Nature* **431**, 699-703, doi:10.1038/nature02965 (2004).

257 Basu, J. *et al.* Gating of hippocampal activity, plasticity, and memory by entorhinal cortex long-range inhibition. *Science (New York, N.Y.)* **351**, aaa5694, doi:10.1126/science.aaa5694 (2016).

258 Lee, I., Hunsaker, M. R. & Kesner, R. P. The role of hippocampal subregions in detecting spatial novelty. *Behavioral neuroscience* **119**, 145-153, doi:10.1037/0735-7044.119.1.145 (2005).

259 Griffin, A. L., Eichenbaum, H. & Hasselmo, M. E. Spatial representations of hippocampal CA1 neurons are modulated by behavioral context in a hippocampus-dependent memory task. *J Neurosci* **27**, 2416-2423, doi:10.1523/jneurosci.4083-06.2007 (2007).

260 Greene, P., Howard, M., Bhattacharyya, R. & Fellous, J. M. Hippocampal anatomy supports the use of context in object recognition: a computational model. *Computational intelligence and neuroscience* **2013**, 294878, doi:10.1155/2013/294878 (2013).

261 McHugh, T. J. *et al.* Dentate gyrus NMDA receptors mediate rapid pattern separation in the hippocampal network. *Science (New York, N.Y.)* **317**, 94-99, doi:10.1126/science.1140263 (2007).

262 McHugh, T. J. & Tonegawa, S. CA3 NMDA receptors are required for the rapid formation of a salient contextual representation. *Hippocampus* **19**, 1153-1158, doi:10.1002/hipo.20684 (2009).

263 Choi, W.-S. *et al.* Conditional deletion of Ndufs4 in dopaminergic neurons promotes Parkinson's disease-like non-motor symptoms without loss of dopamine neurons. *Scientific reports* **7**, 44989, doi:10.1038/srep44989 (2017).

264 Lee, S. *et al.* Shank2 Deletion in Parvalbumin Neurons Leads to Moderate Hyperactivity, Enhanced Self-Grooming and Suppressed Seizure Susceptibility in Mice. *Frontiers in molecular neuroscience* **11**, 209-209, doi:10.3389/fnmol.2018.00209 (2018).

265 Burket, J. A. *et al.* Effects of VU0410120, a novel GlyT1 inhibitor, on measures of sociability, cognition and stereotypic behaviors in a mouse model of autism. *Progress in neuro-psychopharmacology & biological psychiatry* **61**, 10-17, doi:10.1016/j.pnpbp.2015.03.003 (2015).

266 Burket, J. A., Benson, A. D., Tang, A. H. & Deutsch, S. I. NMDA receptor activation regulates sociability by its effect on mTOR signaling activity. *Progress in neuro-psychopharmacology & biological psychiatry* **60**, 60-65, doi:10.1016/j.pnpbp.2015.02.009 (2015).

267 Deutsch, S. I., Burket, J. A., Benson, A. D. & Urbano, M. R. NMDA agonists for autism spectrum disorders: progress and possibilities. *Future Neurology* **10**, 485-500, doi:10.2217/fnl.15.28 (2015).

268 Deutsch, S. I. *et al.* D-cycloserine improves sociability and spontaneous stereotypic behaviors in 4-week old mice. *Brain research* **1439**, 96-107, doi:10.1016/j.brainres.2011.12.040 (2012).

269 Rubenstein, J. L. & Merzenich, M. M. Model of autism: increased ratio of excitation/inhibition in key neural systems. *Genes, brain, and behavior* **2**, 255-267 (2003).

270 Ebert, D. H. & Greenberg, M. E. Activity-dependent neuronal signalling and autism spectrum disorder. *Nature* **493**, 327-337, doi:10.1038/nature11860 (2013).

271 Cardin, J. A. *et al.* Driving fast-spiking cells induces gamma rhythm and controls sensory responses. *Nature* **459**, 663-667, doi:10.1038/nature08002 (2009).

272 Gogolla, N. *et al.* Common circuit defect of excitatory-inhibitory balance in mouse models of autism. *Journal of neurodevelopmental disorders* **1**, 172-181, doi:10.1007/s11689-009-9023-x (2009).

273 Gogolla, N., Takesian, A. E., Feng, G., Fagiolini, M. & Hensch, T. K. Sensory integration in mouse insular cortex reflects GABA circuit maturation. *Neuron* **83**, 894-905, doi:10.1016/j.neuron.2014.06.033 (2014).

274 Sohal, V. S., Zhang, F., Yizhar, O. & Deisseroth, K. Parvalbumin neurons and gamma rhythms enhance cortical circuit performance. *Nature* **459**, 698-702, doi:10.1038/nature07991 (2009).

275 Yizhar, O. *et al.* Neocortical excitation/inhibition balance in information processing and social dysfunction. *Nature* **477**, 171-178, doi:10.1038/nature10360 (2011).

276 Wohr, M. *et al.* Lack of parvalbumin in mice leads to behavioral deficits relevant to all human autism core symptoms and related neural morphofunctional abnormalities. *Translational psychiatry* **5**, e525, doi:10.1038/tp.2015.19 (2015).

277 Filice, F., Vorckel, K. J., Sungur, A. O., Wohr, M. & Schwaller, B. Reduction in parvalbumin expression not loss of the parvalbumin-expressing GABA interneuron subpopulation in genetic parvalbumin and shank mouse models of autism. *Molecular brain* **9**, 10, doi:10.1186/s13041-016-0192-8 (2016).

278 Kosaka, T. & Heizmann, C. W. Selective staining of a population of parvalbumin-containing GABAergic neurons in the rat cerebral cortex by lectins with specific affinity for terminal N-acetylgalactosamine. *Brain research* **483**, 158-163 (1989).

279 Filice, F. & Schwaller, B. Parvalbumin and autism: different causes, same effect? *Oncotarget* **8**, 7222-7223, doi:10.18632/oncotarget.14238 (2016).

280 Hashemi, E., Ariza, J., Rogers, H., Noctor, S. C. & Martinez-Cerdeno, V. The Number of Parvalbumin-Expressing Interneurons Is Decreased in the Prefrontal Cortex in Autism. *Cerebral cortex (New York, N.Y. : 1991)* **27**, 1931-1943, doi:10.1093/cercor/bhw021 (2017).

281 Shi, S. H. *et al.* Rapid spine delivery and redistribution of AMPA receptors after synaptic NMDA receptor activation. *Science (New York, N.Y.)* **284**, 1811-1816 (1999).

282 Song, I. & Huganir, R. L. Regulation of AMPA receptors during synaptic plasticity. *Trends in neurosciences* **25**, 578-588 (2002).

283 Mayer, M. L. Glutamate receptor ion channels. *Current Opinion in Neurobiology* **15**, 282-288, doi:10.1016/j.conb.2005.05.004 (2005).

284 Greger, I. H., Ziff, E. B. & Penn, A. C. Molecular determinants of AMPA receptor subunit assembly. *Trends in neurosciences* **30**, 407-416, doi:10.1016/j.tins.2007.06.005 (2007).

285 Shepherd, J. D. Memory, plasticity and sleep - A role for calcium permeable AMPA receptors? *Frontiers in molecular neuroscience* **5**, 49-49, doi:10.3389/fnmol.2012.00049 (2012).

286 Ha, H. T. T. *et al.* Shank and Zinc Mediate an AMPA Receptor Subunit Switch in Developing Neurons. *Frontiers in Molecular Neuroscience* **11**, doi:10.3389/fnmol.2018.00405 (2018).

287 Lu, J. *et al.* Postsynaptic positioning of endocytic zones and AMPA receptor cycling by physical coupling of dynamin-3 to Homer. *Neuron* **55**, 874-889, doi:10.1016/j.neuron.2007.06.041 (2007).

288 Henley, J. M. & Wilkinson, K. A. AMPA receptor trafficking and the mechanisms underlying synaptic plasticity and cognitive aging. *Dialogues in clinical neuroscience* **15**, 11-27 (2013).

289 Uchino, S. *et al.* Direct interaction of post-synaptic density-95/Dlg/ZO-1 domain-containing synaptic molecule Shank3 with GluR1 alpha-amino-3-hydroxy-5-methyl-4-isoxazole propionic acid receptor. *Journal of neurochemistry* **97**, 1203-1214, doi:10.1111/j.1471-4159.2006.03831.x (2006).

290 Verpelli, C. *et al.* Importance of Shank3 protein in regulating metabotropic glutamate receptor 5 (mGluR5) expression and signaling at synapses. *The Journal of biological chemistry* **286**, 34839-34850, doi:10.1074/jbc.M111.258384 (2011).

291 Raynaud, F. *et al.* Shank3-Rich2 interaction regulates AMPA receptor recycling and synaptic long-term potentiation. *J Neurosci* **33**, 9699-9715, doi:10.1523/jneurosci.2725-12.2013 (2013).

292 Mejias, R. *et al.* Gain-of-function glutamate receptor interacting protein 1 variants alter GluA2 recycling and surface distribution in patients with autism. *Proc Natl Acad Sci U S A* **108**, 4920-4925, doi:10.1073/pnas.1102233108 (2011).

293 Mao, L., Takamiya, K., Thomas, G., Lin, D. T. & Huganir, R. L. GRIP1 and 2 regulate activity-dependent AMPA receptor recycling via exocyst complex interactions. *Proc Natl Acad Sci U S A* **107**, 19038-19043, doi:10.1073/pnas.1013494107 (2010).

294 Wang, X. *et al.* Synaptic dysfunction and abnormal behaviors in mice lacking major isoforms of Shank3. *Human molecular genetics* **20**, 3093-3108, doi:10.1093/hmg/ddr212 (2011).

295 Bozdagi, O. *et al.* Haploinsufficiency of the autism-associated Shank3 gene leads to deficits in synaptic function, social interaction, and social communication. *Mol Autism* **1**, 15, doi:10.1186/2040-2392-1-15 (2010).

296 Carlson, G. C. Glutamate receptor dysfunction and drug targets across models of autism spectrum disorders. *Pharmacology, biochemistry, and behavior* **100**, 850-854, doi:10.1016/j.pbb.2011.02.003 (2012).

297 Janssen, B. J. C. *et al.* Neuropilins lock secreted semaphorins onto plexins in a ternary signaling complex. *Nature structural & molecular biology* **19**, 1293-1299, doi:10.1038/nsmb.2416 (2012).

298 Kong, Y. *et al.* Structural Basis for Plexin Activation and Regulation. *Neuron* **91**, 548-560, doi:10.1016/j.neuron.2016.06.018 (2016).

299 Zikopoulos, B. & Barbas, H. Changes in prefrontal axons may disrupt the network in autism. *The Journal of neuroscience : the official journal of the Society for Neuroscience* **30**, 14595-14609, doi:10.1523/JNEUROSCI.2257-10.2010 (2010).

300 Martínez-Cerdeño, V. Dendrite and spine modifications in autism and related neurodevelopmental disorders in patients and animal models. *Developmental neurobiology* **77**, 393-404, doi:10.1002/dneu.22417 (2017).

301 Lei, H. *et al.* Axon guidance pathways served as common targets for human speech/language evolution and related disorders. *Brain and language* **174**, 1-8, doi:10.1016/j.bandl.2017.06.007 (2017).

302 Zaslavsky, K. *et al. SHANK2 mutations associated with autism spectrum disorder cause hyperconnectivity of human neurons*. Vol. 22 (2019).

303 Rabaneda, L. G., Robles-Lanuza, E., Nieto-Gonzalez, J. L. & Scholl, F. G. Neurexin dysfunction in adult neurons results in autistic-like behavior in mice. *Cell Rep* **8**, 338-346, doi:10.1016/j.celrep.2014.06.022 (2014).

304 Lee, E.-J. *et al.* Trans-synaptic zinc mobilization improves social interaction in two mouse models of autism through NMDAR activation. *Nature Communications* **6**, 7168, doi:10.1038/ncomms8168 (2015).

305 Manzerra, P. *et al.* Zinc induces a Src family kinase-mediated up-regulation of NMDA receptor activity and excitotoxicity. *Proceedings of the National Academy of Sciences of the United States of America* **98**, 11055-11061, doi:10.1073/pnas.191353598 (2001).

306 Keifer, J. & Zheng, Z. AMPA receptor trafficking and learning. *The European journal of neuroscience* **32**, 269-277, doi:10.1111/j.1460-9568.2010.07339.x (2010).

307 Kessels, H. W. & Malinow, R. Synaptic AMPA receptor plasticity and behavior. *Neuron* **61**, 340-350, doi:10.1016/j.neuron.2009.01.015 (2009).

308 Krestel, H. E., Mayford, M., Seeburg, P. H. & Sprengel, R. A GFP-equipped bidirectional expression module well suited for monitoring tetracycline-regulated gene expression in mouse. *Nucleic acids research* **29**, E39 (2001).

309 Zhu, P. *et al.* Silencing and Un-silencing of Tetracycline-Controlled Genes in Neurons. *PloS one* **2**, e533, doi:10.1371/journal.pone.0000533 (2007).

310 Telford, E. J. *et al.* Preterm birth is associated with atypical social orienting in infancy detected using eye tracking. *Journal of Child Psychology and Psychiatry* **57**, 861-868, doi:10.1111/jcpp.12546 (2016).

311 Meldrum, S. J. *et al.* Autism spectrum disorder in children born preterm-role of exposure to perinatal inflammation. *Front Neurosci* **7**, 123-123, doi:10.3389/fnins.2013.00123 (2013).

312 Harel-Gadassi, A. *et al.* Risk for ASD in Preterm Infants: A Three-Year Follow-Up Study. *Autism Res Treat* **2018**, 8316212-8316212, doi:10.1155/2018/8316212 (2018).

313 Fenoglio, A., Georgieff, M. K. & Elison, J. T. Social brain circuitry and social cognition in infants born preterm. *Journal of neurodevelopmental disorders* **9**, 27, doi:10.1186/s11689-017-9206-9 (2017).

314 Landa, R. J., Gross, A. L., Stuart, E. A. & Faherty, A. Developmental trajectories in children with and without autism spectrum disorders: the first 3 years. *Child development* **84**, 429-442, doi:10.1111/j.1467-8624.2012.01870.x (2013).

Appendix

Appendix 1: Primer sequences

All primers were designed with the Primer3, Primer-BLAST tools or taken from the Universal Probe Library Assay Design Center (Roche).

Cre-Primer: F: 5’-GCGATTATCTTCTATATCTTCAGG-3’
R: 5’-GCCAATATGGATTAACATTCTCCC-3’

Arflox primer: F: 5’-AGCCTGTATACTCAGTTGGGG-3’
R: 5’-AATGCATCACATTAAGTTGATACC-3’

Sry-primer: F: 5’-TATGGTGTGGTCCCGTGGTG-3’
R: 5’-ATGTGATGGCATGTGGCTTCC-3’

Ca25-primer: 5’-GCTCAGAAGCCCCAAGCTCG-3’
Casli3-primer: 5’-TAAGCAGCTCTAATGCGCTGTTA-3’
Cas25as-primer: 5’-CAGCGCCTAACTCTGGACACC-3’

β-globin 1-primer: 5’-CAGTGGTATTTGGCCAGGGCA-3’
β-globin as1-primer: 5’-ATAATTTGTCAGCAGTTTAAGGTTGCAAAC-3’
β-globin as2-primer: 5’-GAATATTTCTGCATATAACTGGCTGGCG-3’

Primer sequences of qPCR are given in the following table

Primer	**Sequence (5'-3')**
18S_F	GATGGGCGGCGGAAAATAG
18S_R	GCGTGGATTCTGCATAATGGT
GAPDH_F	CTGGGCTACACTGAGCACC
GAPDH_R	AAGTGGTCGTTGAGGGCAATG
HPRT1_F	TGATAGATCCATTCCTATGACTGTAGA
HPRT1_R	AAGACATTCTTTCCAGTTAAAGTTGAG
HSPD1_F	GATGGAGAAGCTCTAAGTACACT
HSPD1_R	GCTGGTTCTTTCTATTGTCACCA
SDHA_F	TGGGAACAAGAGGGCATCTG
SDHA_R	CCACCACTGCATCAAATTCATG
SHANK1_F	CTCCCTGCGTTCCAAATCTA
SHANK1_R	GGCTGCTGCTCGTACTCC
SHANK2_F	CTTTGGATTCGTGCTTCGAG
SHANK2_R	CATCCACGGACTCCAGGTA
SHANK3_F	TTCCACGGACCAAGTCTGTA
SHANK3_R	GTCTTGCATCGAGGTGCTC
MECP2_F	GTGGAGTTGATTGCGTACTTCG
MECP2_R	CCCTCTCCCAGTTACCGTGAA
PSD95_F	TCACAACCTCTTATTCCCAGCA
PSD95_R	CATGGCTGTGGGGTAGTAGTCG
18s_F	CTTAGAGGGACAAGTGGCG
18s_R	ACGCTGAGCCAGTCAGTGTA
Gapdh_F	ACAGTCCATGCCATCACTGCC
Gapdh_R	GCCTGCTTCACCACCTTCTTG
Hprt1_F	TCCTCCTCAGACCGCTTTT
Hprt1_R	CCTGGTTCATCATCGCTAATC
Hspd1_F	AGCTGTTACAATGGGGCCAA
Hspd1_R	ATCCCCAGCCTCTTCGTTTG
Sdha_F	CATGCCAGGGAAGATTACAAA
Sdha_R	GTTCCCCAAACGGCTTCT
mShank1_F	GTCCTACCAGGCGCAAGGCG
mShank1_R	CCCAGAAGCCTCCTTCCCCGA

mShank2_F	TGCTGCCAGTGACTGCATTATTGA
mShank2_R	CAGGGCTGGAAATGCTGGCGT
mShank3_F	AGGGAACCGTGAAGGGCCGA
mShank3_R	TGGCGGAAGAGACGCTTCGT
Mecp2_F	GCGAGGAGGAGAGACTGGA
Mecp2_R	TTCTTGTCTTTCTTCGCCTTCT
Psd95_F	CTCTGCGAAGCAACCCCAA
Psd95_R	TCTTCGTCGCTGGCGTCAATTA
mAr_F	GCCTCCGAAGTGTGGTATCC
mAr_R	TGGTCCCTGGTACTGTCCAA

Appendix 2: Buffers recipes

Buffers recipes for gel electrophoresis

50x TAE

2420 g Tris

571 ml acetic acid

186.12 g EDTA

→ 10 L H_2O

20x E-Buffer

484.4 g (800 mM) Tris

164.0 g (400 mM) Sodium acetate

74.4 g (40 mM) EDTA

—> dissolve in ddH2O, adjust pH to 8.3 with acetic acid (100 %)

—> 5 L ddH_2O

Buffer recipes for western blot

RIPA buffer (cell lysis buffer for protein isolation)

0.606 g Tris

0.877 g NaCl

1 ml 10% SDS

5 ml 10% Sodium deoxycholate

1 ml NP-40

→ 100 ml H2O

5x SDS protein loading dye

0.225 M Tris-HCl

50% Glycerol

5% SDS

0.05% bromophenol blue

0.25 M DTT

10x Running Buffer

10.09 g SDS

30.3 g Tris

144 g Glycine

—> 1 L ddH2O

10x TBS

88 g NaCl

24.2 g Tris

700 ml ddH2O

—> adjust pH to 7.6 with HCl

—> 1 L with ddH2O

1x TBS-T

Dilute 10x TBS 1:10 in ddH2O to make 1 L of 1x TBS and add 1 ml of tween

10x Transfer buffer

144 g Glycine

30.3 g Tris

2000 ml Methanol

50 ml 10% SDS

—> 1 L with ddH2O

Resolving Tris Glycine gel 8%

H_2O	4.6 ml
30% acrylamide mix	2.7 ml
1.5 M Tris (pH 8.8)	2.5 ml
10% SDS	100 µl
10% ammonium persulfate	100 µl
TEMED	6 µl

Stacking Tris Glycine gel

H_2O	1.4 ml
30% acrylamide mix	330 µl
1 M Tris (pH 6.8)	250 µl
10% SDS	20 µl
10% ammonium persulfate	20 µl
TEMED	2 µl

Appendix 3: nCounter probe sequences

nCounter probe sequences for *Ar*^{NesCre} mice

Gene	Probe	Sequence
Gapdh	A	ATGGGCTTCCCGTTGATGACAAGCTTCCCATTCTCCCTCAAGACCTAAGCGACAGCGTGACCTTGTTTCA
	B	CGAAAGCCATGACCTCCGATCACTCATTTGATGTTAGTGGGGTCTCGCTCCTGGAAGATGGTG
Hspd1	A	CACAGTTCTTCCCTTTGGCCCCATTGTAACAGCTACAGCATCTGCTAAAACATCCTCTTCTTTTCTTGGTGTTGAGAAGATGCTC
	B	CGAAAGCCATGACCTCCGATCACTCGTGACCCCATCTTTTGTTACTTTGGGACTTCCCCAACTCTGTTCAATAAT
Sdha	A	GTAATCATACTCATCGACCCGCACTTTGTAATCTTCCCTGGCATGGGCTCCACAATTCTGCGGGTTAGCAGGAAGGTTAGGGAAC
	B	CGAAAGCCATGACCTCCGATCACTCCAGTGTTCCCCAAACGGCTTCTTCTGCTGTCCCTGGATGGGCTTGGA
Hprt1	A	AACAAATCTAGGTCATAACCTGGTTCATCATCGCTAATCACGACGCTGGGCTGTTGAGATTATTGAGCTTCATCATGACCAGAAG
	B	CGAAAGCCATGACCTCCGATCACTCGAGGAATAAACACTTTTTCCAAATCCTCGGCATAATGATTAGGTATACAA
Shank1	A	TCACCGCCATGAAGGAGCGACCGGGTACCGCTGAATAGAGCTTCCTACGTCTTTCGGGTTATATCTATCATTTACTTGACACCCT
	B	CGAAAGCCATGACCTCCGATCACTCCTTTACTCAGAGAGATCTCCCCCTCGCCTTGCGCCTGGTAGGACT
Shank2	A	TCCACGGACTCCAGGTACTGCAGGGCTGGAAATGCTGGCGTGGGTGTGAACAACAGCCACTTTTTTTCCAAATTTTGCAAGAGCC
	B	CGAAAGCCATGACCTCCGATCACTCTCCTTAGTCCGGCTTGCCATGCCACCCCACCTTCA
Shank3	A	CTTCGTCCGGTCCTCTCTGGTTTCATGCCGGGTGTCATACTGTCGCACCGTGTGGACGGCAACTCAGAGATAACGCATAT
	B	CGAAAGCCATGACCTCCGATCACTCTGTGAAGTGAGGCTGTCATAGGAACCCACAGTGTAGTGGCGGAAGAGACG
Mecp2	A	TGAACACCTTCTGATGCTGCTGCCTTTGGTCTCCCAGCCTGGAGTTTATGTATTGCCAACGAGTTTGTCTTT
	B	CGAAAGCCATGACCTCCGATCACTCGCATCTTGACAACAAGTTTCCCAGGGCTCTTCTCCAGGACCCTTTTCACC
Psd95	A	GGCCTGGCTCAAGAAACCGCAGTCCTTGGTCTTGTCGTAGTCAAACAAACTGGAGAGAGAAGTGAAGACGATTTAACCCA
	B	CGAAAGCCATGACCTCCGATCACTCTCGTCGCTGGCGTCAATTACATGAAGCACATCCCCAAAGTGGAAGCTCAG
Erα	A	AGGCTTCACTGAAGGGTCTAGAAGGATCATATTCAGAATAGATCATGGGCCCAGCAGACCTGCAATATCAAAGTTATAAGCGCGT
	B	CGAAAGCCATGACCTCCGATCACTCCTCCCTATCTGCTAGGTTGGTCAATAAGCCCATCATTG
Erβ	A	GCCAGACGGACTGACTGCTGCTGGGAAGAGATTCCACTCTTCGAAATCACCCTGCCAATGCACTCGATCTTGTCATTTTTTTGCG
	B	CGAAAGCCATGACCTCCGATCACTCTGCCCTTGTTACTGATGTGCCTGACATGAGAAAGAAGCATCAGGAGGTTG

nCounter probe sequences for $Tg^{SHANK2A}$ and $Tg^{SHANK2AR462X}$ mice

Gene	Probe	Sequence
Gapdh	A	ATGGGCTTCCCGTTGATGACAAGCTTCCCATTCTCCCTCAAGACCTAAGCGACAGCGTGACCTTGTTTCA
	B	CGAAAGCCATGACCTCCGATCACTCATTTGATGTTAGTGGGGTCTCGCTCCTGGAAGATGGTG
Hspd1	A	CACAGTTCTTCCCTTTGGCCCCATTGTAACAGCTACAGCATCTGCTAAAACATCCTCTTCTTTTCTTGGTGTTGAGAAGATGCTC
	B	CGAAAGCCATGACCTCCGATCACTCGTGACCCCATCTTTTGTTACTTTGGGACTTCCCCAACTCTGTTCAATAAT
Sdha	A	GTAATCATACTCATCGACCCGCACTTTGTAATCTTCCCTGGCATGGGCTCCACAATTCTGCGGGTTAGCAGGAAGGTTAGGGAAC
	B	CGAAAGCCATGACCTCCGATCACTCCAGTGTTCCCCAAACGGCTTCTTCTGCTGTCCCTGGATGGGCTTGGA
Hprt1	A	CTCCGGAAAGCAGTGAGGTAAGCCCAACGCTCTCCCTGTTGAGATTATTGAGCTTCATCATGACCAGAAG
	B	CGAAAGCCATGACCTCCGATCACTCCAAAAAGCGGTCTGAGGAGGAAGCCGGCGGAGGAGGTGCTACCG
Pgk1	A	GAGGAGAACAGCGCGGCAGACGTGCGCTTTTGAAGCGTGCAGAATGCCAAAGACGCCTATCTTCCAGTTTGATCGGGAAACT
	B	CGAAAGCCATGACCTCCGATCACTCAAGCGACATTTTGGCAACACCGTGAGGTCGAAAGGCCCGGAGATGAGGAA
Gpi1	A	GGCCCCCAGAATGAAGGGTGTCAGCTTGGTAAACACAATAGAGTTGGTCGCGAACCTAACTCCTCGCTACATTCCTATTGTTTTC
	B	CGAAAGCCATGACCTCCGATCACTCTCCCACATGATGCCCTGAACAAAGATCTTGTGCTCATACATGGCAATCAA
Shank1	A	GAAGGCCGGTCATAACTTGGCTGGGAGCGGTGGTGAGGATCAAAGCTCGACTTTCGGGTTATATCTATCATTTACTTGACACCCT
	B	CGAAAGCCATGACCTCCGATCACTCCGATAGATTTCTGCCGGAGCATAAGGCCAGGTCCGGGAGGCAGGAAA
Shank2	A	GCAGAAATAAAGACAGCAAGTTAAGCAAGCAGGGCACGATCCTGTCCACACAACAGCCACTTTTTTTCCAAATTTTGCAAGAGCC
	B	CGAAAGCCATGACCTCCGATCACTCAACTCCGTGTGACTTCATTTTGGCCACCCTGGAATTATGCTAATCTGTTT
Shank3	A	CTTCGTCCGGTCCTCTCTGGTTTCATGCCGGGTGTCATACTGTCGCACCGTGTGGACGGCAACTCAGAGATAACGCATAT
	B	CGAAAGCCATGACCTCCGATCACTCTGTGAAGTGAGGCTGTCATAGGAACCCACAGTGTAGTGGCGGAAGAGACG
Venus	A	GGCTGTTGTAGTTGTACTCCAGCTTGTGCCCCAGGATGTTGCCTGGAGTTTATGTATTGCCAACGAGTTTGTCTTT
	B	CGAAAGCCATGACCTCCGATCACTCGTTGGCCTTGATGCCGTTCTTCTGCTTGTCGGCGGTGATATAGACGTTGT
Homer1	A	ACTGAAGATCTCCTCCTGCTGATTCCTGTGAAGGGGTACTGCAGATAAGGTTGTTATTGTGGAGGATGTTACTACA
	B	CGAAAGCCATGACCTCCGATCACTCGGGTGTTCTCTCATCGTCTGTCCCATTGATACTTTCTGGTGTCAAAGGAG
Dlgap1	A	TTCGTCGTCCTGGGAGCAGCCCTTTTCGATGGCCCGCACATAGCTGTGCTTCCTTCCTGTGTTCCAGCTACAAACTTAGAAAC
	B	CGAAAGCCATGACCTCCGATCACTCCTCACGGTGGTGGTTGTGCGTGGAGGGGAGGACGACCGCAGCGACACGCA
Grm5	A	TGAGAGTGTCATATTTGGGAGAGGATGGGATGCAGAGGGCATAAAATTGGTTTTGCCTTTCAGCAATTCAACTT
	B	CGAAAGCCATGACCTCCGATCACTCGTTTCCAGTGGCTCACAACGATGAAGAACTCTGCGTGTAATCTCTGATGA
Slc17a7	A	TTTGGCAGATAAATCCTCCAGGAATCTGAGTGACAATGTAGCCCCAGAAACTGGTCAAGACTTGCATGAGGACCCGCAAATTCCT
	B	CGAAAGCCATGACCTCCGATCACTCTGGAGGTAGCCACAATGGCAAAGCCAAAGACCCTGTTGGCTGCGAATT
Slc17a6	A	GCCAACTGTTGTAGTTGTGCTCTCTAAAATGGTGATGGGTCCAACGAATACTTTCGTTGGGACGCTTGAAGCGCAAGTAGAAAAC

	B	CGAAAGCCATGACCTCCGATCACTCATGATCCAGTAGCTTTGGCTTCCTAACTTCTGTAGGATGACATGT
Grin1	A	CGTAGACCTGGCTAGAGATGAGGTCCTCACACACTGACAGCCAGCAGACCTGCAATATCAAAGTTATAAGCGCGT
	B	CGAAAGCCATGACCTCCGATCACTCAGTGAAGTGGTCGTTGGGAGTAGGCGGGTGACTAACTAGGATAG
Grin2a	A	AAGACCAGGCCCCAGAGGAGCCATATAGCTTTTCCAATGGTAAAAGAAGGCCTGCCAATGCACTCGATCTTGTCATTTTTTTGCG
	B	CGAAAGCCATGACCTCCGATCACTCCTGGTTGTGCCTTTAGGATTCTGGACGGGCACAGAATTGTTG
Dlg4	A	GGCCTGGCTCAAGAAACCGCAGTCCTTGGTCTTGTCGTAGTCAAACAAACTGGAGAGAGAAGTGAAGACGATTTAACCCA
	B	CGAAAGCCATGACCTCCGATCACTCTCGTCGCTGGCGTCAATTACATGAAGCACATCCCCAAAGTGGAAGCTCAG
Grin2b	A	CACCCTACTGTAATGGCTCTTTCACAAAGCCTTATACGAAGAGCTTTCCCCTGAGGCTGTTAAAGCTGTAGCAACTCTTCCACGA
	B	CGAAAGCCATGACCTCCGATCACTCCCCCTTTCTCACTAACCCTACCGTTAATGACTAAAAACATCCCCCTCTCT
Gria1	A	AACTCGATTAAGGCAACCAGCATGGCCAATCCCAGCCCTCTAGGACGCAAATCACTTGAAGAAGTGAAAGCGAG
	B	CGAAAGCCATGACCTCCGATCACTCTCAAACAGAAACCCTTCATCCGCTTCGACTCGCTACGGGATTTGTAGCAG
Gria2	A	CTTCTTTGACCGTTTTCCTCAGCAAATTAGATCCTCTGCATTTTGAGGCCACGCGATGACGTTCGTCAAGAGTCGCATAATCT
	B	CGAAAGCCATGACCTCCGATCACTCAAAAGTAGAGCATCCACAAAATATCCCCTCGTTTCCCTTTCCTCCTTTTC
Gria3	A	TCAGTGGTGTTCTGGTTGGTGTTGTATAACTGCACAGCAAAGCGGAAAGCCATTTGGAATGATGTGTACTGGGAATAAGACGACG
	B	CGAAAGCCATGACCTCCGATCACTCTATTGGAGGAATCCAAGTGGTCTACGTGGTAGTTCAAATGGAAGGGCTTC
Syngap1	A	TCATGAAGCCCAGGAAGTCCTCCTTTGAGGTAAACTTGGAAAAGTTGGCCCACAAGAATCCCTGCTAGCTGAAGGAGGGTCAAAC
	B	CGAAAGCCATGACCTCCGATCACTCCTCATACAAGAACTGCTGCATAGAGCCCCACTCCAGCTCCAGAAACTCAT
Drd2	A	CGATGGAGGAGTAGACCACGAAGGCAGGGTTGGCAATGATACACTCATTCCTTGACGTAGATTGCTATCAGGTTACGATGACTGC
	B	CGAAAGCCATGACCTCCGATCACTCGATTTTGATATAGACCAGCAGGGTGACGATGAAGGGCACGTAGAACGAGA
Htr2a	A	AAGTTTTGTATCCGGTGAGAATCTTTCAGCCAATTCTCGGGTTGGATATGCTTACAGATCGTGTGCTCATGACTTCCACAGACGT
	B	CGAAAGCCATGACCTCCGATCACTCAGCAGTGTGGAGCATTTGGAGACACAAACGTGTTCCTGGTTAAGGAAGAA
Oxtr	A	TAAGTCCAGAATTAAGTCTGGGTATTTCAAAGGGACTCCAGAGTGCACAGCAGCAAGAAGGAGTATGGAACTTATAGCAAGAGAG
	B	CGAAAGCCATGACCTCCGATCACTCGTGGATCTACAGATTCTAGGCTTTTTGGAAGCGCCCTTGATATATTTCAG
Gabra1	A	CTGGTCTCAGACGATTGTCATAACCGTCCAGCAGTCGGTCCAAAATTCCGGGAATCGGCATTTCGCATTCTTAGGATCTAAA
	B	CGAAAGCCATGACCTCCGATCACTCACTGGTGACGAAAATGTCGGTCTTCACTTCAGTTACACGCTCTCCCAAAC
Grm1	A	CTATGTCACTCCACTCGAGGTAACGGATAGTAATGGGCTCACAGCCGCTATGCAGACGAGCTGGCAGAGGAGAGAAATCA
	B	CGAAAGCCATGACCTCCGATCACTCTAGCGTCACGAGGATGCCCAGGCAAGAAAAGGCGATGGCTATGATGGATT

Appendix 4: Synaptosome proteomic analysis in the hippocampus of $Tg^{SHANK2A}$ and $Tg^{SHANK2AR462X}$ mice

For $Tg^{SHANK2A}$

Gene	Control vs $Tg^{SHANK2A}$ | log2 fold change	Control vs $Tg^{SHANK2A}$ | FDR adjusted p-values
Kif1a	1.122474884	1.14E-09
Eva1a	0.635968261	2.18E-07
Rae1	0.597712327	4.16E-07
Shank3	-0.592462511	4.16E-07
Pgls	0.680475358	6.77E-07
Mycbp2	0.811999939	1.92E-05
Map7d2	0.47887933	6.17E-05
Shank2	1.258631909	7.34E-05
Ndrg3	0.315048213	0.000106211
Apba2	0.40003458	0.000136591
Shank1	-0.428723287	0.000250898
C1qc	-0.586927084	0.000307778
Slc6a7	-0.347217651	0.000526456
Serpinb1a	-0.841930491	0.000829553
Cadm3	-0.390571275	0.001254315
Rgs14	-0.497653943	0.001389282
Cd44	-0.346112006	0.001575027
Homer2	0.376288701	0.00190151
Mapk10	0.221912197	0.002903784
Rasgrp1	-0.355467726	0.003147952
Nptxr	-0.281252663	0.003191833
Grm3	-0.457778491	0.003526421
Cyb5r1	-0.352127373	0.004473184
Dkk3	-0.297810886	0.005653321
Pgm2l1	0.565646527	0.00621139
Stxbp6	-0.66412202	0.007668076
Slc18a2	-0.238766089	0.007850403
Idh2	0.321774881	0.009811683
Snph	-0.284572087	0.009811683
Sccpdh	-0.27468463	0.010398508
Slc25a22	-0.342067674	0.010398508
Epha4	-0.263419979	0.010548993
Rasal1	-0.27179138	0.012534902
Snx27	0.266420027	0.012630323
Slc16a1	-0.412377332	0.012630323
Rmnd1	-0.274691876	0.013283452

Ptprn2	-0.694571215	0.013283452
S100a13	-0.312927979	0.01329418
Nwd2	-0.317893646	0.01329418
Fam171a2	-0.312149199	0.013555972
Tmem132a	-0.417145822	0.013555972
Cntnap1	-0.225628975	0.014006395
Traf3	-0.631770347	0.014798405
2010300c02rik	0.470547125	0.015369165
Rac3	-0.287101422	0.015433729
Stxbp5	-0.282052748	0.016913791
Vti1a	-0.258452469	0.016983656
Rab15	-0.974290132	0.016983656
Ptprs	-0.281267124	0.017272138
Dgkb	-0.344567694	0.01799354
Atp8a1	-0.212135869	0.018101232
Gltp	-0.341492081	0.019484466
Lman1	0.250195508	0.019917694
Baiap2	-0.217700561	0.020319399
Scamp4	-0.312880145	0.020319399
Abhd3	-0.361977256	0.020319399
Pip4k2c	0.450513784	0.021473279
Stx16	-0.287488552	0.021473279
Rimbp2	-0.217296232	0.024377846
Syt17	-0.492892907	0.024377846
Cacng8	-0.262163524	0.024647245
Mlf2	-0.31437065	0.024647245
Gria1	-0.30045553	0.026246019
2310061i04rik	-0.334277601	0.027688403
Nos1	-0.255445978	0.028245011
Them4	-0.189069975	0.028717854
Ppap2b	-0.28285279	0.029058358
Unc5c	-0.458229666	0.029058358
Coro2b	-0.292554824	0.029177482
Calu	0.283983932	0.029547219
Itm2b	-1.040993344	0.029547219
Myadm	-0.17252979	0.029774913
Rtn4ip1	-0.347207271	0.029874312
Cpne5	-0.267101556	0.030369767
Cpne6	-0.279278566	0.030369767
Smpd3	-0.363975358	0.030369767
Kcnn2	-0.275269374	0.031125458
Rab11fip2	-0.253095199	0.031721149
Il1rap	-0.268933682	0.032073907

Plxna1	-0.262771204	0.032683728
Rmdn3	-0.29787384	0.032683728
Synpr	-0.358142355	0.032683728
Rpl13a	0.320273311	0.037105449
Bsg	-0.199095201	0.037224236
Atp6v0d1	-0.211354153	0.037224236
Txnl1	0.40481663	0.042397632
Pycrl	-0.307193967	0.042397632
Plxna2	-0.390853418	0.042397632
Samm50	-0.217931489	0.04375461
Gm996	-0.296431502	0.04375461
Svop	-0.430162468	0.044266769
Myo18a	0.547427858	0.04644443
Gng7	-0.296499281	0.04644443
Vdac1	-0.186149907	0.04852333
Mark4	-0.213873421	0.04852333
Syt12	-0.238310408	0.04852333
Mtch2	-0.286659187	0.04852333
Slc6a11	-0.395320579	0.04852333
Ipo5	0.238257927	0.048562036
Map1lc3b	-0.161568702	0.048778909
Pmm1	0.445271034	0.048889438
Pdcl	-0.248255577	0.048889438
Gpx1	0.16857488	0.050092878
Fam210a	-0.243252202	0.050092878
Wfs1	-0.426432596	0.050092878
Tpm4	0.341181093	0.050298941
Gprc5b	-0.237953556	0.050298941

For *Tg*^{SHANK2AR462X}

Gene	Control vs *Tg*^{SHANK2AR462X} | log2 fold change	Control vs *Tg*^{SHANK2AR462X} | FDR adjusted p-values
Kif1a	0.870412262	4.63E-09
Ndrg3	0.306349697	3.41E-05
Rae1	0.495970752	0.000274634
Apba2	0.289942235	0.000499013
Mycbp2	0.685342092	0.000722405
Pgm2l1	0.597170306	0.002230564
Rgs14	-0.474542693	0.002230564
Cpne4	-0.294877801	0.002830756
Ermp1	-0.245749763	0.008358106
Pgls	0.254343851	0.010176294
Lancl1	0.231332812	0.013645122
Rimbp2	-0.270407782	0.013645122
Epha4	-0.196126477	0.013645122
Nwd2	-0.350761804	0.013645122
Serpinb1a	-0.448180145	0.013645122
Anxa11	-0.401698302	0.022434897
Ca4	1.635201324	0.027671
Plxna1	-0.317544143	0.027671
Map7d2	0.309353916	0.027864551
Pld3	0.205933469	0.027864551
Lxn	0.355360482	0.029387066
Ech1	-0.339782174	0.029387066
Gria1	-0.288694363	0.029387066
Nos1	-0.188663274	0.029595978
Ptprn2	-0.664626969	0.030111267
Scn8a	-0.221685002	0.030268813
Acot13	-0.212144629	0.030289017
Rhoa;rhoc	0.287678648	0.030289017
Ppm1f	-0.195102468	0.030289017
Pex11b	-0.200591863	0.032101342
Kit	-0.508559449	0.032101342
Plxna4	-0.249105577	0.032101342
Wbscr17	-0.26710312	0.033011016
Stxbp6	-0.563376886	0.033011016
Clcn6	0.171758858	0.033737627
Uchl1	0.400391828	0.034195896
Rtn4ip1	-0.348146309	0.034195896
Cadm3	-0.289321917	0.034195896
Cryz	-0.236269806	0.036849927

Ccdc177	-0.192598836	0.037525782
Slc35f1	0.632444371	0.040580386
Gpr56	0.33786522	0.040580386
Pgbd5	-0.219782996	0.040580386
Them6	-0.289408107	0.041542566
6330403a02rik	-0.218986619	0.041542566
Gm20671;pisd	-0.333491941	0.041542566
Cpne7	-0.413482633	0.041542566
Cntnap1	-0.204233402	0.041542566
Cpne5	-0.281118121	0.041542566
Hsd17b8	-0.208092459	0.044621876
Pde1a	0.316988873	0.04541138
Vps16	0.135736026	0.048906198
Tnks1bp1	-0.221357526	0.048906198
Slc7a14	-0.245379863	0.048906198
Cpne6	-0.279941823	0.049821894

Appendix 5: Summary of the behavioral analysis

Name of the behavioral experiment	Parameter	$Tg^{SHANK2A}$	$Tg^{SHANK2A}$ + dox	$Tg^{SHANK2A}$ + P0 dox		$Tg^{SHANK2AR462X}$	$Tg^{SHANK2AR462X}$ +dox
SHIRPA	Weight	↓30 %	↓30 %	↓10 %		↓10 %	
	Body position						
	Spontaneous activity	↑	↑	↑			
	Tremor						
	Twitches	↑	↑				
	Defecation						
	Urination						
	Visual Placing						
	Body Tone						
	Pinna Reflex						
	Corneal Reflex	↑	↑	↑			
	Toe Pinch						
	Crossed extensor reflex						
	Suspended hind limb splay						
	Trunk curl						
	Limb grasp						
	Horizontal rotation response						
	Catalepsy			↑			
	Negative geotaxis						
Balance test	Score	↓					
LABORAS	Number of locomotion	↑	↑	↑		↑	↑
	Average speed	↑	↑	↑		↑	↑
	Duration of eating	↑	↑				↑
	Duration of drinking		↓				
	Number of rearing	↑	↑	↑			
	Number of self-grooming					↓	↓
	Number of climbing						
Visual stereotypic behavior	Jumping		n.a.	n.a.		↑	n.a.
	Self-grooming	↑	n.a.	n.a.			n.a.
	Digging	↓	n.a.	n.a.		↓	n.a.
Open field test	Number of visits to the center of the arena	↓		↓			↓
	Distance in the center of the arena	↓		↓			↓
Dark/light compartment	Latency to visit light	↑	↑	↑		↑?	
	Number of visits to light	↓	↓	↓		↑?	↓
Neophobia	Number of contacts	↓	↓				↓
	Latency to the first contact	↑		↑		↑	↑
Cliff avoidance	CAR	↓	↓	↓		↓	↓
Nesting	Score	↓	↓				
Burrowing	Remaining food pellets after 2h	↑	↑	↑		↑	↑

	Remaining food pellets after 12h	↑	↑			↑	↑
Novel object recognition	Number of contacts	↓?				↑	
Three-chamber social test	Number of all contacts	↓					
Direct social interaction	Number of all contacts	↓				↑	
Puzzle box (session)	Latency	↑ 1, 8, 10	↑ 1-10	↑1, 8-10		↑ 5,6, 7	↑ 5,6, 10
Fear conditioning	Acquisition	↓	↑			↓	
	Context memory					↓	
	Cued memory		↑				↑

↑: increase, ↓: decrease, n.a. : not applicable, empty space: no difference compared to control mice